JICA

ASEAN-JAPAN COOPERATION ON MATERIALS SCIENCE AND TECHNOLOGY

2nd SEMINAR ON CORROSION AND PROTECTION

BANGKOK, THAILAND
30 JUNE - 2 JULY 1992

SPONSORED BY: JAPAN INTERNATIONAL COOPERATION AGENCY (JICA)

ORGANISED BY: THAILAND INSTITUTE OF SCIENTIFIC AND TECHNOLOGICAL RESEARCH (TISTR)

SEMINAR ON CORROSION AND PROTECTION (2nd : 1992 : BANGKOK).

THE 2nd SEMINAR ON CORROSION AND PROTECTION, 30 JUNE - 2 JULY 1992, SIAM CITY HOTEL, BANGKOK, THAILAND.

List of Contents

17. Present Status of the Metal Protection and Finishing Industries in Malaysia
18. The Effect of Ultraviolet Radiation on the Bonding Between Organic Polymer and Metal Substrate
19. Bangkok Metropolis and Its Air pollution Problem
20. Coating for Pipelines and other Underground Structures
21. Preservation of Ship's Hull
22. Corrosion and Protection
23. Study on the Properties of Organic Paints for Steel Structure Subjected to Natural Exposure

General Information

Conference Secretarial

The Secretarial will be pleased to handle your enquires (whenever possible). Please refer to any of the Following Secretarial Personnel:

Mr.Pakomthep	Migasena
Mr.Sermkiat	Kulkowit
Ms.Siriluck	Kewdoknoi
Ms.Naetsai	Chulasai
Ms.Korrakoch	Meechumnarn
Mr.Wirach	Chantra
Ms.Ubolwan	Hongcharoensri
Mr.Panya	Gatpan
Ms.Vanitsri	Goatpetch
Ms.Phensri	Nonsrichai
Ms.Wanngam	Thanavanitchnam

Airlines		Telephone number
i	Royal Brunei Airlines (RJ)	2354764
ii	Garuda Indonesia (GA)	2330981-2
iii	Malaysian Airlines (MH)	2365871-5
iv.	Philippines Airlines (PR)	2332350-2
v.	Singapore Airlines (SQ)	2360440
vi.	Thai Airways International (TG)	2333810
vii.	Qantas Airways (QF)	2376268-75
viii.	Japan Airlines (JL)	2349111

Other Information

Embassies		Telephone number
i.	Embassy of Brunei Darussalam	2605886-7
		Fax : 2605884
ii.	Philippines Embassy	2590140
		Fax : 2597373
iii.	Embassy of the Republic of Indonesia	2523135-40
		Fax : 2551267
iv.	Embassy of Malaysia	2861390-2
		Fax : 2872348
v.	Embassy of Japan	2526151-9
		Fax : 2534153
vii.	Embassy of the Replublic of Singapore	2862111
		Fax : 2872578

Welcome Address and Report

to

Mr.Kasem Snidvongs

Permanent Secretary, Ministry of Science, Technology and Environment

by

Mr.Chalermchai Honark

Deputy Governor, Thailand Institute of Scientific and Technological Research

---

Khun Kasem Snidvongs Permanent Secretary of Ministry of Science, Technology and Environment,Distinguished Participants, Ladies and Gentlemen.

First and foremost I wish to take this opportunity to welcome our colleagues from ASEAN, officials from Japan and Thai participants to this meeting once again and some of you have already visited Thailand and attended the first seminar and other function of the project in 1990. We are happy and honored to have you all here. I hope that your deliberations be fruitful and all of you will enjoy a most pleasant and memorable stay in Thailand.

On behalf of Atmospheric Corrosion : Organic Coatings Project, I would like to express my deep gratitude to the Permanent Secretary of the Ministry of Science, Technology and Environment for presiding over the opening ceremony of the seminar on "Corrosion and Protection". I would also like to extend my appreciation to the Japanese Government and to all distinguished guests for your kind cooperation in gathering here.

May I take this opportunity to report to you the objective and background of this seminar as follows:

Almost ten years back during the time when His Excellency Yasuhiro Nakasone, the former Japanese Prime Minister, visited ASEAN countries in 1983, he advocated meetings of ministerial and expert levels for the purpose of exchanging views and opinions on technical cooperation progress in the field of Science in order to share scientific technology among ASEAN countries. After several such meetings between Japan and ASEAN countries, the desired fields and scopes were agreed upon in 1987, and Material Science Technology was one of them. As to this field, the Japanese Government would provide project type cooperation toward each ASEAN member country as follows:

- Corrosion of reinforced concrete structures, Project of Brunei
- Characterization of polymeric materials, Project of Indonesia
- Characterization of fine ceramics, Project of Malaysia
- Atmospheric corrosion-metallic coatings, Project of the Philippines
- Prevention of corrosion in structures, Project of Singapore
- Atmospheric corrosion-organic coatings, Project of Thailand

As for Thailand, in 1987 the Record of Discussion for the ASEAN Project was signed between the Japanese mission and the authorities of the Royal Kingdom of Thailand and the project started to be implemented in August 1988 with the following aims:

1. To evaluate the durability of organic coated metals by outdoor exposure tests and accelerating tests.
2. To study various methods of the measurement on corrosion of metals and degradation of organic coatings.
3. To contribute to the development of corrosion prevention technology.

According to the agreement of the joint ASEAN-JAPAN expert meeting held firstly in Bali, Indonesia, followed by the meetings in Cha-am, Thailand and Genting Highlands, Malaysia. The fourth joint meeting was held in Manila, Philippines last year. We are happy to inform that one of the unique characters of ASEAN-Japan Cooperation Programme, the multilateral activities such as seminars, training, and collaborative research work had been commented in each ASEAN member country succesfully. Moreover, the Japanese mutual consultation team, were sent to each country to review the progress of the project, discuss the research and general activities of the projects and that we hope to complete our target to contribute to the development of corrosion prevention technology to the nation, not only Thailand but also the regional as the whole. This seminar will summarize all the results of the activities concerning corrosion in ASEAN countries and also the presentation of 22 papers from Japan, ASEAN and other local organizations from both the government and private sectors.

It is now the auspicious moment. May I have the honor of inviting Permanent Secretary of Ministry of Science, Technology and Environment to declare open and give blessings to the seminar on "Corrosion and Protection".

Opening Address

by

Mr.Kasem Snidvongs

Permanent Secretary, Ministry of Science, Technology and Environment

at

The 2nd Seminar on "Corrosion and Protection"

Siam City Hotel, Bangkok Thailand

Tuesday 30 June, 1992

Distinguished Participants:

It is a privilege and great pleasure for me to have an opportunity to preside over the opening ceremony of the seminar on "Corrosion and Protection". This seminar is jointly organized by Japan International Cooperation Agency (JICA) and Thailand Institute of Scientific and Technological Research.

I am pleased to be at this seminar because I have learned that at present many Thai researchers are interested in certain natural phenomena which creates a great loss. Such phenomenon is the destruction or the corrosion of materials caused by human unawareness. The corrosion damage is worth more than one hundred thousand million baht a year and is going to be greater if we still develop industry without considering its impact on the environment, or if we utilize our natural resources without proper management. Although such concern is still limited among researcher, it is a good start and would benefit the country in the future.

In Thailand, the loss of corrosion material has not yet been evaluated. But I could give you some examples which illustrate the corrosion damage and the cost of protection that is the fast growing rate of the auto body repair shop in Bangkok and all districts throughout the country. The circulating sum of capital in this business is certainly not less than one thousand million baht a year. The cause of the losses are well known to us and no one could deny that the damage is still going on as long as we do not have new materials and proper protection.

However, I am proud that there are a number of experts who are paying attention to this problem and try to find the real cause and search for the preventive measures. One more important of atmospheric pollutant is that some corrosive atmosphere such as SO_2, NO_2, H_2S is harmful to human life which is a big campaign for Thailand to eliminate those pollutant.

On behalf of the Ministry of Science, Technology and Environment, I wish to express my sincere appreciation and thank to all of the guest speakers and distinguished participants to devote your time for sharing experience and knowledge which will be benificial to your work and economic development of the country. I also wish to express a special thank to the Government of Japan and all Japanese experts for their support in this project. I do hope that the results of this seminar shall be further developed and expanded to enhance the capability of the country in the field of material science.

At this propitious moment, I hereby declare open the seminar on "Corrosion and Protection:. I do wish all of you a resounding success in both your work and your private life.

Thank you

ASEAN-JAPAN COOPERATION PROGRAMME ON MATERIALS SCIENCE AND TECHNOLOGY

2nd SEMINAR/WORKSHOP ON CORROSION AND PROTECTION IN THAILAND 1992

30th JUNE - 2nd JULY 1992

SIAM CITY HOTEL

BANGKOK, THAILAND

List of Speaker

JAPAN

Prof. Dr. Toshio Shibata
Faculty of Engineering
Osaka University,
Osaka, Japan

Assoc.Prof. Dr. Hideaki Takahashi
Faculty of Engineering,
Hokkaido University,
Hokkaido, Japan

ASEAN

Brunei

Mr. Ak Menuddin PLW Pg Hj Yussof
Public Works Department Ministry of Development
Brunei Darussalam

Indonesia

Dr.-Ing. Faraz Umar
Institute of Technology Bandung, JL Ganesha
No.10-Bandung 40132 Indonesia

Dr. Sunara Purwadaria
Institute of Technology Bandung, JL Ganesha
10 Bandung 401321 Indonesia

Mr. A.D. Wiyono
UPT-LUK, BPPT Puspiptek
Serpong Indonesia

Malaysia

Dr. Mustaza Hj. Ahmadun
SIRIM, P.O. Box 7035, 40911
Shah Alam, Malaysia

Dr. Jamaliah Idris
Fakulti Kejuruteraan Jentera University
Teknologi Malaysia Karung
Berkunui 791 Johor Bahru 80990 Johor

Mr. Azman Bin A. Aziz
Petronas, LOT 1026 PKNS
Industrial Estate 52100
ULU Kelang, Selangor, Malaysia

Philippines

Dr. Lilia Silao
DE LA SALLE UNIV. 2401 Taft Ave.,
Manila Philippines

Ms. Cynthia V. Bernas
Industrial Technology Development Institute
Bicutan Taguig Manila, Philippines

Dr. Ner Cruz-Rodriguez
Industrial Technology Development Institute
Bicutan Taguig Manila Philippines

Singapore

Dr. Huang Xianya
Singapore Institute of Standard and Industrial Research
1 Science Park Drive, Singapore 0511

Thailand

Dr. Ladawal Chotimongkol
Thailand Institute of Scientific and Technological Research
196 Phahonyothin Rd. Chatuchak, Bangkok 10900

Commander Mana Naknawedee
Pom Prachul Dockyard , Naval Dockyard Department
Royal Thai Navy

Dr. Supat Wangwongwatana
Department of Pollution Control,
61/1 Soi Phibunwatana 7, Rama VI,
Bangkok 10400

Dr. Somchai Tongtem
Faculty of Science, Chiang-Mai University,
Chiang-Mai 50000

Dr. Sermkiat Chomchanyong
Chiang-Mai University,
Chiang-Mai 50000

Mr. Vinij La-ongsuwan
TOA Paint (Thailand) Co., Ltd.

Mr. Narong Sukapaddhi
Thai oil Co., Ltd.
Sriracha Refinery, Chonburi

Ms. Taveeporn Khumthong
Thai Kansai Paint Co., Ltd.
180 Thaparug Rd. Somrong-Nua,
Samutprakarn Thailand 10270

Mr. Soravuth Judabong
Thailand Institute of Scientific and Technological Research
196 Phahonyothin Rd. Chatuchak, Bangkok 10900

ASEAN-JAPAN COOPERATION PROGRAMME ON MATERIALS SCIENCE AND TECHNOLOGY

2nd SEMINAR/WORKSHOP ON CORROSION AND PROTECTION IN THAILAND 1992

30th JUNE - 2nd JULY 1992

SIAM CITY HOTEL

BANGKOK, THAILAND

List of participant

JAPAN

Prof. Dr. Toshio Shibata
Faculty of Engineering
Osaka University,
Osaka, Japan

Assoc.Prof. Dr. Hideaki Takahashi
Faculty of Engineering,
Hokkaido University,
Hokkaido, Japan

Ms. Kuni Sato
Fist Secretary
Embassy of Japan

Mr. Masahiko Metoki
Second Secretary
Embassy of Japan

Mr.Tokuhisa Ishiwata
Assistant Resident Representative
JICA Thailand Office

Mr. Koji Yamamoto
Director
for Co-research and Coordination in Bangkok
National Space Development Agency of Japan
B.B. Building 13 F Room No.12
54 Asoke Rd., Sukhumvit 21
Bangkok 101 0 , Thailand

Mr. Toshiharu Murata
Port Advisor
Technical Department, Port Authority of Thailand
Sunthornkosa Rd., Klong Toey, Bangkok 10110

Mr. Shigeki Kirihara
JICA Long-term Expert on Atmospheric Corrosion
JAPAN-ASEAN Cooperation on Science and Technology in Thailand

Ms. Mineko Sato
JICA Long-term Expert on Atmospheric Corrosion
JAPAN-ASEAN Cooperation on Science and Technology in Thailand

Mr. Hideo Nagai
JICA Long-term Expert on Atmospheric Corrosion
JAPAN-ASEAN Cooperation on Science and Technology in Thailand

ASEAN

Brunei

Mr. Ak Menuddin PLW Pg Hj Yussof
Public Works Department Ministry of Development
Brunei Darussalam

Mr. Rahman Hj. Abu Baker
Public Works Department Ministry of Development
Brunei Darussalam

Ms Lee Siew Hung
Public Works Department Ministry of Development
Brunei Darussalam

Indonesia

Dr.-Ing. Faraz Umar
Institute of Technology Bandung, JL Ganesha
No.10-Bandung 40132 Indonesia

Dr. Sunara Purwadaria
Institute of Technology Bandung, JL Ganesha
10 Bandung 401321 Indonesia

Mr. A.D Wiyono
UPT-LUK, BPPT Puspiptek
Serpong Indonesia

Malaysia

Dr. Mustaza Hj. Ahmadun
SIRIM, P.O. Box 7035, 40911
Shah Alam, Malaysia

Dr. Jamaliah Idris
Fakulti Kejuruteraan Jentera University
Teknologi Malaysia Karung
Berkunui 7 1 Johor Bahru 80990 Johor

Mr. Azman Bin A. Aziz
Petronas, LOT 1026 PKNS
Industrial Estate 52100
ULU Kelang, Selangor, Malaysia

Philippines

Dr. Lilia Silao
DE LA SALLE UNIV. 2401 Taft Ave.,
Manila Philippines

Ms. Cynthia V. Bernas
Industrial Technology Development Institute
Bicutan Taguig Manila, Philippines

Dr. Ner Cruz-Rodriguez
Industrial Technology Development Institute
Bicutan Taguig Manila Philippines

Singapore

Dr. Huang Xianya
Singapore Institute of Standard and Industrial Research
1 Science Park Drive, Singapore 0511

Thailand

Dr. Ladawal Chotimongkol
Thailand Institute of Scientific and Technological Research
196 Phahonyothin Rd. Chatuchak, Bangkok 10900

Dr. Paritud Bhandhubanyong
Faculty of Engineering
Chulalongkorn University
Thanon Phaya Thai, Bangkok 10330

Dr. Monthop Valayapetre
Department of Mineral Resources (DMR)
Thanon Rama VI, Bangkok 10400

Mr. Pakdi Thongcharoen
Department of Mineral Resources (DMR)
Thanon Rama VI, Bangkok 10400

Miss. Wanasri Samanasen
The National Research Council of Thailand (NRCT)
196 Thanon Phahon Yothin, Chatuchak,
Bangkok 10900

Miss. Choosri Keedumrongkool
The National Research Council of Thailand (NRCT)
196 Thanon Phahon Yothin, Chatuchak,
Bangkok 10900

Commander Mana Naknawedee
Pom Prachul Dockyard, Naval Dockyard Department
Royal Thai Navy

Dr. Supat Wangwongwatana
Department of Pollution Control,
61/1 Soi Phibunwatana 7, Rama VI,
Bangkok 10400

Dr. Somchai Tongtem
Faculty of Science, Chiang-Mai University,
Chiang-Mai 50000

Dr. Sermkiat Chomchanyong
Chiang-Mai University,
Chiang-Mai 50000

Mr. Vinij La-ongsuwan
TOA Paint (Thailand) Co., Ltd.

Mr. Narong Sukapaddhi
Thai oil Co., Ltd.
Sriracha Refinery, Chonburi

Ms. Taveeporn Khumthong
Thai Kansai Paint Co., Ltd.
180 Thaparug Rd. Somrong-Nua,
Samutprakarn Thailand 10270

Mr. Soravuth Judabong
Thailand Institute of Scientific and Technological Research
196 Phahonyothin Rd. Chatuchak, Bangkok 10900

Ms. Kannika Sthapitanonda
Thailand Institute of Scientific and Technological Research
196 Phahonyothin Rd. Chatuchak, Bangkok 10900

Ms. Peesamai Jenvanitpanjakul
Thailand Institute of Scientific and Technological Research
196 Phahonyothin Rd. Chatuchak, Bangkok 10900

Ms. Salaisophin Komarakul Na Nakorn
Thailand Institute of Scientific and Technological Research
196 Phahonyothin Rd. Chatuchak, Bangkok 10900

Dr. Prasonk Sricharoenchai
Faculty of Engineering
Chulalongkorn University
Phaya Thai Rd. Bangkok 10330

Mr. Sangsit Treesuwan
Kasetsart University
50 Phahon Yothin Rd. Chatuchak
Bangkok 10900

Mr. Visit Kasempimolporn
Songkhalnkarin University Hat Yai
Songkla 90110

Mr. Somboon Tenghongchareon
Rajamangala Institute of Technology : Bangkok Technical Campus
2 Nanglinji Rd. Yannawa,
Bangkok 10120

Mr. Witoon Swadiluksa
Rajamangala Institute of Technology : North Bangkok Campus
1381 Piboonsongkrarm Rd. Bangsue
Bangkok 10800

Miss. Duangrudee Supatimusro
Rajamangala Institute of Technology : Nonthaburi Campus
7/1 Nonthaburi 1 Rd. Suanyai, Amphur Muang
Nonthaburi 11000

Ass.Prof. Pornsak Attavanich
King Mongkut's Institute of Technology Lat Krabang (KMITL)
Chalongkrung Rd. Lat Krabang District,
Bangkok 10520

Mr. Somkid Thanaruongsakulthai
King Mongkut's Institute of Technology North Bangkok (KMITNB)
1518 Pibulsongkram Rd. Khet Bangsue,
Bangkok 10800

Miss. Siriporn Chayutipun
King Mongkut's Institute of Technology North Bangkok (KMITNB)
1518 Pibulsongkram Rd. Khet Bangsue,
Bangkok 10800

Mr. Suwan Soontareerat
King Mongkut's Institute of Technology Thonburi
91 Suksawat 48 Bangmod , Khet Ratburana
Bangkok 10140

Mrs. Medini Mukdasiri
King Mongkut's Institute of Technology Thonburi
91 Suksawat 48 Bangmod , Khet Ratburana
Bangkok 10140

Mr. Choochat Nitipanyawong
King Mongkut's Institute of Technology Thonburi
91 Suksawat 48 Bangmod , Khet Ratburana
Bangkok 10140

Mr. Krirkchai Rayanasukwong
Department of ASEAN Affairs
Thanon Si Ayutthaya,
Bangkok 10400

LT. Lalida SuparoJanee
Naval Science Department
Arun-Amarin Rd.
Bangkok 10600

Mr. Pansa Buranawanich
Department of Mineral Resources (DMR)
Thanon Rama VI, Bangkok 10400

Mrs. Saipin Suebsantikul
Department of Science Service
Cable Address : DPESCIE
Bangkok 10400

Mr. Surasak Pongpansook
Office of Atomic Energy for Peace (OAEP)
Vibhavadi Rangsit Rd. Chatuchak,
Bangkok 10900

Mrs. Supranee Srisuda
Office of the National Economic and Social Development Board
962 Krung Kasem Rd.
Bangkok 10100

Mr. Thonglor Phoomglin
Department of Energy Affairs (DEA)
Saphan Kasat Suk,
Bangkok 10330

Mr. Supachai Sri-israporn
Petroleum Authority of Thailand
555 Vibhavadi Rangsit Rd. Chatuchak,
Bangkok 10900

Mr. Atchanai Ratanasit
Petroleum Authority of Thailand
Prakanong Oil Depot
Argnarong Rd., Kaung Toey,
Bangkok 10250

Mr. Witaya amwong
Petroleum Authority of Thailand
555 Vibhavadi Rangsit Rd. Chatuchak,
Bangkok 10900

Mr. Punsak Tiramongkol
Pollution Control Department
Soi Phibun Watthana 7, Rama VI Rd.
Bangkok 10400

Mr. Somboon Arayaskul
The Electricity Generating Authority of Thailand (EGAT)
53 Charan Sanid Rd. Wong, Bang Kruai
Nonthaburi 11000

Mr. Tanee Jumneonkara
The Electricity Generating Authority of Thailand (EGAT)
53 Charan Sanid Rd. Wong, Bang Kruai
Nonthaburi 11000

Mr. Sombat Paneiam
The Expressway and Rapid Transit Authority of Thailand (ETA)
Phahon Yothin Rd. Lat Yao, Chatuchak,
Bangkok 10900

Miss. Ruchnee Jiar-ajala
The Department of Highways
Si Ayutthaya Rd.,
Bangkok 10400

Mrs. Jiraporn Srirarai
The Department of Highways
Si Ayutthaya Rd.,
Bangkok 10400

Mr. Sathit Keatikumjorn
The Industrial Estate Authority of Thailand (IEAT)
618 Nikhom Makkasan Rd. Ratchathewi,
Bangkok 10400

Mr. Santichai Horpaopun
The Industrial Estate Authority of Thailand (IEAT)
618 Nikhom Makkasan Rd. Ratchathewi,
Bangkok 10400

Mr. Viwat Summachevavat
The Industrial Estate Authority of Thailand (IEAT)
618 Nikhom Makkasan Rd. Ratchathewi,
Bangkok 10400

Mr. Nukul Subcharoen
The Meteorological Department (MET)
4353 Bang Na,
Bangkok 10260

Mr. Pornlers Santipaporn
The Metropolitan Waterworks Authority (MWA)
18/137 Pracha Chuen Rd. Tung song Hong,
Don Muang, Bangkok 10210

Mr. Suwan Cheiwchansilp
The Metropolitan Waterworks Authority (MWA)
18/137 Pracha Chuen Rd. Tung song Hong,
Don Muang, Bangkok 10210

Miss. Prinda Butayothee
The National Research Council of Thailand (NRCT)
196 Phahon Yothin Rd. Chatuchak,
Bangkok 10900

Mr. Somchai Montburinont
The Provincial Waterworks Authority (PWA)
72 Chaeng Watana 1 Rd. Lak si,
Bang Khen , Bangkok 10210

Mr. Nibhon Premkamol
The Secretariat of the National Assembly
U-Thong Nai Rd.
Bangkok 10300

Miss. Anarat Tungpanithannan
Test and Development Organization of Thailand
65 Phathumsumphum Rd.
Amphor Muang, Phathumthanee 12000

Mrs. Chongkolnee Chottivitayatanin
Test and Development Organization of Thailand
65 Phathumsumphum Rd.
Amphur Muang, Phathumthanee 12000

Miss. Kanogporn Nuntamanop
Test and Development Organization of Thailand
65 Phathumsumphum Rd.
Amphur Muang, Phathumthanee 12000

Miss. Pornampai Punpocha
Test and Development Organization of Thailand
65 Phathumsumphum Rd.
Amphur Muang, Phathumthanee 12000

Miss. Niramon Wilamas
Corro-Coat (Thailand) Co., Ltd.
45 Moo 26 Soi Watmahawong
Poochaosamingprai Rd.,
Samuthprakarn 10130

Mr. Chatchaval Asavakanoksilp
Dimet (Siam) Co., Ltd.
1048 Soi Poonsin Sukhumwit 64
Bangchak Phakanong,
Bangkok 10260

Mr. Boonying Intanapasat
Dimet (Siam) Co., Ltd.
1048 Soi Poonsin Sukhumwit 64
Bangchak Phakanong,
Bangkok 10260

Dr. Athikom Bangviwat
Esso Standard Thailand Co., Ltd.
Manufacturing Department
P.O. Box 18 Sriracha
Cholburi 20110

Miss. Kesirin Thovanish
Jotun Thailand Co., Ltd.
45 Moo 4 Soi Watmahawong
Poochaosamingprai Rd. Somrongtai
Prapadang Samuthprakarn 10130

Miss. Prapatsorn Thobhunme
Jotun Thailand Co., Ltd.
45 Moo 4 Soi Watmahawong
Poochaosamingprai Rd. Somrongtai
Prapadang Samuthprakarn 10130

Miss. Siriwan Tantawechkij
Jotun Thailand Co., Ltd.
45 Moo 4 Soi Watmahawong
Poochaosamingprai Rd. Somrongtai
Prapadang Samuthprakarn 10130

Mr. A. Soeda
Thai Kansai Paint Co., Ltd.
180 Moo 3 Thepavah Rd.,
Amphur Muang,
Samutprakan 10270

Mr. H. Inada
Thai Kansai Paint Co., Ltd.
180 Moo 3 Thepavah Rd.,
Amphur Muang,
Samutprakan 10270

Mr. Thaweesak Sripusitto
Pha-Dange Indrustrial Co., Ltd.
Amphur Muang, Tak 63000

Mr. Somkiat Rodsakul
Pha-Dange Indrustrial Co., Ltd.
Amphur Muang, Tak 63000

Mr. Arnoopon Chaklang
Pha-Dange Indrustrial Co., Ltd.
Amphur Muang, Tak 63000

Ms. Kallaya klaithong
The Bangchak Petroleum Co., Ltd.
210 Sukhumwit 64 Phakanong
Bangkok 10260

LT. Bodin Choochartchaikulkarn
The Bangchak Petroleum Co., Ltd.
38 Srinakarin Rd. Prawet,
Bangkok 10260

Mr. Piyawong Thithiwong
The Bangchak Petroleum Co., Ltd.
38 Srinakarin Rd. Prawet,
Bangkok 10260

Mr. Veera Varanyanond
Valence Corporation Co., Ltd.
156/5-9 Petchburi Rd., Ratthewee
Bangkok 10400

Mr. Tanin Jamkrajang
Charoenwattana Co., Ltd.
2/1 Soi Yimprayoon Bang Kae,
Phasee Charoen, Bangkok 10160

Mr. Prajobpan Setthabute
Charoenwattana Co., Ltd.
2/1 Soi Yimprayoon Bang Kae,
Phasee Charoen, Bangkok 10160

Thailand Institute of Scientific and Technology Research

Dr. Nongluck	Pankurddee
Mr. Vichian	Auimmode
Mr. Pisut	Chullarerk
Mr. Orachun	Keowkangwal
Mr. Pratip	Vongbandit
Mr. Raewat	Laopaiboon
Mr. Sumate	Poomiapiradee
Ms. Duangrudee	Mongkalakorn
Ms. Rujeeporn	Pookrongta
Ms. Siriporn	Larpkiattaworn
Mr. Kriengkrai	Imsompoch
Mr. Panya	Suadee
Ms. Piyanun	Manee
Mr. Prachun	Onpuckdee
Mr. Manud	Gedgrew
Mr. Suchat	Saengkaew
Mr. Chalermpol	Chullarerk
Mr. Chumporn	Thaworn
Mr. Chanin	Surainark
Mr. Udom	Nongruang
Ms. Jiamjit	Suwan
Ms. Arunee	Srimongkolpipaht

ASEAN-JAPAN COOPERATION PROGRAMME ON MATERIALS SCIENCE AND TECHNOLOGY

2nd SEMINAR/WORKSHOP ON CORROSION AND PROTECTION IN THAILAND 1992

30th JUNE - 2nd JULY 1992

SIAM CITY HOTEL

BANGKOK, THAILAND

PROGRAMME

DAY 1, TUESDAY 30 JUNE 1992

08:30 - 08:55	Registration of all participants
09:00	Arrival of Guests of Honour
09:00 - 09:15	Welcome Address and Report by Deputy Governor of Thailand Institute of Scientific and Technological Research (TISTR)
09:15 - 09:30	Address by Embassy of Japan
09:30 - 09:45	Opening Address by Permanent Secretary for Ministry of Science, Technology and Environment
09:45 - 10:00	Coffee Break

Session A :

10:00 - 10:30	**"Atmospheric Corrosion : Organic-Coatings"** by Dr.Ladawal Chotimongkol, Project Team Leader, TISTR, Thailand
10:30 - 11:30	**"Recent Investigation on Anodizing of Aluminum and It's Alloys"** by Associate Prof. Hideaki Takahashi, Hokkaido University, Japan

11.30 - 12.00	"Structural Repair to Reinforced Concrete Beam in Tungku Landless Housing Settlement Scheme, Nagara Brunei Darussalam" by Ak.Menuddin PLW Pg. Hj. Yussof, Structural Section, Public Works Department, Brunei Darussalam
12.00 - 13.30	Lunch

Session B :

13.30 - 14:00	"Application of Potential - pH (Pourbaix) Diagram in Aqueous Corrosion" by Dr.Sunara Purwadaria, Institute of Technology Bandung, Indonesia
14:00 - 14:30	"Protective Coatings for Offshore Structures and Equipment" by Mr.Azman Bin A. Aziz, Petroleum Research Institute, Malaysia
14:30 - 15:00	"Atmospheric Corrosion of Galvanized Roofing Materials at Makban Geothermal Power Plant Complex" by Ms.Cynthia V. Bernas, Industrial Technology Department Institute, Philippines
15:00 - 15:20	Coffee Break

Session C :

15:20 - 15:50	"Mechanism of Stress Corrosion Cracking (SCC) of Titanium Alloys in Nearly Neutral Chloride Aqueous Solution" by Dr.Huang Xianya, Singapore Institute of Standards and Industrial Research, Singapore
15:50 - 16:20	"Creep Damage of Catalyst Tube and Pigtail Outlets in Steam Reformer Furnace of Hydrogen Manufacturing Unit" by Mr.Narong Sukapaddhi, Thai Oil Co.,Ltd., Thailand
16:20	Close of Day 1

Day 2, WEDNESDAY 1 JULY 1992

Session D :

09:00 - 10:00	"Recent Progress in Scanning Microprobe Systems for Electrochemical Corrosion Measurement" by Prof.Toshio Shibata, Osaka University, Japan
10:00 - 10:20	"Stress Corrosion Cracking on Some Components Used in Oil Industry" by Mr. A.D. Wiyono, UPT-Laboratorium UJI Konstruksi, BPP-Teknologi, Puspiptek Serpong, Indonesia
10:20 - 11:40	"Corrosion Performance of Deformed Galvanized Coatings" by Dr.Jamaliah Idris, Universiti Teknologi Malaysia, Malaysia
10:40 - 11:00	Coffee Break

Session E :

11:00 - 11:20	"Evaluation of Corrosion Protective Properties of Coated Steels after Chemical Conversion Treatments by AC Impedance Measurement and Scanning Vibrating Electrode Technique" by Dr.Lilia Silao, De La Salle University, Philippines
11:20 - 11:40	"Corrosion Test of Plated Products for The Study of Service Life" by Dr.Sermkiat Jomjanyong, Chiangmai University, Thailand
11:40 - 12:00	"The Chlorination of Selected Commercial Alloys at High Temperature" by Dr.Somchai Tongtem, Chiangmai University, Thailand
12:00 - 13:30	Lunch

Session F :

13:30 - 13:50	**"Electroplating of Tin from Halogen Baths for Decorative and Corrosion Protective Purposes"** by Dr.-Ing Faraz Umar, Institute of Technology Bandung, Indonesia
13:50 - 14:20	**"Present Status of The Metal Protection and Finishi g Industries in Malaysia"** by Dr.Mustaza Hj. Ahmadun, Standards & Industrial Research Institute of Malaysia, Malaysia
14:20 - 14:40	**"The Effect of Ultraviolet Radiation on the Bonding Between Organic Polymer and Metal Substrate"** by Ms.Ner C. Rodriquez, Industrial Technology Development Institute, Philippines
14:40 - 15:00	**"Bangkok Metropolis and Its Air Pollution Problem"** by Dr.Supat Wangwongwatana, Department of Pollution Control, Thailand
15:00 - 15:20	Coffee Break

Session G :

15:20 - 15:40	**"Coating for Pipelines and Other Underground Structures"** by Mr.Vinij La-Ongsuwan, TOA Paint (Thailand) Co.,Ltd., Thailand
15:40 - 16:00	**"Preservation of Ship's Hull** by CDR. Mana Naknaewdee, Naval Dockyard Department, Thailand
16:00 - 16:20	**"Corrosion and Protection"** by Ms.Taveeporn Khumthong, Thai Kansai Paint Co.,Ltd., Thailand

16:20 - 16:40	"Study on the Properties of Organic Paints for Steel Structure Subjected to Natural Exposure" by Mr.Soravuth Judabong, TISTR, Thailand
16:40	Close of Day 2

DAY 3, THURSDAY 2 JULY 1992

Session H :

09:00 - 10:00	Panel Discussion : Chairman Session A,B,C,D
10:00 - 10:30	Coffee Break
10:30 - 12:00	Panel Discussion : Chairman Session E,F,G
12:00 - 12:15	Closing
12:15 - 17:00	Factory Visit

Note : The visit will be conducted in two groups, A & B
Lunch box will be served on the bus

Group A : Honda Car (Thailand) Co.,Ltd.
(50 persons only)

Group B : Bangkok Container Industry Co., Ltd.
(30 persons only)

Introduction to Atmospheric Corrosion-Organic Coating Project

Ladawal Chotimongkol

Metal and Material Technology Department
Thailand Institute of Scientific and Technological Research

Background Information

ASEAN-Japan Cooperation Programme on Materials Science and Technology

The former Japanese Prime Minister, Mr.Nakasone, proposed the cooperation programme on Materials Science and Technology between ASEAN countries and Japan in 1983. The objective of this programme is to strengthen the basis and to contribute to the upgrading of research level on Materials Science and Technology of ASEAN, because ASEAN counties are rich in natural resources.

This cooperation programme comprises six national projects to be implemented in each host country of ASEAN.

They are :

(1) Brunei Darussalam

Project on Corrosion of Reinforced Concrete Structures

September 1987 - September 1990

September 1990 - September 1992

(Follow-up)

(2) Indonesia

Project on Characterization of Polymeric Materials

October 1987 - September 1992

(3) Malaysia

Project on Characterization of Fine Ceramics

November 1987 - November 1991

November 1991 - November 1992

(Follow-up)

(4) The Philippines

Project on Atmospheric Corrosion Metallic Coatings

October 1987 - October 1992

(5) Singapore

Project on Prevention of Corrosion in Structures

October 1987 - September 1990

October 1990 - September 1992

(Extension)

(6) Thailand

Project on Atmospheric Corrosion-Organic Coatings

November 1987 - November 1992

Project on Atmospheric Corrosion-Organic Coatings

Objectives

1. To evaluate the durability of metals, organic coated metals by outdoor exposure test and accelerated test.
2. To study various methods of the measurement on corrosion of metals and degradation of organic coatings.
3. To contribute to the development of corrosion prevention technology.

Study Framework

1. Research on atmospheric corrosion.
2. Acceptance of Thailand researcher to Japan.
3. Dispatch of Japanese researcher to Thailand.
4. Multilateral activities.
   - training programme
   - collaborative research work
   - seminar

Duration

From November 30, 1987 to November 29, 1992 (5 Years)

Chronological Record

May 1983

During the visit of former Japanese Prime Minister, Mr.Nakasone, to the ASEAN countries, a conference at the ministerial level was proposed, as well as a meeting among scientists, to discuss an ASEAN-Japan Cooperation in Science and Teohnology.

November - December 1983

A conference between ministers in charge of ASEAN-Japan Cooperation in Science and Technology was held in Tokyo, Japan

March 1984

At the meeting of the ASEAN Committee on Science and Technology (COST) in Baguio, The Philippines, ASEAN countries suggested three cooperation subjects : Biotechnology, Microelectronics and Materials Science.

December 1984

A basic agreement was achieved at a high level ASEAN-Japan Meeting held in Jakarta, Indonesia.

April 1985

At the twelfth ASEAN COST Meeting in Brunei Darussalam, the proposal of Japan on Cooperation on Materials Science and Technology was accepted.

May 1985

The Ambassador of Japan to Indonesia and the Chairman of ASEAN COST exchanged notes on the Cooperation Programme. It included topics of selected activities in respective ASEAN countries.

August 1985 - February 1986

Four Japanese Preliminary Survey Teams were dispatched to the ASEAN countries.

The Japanese Implementation Survey Team visited Thailand for the propose of working out the details of the technical cooperation programme concerning the project on Atmospheric Corrosion-Organic Coatings.

February 1987

The Japanese Expert Team and the ASEAN Working Group on Materials Science and Technology (AWGMST) reached agreement and signed minutes at the Experts Meeting of ASEAN-Japan Cooperation on Materials Science and Technology in Bandung, Indonesia.

November 1987

Dr.Krissanapong Kirtikara, Leader of Thailand Delegation, Ministry of Science, Technology and Energy of Thailand and Dr.Toshiro Fukushima, Leader of Implementation Survey Team, JICA, signed the record of discussions for the ASEAN Project on Atmospheric Corrosion-Organic Coatings.

August 1988

The first Joint Meeting between the ASEAN Working Group on Materials Science and Technology and Japanese Delegation on ASEAN-Japan Cooperation on Materials Science and Technology was held in Bali, Indonesia, to discuss the Multilateral aspects of ASEAN-Japan Cooperation on Materials Science and Technology.

November 1988

The Japanese Mutual Consultation Team was sent to Thailand for the purpose of discussing the smooth and successful implementation of the project.

August 1989

The Second Joint Meeting between the ASEAN Working Group and Japanese Delegation on ASEAN-Japan Cooperation was held in Cha-Am, Thailand to review projects of each country and to implement the multilateral activities.

December 1989

The Japanese Advisory survey team was sent to Thailand to review the progress of the project and discuss further project activities.

August 1990

The Third Joint Meeting between the ASEAN Sub-Committee on Materials Science and Technology (ASCMST) and Japanese Delegation on ASEAN-Japan Cooperation on materials Science and Technology was held in Genting Highlands, Malaysia to review projects of each country and to implement multilateral activities in 1990-1992.

November 1990

The Japanese Mutual Consultation Team was sent to Thailand to review the progress of the project and discuss the research and general activities of the project.

Research Activities

Corrosion research activities in TISTR as focal point are concentrated on the Atmospheric Corrosion Programme which is supported by JICA.

Long term exposure sites to study the behavior of materials under different environments such as marine, industrial, urban and rural environments have been established. This test programme is undertaken to investigate the effect of environmental factors; such as solar radiation, temperature, moisture, normal air constituents, acid rain and pollutants upon atmospheric corrosion. There are 4 categories of selected materials for this programme.

1. Bare metal
2. Metallic coated steel
3. Organic coated steel
4. Plain & coated fibre reinforced plastic.

Accelerated corrosion test and simulated test are also included in corrosion research activities. These studies will provide information as an estimation of the final result of the Atmospheric Corrosion Project.

Accelerated Corrosion Test.

- Combined cyclic corrosion test.
  to accelerate effects of marine environment.
- Weathering meter test.
  to accelerate effects of sunshine in deteriorating organic coating.
- Gas corrosion test.
  to study effect of pollution gas on corrosion of materials in the industrial environments.

Characterization and Identification

- Characterization and identification of multilayer corrosion products have been performed by using electron probe, microanalyzer and X-ray diffractometer.
- Study on deterioration of organic coating
- Study on corrosion mechanism by electrochemical techniques.

Multilateral Activities

As one of the ugique characters of ASEAN-Japan Cooperation Programme, Thailand Institute of Scientific and Technological Research and JICA conduct the multilateral activities.

The objectives of each activity are :

1. training programme
2. collaborative research work
3. seminar

See all details in Annex A.

Technical Exchange Team from ASEAN

- Indonesia technical exchange team visited Thailand project during July 20-21, 1989.
- Malaysia technical exchange team visited Thailand project during March 5-6, 1990.
- Philippines technical exchange team visited Thailand project during May 19-24, 1990.
- Singapore technical exchange team visited Thailand project during June 19-22, 1991.

Thailand project also visited ASEAN member country during 16 July - 1 August 1990.

ORGANIZATION CHART

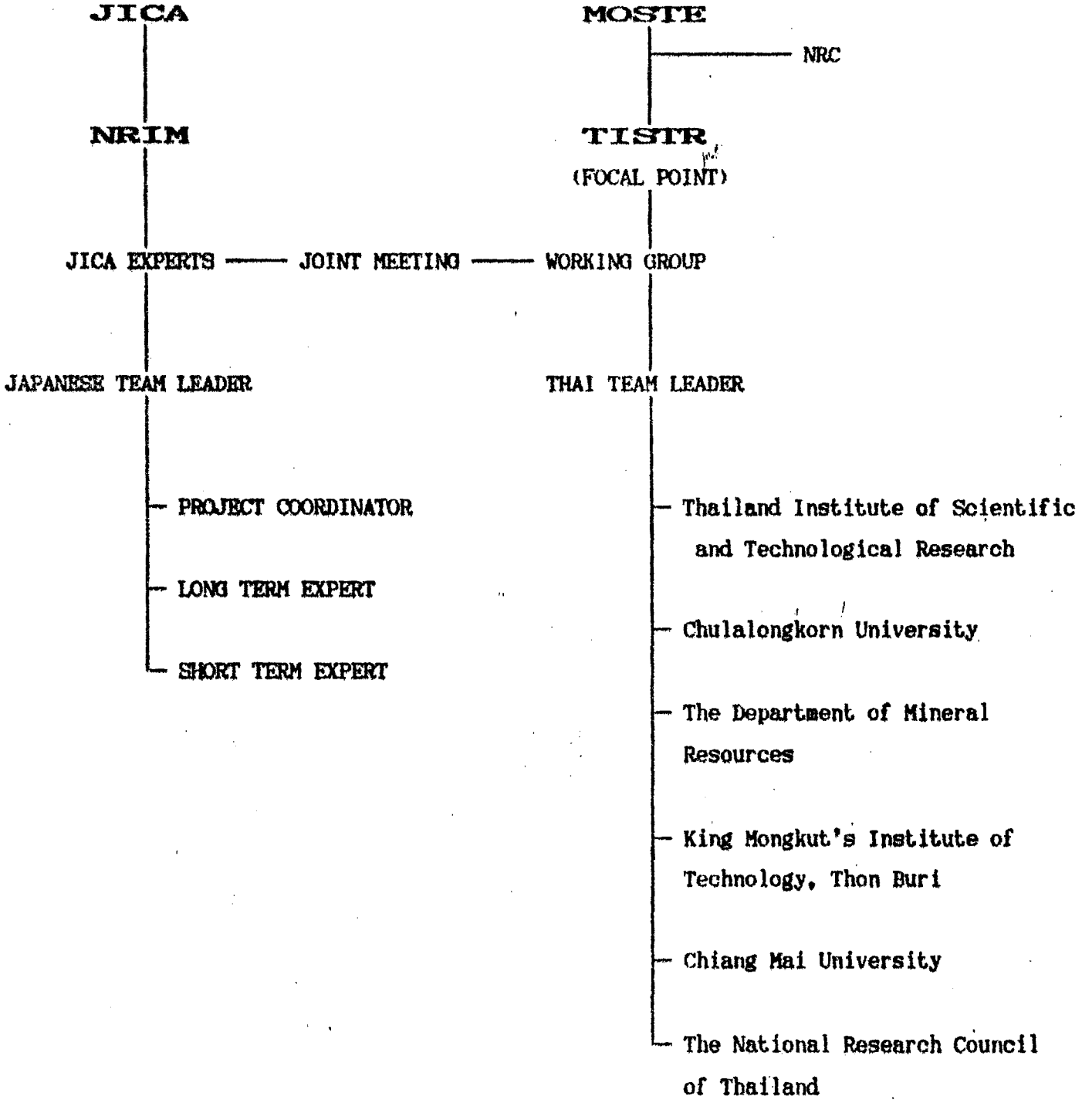

Annex A

Multilateral Activities

TRAINING PROGRAMME FISCAL YEAR 1989/1990

COUNTRY	TIME/DURATION	NUMBER OF PARTICIPANTS	TITLE	PARTICIPANTS FROM THAILAND
BRUNEI DARUSSALAM	5-17 March 1990	2 from each ASEAN country plus others from host country	Study on Corrosion of Reinforced Concrete Structure in Brunei Darussalam	1. Mr.Pakdi Thongcharoen, DMR 2. Mr.Panich Voottipruex, TISTR
INDONESIA	3-30 November 1990	1 from each ASEAN country plus others from host country	Characterization of Polymeric Materials	1. Mr.Wachirapan Pattanachot, CU
MALAYSIA	18 November - 15 December 1990	1 from each ASEAN country plus others from host country	Instrumental Analyses Fine Ceramics	Miss Pornthip Laoprasopwattana, TISTR
PHILIPPINES	7 January - 2 February 1991	1 from each ASEAN country plus others from host country	Atmospheric Corrosion -Metallic Coatings	1. Mr.Supachai Surapa[illegible], DMR
SINGAPORE	1-28 February 1990	1 from each ASEAN country plus others from host country	Corrosion Measuring and Evaluation Methods	1. Mr.Sa-ard Aurakararaksun, Waterworks Authorit[illegible]
THAILAND	16 October - 12 November 1990	1 from each ASEAN country plus others from host country	Environmental Analyses	Five participants from other ASEAN countries

TRAINING PROGRAMME FISCAL YEAR 1991

COUNTRY	TIME/DURATION	NUMBER OF PARTICIPANTS	TITLE	PARTICIPANTS FROM THAILAND
BRUNEI DARUSSALAM	-	-	-	-
INDONESIA	28 September - 27 October 1991	1 from each ASEAN country plus others from host country	Characterization of Polymeric Materials	1. Mr.Prinya Aroonvisoot, Prince of Songkhla University
MALAYSIA	13 May - 11 June 1991	1 from each ASEAN country plus others from host country	Characterization of Ceramic Powder	1. Mr.Nimit Sriprang, CMU
PHILIPPINES	8 July - 7 August 1991	1 from each ASEAN country plus others from host country	Statistical Evaluation of Corrosion-Multiple Regression	1. Miss Siripan Nilpairach, CU (waived) 2. Mr.Wim Nhuapeng, CU (waived)
SINGAPORE	-	-	-	-
THAILAND	11 November - 6 December 1991	1 from each ASEAN country plus others from host country	Instrumental Analyses	Five participants from other ASEAN countries

TRAINING PROGRAMME FISCAL YEAR 1992

COUNTRY	TIME/DURATION	NUMBER OF PARTICIPANTS	TITLE	PARTICIPANTS FROM THAILAND
BRUNEI DARUSSALAM	22 June - 4 July 1992	2 from each ASEAN country plus others from host country	Corrosion of Reinforced Concrete Structures	1. Dr.Somkiat Rungthongbaisuree, KMITT 2. Dr.Ekkasit Limsuwan
INDONESIA	30 May - 28 June 1992	1 from each ASEAN country plus others from host country	Characterization of Polymeric Materials	1. Ms.Sirina Puthanarak
MALAYSIA	-	-	-	-
PHILIPPINES	-	-	-	-
SINGAPORE	May 1992			
THAILAND	-	-	-	

TRAINING IN JAPAN

FISCAL YEAR	DURATION	TITLE	THAI TRAINEE
1988	27 October - 10 December 1988	Instrumental Analyses	Miss Nandh Thavarungkul, KMITT
	10 January - 18 July 1988	Corrosion Monitoring	Miss Korakoch Meechumnarn, TISTR
	16 January - 15 March 1989	Instrumental Analyses	Mr.Sathid Therkiattikul, DMR
1989	11 September - 10 December 1989	Instrumental Analyses	Miss Suthipa Masuthon, TISTR
	11 September - 10 December 1989	Accelerated Test	Mr.Verra Loha, KMITT
	20 February - 19 May 1990	Surface Analyses	Mr.Pansa Buranawanich, DMR.
1990	29 November 1990 - 28 February 1991	Surface Treatment for Organic Coating	Dr.Sumalee Wongchan, CU
	10 January - 10 May 1991	Organic Coating and Evaluating	Mr.Serakiat Kulkowit, TISTR
1991	24 September 1991 - 21 March 1992	Instrumental Analysis for Corrosion Monitoring and Testing	Mr.Choochat Nitipanyawong, KMITT
	28 January - 7 July 1992	Electrochemistry Technique for Atmospheric Corrosion-Organic Coatings	Miss Niramon Thamuddhamusilp, TISTR
	10 March - 7 July 1992	Organic Coatings Technique	Mr.Pradoong Suanpoot, CMU
1992	3 months	Environmental Analysis	Ms.Naetsai Chulasai, TISTR
	3 months	Polymer /or Organic Coating Technology	Ms.Waraporn Rungruangkakokkul, CU

COLLABORATIVE RESEARCH WORK FISCAL YEAR 1990

COUNTRY	TITLE	DURATION	PARTICIPANTS FROM THAILAND
BRUNEI DARUSSALAM	Corrosion of steel bar in reinforced concrete structures Corrosion of reinforced concrete structures 1. Basic Corrosion in R.C. Structures 2. Maintenance of R.C. Structures	10 May - 10 August 1990	
INDONESIA	1. Characterization of Polymers Used in Adhesives 2. Characterization of Polymers Membranes 3. Comparibility of Binary Polymeric Mixtures 4. Characterization of Polymers after Accelerated Thermal and Mechanical Treatment	1 December 90 - 28 February 1991	
MALAYSIA	1. Preparation of some rare earth addition glass 2. Properties microstructure relationship of SiC or Si_3N_4 Characterization of fine Ceramics 1. Aluminosilicate glasses doped with rare-earth oxides 2. The microstructure of silicon carbides	5 August - 2 November 1990	Miss Chutima Tantigate, TISTR
PHILIPPINES	Atmospheric Corrosion-Metallic Coatings	19 November 90 - 9 March 1991	Miss Pakarat Hanvivatvong, DMR
SINGAPORE	1. Corrosion Prevention for Port and Harbour Structures 2. Corrosion Prevention for Dringking Water Storage Tanks	1 January - 31 March 1991	Mr.Wuttipong Muangnoi, KMITT
THAILAND	Accelerated Corrosion Tests on Materials Accelerated Corrosion Tests on Steel Structure	8 October 90 - 7 January 1991	Two participants from Brunei and Indonesia

COLLABORATIVE RESEARCH WORK FISCAL YEAR 1991

COUNTRY	TITLE	DURATION	PARTICIPANTS FROM THAILAND
BRUNEI DARUSSALAM	-	-	-
INDONESIA	Characterization of Polymeric Materials	22 September-22 December 1991	Miss Sireerat Charuchinda, Ministery of Indusry
MALAYSIA	Characterization of Fine Ceramics	13 May - 10 August 1991	Dr.Ladawal Pdungsap, MU
PHILIPPINES	Monitoring of Atmospheric Corrosion Rate by Electrochemistry Impedance Method	15 September-15 December 1991	Miss Siriluck Kewdoknoi, TISTR
SINGAPORE	Cathodic Protection	1 January - 31 March 1992	-
THAILAND	Accelerated Corrosion Tests on Organic Coatings	16 September91 - 14 Marcch 1992	Participant from the Philippines

COLLABORATIVE RESEARCH WORK FISCAL YEAR 1992

COUNTRY	TITLE	DURATION	PARTICIPANTS FROM THAILAND
BRUNEI DARUSSALAM	-	-	-
INDONESIA	-	-	-
MALAYSIA	Collaborative Research Programme on Glass Ceramics	17 May - 14 August 1992	-
PHILIPPINES	-	-	-
SINGAPORE	-	-	-
THAILAND	-	-	-

SEMINAR/WORKSHOP FISCAL YEAR 1990

COUNTRY	TIME/DURATION	NUMBER OF PARTICIPANTS	TITLE	PARTICIPANTS FROM THAILAND
BRUNEI DARUSSALAM	6-8 August 1990	3 from each ASEAN country plus others from host country	Study on Corrosion of Reinforced Concrete Structure	1. Mr.Pakhomthep Migasena, TISTR 2. Dr.Ekkasit Limsuwan, CU 3. Mr.Pansa Buranwanich, DMR
INDONESIA	7-9 March 1991	3 from each ASEAN country plus others from host country	Characterization of Polymeric Materials	1. Mrs.Jurai Supamanonda, TISTR 2. Miss Sirijutaratana Covavisaruch, CU 3. Mrs.Suda Kiatkamtornwong, CU
MALAYSIA	-	-	-	-
PHILIPPINES	4-9 March 1991	3 from each ASEAN country plus others from host country	Atmospheric Corrosion -Metallic Coatings	1. Mr.Wikrom Vajaragupt, CU 2. Dr.Chatchai Somsiri, CU 3. Mr.Detchana Chutinara, DMR
SINGAPORE	17-19 September 1990	3 from each ASEAN country plus others from host country	Corrosion of Structures	1. Miss Korrakoch Meechumnarn, TISTR 2. Miss Nongyow Chtivanitchayakul, TISTR 3. Miss Suthipa Masuthon, TISTR
THAILAND	17-19 October 1990	3 from each ASEAN country plus others from host country	Atmospheric Corrosion -Organic Coatings	102 participants attended the seminar

SEMINAR/WORKSHOP FISCAL YEAR 1991

COUNTRY	TIME/DURATION	NUMBER OF PARTICIPANTS	TITLE	PARTICIPANTS FROM THAILAND
BRUNEI DARUSSALAM	-	-	-	-
INDONESIA	-	-	-	-
MALAYSIA	1-2 October 1991	3 from eacn ASEAN country plus others from host country	Characterization of Fine Ceramics	1. Dr.Somchai Thongtem, CMU 2. Dr.Nopadol Chaikum, MU. 3. Dr.Nongluck Pankuddee, TISTR
PHILIPPINES	-	-		-
SINGAPORE	-	-		-
THAILAND	-			-

SEMINAR/WORKSHOP FISCAL YEAR 1992

COUNTRY	TIME/DURATION	NUMBER OF PARTICIPANTS	TITLE	PARTICIPANTS FROM THAILAND
BRUNEI DARUSSALAM	3-5 August 1992	3 from each ASEAN country plus others from host country	Corrosion of Reinforced Concrete Structures	1. Dr.Hongluck Panichpakdee, TISTR 2. Ms.Kannika Sthapitanonda, TISTR 3. Ms.Siriluck Kewcharoenwong, TISTR
INDONESIA	29 June - 1 July 1992	3 from each ASEAN country plus others from host country	Characterization on Polymeric Materials	1. Dr.Suda Kiatkamjornwong, CU 2. Dr.Sirijutaratana Covavisaruch, CU 3. Ms.Arunee Hunsacharoonroj, CU
MALAYSIA	-	-	-	-
PHILIPPINES	1-6 June 1992	3 from each ASEAN country plus others from host country	Corrosion of Metals	1. Dr.Somchai Thongtem, CMU 2. Dr.Paritud Bhandhubanyong, CU 3. Mr.Pakdi Thongcharoen, DMR
SINGAPORE	20-24 September 1992	5 from each ASEAN country plus others from host country	Final ASEAN Reginal Seminar	1. Mr.Shigeki Kirihara 2. Dr.Ladawal Chotimongkol, TISTR 3. Dr.Somchai Thongtem, CMU 4. Asst.Prof.Wikrom Vajaragupta, CU 5. Mr.Anurak Petiraksakul, KMITT
THAILAND	30 June - 2 July 1992	3 from each ASEAN country plus others from host country	Corrosion and Protection	

RECENT INVESTIGATION ON ANODIZING OF ALUMINUM AND ITS ALLOYS

Hideaki TAKAHASHI
Faculty of Engineering, Hokkaido University,
Sapporo 060, Japan

abstract

The paper consists of three parts: general, anodizing of ADC-12 aluminum die-casting alloy, and anodizing of aluminum covered with thermal oxide film.

In the first part, the application and structure of oxide film formed on aluminum are described. The oxide films formed on aluminum can be classified into four types: porous anodic oxide film, barrier anodic oxide film, thermal oxide film, and hydroxide film. The change in the structure of oxide films with the combination of treatments is also described.

In the middle, the distinctive feature of the formation ofporous anodic oxide films on an aluminum die-casting alloy, ADC-12, which includes ca. 10wt%-Si and 2wt%-Cu as well as other alloying elements, is compared with that of casting and rapidly solidified alloys. Some techniques for improving the disadvantages in the anodizing of ADC-12 are proposed.

In the last, described is the formation of crystalline barrier type anodic oxide films on aluminum covered with thermal oxide films. The anodic oxide film has a high electric field sustaining ability, and much amount of voids. The void structure of anodic oxide films strongly depends on the pretreatment.

RECENT INVESTIGATION ON ANODIZING OF ALUMINUM AND ITS ALLOYS

Hideaki TAKAHASHI
Faculty of Engineering, Hokkaido University, Sapporo 060, Japan

GENERAL

Anodizing of aluminum and its alloys is one of the important process in metal finishing, and has been developed for many years mainly for the purpose of the formation of oxide films with anticorrosive and decorative properties. Now a day, the anodic oxide films are used in many fields, due to their unique morphology and properties, as shown in Table 1.

Table 1 Application of anodic oxide films on aluminum and its alloys

Properties		Application
Physical	Hardness Anti-abrasion Lubricity Morphology	bearing, cylinder gear, bolt/nut lubricating alumite molecule separating membrane, super grid
Chemical	Anticorrosion Adhesion Wettability Dye-affinity Catalytic property	window/door frame organic coating PS-plate dyeing for(decoration) catalyzer
Electric & Magnetic	Dielectric property Insulating property Magnetic property	electrolytic capacitor, humidity sensor printed wiring board, IMST, alumite cable memory storage disk, rotary encoder
Optical	E.L. Absorption	luminescent display solar-heat collector, optical wave-guide

Aluminum has a strong chemical affinity with oxygen, and thus is covered with a thin air-formed oxide film. The air-formed oxide film is too ambiguous to be used as a device in sophisticated electric and optical instruments, because it's properties

depend on the preparation process of the substrate. By anodizing, heat treatment, and hydrothermal treatment, well-defined surface films can be obtained, and these are suitable for applying their physical, chemical, electric, and optical properties in the modern technology. Surface films formed on aluminum can be classified into four types, as shown in Table 2.

Table 2 Oxide and hydroxide films formed on aluminum

type	process	medium
porous oxide film	anodizing	H_2SO_4, $H_2C_2O_4$, H_3PO_4, NaOH
barrier oxide film	anodizing	neutral borate, phosphate, and citrate solutions
thermal oxide film	heating	air, oxygen
oxyhydroxide film	boiling	hot water

The porous type oxide film, which is formed by anodizing in acid or alkali solutions, has a lot of number of pores perpendicular to the metal substrate. The pores are isolated from the metal substrate by a thin and hemispherical-shape oxide layer, so called barrier layer. The number of pores($N:10^{9} - 10^{11}/cm^2$), pore diameter($D:10 - 100$ nm), and barrier layer thickness($\delta:5 - 100$ nm) are functions of primarily applied anode potential, E_a, and the total film thickness is proportional to the current density and anodizing period. A maximum of film thickness is reached to be at most several hundred μm because of the chemical dissolution of oxide during anodizing.

The unique morphology of the porous type oxide films is a key for the application of the film to modern technology. By stripping the film from the substrate, and removing the barrier layer, a membrane with pores, whose number and size are well-defined, can be obtained. Such a membrane are suitable for separating gas molecules and polymerized compounds, and also can be used as the "super-grid" for transmission electron microscopy.

When alternative current is applied to aluminum covered with porous type oxide film in solutions including metal ions such as Fe, Ni, and Co, the metal deposits in the pores to produce colored oxide films. This process is called the "electrolytic coloring", and has been established in anodizing industry. The metal deposited in the pores shows an anisotropy in magnetic property, and this property can be utilized in electromagnetic devices such as memory storage disk and rotary encoder.

Barrier type oxide films, which formed by anodizing in neutral electrolyte solutions, are thin and compact. The thickness, δ, of the oxide films is proportional to the anode potential, E_a, showing a proportionality constant of 1.3 - 1.6 nm/V.

The value of δ is limited to be less than 1 μm by the dielectric breakdown phenomena. Thus, the barrier oxide film has less protective property for corrosion, and utilized as dielectric or insulating film in electrolytic capacitor, humidity sensor, and so on.

Thermal oxide films formed by heating in air above 500 °C include a crystalline oxide of γ-alumina and shows a terminal thickness of ca. 30 nm. Anodizing of thermal oxide covered aluminum in a neutral solution allows the growth of anodic oxide films with a crystalline oxide. The oxide films thus obtained shows a high electric sustaining ability.

Oxyhydroxide films obtained by immersing aluminum in boiling pure water are composed of two layers: an outer porous layer and inner dense layer. The thickness of the inner and outer layers reaches about 300 nm after 30 min immersion. The hydroxide film shows a crystal structure of pseudo-boehmite and chemical composition of $Al_2O_3 \cdot 2\text{-}2.5H_2O$. The hydrothermal treatment of aluminum is carried out as a pretreatment of organic coating. The porous outer layer is possibly responsible for the good adhesion with organic coatings. Anodizing of aluminum covered with the hydroxide films causes the "composite oxide film" to grow. The composite oxide film includes crystalline oxide and shows a high ability for sustaining electric field. The application of the composite oxide films as dielectric material has been established in electrolytic capacitor manufacturing industry.

As described above, the morphology, crystal structure, and chemical composition of oxide/oxyhydroxide films formed on aluminum strongly depend on the film formation condition. If oxide films are formed on aluminum alloys instead of pure aluminum, the growth mechanism of oxide would be affected considerably by alloying elements and microstructure of the substrate. The combination of the four processes described above should be investigated for further development of technology with surface oxide films on aluminum and its alloys.

In the second section of this paper, two topics are described in the following.

1) Film formation mechanism of porous anodic oxide films on aluminum die casting alloy, and

2) Electron microscopic study of anodic oxide films on aluminum with thermal oxidation.

FILM FORMATION MECHANISM OF POROUS ANODIC OXIDE FILMS ON AN ALUMINUM DIE-CASTING ALLOY

Hideaki TAKAHASHI, Keiichi WATANABE, Ryusaburo FURUICHI, and Masahiro SEO
(Faculty of Engineering, Hokkaido University, Sapporo 060, Japan)

ABSTRACT

A commercial aluminum die-casting alloy, ADC12(85.5Al-10.7Si-2.1Cu-Fe-Mn-Zn-Ni-Sn) was anodized galvanostatically in a sulfuric acid solution to examine the formation behavior of porous anodic oxide films by potential measurements, chemical analyses, evolved-gas volume measurements, X ray diffraction measurements and electron microscopy. The results were compared with those from several Al-Si-Cu ternary alloys prepared by casting and rapid solidification.

During anodizing, the anode potential, E_a, increased with time, t_a, to a steady value, E_a^*. The value of E_a^* for ADC12 was similar to that for Al-10.7Si-3Cu rapidly solidified alloy. The high E_a^* value for ADC12 was found to be either due to the high Si- and moderate Cu-content, or the development of eutectic structure formed by the relatively high solidification rate of the specimen. ADC12 showed a high partial current for gas evolution and low partial current for film formation, and film dissolution. This behavior correlated with the effects by trace alloying elements in addition to Si and Cu.

Electron microscopy showed that films formed on ADC12 have non-uniform thicknesses, and that the average thickness is relatively low. The non-uniformity of film thickness was attributed to the concentration of current into sites where α-aluminum phase had developed. The small average thickness was due to the low film formation rate, which was caused by the high partial current for gas evolution.

INTRODUCTION

The aluminum alloy, ADC12, is a Japanese industrial standard die-casting alloy, and includes about 10%-Si and 2%-Cu as well as other trace alloying elements. The die-casting alloy has good mechanical properties, and is used in various parts of vehicles, aircraft, household articles, and so on.

Anodizing of ADC12 in acid solutions is not performed due to 1)high electric-power consumption, 2)low film-formation efficiency, 3)films with uneven thickness and grayish-black color. There are several investigations of the formation of porous anodic oxide films on ADC12[1-5], but the details in the film formation mechanism have not been established yet. In the present investigation, the formation of anodic oxide film on ADC12 was examined in a sulfuric acid solution and compared with Al-Si-Cu ternary alloys.

EXPERIMENTAL

1)Specimen: a)ADC12 plate specimens supplied by the Research Institute of Aluminum

Die-casting Alloy Finishing was cut into 1x1 cm^2 and embedded into an epoxyl resin. The chemical composition of ADC12 is as in Table 1. b)Al-10.7wt%Si-(0-5wt%)Cu casting alloy(CA) specimens were prepared by melting the mixture in an alumina crucible at 973 K and pouring it on a Cu plate at room temperature. The solidified blocks were cut into 1x1 cm^2 and embedded in epoxyl resin. c)Al-10.7wt%Si-(0-5wt%)Cu rapidly solidified alloy(RSA) specimens were prepared by melting the mixture by radio high-frequency heating and dropping the melt on a Cu roll, rotating at a high speed in a N_2 atmosphere.

Table 1 Chemical composition of ADC12(wt%)

Al	Si	Cu	Fe	Mn	Mg	Zn	Ni	Sn
Bal.	10.7	2.05	0.91	0.16	0.10	0.49	0.04	0.01

2)Pretreatment: The ADC12 and CA specimens were polished mechanically with wet emery paper and cloth with diamond polishing suspension. After removing the outer 100 μm layer by polishing, the specimens were degreased with acetone. The RSA specimen was degreased with acetone prior to the experiments.

3)Anodizing: Pretreated ADC12 and CA specimens were set in a specimen holder and anodized in 0.2 dm^3 of 10 wt%-H_2SO_4 at 293 K by supplying a constant current density of i_a = 100 A/m^2. The details of the assembly for anodizing have been described elsewhere[4]. The RSA specimen was hung by a clip to anodize in the sulfuric acid solution after masking the backside and periphery of specimens. The change in anode potential, E_a, with anodizing time, t_a, was followed with a recorder.

4)Amount of dissolved Al^{3+} ions: During anodizing an aliquot of the solution was taken at 5 min intervals to analyze the amount of dissolved Al^{3+} ions, W_d, by colorimetry with the oxinate extraction method.

5)Amount of evolved gas: The amount of gas evolved on the specimen, V_g, was measured by using a gas-collecting tool and an H-shape cell, where anode chamber was separated from cathode chamber with fritted glass.

6)Scanning electron microscopy(SEM): Before/after anodizing the specimens were etched lightly and evaporated with gold to examine the structure of the metal substrate and oxide film by SEM.

7)X ray diffraction measurements(XRD): The crystal structure of the metal substrate was examined by XRD.

RESULTS AND DISCUSSION

1)Structure of the metal substrate: Fig. 1 shows the scanning electron micrographs of a)ADC12, b)Al-10.7Si-3Cu-CA, and c) Al-10.7Si-3Cu-RSA specimens. In ADC12, Si eutectic particles and Si-(Fe, Mn) eutectic rods are observed in α-aluminum matrix(black part). The Al-10.7Si-3Cu-CA and -RSA specimens show Si eutectic particles in α-aluminum matrix. The Si eutectic particles become smaller in the order; CA > ADC12 > RSA specimen. The RSA specimen shows a fully developed eutectic structure because of the high solidification rate. Although the θ-Al_2Cu phase could not be distinguished by SEM, XRD measurements indicated the existence of trace amount of θ-Al_2Cu phase in ADC12 and both CA and RSA specimens with more than 3% of C_{Cu}.

2)Anode potential: Fig.2 shows the change in the anode potential, E_a, with anodizing time, t_a, for ADC12, Al-10.7Si-3Cu-CA, and -RSA as well as pure Al casting specimens. The pure Al specimen shows a rapid increase in E_a in the very early stage and a steady E_a value, E_a^*, after the initial transition period. All curves except for

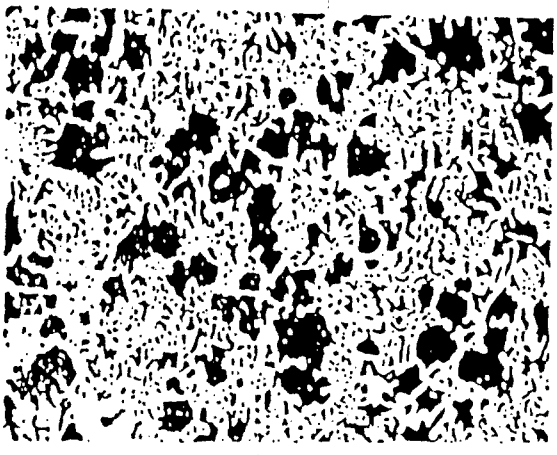

(a)

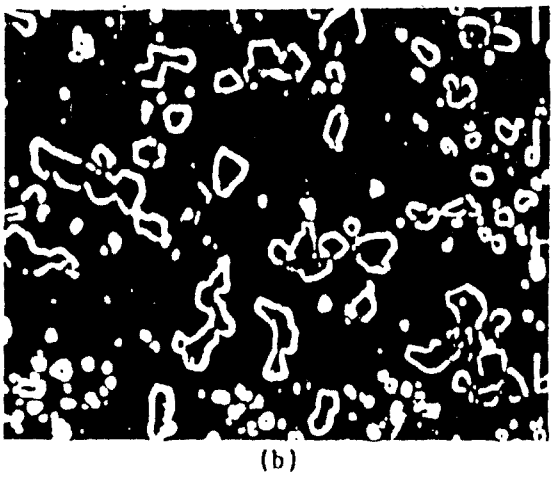

(b)

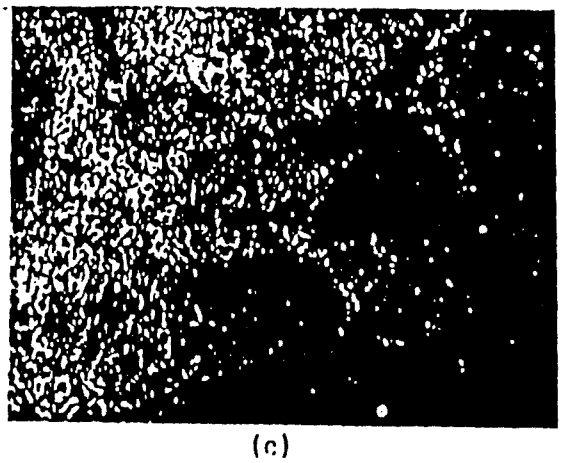

(c)

Fig. 1 Scanning electron micrographs of a)ADC12, b)Al-10.7Si-3Cu casting alloy, and c)Al-10.7Si-3Cu rapidly solidified alloy.

20 μm

pure Al show gradual increases in E_a after the initial rapid increase to reach almost steady values, E_a^*. The value of E_a^* depends strongly either on the chemical composition or solidification rate of the specimen. Fig. 3 shows the relationship between E_a^* and copper content, C_{Cu}, in the different types of specimen. The value of E_a^* for both CA and RSA specimens increases with increasing C_{Cu} to reach a maximum at C_{Cu} = 3 %, and beyond this it decreases. The E_a values for RSA specimens are larger than those for CA at all C_{Cu}. The E_a^* value for pure Al casting specimen is the lowest and the value for ADC12 is similar to that for Al-10.7Si-3Cu-RSA specimen.

The maximum in E_a^* at C_{Cu} = 3 % for both CA and RSA specimens can be considered as a result of the θ-Al_2Cu phase at C_{Cu} > 3%. The high E_a^* value for ADC12 correlates with the high Si and moderate Cu contents and fully developed eutectic structure produced by the relatively high solidification rate.

3)Film dissolution and gas evolution: Figs. 4-a and -b show the changes in the amount of dissolved Al^{3+} ions, W_d, and the evolved gas volume, V_g, with anodizing time, t_a, obtained for ADC12, Al-10.7Si-3Cu-CA and -RSA specimens. As can be seen from Fig. 4, W_d and V_g increase almost linearly with t_a, at different rates for different specimens. The partial dissolution current, i_d, and the partial gas evolution current, i_g, are expressed by the following equations.

$$i_d = (dW_d/dt_a)(nF/M_{Al}) \quad (1)$$

$$i_g = (dV_g/dt_a)(n'F/V_0) \quad (2)$$

where, n(= 3) and n'(= 4) are the valence of Al, and O_2, F is the Faraday constant, and V_0 is the volume of 1 mol of O_2 gas at the standard temperature and pressure.

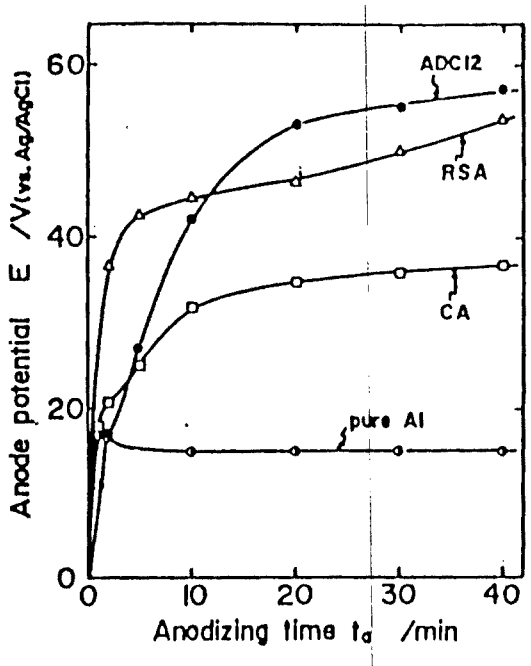

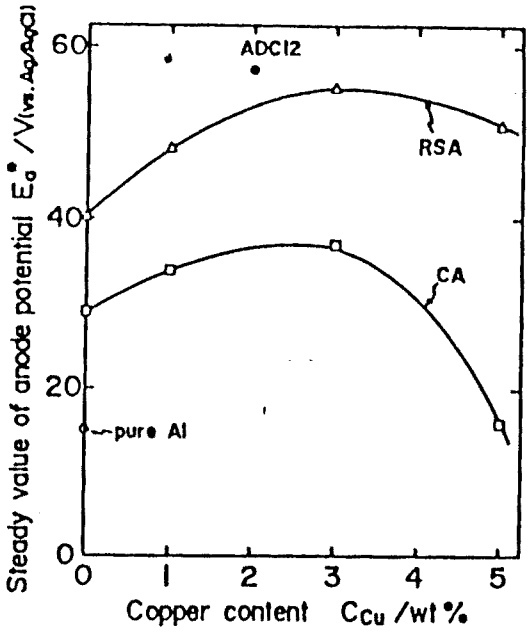

Fig. 2 (left) Time variation in the anode potential, E_a, during anodizing of a)ADC12, b)Al-10.7Si-3Cu casting alloy(CA), c)Al-10.7Si-3Cu rapidly solidified alloy(RSA), and d)pure Al casting specimens. Anodizing was performed in 10%H_2SO_4 at 293 K and 100 A/m^2.

Fig. 3 (right) Relationship between the steady value of anode potential, E_a^*, and copper content in a)ADC12, b)Al-10.7Si-(0-5)Cu casting alloy(CA) and c)Al-10.7Si-(0-5)Cu rapidly solidified alloy(RSA), and d)pure Al casting specimens. Anodizing conditions are as in Fig. 2.

By neglecting the dissolution of alloying elements other than Al, the partial oxide formation current, i_{ox}, is calculated by;

$$i_{ox} = i_a - (i_d + i_g) \qquad (3)$$

The changes in i_{ox}, i_d, and i_g with copper content, C_{Cu} are shown in Fig. 5-a(CA specimens) and Fig. 5-b(RSA specimens). Both CA and RSA specimens show that, with increasing C_{Cu}, i_d and i_g increase and i_{ox} decreases. In all C_{Cu}, i_d for RSA is lower than that for CA specimens, but i_g shows an opposite tendency. The i_{ox} values for RSA are similar to those for CA specimens. In Fig. 5-b, i_d, i_g, and i_{ox} for casting pure Al and ADC12 are also indicated. The pure Al shows no gas evolution, i.e. $i_g = 0$, and relatively high i_{ox}, while ADC12 shows relatively low i_d and i_{ox}, and high i_g.

Fig. 5 hence suggests that the partial currents of i_d, i_g, and i_{ox} are strongly affected by the chemical composition of specimens, and slightly influenced by the solidification rate, i.e. the development of the eutectic structure. In CA specimens, the increase in Si content, C_{Si}, causes i_g to increase, and i_d and i_{ox} to decrease. On the other hand, the increase in C_{Cu} causes i_d and i_g to increase and i_{ox} to decrease. The relatively high i_g and low i_d and i_{ox} for ADC12 can be explained as a result of the influence of trace alloying elements in addition to the effect of Si and Cu.

4)Film structure: Fig. 6 is electron micrographs of sections of 40 min anodized specimens of a)ADC12, b)Al-10.7Si-3Cu-CA, c)Al-10.7Si-3Cu-RSA, and d)pure Al casting specimens. The pure Al and RSA specimens have oxide films with uniform thickness of

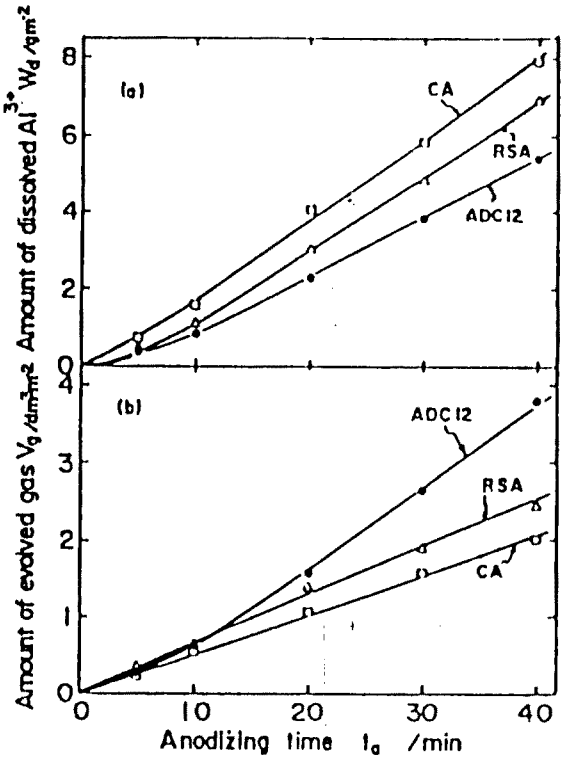

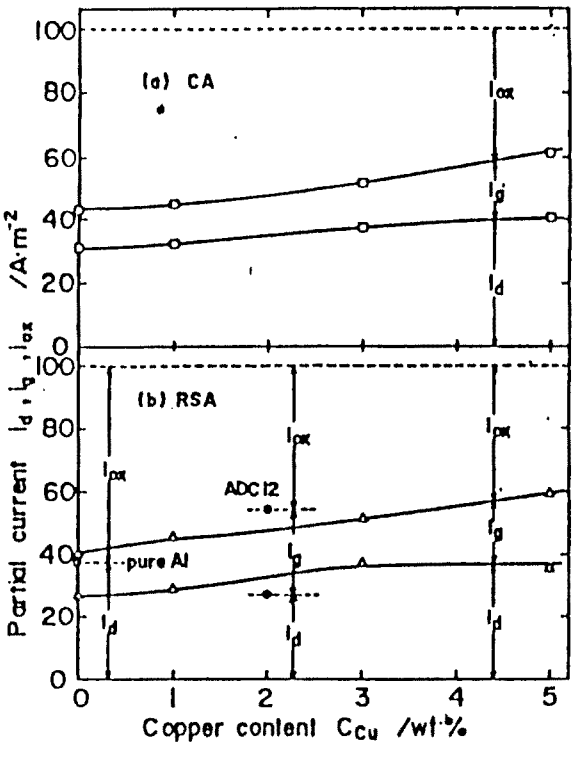

Fig. 4 (left) Changes in the amounts of dissolved Al^{3+}, W_d, and evolved gas, V_g, with anodizing time, t_a, for a)ADC12, b)Al-10.7Si-3Cu casting alloy(CA), and c)Al-10.7Si-3Cu rapidly solidified alloy(RSA). Anodizing conditions are as in Fig. 2.

Fig. 5 (right) Changes in the partial currents for Al-dissolution, i_d, gas evolution, i_g, and oxide formation, i_{ox}, with copper content in a)Al-10.7Si-(0-5)Cu casting alloys(CA) and b)Al-10.7Si-(0-5)Cu rapidly solidified alloys(RSA). In Fig. 5-b, the values for ADC12 and pure Al casting specimens are also indicated. Anodizing conditions are as in Fig. 2.

14 and 11 μm. The thicknesses of oxide films formed on CA and ADC12 are non-uniform and in average 11 and 7 μm. The thin oxide film on ADC12 is evidently due to the high i_g and low i_{ox}(see Fig. 5-b).

The non-uniformity in the thickness of oxide films formed on ADC12 and CA specimen can be explained by the results of the distribution of local current. The current may concentrate on sites where α-Al phase develops, because a high electric resistant barrier layer may be produced on sites where the eutectic structure is predominant. The uniform thickness of oxide films on the rapidly solidified alloy is clearly correlated with the fully developed eutectic structure.

CONCLUSION

Anodic oxide film formation on ADC12 in a sulfuric acid solution was examined by comparing the behavior on Al-Si-Cu ternary alloys prepared by casting and rapid solidification. The following is concluded.

1. High anode potential observed for ADC12 is caused by the high Si content and moderate Cu content, and by the relatively high solidification rate. Development of

eutectic structure in the metal substrate may cause the formation of the high electric-resistant barrier layer in the oxide film.

2. During anodizing, ADC12 shows a high partial current for gas evolution and low partial current for oxide formation. The high gas-evolution current is caused by trace alloying elements in ADC12 as well as Si and Cu.

3. The oxide film formed on ADC12 is relatively thin and has non-uniform thickness. The non-uniformity in the film thickness is due to the local current distribution, which is caused by the distribution of eutectic particles in the α-Al matrix.

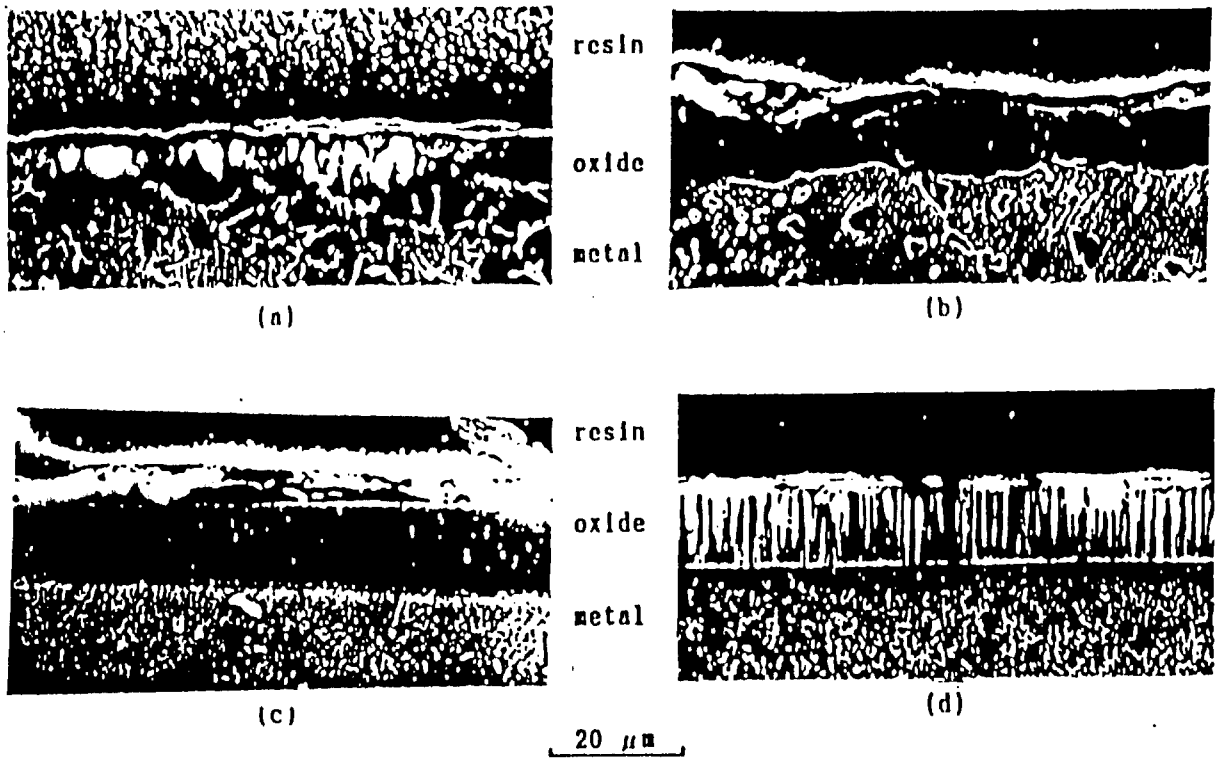

Fig. 6 Scanning electron micrographs of sections of 40 min anodized specimens of a)ADC12, b)Al-10.7Si-3Cu casting alloy, c)Al-10.7Si-3Cu rapidly solidified alloy, and d)pure Al casting. Anodizing conditions are as in Fig. 2.

ACKNOWLEDGEMENTS

The authors thank Prof. K. Hashimoto, Tohoku University, for suggestions on the preparation of rapidly solidified alloy specimens. Financial support of this investigation from the Light Metal Education Foundation of Japan is greatly appreciated.

REFERENCES

1)S. Hoshino, T. Imamura, S. Matsumoto: Abstract of 73th Annual Meeting of Metal Finishing Soc. Jpn., p.82 (1986)
2)I. Mita and H. Miyasaka: J. Metal Finishing Soc. Jpn., 39, 323 (1988)
3)Y. Fukuda, T. Fukushima, and Y. Fukuda: Abstract of 78th Annual Meeting of Metal Finishing Soc. Jpn., p.234 (1988)
4)H. Takahashi, K. Watanabe, S. Hashimoto, and R. Furuichi: J. Metal Finishing Soc. Jpn., 41, 423 (1990)
5)I. Mita: Abstract of 82th Annual Meeting of Metal Finishing Soc. Jpn., p.200 (1990)

J. Electron Microsc. 40: 101-109 (1991)

Electron Microscopic Study of Anodic Oxide Films Formed on Aluminum with Thermal Oxidation

Hideaki Takahashi, Chiko Ikegami, Masahiro Seo and Ryusaburo Furuichi*

*Electrochemistry Laboratory, and *Analytical Chemistry Laboratory, Faculty of Engineering, Hokkaido University, N13 W8, Kita-ku, Sapporo, 060 Japan*

The effects of thermal oxidation on the formation of barrier-type oxide films on aluminum were investigated by electron microscopy, gravimetry, and chemical analysis. Highly pure aluminum specimens were heated in air at 773–873 K for 1–24 hr, and then anodized in a neutral borate solution at 353 K with a constant current density of 50 A/m². Thermal oxide films were found to have a terminal thickness of ca. 30 nm after long heating periods, and to have a crystalline structure of γ-alumina. During anodizing, the rate of increase in the anode potential, E_a, for heat-treated specimens was twice as high as that for unheated specimens. The formation efficiency of anodic oxide films was 0.80 for heated specimens and 0.72 for unheated specimens. Anodic oxide film formed on heated specimens was a single layer including γ-alumina, and had a low thickness/E_a ratio of 0.77 nm/V. At high E_a, amorphous oxide islands were formed in the anodic oxide layer through the local breakdown of the crystalline oxide.

Key words: aluminum, anodic oxide film, thermal oxidation

Many authors have reported that anodizing of aluminum in the presence of thermal oxide films causes the formation of barrier-type oxide films including crystalline oxide.[1-12] This phenomenon is important to the electrolytic capacitor manufacturing industry and also scientifically interesting because the oxide crystallization assisted by electric field across the oxide is involved.

The structure of the anodic oxide films appears to change considerably with conditions of pretreatment, heating and anodizing. Alwitt and Takei[2] have investigated anodizing of NaOH-etched aluminum in 5 g/dm³ ammonium citrate solution at 343 K at 50 A/dm² after heat treatment in air for 20 min at 798 K. They have reported that anodic oxide film is a single layer including γ'-alumina and its thickness/voltage ratio is 0.90 nm/V for the oxide film formed by anodizing up to 140 V. Shimizu et al.[4,5] have heated electropolished aluminum in air for 15 min at 773 K and then anodized this in 0.05 mol/dm³ ammonium penta-borate solution at 298 K at 50 A/dm². Using electron microscopy, they found that discrete γ'-alumina islands are produced at the middle part of the amorphous anodic oxide film. Crevecoeur and de Wit[7] have heated HF-etched specimen for 15 min at 823 K and then anodized this in 20 g/dm³ ammonium penta-borate at 297 K with a potential sweep technique. The anodic oxide film thus formed was found to consist of an outer amorphous oxide layer, a middle crystalline oxide layer, and an inner amorphous oxide layer; the film thickness/voltage ratio was 1.0 nm/V. Recently Alwitt et al.[9] reported that anodic oxide films formed by anodizing up to 80 V under the same condition as shown in ref. 2, consist of an outer crystalline oxide layer and an inner amorphous oxide layer.

These structural changes in the anodic oxide films may be explained as a result that the crystallization of amorphous oxide during anodizing is strongly influenced by the conditions of pretreatment, heating, and anodizing. A heating period of 15–20 min at 773–823 K seems to result in nuclei of γ-alumina in the thermal oxide film, and the γ-alumina nuclei may act as seeds for crystals in the formation of crystalline oxide during anodizing.[1,5] Hence, higher heating temperature, longer heating period, and higher anodizing temperature are expected to enhance the formation of crystalline anodic oxide films.

In the present investigation, the formation of anodic oxide films at 353 K after relatively long periods of heat treatment was investigated by electron microscopy, gravimetry, and chemical analysis.

EXPERIMENTAL

1) *Specimen*

Highly pure aluminum foil (99.99%) was electropolished in an acetic acid/perchloric acid solution and then rinsed with distilled water. After dipping in acetone, the specimens were kept in a desiccator prior to the experiments. The surface area of the specimens was 6 cm² for all the experiments except for gravimetry, where specimens with 20 cm² were used to obtain an appreciable weight gain during thermal oxidation.

2) *Thermal oxidation*

Specimens were kept in an electric furnace in air for different periods, t_h, at T_h = 773, 823, and 873 K. In the furnace the specimens were hung on hooks with a small hole at the branch of specimens in order to allow the thermal oxide film to form uniformly on all surfaces of the specimens. The time variation in the weight gain of

specimens, ΔW, during heating, t_h, was examined with a micro balance.

3) Anodizing

Specimens with/without heat treatment were anodized in a 0.5 mol/dm³ H_3BO_3/0.05 mol/dm³ $Na_2B_4O_7$ solution (pH=7.4) by supplying a constant current density of $i_a = 50\,A/m^2$. During anodizing, the solution was stirred moderately with a magnetic stirring bar, and the solution temperature was kept at 353.2+0.2 K. The counter electrode was Pt-plate, and the anode potential, E_a, was measured against an Ag/AgCl reference electrode. The change in the amount of dissolved Al^{3+}, W_d, with anodizing time, t_a, was determined by an oxinate extraction method.[13]

4) Electron microscopy

Heated and anodized specimens were embedded in an epoxy resin to make sliced samples by ultra-thin sectioning technique with a diamond knife.[14] The sliced samples were placed up on copper grids to observe the cross sections of specimens under a transmission electron microscope (Hitachi H700-H) at 200 kV.

Both thermal and anodic oxide films were also removed from the metal substrate by immersing specimens in a saturated $HgCl_2$ solution to observe the film structure and electron diffraction.

RESULTS AND DISCUSSION

1) Formation of thermal oxide film

Figure 1 shows the time variation in the weight gain, ΔW, of specimens during heat treatment at different temperatures, T_h. At each T_h, ΔW increases with heating time, t_h, and reaches a steady value after a certain t_h. Higher T_h shows a higher rate of increase in ΔW, and a shorter period for attaining a steady value of ΔW. The steady values of ΔW are between 4.0 and 5.0×10^{-4} g/dm², decreasing slightly with increasing T_h.

The ΔW vs. t_h curves obtained here show good agreement with those reported by Dignam et al.[15,16] and Eldridge et al.[17] Using electron microscopy in addition to gravimetry, they showed that γ-alumina crystallite nuclei grow laterally underneath an outer amorphous oxide layer by oxygen ion transport via local channels across the outer oxide layer, and that a terminal thickness is achieved after the crystallite islands coalesce. The kinetic results in Fig. 1 can be easily understood by their explanation.[15-17]

Figure 2 shows electron micrographs obtained from the specimen heated at $T_h = 823$ K for $t_h = 3$ hr. Figure 2a corresponds to the stripped film and Fig. 2b to the cross section. It can be seen from Fig. 2 that the thermal oxide film has non-uniform thickness which depends on the crystal grains, and fully crystallized parts (black parts) are observed randomly. Eldridge et al.[17] have shown in the experiments with single-crystal specimens that the terminal film thickness depends on the crystal orientation

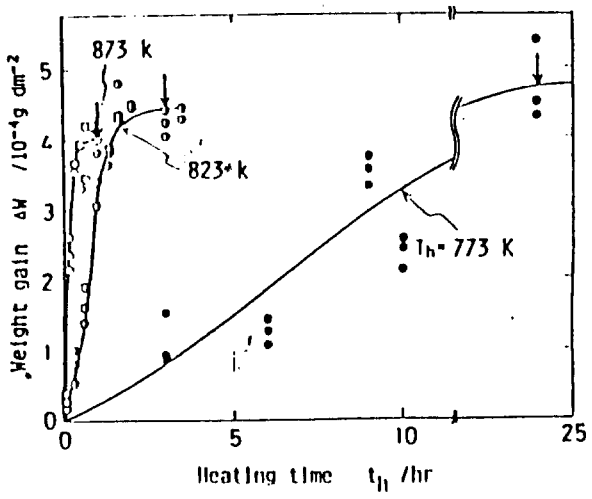

Fig. 1. Change in the weight gain, ΔW, of electropolished specimens with heating time, t_h.

of the metal substrate and decreases in the order (110)>(100)>(111). The non-uniform film thickness observed in the present study may be due to the dependence of the terminal film thickness on the crystal grain facet in the metal substrate.

Figure 2b also shows that the average of the terminal thickness of thermal oxide films is ca. 30 nm. Assuming the density of thermal oxide film to be $\rho = 3.5\times10^{-3}$ g/dm³, the weight gain data yields an average thickness of 25–30 nm.

The inserted photo in Fig. 2 is an electron diffraction pattern obtained from the stripped film, indicating the evidence of γ-alumina (Table 1). This agrees with the results reported by many authors.[1,10,16,17]

2) Formation of anodic oxide film

In order to examine the effects of thermal oxide films on the formation of oxide during the subsequent anodizing, aluminum specimens were heated at 773 K for 24 hr, 823 K for 3 hr, and 873 K for 1 hr, so that the entire surface was covered by γ-alumina film with terminal thicknesses. Anodic oxide film formation on such heavily oxidized specimens will now be described by comparing it with film formation on unheated (electropolished) specimens.

Figure 3 shows the change in the anode potential, E_a, with anodizing time, t_a, obtained for heated and unheated specimens. For the unheated specimens, E_a increases linearly from zero with a slope of 40 V/min. For the heated specimens, E_a shows a potential jump of 20 V approximately at the very initial stage of anodizing, after which it increases linearly with a slope of ca. 89 V/min. Above $E_a = 300$ V, the slope of the curves decreases due to dielectric breakdown of oxide films. The curves frequently show abrupt decrease and increase in E_a in the range between 150 and 250 V. It is clear that the shape of the curves for heated specimens changes little with T_h and t_h. This may be understood as a result of the development of thermal oxide films

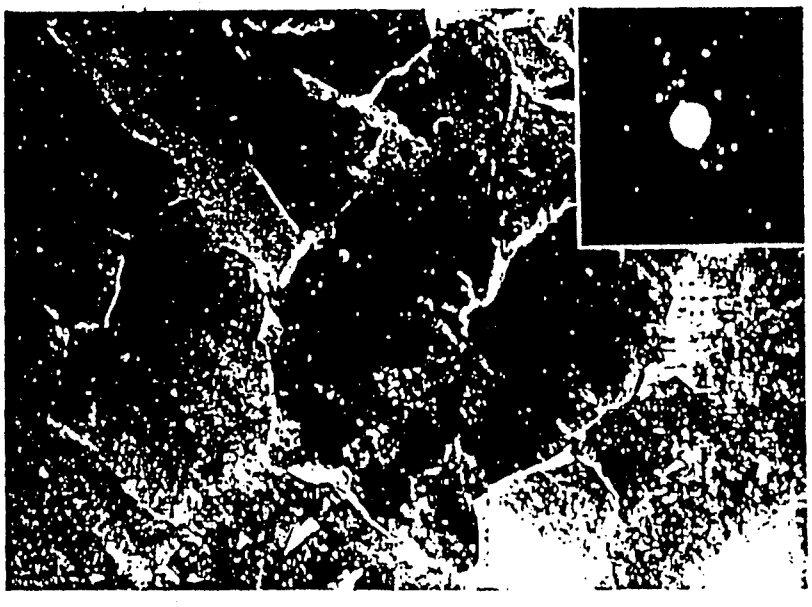

a

100 nm

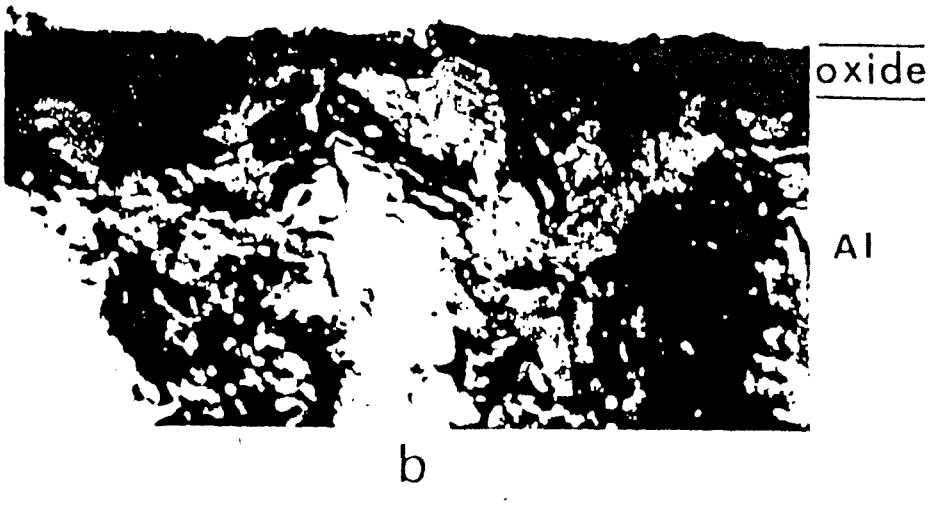

b

Fig. 2. Electron micrographs of thermal oxide film formed by heat treatment in air at 823 K for 3 hr. a) stripped film, b) vertical cross section. The inserted photo is the electron diffraction pattern of the thermal oxide film.

with terminal thicknesses.

The initial jump of E_a for heated specimens is due to the high field sustaining capability of the thermal oxide film. The film thickness/voltage ratio for the thermal oxide film can be calculated to be 2–1.7 nm/V (see Fig. 2b). Beck et al.[18] have reported 2.6 nm/V for the film thickness/voltage ratio of thermal oxide films formed on NaOH-etched aluminum. The value obtained in the present investigation is smaller than their value,[18] and this is due to the different pretreatment.

The slope of the E_a vs. t_a curves for heated specimens is more than twice as steep as that for the unheated specimens. This significant difference can be explained in terms of the film formation efficiency and the high field sustaining capability of the crystalline oxide film. The detail will be described in the following sections.

The mechanism of the abrupt decrease and increase in E_a during anodizing of heated specimens is ambiguous.

A similar behavior has been reported by Yamakawa et al.[19] during anodizing of aluminum covered with hydroxide film. They suggested that this phenomenon is due to the penetration of electrolyte into voids in the film and to fill the voids with new oxides.

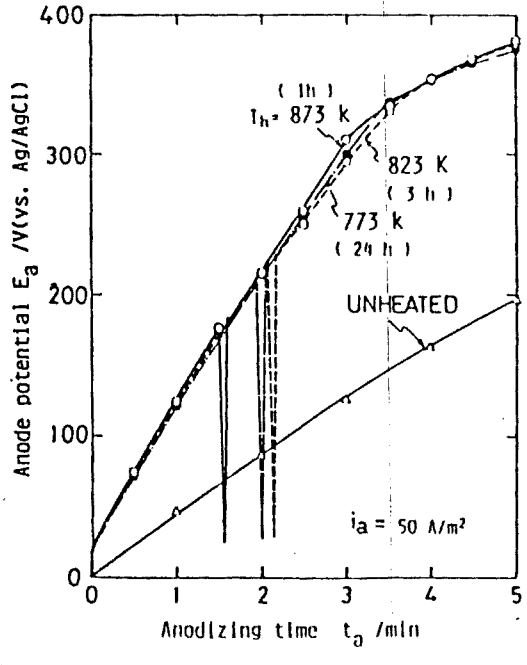

Fig. 3. Time variation in the anode potential, E_a, during anodizing, from heated specimens (at 773 K for 24 hr, 823 K for 3 hr, and 873 K for 1 hr) and unheated specimens. Anodizing was carried out at a constant c.d. of 50 A/dm² in 0.5 mol/dm³ H_3BO_3/0.05 mol/dm³ $Na_2B_4O_7$ solution at 353 K.

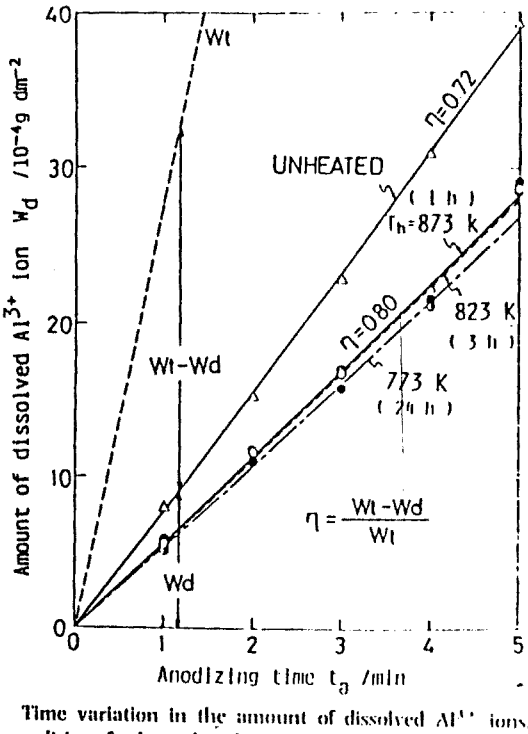

Fig. 4. Time variation in the amount of dissolved Al^{3+} ions, W_d, during anodizing, for heated and unheated specimens. Conditions of heating and anodizing are as in Fig. 3.

3) *Film formation efficiency*

Figure 4 shows the change in the amount of dissolved Al^{3+} ions, W_d, with anodizing time, t_a, for heated and unheated specimens. For each specimen, W_d increases linearly with t_a. The slope of the curves for heated specimens depends little on T_h and t_h, and it is more gentle than that for unheated specimens. Assuming that no side reactions like oxygen evolution take place, the film formation efficiency, η, is calculated by the following equation:

$$\eta = (W_t - W_d)/W_t , \qquad (1)$$

where W_t is the total amount of oxidized Al, and calculated from $W_t = (i_a t_a / nF) M_{Al}$ (n: valency of Al^{3+}; F: Faraday constant; M_{Al}: atomic weight of Al). The value of η obtained with Eq. (1) is 0.72 for unheated specimens and 0.80 for heated specimens. The improvement of η with heat treatment may be explained either by the formation of crystalline anodic oxide film, where the electrochemical dissolution occurs at a slow rate, or by the decrease in the transport number of Al^{3+} ions during anodizing.

4) *Structure of anodic oxide film*

Figure 5(a) and (b) show electron micrographs of cross sections of 2-min- and 5-min-anodized specimens without heat treatment, respectively. Anodic oxide films formed on unheated specimens are found to consist of a porous outer layer and a dense inner layer. The thickness of both outer and inner layers increases with t_a. The electron diffraction of 5-min anodic oxide film removed from the metal substrate showed a halo pattern, suggesting amorphous oxide.

The morphology of these films is very similar to that obtained in a previous investigation,[20] where anodic oxide films were formed potentiostatically at 293–333 K in the same solution as in this investigation. Under potentiostatic conditions and at relatively high temperatures, the porous outer layer became thicker with t_a, and the inner layer thickness remained constant. After long anodizing, the interface between oxide/metal substrate

Table 1. Diffraction spectra obtained from thermal and anodic oxide films.

Lattice plane (hkl)	Spacing (nm) and intensity		
	Standard[17]	Thermal*	Anodic**
111	0.456 mf	0.463 f	0.455 f
220	0.280 f	0.282 f	--
311	0.239 ms	0.241 vs	0.237 m
222	0.228 m		
400	0.200 vs	0.196 m	0.202 vs
511	0.152 f	0.156 m	--
440	0.140 vs	0.141 s	0.142 s
533	0.119 f	0.120 m	0.117 m

* Thermal oxide was formed by heat treatment at 823 K for 3 hr.
** Anodic oxide was formed by anodizing at 50 A/m² for 5 min after the heat treatment described above.

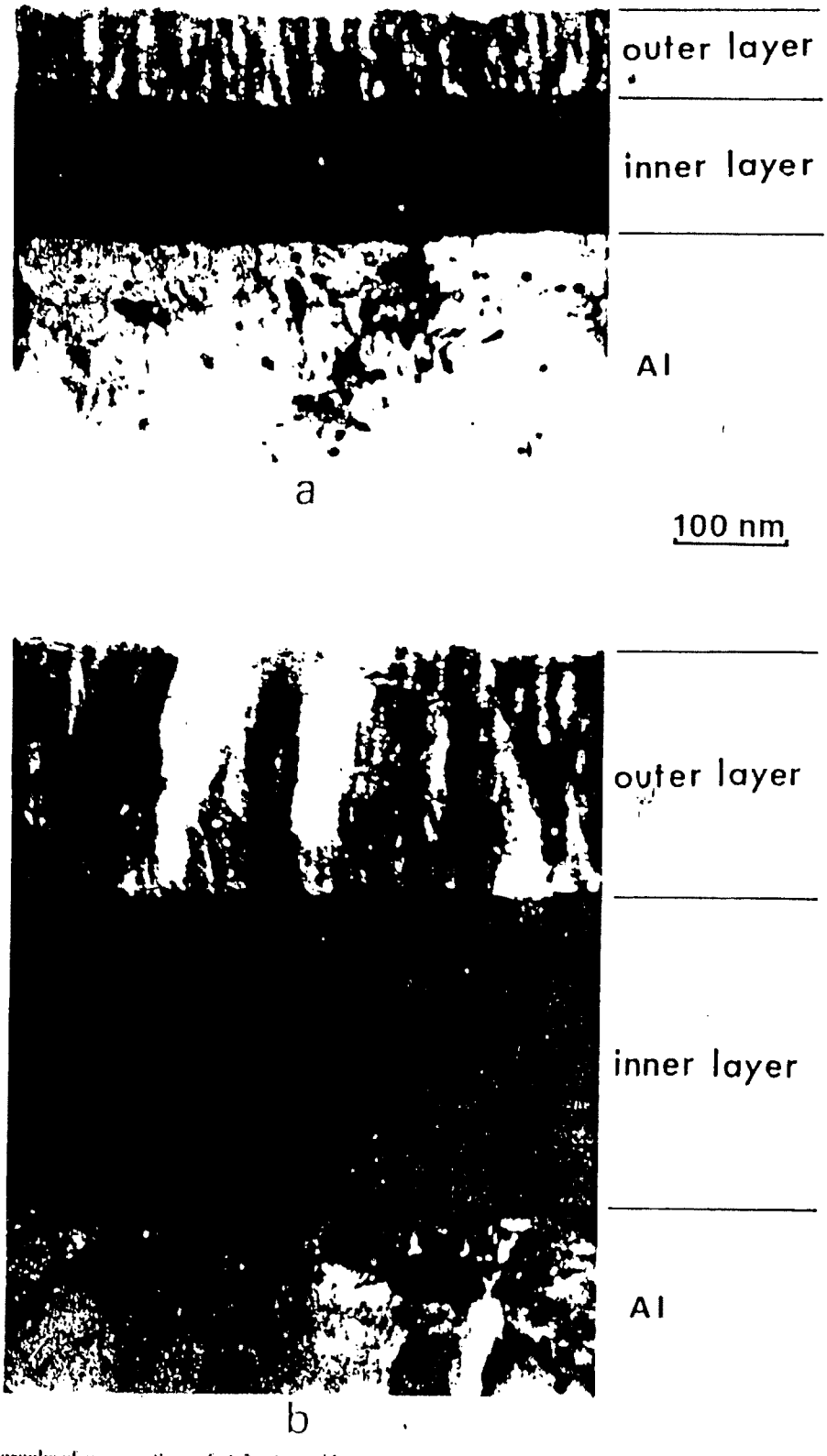

Fig. 5. Electron micrographs of cross sections of a) 2-min and b) 5-min anodic oxide films formed on unheated specimens. Anodizing conditions are as in Fig. 3.

became rounded and the film changed to porous oxide films similar to that formed in acidic solutions. Hence, the anodic oxide films shown in Fig. 5 are expected to be precursors of the porous oxide film and only the inner layer can sustain a high field of anode potential.

Figure 6 shows electron micrographs of the stripped

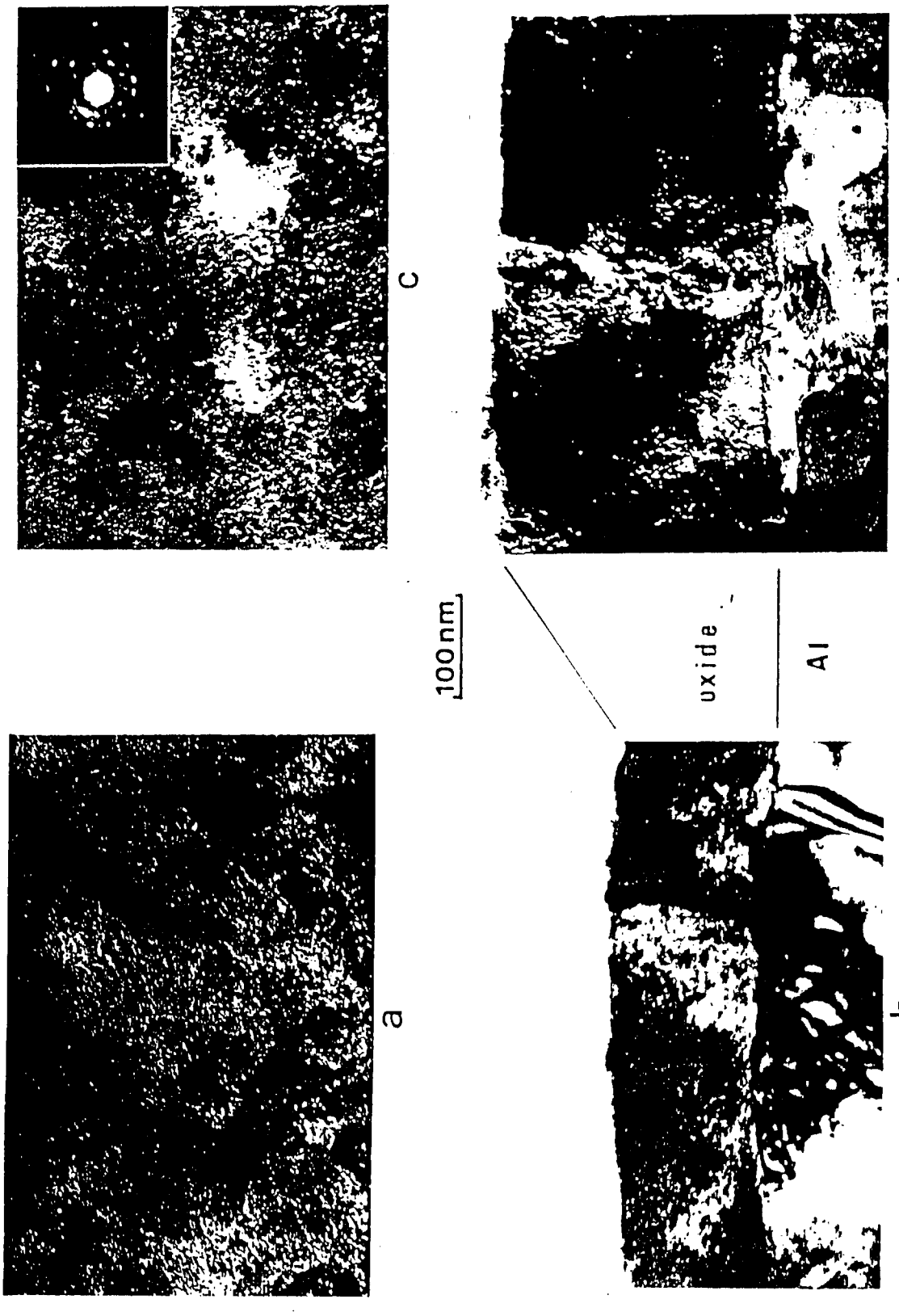

Fig. 6. Electron micrographs of stripped films and cross sections of 2-min (a and b) and 5-min anodic oxide films (c and d) formed on specimens with heat treatment at 823 K for 3 hr. Inserted photo is the electron diffraction pattern of the 5-min anodic oxide film. Anodizing conditions are as in Fig. 3.

films and the cross sections of 2-min- (Fig. 6(a) and (b)) and 5-min-anodized (Fig. 6(c) and (d)) specimens, which have been heated for 3 hr at 823 K. The anodic oxide films formed after the heat treatment appear to consist of a single dense oxide layer. Thickness of the oxide film increases with t_a. Electron diffraction obtained from the removed film (inserted photo in Fig. 6a) shows evidence of a crystalline oxide of γ-alumina in the anodic oxide films (Table 1). Detailed examination of the structure of the anodic oxide films suggests that the crystallinity of the oxide is not uniform and that there are numerous small voids in the oxide. The voids can be considered to be produced by crystallization of amorphous oxide under a high electric field, as described later.

The single layer structure is very similar to the structure reported by Alwitt and Takei,[2] which was obtained by anodizing in a neutral citrate solution at 343 K after 798 K heat treatment for 20 min. At room temperature, anodizing of aluminum covered with crystalline thermal oxide film has been reported to cause the formation of a three-layered oxide film, which consists of an outer amorphous oxide layer, middle crystalline oxide layer, and inner amorphous oxide layer.[4,7,9,12] The differences in the film structure will be described below.

During anodizing, the formation of amorphous oxide takes place both at the electrolyte/oxide and oxide/metal interface by the transport of Al^{3+} and O^{2-} ions. In the middle part of the oxide film, the amorphous oxide crystallizes under the high electric field through contact with the γ-alumina which has been formed by thermal oxidation. At high anodizing temperatures, the rate of crystallization can be expected to be high. In addition, a part of the oxide formed at the electrolyte/oxide interface dissolves electrochemically (see Fig. 4). The enhancement in crystallization of amorphous oxide at high anodizing temperatures has been observed for the anodic oxide film formation on aluminum after hydrothermal treatment.[21] The enhancement in crystallization and dissolution of oxide may result in the formation of the single layer structure observed in this investigation. The crystallization of amorphous oxide may cause a volume shrinkage of oxide, and allow the oxide film to produce numerous voids.

A comparison of Fig. 3 with Figs. 5 and 6 gives the relationship between the thickness of anodic oxide films, δ, and the anode potential, E_a, and is shown in Fig. 7. For anodic oxide films formed on unheated specimens, only the inner layer thickness is plotted as only this layer sustains the electric field. The film thickness, δ, is apparently proportional to E_a for both types of anodic oxide film, and δ for heated specimens does not depend on T_h and t_h. The slope of the curves gives the film thickness/E_a ratio as 1.45 nm/V for unheated specimens and 0.77 nm/V for heated specimens. The value for unheated specimens agrees well with that reported for barrier-type amorphous oxide films.[20]

The value obtained for heated specimens, 0.77 nm/V, is much smaller than that for unheated specimens. This

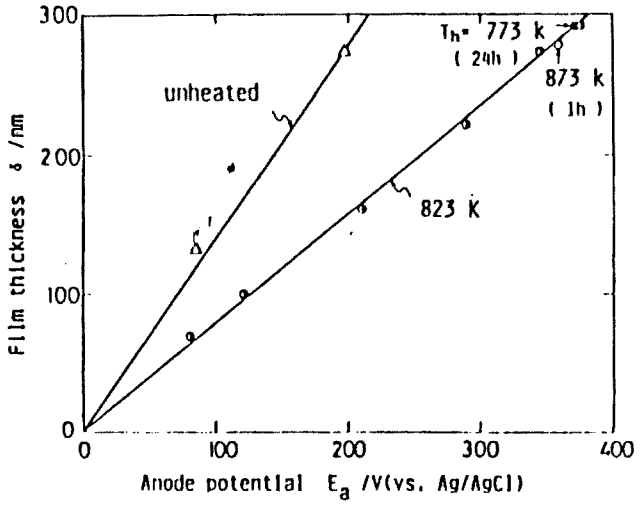

Fig. 7. Relationship between anodic oxide film thickness, δ, and anode potential, E_a, obtained from heated and unheated specimens. Anodizing conditions are as in Fig. 3.

is because the anodic oxide films formed on heated aluminum have a single layer of γ-alumina which can sustain a higher electric field. Many authors reported that anodic oxide films, formed after the heat treatment and hydrothermal treatment, include γ'-alumina crystals[2,4,21,22] and that the anodic oxide films have low values of 0.85–1.25 nm/V for the film thickness/E_a ratio.[1,2,4,5,7,9,12,21,25] The value obtained in the present investigation is smaller than any of the values reported in these papers. This can be explained as a result of the different crystal structure between them. Longer heat treatments may allow γ-alumina crystals to develop fully in the thermal oxide film, and the crystals may act as seeds for the formation of γ-alumina in the anodic oxide films during anodizing.

5) *Local structure of anodic oxide film*

Figure 8a shows a low magnification electron micrograph of the stripped film, obtained from the specimens anodized for 5 min after heat treatment for 3 hr at 823 K. It can be seen from Fig. 8a that there are black islands with a diameter of 0.1–1.0 μm. These black islands may correspond to the amorphous oxide formed locally in the crystalline oxide layer, and this can be supported from Fig. 8b, in which a thicker amorphous oxide island is observed.

As these black islands were not observed in the stripped film obtained by anodizing for 2-min-anodized specimens, it is considered that the formation of the amorphous oxide islands takes place through the local breakdown of crystalline oxide layer at the last stage of anodizing. Possibly, this correlates with the abrupt increase and decrease in the anode potential, E_a, observed during anodizing for the heated specimens (see Fig. 3). Further investigation will be necessary to clarify the mechanism of the amorphous oxide island formation.

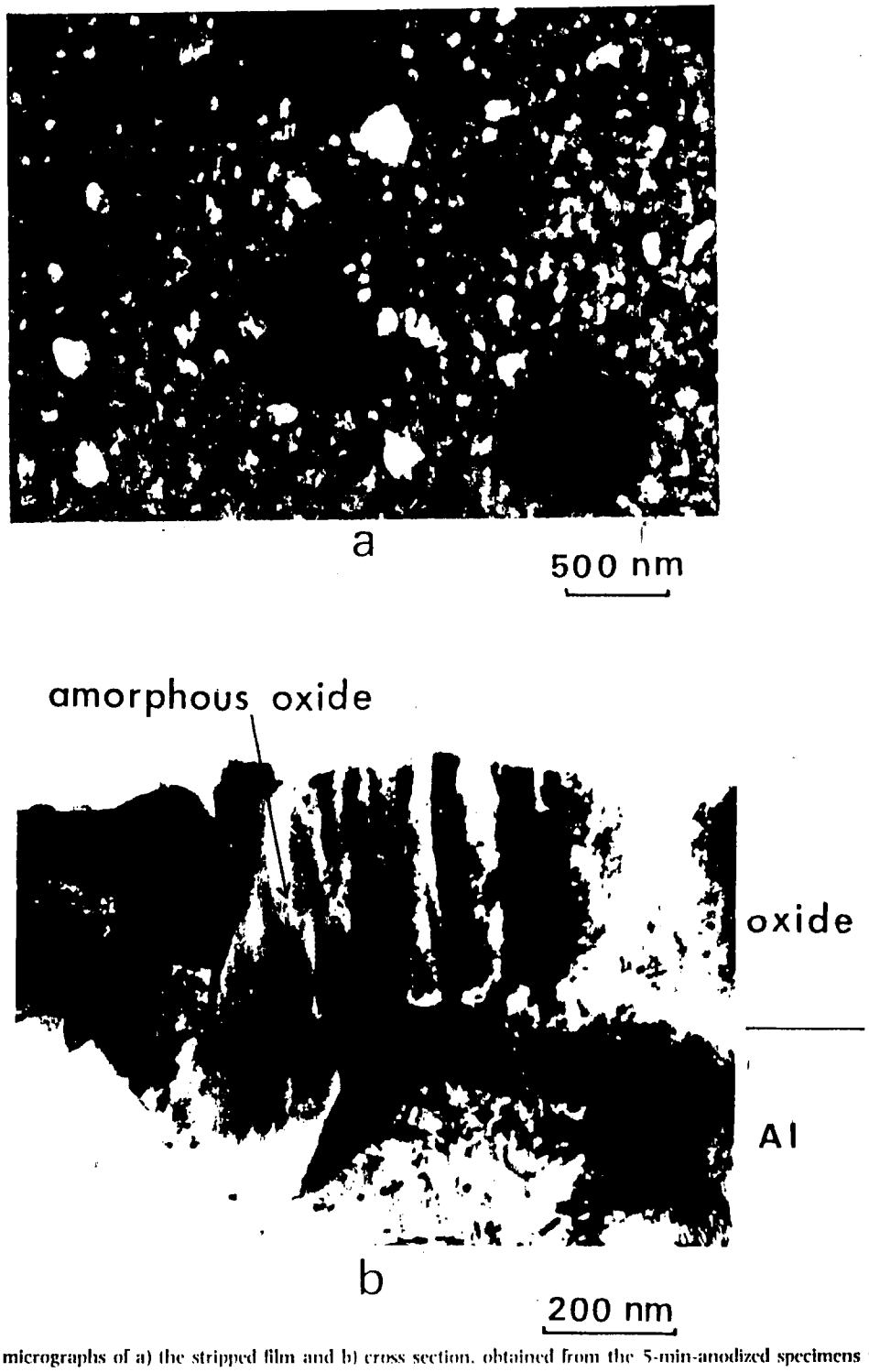

Fig. 8. Electron micrographs of a) the stripped film and b) cross section, obtained from the 5-min-anodized specimens with heat treatment at 823 K for 3 hr. Anodizing conditions are as in Fig. 3.

CONCLUSION

Very pure aluminum was thermally oxidized at $T_h = 773$–873 K for $t_h = 1$–24 hr and then anodized galvanostatically in a neutral borate solution at 353 K. The influence of heat treatment on anodic oxide film formation was examined by electron microscopy, gravimetry, and chemical analysis. The following are the conclusions.

1) Thermal oxide films formed by long periods of heat treatment have a terminal thickness of ca. 30 nm, which decreases slightly with increasing T_h. These films include γ-alumina crystals.

2) During anodizing, the rate of increase in the anode potential, E_a, for fully oxidized specimen is much higher than that for unheated specimens, and it does not depend on T_h.

3) The efficiency of anodic oxide film formation is 0.80 for heated specimens and 0.72 for unheated specimens.

4) Anodic oxide films formed on heated specimen have a single layer structure of crystalline oxide, and show a low 0.77 nm/V film thickness/E_a ratio. At high E_a region, amorphous oxide islands are formed through the local breakdown of crystalline oxide layer.

Acknowledgments. Financial support of this investigation from the Light Metal Education Foundation of Japan is greatly appreciated. The authors also thanks Dr. R. S. Alwitt, Dr. M. J. Graham, and Prof. Heishichiro Takahashi for valuable discussion and suggestions.

REFERENCES

1) Alwitt RS: Crystalline anodic oxide films on aluminum. J Metal Finishing Soc Jpn, 32: 226–234 (1981)
2) Alwitt RS, Takei H: Crystalline aluminum oxide films. In: Froment M, ed. Passivity of metals and semiconductors. Elsevier Science Publishers B. V., Amsterdam, 741–746 (1983)
3) Bernard WJ, Florio MS: Anodic oxide growth on aluminum in the presence of a thin thermal oxide layer. J Electrochem Soc 132: 2319–2322 (1985)
4) Shimizu K, Kobayashi K, Nishibe H: Influence of thermal oxide layer on the growth and structure of barrier anodic films on aluminum. J Jpn Inst Light Metals 35: 553–561 (1985)
5) Shimizu K, Kobayashi K, Nishibe H: The structure of barrier anodic films formed on aluminum covered with a layer of thermal oxide. J Electrochem Soc 133: 140–141 (1986)
6) Kobayashi K, Shimizu K, Teranishi D: Influence of electrolyte on the development of γ'-alumina in the barrier oxide layers formed on aluminum covered with a thin layer of thermal oxide. J Jpn Inst Light Metals 36: 81–88 (1986)
7) Crevecoeur C, de Wit HJ: The anodization of heated aluminum. J Electrochem Soc 134: 808–816 (1987)
8) Alwitt RS: Thickness-dependent properties of amorphous anodic alumina films. J Electrochem Soc 134: 1891–1896 (1987)
9) Alwitt RS, Ortega C, Thorne N, Seljka J: Ion transport through duplex amorphous/crystalline barrier aluminum oxide films. J Electrochem Soc 135: 2695–2700 (1988)
10) Kobayashi K, Shimizu K: Behavior of γ-alumina during anodic oxidation of aluminum. J Jpn Inst Light Metals 38: 91–95 (1988)
11) Kobayashi K, Shimizu K: Scanning electron microscopy of crystalline barrier anodic oxide films on aluminum. J Metal Finishing Soc Jpn 40: 484–485 (1989)
12) Kobayashi K: The structure of barrier anodic film on aluminum. J Metal Finishing Soc Jpn 40: 1328–1331 (1989)
13) Takahashi H, Saito H, Nagayama M: Effects of electrolyte anions on the formation of barrier type oxide films on aluminum. J Metal Finishing Soc Jpn 33: 225–231 (1982)
14) Takahashi H, Nagayama M, Akahori H, Kitahara A: Electron microscopy of porous anodic oxide films on aluminum by ultra-thin sectioning technique. Part 1, the structural change of the film during the current recovery period. J Electron Microsc 22: 149–157 (1973)
15) Dignam MJ, Fawcett WR, Bohni H: The kinetics and mechanism of oxidation of superpurity aluminum in dry oxygen. I. Apparatus description and the growth of amorphous oxide. J Electrochem Soc 113: 656–662 (1966)
16) Dignam MJ, Fawcett WR: The kinetics and mechanism of oxidation of superpurity aluminum in dry oxygen. II. The growth of crystallites of γ-alumina. J Electrochem Soc 113: 663–671 (1966)
17) Eldridge JI, Hussey RJ, Mitchell DF, Graham MJ: Thermal oxidation of single-crystal aluminum at 823 K. Oxidation Metals 30: 110–128 (1988)
18) Beck AF, Heine MA, Caule EJ, Pryor MJ: The kinetics of the oxidation of Al in oxygen at high temperature. Corros Sci 7: 1–22 (1967)
19) Yamakawa S, Ohsawa S, Numazawa A, Iida T, Sato K, Takahashi M, Hoshino K: Self-restoration-forming phenomenon. Proceedings of the 6th ARS Kyoto Conference, 85–92 (1989)
20) Takahashi H, Nagayama M: Electrochemical behaviour and structure of anodic oxide films formed on aluminum in a neutral borate solution. Electrochim Acta 23: 279–286 (1978)
21) Takahashi H, Umehara Y, Miyamoto T, Fujimoto N, Nagayama M: Anodizing of aluminum covered with hydroxide. I. Formation of hydroxide and composite oxide films. J Metal Finishing Soc Jpn 38: 67–73 (1987)
22) Kobayashi K, Shimizu K, Fujisawa A: The structure of barrier anodic films formed on aluminum covered with a layer of hydrous oxide. J Jpn Inst Light Metals 35: 611–617 (1985)
23) Hasegawa H, Suganuma E, Funakoshi A: Formation and structure of hydrated/composite oxide films on aluminum. J Metal Finishing Soc Jpn 40: 1422–1426 (1989)
24) Kudo T, Alwitt RS: Cross-sections of hydrous and composite aluminum oxide films. Electrochim Acta 23: 341–345 (1978)
25) Takahashi H, Takahashi K, Furuichi R, Nagayama M: Anodizing of aluminum covered with hydroxide films. IV. Field assisted dehydration of hydroxide formed in high temperature. J Metal Finishing Soc Jpn 40: 1415–1421 (1989)

(Received November 5, 1990; accepted February 25, 1991)

STRUCTURAL REPAIR TO REINFORCED CONCRETE BEAM IN TUNGKU LANDLESS HOUSING SETTLEMENT SCHEME BRUNEI DARUSSALAM

Ak. Menuddin PLW Pg. Hj. Yussof B.Eng(Hon)
M.I. Mohamed Nakeeb C.Eng(London), MI StructE
Engineers, Structural Section, Public Works Department
Brunei Darussalam.

ABSTRACT

This paper discussed the repair method used in repairing a residential structure at Tungku Landless Housing Settlement Scheme, Brunei Darussalam. The deterioration of the structure was caused by both poor quality of materials used and inadequate supervision during the construction. It covers the problems, the options of repair method, the method selected, and the factors considered in the choice of repair method. The paper also discusses present activities for monitoring the effectiveness of the repair method employed.

Introduction

The Tungku Housing Settlement Scheme situated at Mukim Gadong, about 9km from the capital Bandar Seri Begawan. The building was constructed five years ago but structural cracks were observed on the face of the beam. The reinforced concrete floor slab was found to have spalling concrete.

Problems Encountered

1) Deep cracks along the simply supported beam and corroded steel were identified.

2) A cantilever beam at the staircase had a similar defect but the extent of damage was small.

3) Spalling concrete was identified on the reinforced concrete floor slab near the affected simply supported beam.

Method of Investigation

The method of testing carried out were :

1) Visual Inspection of the house and its surrounding environment
   - cracking pattern
   - location and size of cracks

2) Direct Hacking by using chisel and hammer to :
   - remove mortar layer
   - expose condition of surface concrete
   - expose reinforcement for inspection
   - check its concrete cover, bar sizes, arrangement at the beam-column joint and its corrosion state

3) Estimation of concrete in-situ strength by using Rebound Hammer. The results obtained were affected by :
   - surface smoothness
   - moisture condition
   - cracks and voids within or on the concrete
   - types of coarse aggregate used

4) Location, spacing and number of reinforcement within beam and column by using R-meter, a type of non-destructive testing equipment.

Results of Investigation

The results indicated :-

1) the shear failure cracking pattern occurring in this house is most likely to be caused by the bad arrangement of the reinforcement within the beam-column joint and the large spacing between the links. The links spacing distance specified in the structural drawing for the beam is 150mm while the R-meter readings showed the variation from 150 to 230mm. This is an indication of inadequate supervision and poor workmanship.

2) the badly corroded condition of the exposed beam reinforcement is likely to cause more serious spalling of concrete and cracking problem in the future.

3) the thickness of the mortar layer measured ranges from 6mm to 12mm and the cover varies from 10 to 20mm at the hacked region, which is again an indication of poor workmanship.

4) the rebound hammer results showed good strength, but the serious cracking problem found on the floor slab and the wall of the bedroom and the beam surface after hacking the mortar indicates very clear warning of the danger imposed upon the occupants of the house. An immediate and appropriate repair work is deemed necessary before it is too late.

Proposals of Repair Method :

Three options were proposed, which are:-

i) Demolish the entire structure and construct a new one. This method is the easiest but very expensive one.

ii) Surface Repair - wire brush / sand blast the corroded steel and plaster the concrete surface using epoxy cement mortar. This method can be applied only for structurally sound members.

iii) Structural Repair - Replace the steel bar and weakest areas. This method is applied only to structurally unsound members.

Repair Method

For the actual repair work, a combination of option (ii) and (iii) was adopted since some members of the structure were structurally sound and some were unsound. Pressure grouting with high strength non-shrink cementious materials were used for the repair of the structurally unsound members. However, for the floor slabs where the concrete spalled off, epoxy cement mortar was used to plaster the area.

Repair Procedure

a) Install props and jacks for the beams and shoring for the columns.

b) Hack the beam and column using chisel and hammer or any approved method only to expose the main reinforcement and shear links.

c) Butt weld the beam main reinforcement to shear links and column reinforcement.

d) Install Hilti HVA M16 adhesive anchor bolts in accordance with manufacturer's specification and as shown on the drawings.

e) Using a water jet clean the hacked area and apply one coat of the following bonding agent to the exposed concrete area:-
AH P.V.A Bonder
or Hilti CA 420 EP
or any approved equivalent.

f) Apply one coat of Anticorrosion Primer, Araldite CM xh 126AB or approved equivalent to the exposed reinforcement.

g) Install watertight formwork and grouting inlet and bleeding pipes.

h) Pump in the following high strength non-shrink pressure grout in an over flowing sequence and maintain the grout pressure at 30 - 50 psi :-
UniStrong Unigrout
or Hilti CM 651 N
or any approved equivalent

i) Remove the formwork after 48 hours.

j) Paint the affected area to match the existing.

k) Remove props and shoring after one week.

Conclusion.

The method adopted to repair the work was practical and very much cheaper than demolishing the structure and re-build a new one. This method also increased the life time of the structure by increasing its durability. The test results on the finished concrete products gave satisfactory results. Further tests are being carried out to study the following:-

a) Carbonation level
b) Chloride
c) Corrosion level of rebar

The repair work was completed about a year ago, and there is no sign of any further deterioration. However, the present study will confirm the durability of the structure.

Acknowledgment

The results reported here were obtained as a group contribution of Corrosion Unit and Design & Supervision Unit of the Structural Section of Public Works Department.

Lee/AK.pap/May.92

APPLICATION OF POTENTIAL-pH (POURBAIX) DIAGRAM IN AQUEOUS CORROSION

S. Purwadaria[1], A. Sulaiman[2] and S. Soepriyanto[1]

1. Option Metallurgy, Dept. of Mining Eng. Instiut Teknologi Bandung, Jl. Ganesha 10 Bandung 40132 - Indonesia
2. R & D for Metallurgy, LIPI, Jl Sangkuriang Bandung - Indonesia

ABSTRACT

The thermodynamics information describing the onset of stability domains of metal, its oxides/hydroxides and predominan areas of its ions, can be usefully presented in the form of potential-pH isothermal diagrams. The applications of diagrams for explaining the mechanism of metal corrosion and the methods for corrosion prevention thermodynamically, are discussed. The addition of kinetics data to these diagrams enhances the practical usefullness of the diagrams. Construction of experimental potential-pH diagram using the anodic polarization measurement results are necessary to exhibit the conditions atwhich a metal is able to be passivated in acids and the potentials when the passivating film will be breakdown.

PROTECTIVE COATINGS FOR OFFSHORE STRUCTURES AND EQUIPMENT

BY

AZMAN BIN A.AZIZ
PETROLEUM RESEARCH INSTITUTE
PETRONAS
MALAYSIA

ABSTRACT

Corrosion of offshore steel structures and equipment is an important and costly problem in the oil and gas industry. In tropical marine environment such as offshore Malaysia, corrosion is more severe than in temperate countries. Therefore the corrosion phenomena in offshore environment have to be understood and identified before fabrication of an offshore platform can take place.

In general, offshore structures can be divided into four zones based on the conditions they are being exposed to. In atmospheric and splash zones, coating is a common method of protecting the steel from corrosion whereas in immersed and mud zones, cathodic protection is widely used.

In undertaking a coating project, proper planning and coordination is vital since the bulk of cost will be for the implementation rather than for the coating materials. Thus, adequate time should be given to these phases of a coating project.

This paper mainly describes PETRONAS' experiences with regard to the application of the several types of protective coatings that are commonly used on offshore platforms in Malaysia.

1.0 AN OVERVIEW OF THE OIL AND GAS INDUSTRY IN MALAYSIA

The petroleum industry in Malaysia had its beginning in the early twentieth century, when oil was first discovered onshore Miri, Sarawak in 1909. By the end of 1973, a total of 19 oil fields had been discovered offshore Malaysia. The oil embargo in 1973 made oil producing countries realize the importance of controlling their own petroleum resources; Malaysia was no exception. In view of the situation, in August 1974, PETRONAS was formed and vested with the ownership and control of all petroleum resources in Malaysia.

Malaysia is fortunate to have a steady increase in oil and gas reserves. At present, 31 oil and gas reserves and 4 non-associated gas fields are in production in Malaysian waters. A total of 174 offshore platforms are now in operation and these platforms are operated either by PETRONAS' wholly owned subsidiary PETRONAS Carigali, or by Shell and Esso through production sharing contracts. Some of these platforms have been in service for more than 20 years and have undergone much maintenance work.

2.0 CORROSION ENVIRONMENT AND COATING SYSTEMS

The offshore platform environment is divided into atmospheric, splash, immersed and mud zone according to the difference in corrosion conditions. This categorization of the structure is shown in Fig.1. In designing an offshore platform, all four zones have to be taken into account as each zone requires different types of protection techniques. Protective coating is used in the atmospheric and splash zone environments whereas cathodic protection (CP) is applied in the immersed and mud zone environments. However CP will not be discussed in this paper.

2.1 Atmospheric Zone

This zone comprises equipment and structural beams situated from the sea deck to the helicopter deck. They are exposed to high relative humidity (i.e RH > 85%), ultra violet ray, high temperature, rain, salt spray, contaminants and impact that could contribute to the corrosion process.

In these areas, a three or four coat system is used to a total dry film thickness (DFT) of about 200 to 300 μm.

The three coat system normally consists of:

1. Organic zinc rich epoxy	50 μm	DFT
2. High build epoxy with or without micaceous iron oxide (MIO)	150 μm	DFT
3. Polyurethane	50 μm	DFT

The main difference between the three and four coat system is the additional primer where the later utilizes inorganic zinc silicate (IOZ). In order to improve the intercoat adhesion properties, the IOZ primer requires a layer of a tie coat before any high build coating can be applied onto it. The system is as follows:

1. Inorganic zinc silicate primer	50 μm DFT
2. Epoxy tie coat	50 μm DFT
3. High build epoxy with or without MIO	125 μm DFT
4. Polyurethane	50 μm DFT

With good quality surface preparation and application, in general, a total service life of between 6 to 10 years can be expected from both systems. Based on PETRONAS' experiences, minor maintenance has to be carried out from time to time to prevent severe deterioration and to prolong the coating's useful life. Besides the two systems mentioned earlier, there is a trend now in Malaysia towards environmental friendly type of coatings such as isocyanate free polyurethane and water based coatings. However the performance and problems associated with these coatings have not been fully established at this stage.

For areas exposed to high impact and abrasion such as the top deck and helicopter deck, glass filled polyester or glass filled epoxy is used. These coatings can be applied at higher film thicknesses in one or two layers (e.g total DFT of 600 μm - 1000 μm). The glassflakes in the cured film provide high impact and abrasion resistance and at the same time enhance the bond of the resin to the substrate to prevent undercutting of the cured film.

For small and remote platforms, especially offshore Sarawak where coating is done by workbarges and boats, it was found to be economical to use glassflake filled polyester eventhough the materials cost per surface area is two to three times more than that of a conventional multiple coat systems. Savings by a factor of two to three are made on the reduction of barge time, rental of scaffolding and downtime. Only primary and secondary structures are coated with this system whilst small piping, flowline supports, wellheads, manifolds and handrails are coated with conventional systems to avoid

a high degree of wastage.

2.2 Splash Zone

This is the most aggressive environment of the four mentioned earlier. As the seawater spray continually wet the area, it is difficult to maintain in a satisfactory manner. In this area CP is not effective and a high oxygen concentration will cause an increase in corrosion rates. Particular attention is given to the zone from the mean waterline level to approximately ±6 m.

Generally coatings similar to those used for atmospheric zones are employed in the splash zone (e.g jacket legs, conductors and boat landing) but at a greater film thickness. In Malaysia, however a glassflake filled polyester coating is commonly used due to its toughness and impact resistant qualities against waves and floating objects. This type of coating system has the advantage of shorter application and curing time; thus it can be applied in between high tides.

For riser pipes operating at moderate temperature (40 to 80 deg.C) a more superior protective coating is used to control corrosion. A 25mm vulcanized rubber cladding is normally selected. This has to be applied under controlled conditions during fabrication. The pipes are blasted to white metal finish and then coated with a bonding adhesive before being wrapped with neoprene rubber. The component is subsequently cured by steam heating at a temperature of 150 deg.C and 344 kPa for about 3 hours. It is claimed that this type of system can last up to 40 years in the splash zone environment.

3.0 PRE-COATING PREPARATION

The planning and coordination phases are the critical phases in undertaking a coating project offshore. In a coating project the cost of the coating materials amount to roughly 10 to 20 percent of the total cost. The bulk of the total cost is on the application which includes, manpower, tools, surface preparation and transportation. In view of this, it is important to coordinate the operations of the different parties involved to ensure efficiency. Some planning steps have to be carried out before the actual coating job starts.

3.1 Pre-Inspection of the Platform

An evaluation of the overall condition of the platform is normally carried out first in order to get a general picture. This is followed by a detailed inspection of the structures and equipment to determine the percentage of the coating breakdown, area coverage and job scope for the contractor. Consultation with the platform operators on the operating routines and equipment set-up can be helpful in planning the work. The layout of the platform including crane capacity, living accommodation for crew and water capacity has to be studied. Equipment that needs wrapping, drains that need plugging, hot items that require special attention and life lines that require platform shutdown need to be ascertained at this stage.

3.2 Coating Schedule

After the necessary information has been gathered, detailed schedules, listing the items and areas to be coated can be prepared. It serves as a guide for the job scope and eliminates any ambiguities once the job starts. It also enables engineers to estimate the cost of the project. The schedule includes an itemized breakdown of the structure members, vessels, and interconnecting lines that are to be coated, types of surface preparation and coating systems.

3.3 Work Schedule

The work schedule lists the time frame allotted for the job. It includes a breakdown of each of the platform area and an estimated start and completion date for each area. A copy of this schedule is given well in advance to the inspector and contractor's foreman for them to plan their work accordingly. The work schedule will be closely monitored so that the work can be completed on time.

3.4 Pre-job Meeting

The objective of the meeting is to familiarize the respective parties with the coating specifications and company standards. This is where the organization and coordination of the team players take place. The team members include management staff, corrosion and field engineer, coating supplier, contractor's foreman, third party inspector, safety officer and platform supervisor. In this meeting the emphasis is on the cooperation and

communication tendered during the project. Any issues regarding safety and job responsibility are also discussed.

4.0 APPLICATION AND INSPECTION

After the preliminary work has been completed, the coating contractor will be informed so that he can mobilize his equipment, coating materials and personnel as scheduled. The work would begin with wrapping and masking of equipment, erecting the scaffolding and followed by surface preparation. Extra attention should be given when masking and wrapping around instrumentation gadgets, flanges, cables, etc before any blasting or painting work is carried out. This is essential because the overspray and hardening of paint on contaminated areas can cause operational difficulties later on.

The surface preparation technique commonly used is the abrasive air blast cleaning. Applying an exotic coating to a piece of metal without proper surface preparation is a waste of time and money. All coating systems that had been discussed earlier require surface finish equivalent to Swedish Standard Sa 2.5 minimum. Prior to blasting the surface they must be completely free from oil and grease. Weld scars, sharp edges, weld spatter etc also need to be removed. For the conventional multiple coats system, a surface profile of 30-40 μm is normally targetted, whilst 75 to 100 μm is required for glassflake filled polyester in view of its thickness.

Spraying is the most common method of application being used in offshore coating. Two types of spray techniques: conventional spray and airless spray may be applied, depending on the types of coating. However most coatings can be used with either one of them except for glassflake filled polyester which requires an airless spray. The presence of glassflakes causes high wear rate to the equipment; thus, a correct size nozzle tip is essential to prevent overspray.

The prime coat must be applied on the day the surface preparation is completed. Sufficiently dried film thickness has to be applied to cover the high peaks of the surface profile and any coating defects e.g pinholing or inadequate thickness, will be marked and recoated before subsequent coatings are applied.

Inspection is performed to ensure compliance with the specifications. Inspections in general do not only cover the coating proper but also include a check on the type and condition of the equipment, surface preparation, conditions of application and inspection of the final

job. Normally the inspection is done by a third party inspector who reports the daily activities to the field engineer. His responsibility also includes submitting a full report upon completion of the job.

5.0 COMPLETION OF THE JOB

After the coating job at a particular area of the platform is completed, the field engineer together with the contractor's foreman and inspector will carry out a final inspection. Any coating defects that are critical must be repaired before moving to other areas of the platform. Only after the field engineer and the inspector are satisfied with the quality of the coating job can the contractor then proceed with clearing the work site. All the spent grit has to be collected and shipped back to shore for disposal. As a matter of fact, the cleaning of the work site from dust and grit must be carried out at least 1 to 1 1/2 hours before coating application. This is to allow sufficient time for the dust to clear and to prevent it from contaminating newly coated surfaces. The removal of masking and wrappers from the equipment, unpluging of all drains and dismantling of all scaffoldings are also carried out during the clearing stage. All the processes that have been discussed earlier (4.0 and 5.0) are repeated when the coating job starts at another area of the platform until the whole job is completed. Sometimes the coating work has to be stopped temporarily during rainy seasons which normally falls between October and February. The time taken to fully complete the coating job offshore depends mainly on the size of the area that needs to be coated and the complexity of the platform. It can take between 4 months to 1 1/2 years to complete the task.

6.0 CONCLUSION

The successful execution and completion of an offshore coating project is a result of many painstaking hours of preparation and labor-intensive effort. It also depends on the favourable outcome of a variety of factors, including those beyond our control e.g weather conditions. However, four main factors that need to be seriously considered in order to obtain an economical and high quality offshore coating job. They are:

a. Planning
b. Coordination
c. Coating selection

d. Application and inspection

Although the cost of coating materials only amounts to 10 to 20 percent of the total cost, the rest is spent on application and implementation. Therefore, the trend in Malaysia now is to use coating systems that are easier to apply i.e requiring less surface preparation and shorter application time. At the same time, more environment friendly systems are also being looked into. However, as all these systems are still on the 'trial' phase, the performance and problems associated with them have not been fully established yet.

7.0 REFERENCES

1. A. Aziz. A, 'Assessment of Coating Damage on Tembungo-A', Technical Report to PCSB, May 1991

2. Conlin. T, 'Fundamental of Offshore Coating Operations' Journal of Protective Coatings & Linings, September 1990

3. Cornelisse. H. H, 'Painting/Coating Policies and Systems in the Oil and Gas Industry', presented at the 6th Asian-Pacific Corrosion Control Conference in Singapore, September 1989

4. Shang. C. L, 'Corrosion and Protection for the Steel Platform in the Oil Development of the Pearl River Mouth', presented at the 6th Asian-Pacific Corrosion Control Conference in Singapore, September 1989

5. Ali. Z, 'Corrosion Protection of Onshore and Offshore Pipelines, Duyong Gas Field Experience', presented at the 2nd Inter-plant Workshop in Malaysia, May 1989

6. Nockengost. R. F, 'Managing Protective Coatings Project', Journal of Protective Coatings & Linings, May 1988

7. Biddles. P, 'Protective Coating System for Onshore and Offshore Marine Structures', presented at the 2nd Asia-Pacific Corrosion Control Conference in Malaysia, July 1981

Fig.1 SCHEMATIC DIAGRAM OF A TYPICAL OFFSHORE PLATFORM

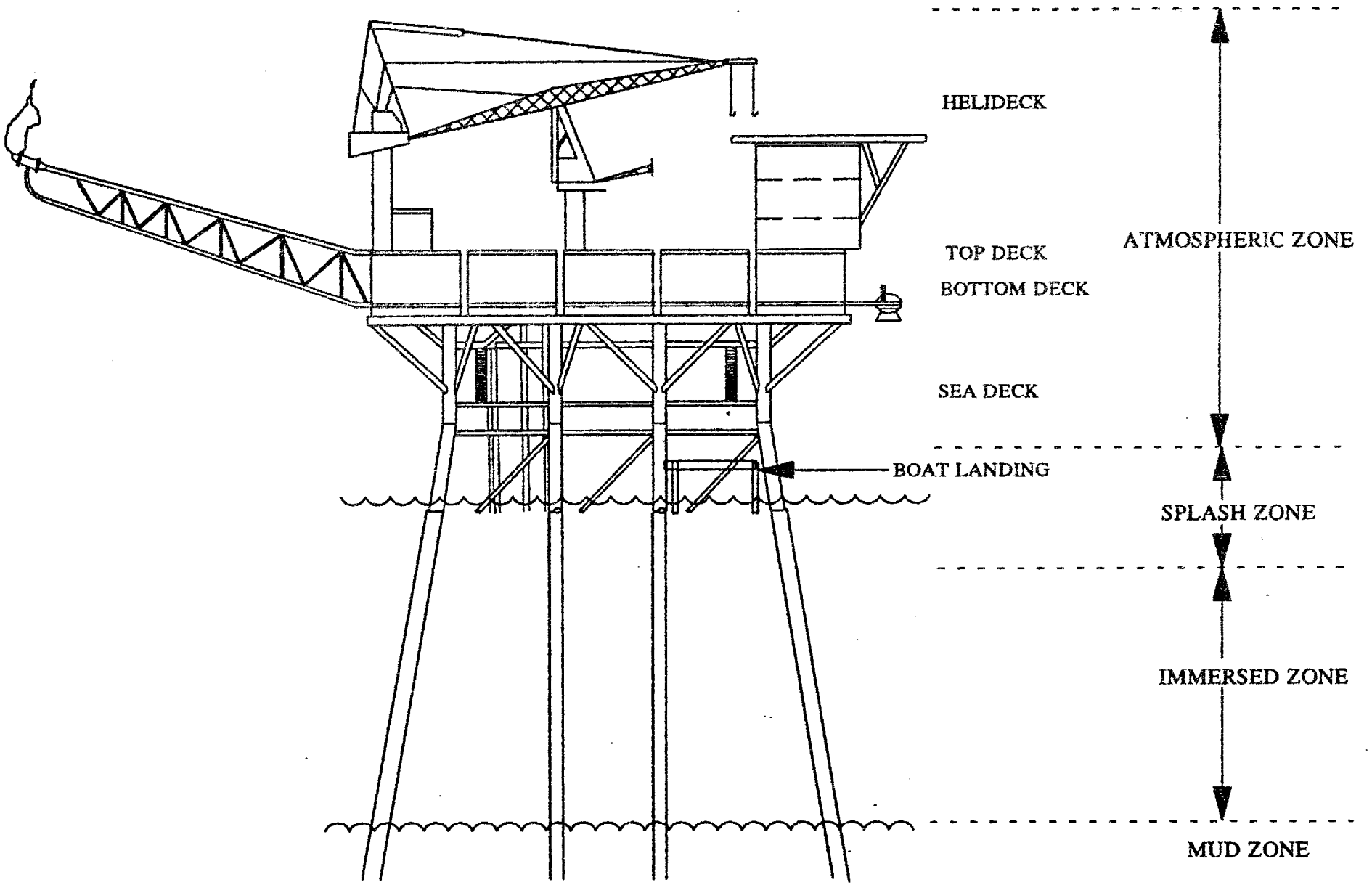

Title : Atmospheric Corrosion of Galvanized Roofing Materials at Makban Geothermal Power Plant Complex

Cynthia V. Bernas and ITDI Corrosion Staff*

Industrial Technology Development Institute
Gen. Santos Ave., Bicutan, Taguig, Metro Manila

Abstract

Exposure test sites were established within the Makban Geothermal Power Plant Complex (MGPPC) to investigate the corrosivitiy of the atmosphere. Two (2) approaches were employed, namely, 1) monitoring of environmental factors (i.e. SO_2, H_2S, airborne salinity or NaCl, dustfall, and time of wetness), and 2) corrosion rate measurement of sample galvanized roofing material by mass loss method.

Evaluation according to ISO proposed category classification of the levels of pollution by SO_2 and NaCl, and time of wetness showed that atmospheric corrosivity ranged from C3 (moderate) to C5 (most severe). However, corrosion rates obtained from the mass loss of galvanized steel specimens were generally higher than ISO given or estimated values.

Corrosion products of selected test specimens were analyzed by XRD, XRF, and SEM/WDX. Estimatation of the service life of galvanized roofing materials at the MGPPC was made based on the corrosion rate measurements obtained. Other roofing materials more suitable to the type of atmosphere were recommended.

---

* N. Rodriguez, A. Viloria, R. Layco, R. Vera Cruz, R. Principe, C. Habana, M. Torre, C. Gayomali, C. Causing, L. de Guzman, and Dr. E. Luis

Mechanism of Stress Corrosion Cracking (SCC) of Titanium Alloys in Nearly Neutral Chloride Aqueous Solution

X. Y. Huang

Metals and Advanced Materials Centre,
Singapore Institute of Standards and Industrial Research,
1 Science Park Drive, Singapore 0511

Abstract

The pH value of the solution in the crack tip region of Ti-5Al-4V and Ti-5Al-2.5Sn under SCC was measured by microelectrode method and indicator paper method to be below 2, while the bulk chloride solution was nearly neutral. The undercritical crack propagation of the SCC in nearly neutral chloride solution was monitored by optical microscope and it was found that micro-cracks had at first been formed in the plastic zone in front of the main crack tip. They then extented themself to join each other and to meet the main crack resulting in discontinuous propagation of the latter. The hydrogen distribution on the fracture surface of SCC was studied by means of SIMS and regular results agreeing with the prediction by fracture mechanics were obtained. Hydride precipitates with fct (a_o=4.44Å, c_o=4.18Å) and bcc (a_o=3.30Å) structure were found on the fracture surface of SCC by XRD and TEM. The fracture surface of SCC was studied by SEM, and it was identified that the fracture surface comprised three different regions, i.e. an intergranular initiation region, a transgranular steady extension region and a rapid rupture one. Based upon these experimental results, the mechanisms of SCC of titanium alloys in nearly neutral chloride aqueous solution, especially the role of hydrogen in SCC of titanium alloys are discussed.

I. Introduction

Titanium and its alloys have been widely used in aerospace, chemical, marine and medical industries because of their high specific strength, corrosion resistance and thermal stability. In some cases, however, titanium alloys suffer from stress corrosion cracking (SCC) in chloride aqueous solutions. Different mechanisms were proposed for SCC of titanium alloys in chloride aqueous solutions. The most important ones are as follows :

(1) Anode path cracking (APC)[1]-[3] : the major argument is that cathodic polarization can inhibit the nucleation and propagation of SCC of titanium alloys.

(2) Cl^-- Attack[4] : It was argued by Beck, that it is Cl^-, but not H^+, which can be enriched in the crack tip region under the potential gradient of the etectric field.

(3) Hydrogen Embrittlement (HE)[5],[6] : hydrogen evolved from the corrosion reaction can penetrate into titanium alloys and cause embrittlement of the materials.

In order to clarify the mechanism of SCC of titanium alloys in chloride aqueous solutions with direct experimental evidences, in the present study, the pH value of the solution in the crack tip region during SCC was measured by two different methods; the undercritical crack propagation of SCC was monitored by optical microscopy; and the fracture surfaces of SCC were investigated by SIMS, SEM and other experimental methods. Based on the experimental results a more comprehensive mechanism for SCC of titanium alloys in chloride aqueous alloys was proposed and discussed.

II. Experimental and Results

Commercially pure titanium, α-type alloy Ti-5Al-2.5Sn and (α+ß)-type alloy Ti-5Al-4V were used in this study. The chemical composition of these materials are listed in Table 1.

Table 1 : Chemical Composition of the experimetal materials

Material	Al	V	Si	Fe	O	H	Ti
C.P.Ti	-	-	-	0.090	0.0090	0.00017	remainder
Ti-5Al-2.5Sn	4.26	-	2.33	0.040	0.0145	0.00145	remainder
Ti-5Al-4V	4.56	3.92	-	0.076	0.0163	0.00069	remainder

In this study, wedge-loaded specimens[7] were used. And 3.5% wt NaCl aqueous solution (pH 6.5) was selected as electrolyte for all experiments. All of Ti-5Al-2.5Sn and Ti-5Al-4V sampels suffered SCC when the applied stress reached a certain level and after a incubation time of about 5 - 15 hours depending on the applied stress and temperature, while none of the pure titanium samples cracked no matter how high the applied stress was.

a. Measurements of the pH valve of the solution in SCC crack tip region

The pH value of the solution in SCC crack tip region was measured by two different methods while the bulk solution remained nearly neutral.

(1) Indicator paper method

After the undercritical crack propagatipn of SCC extended over a few mm, a thin piece of MERK indicator paper was used to touched the crack tip slightly from the outside surface of the sample (similar to the arrangement in Fig. 1) that had been polished and cleaned before the sample was being loaded. At the touch of the crack tip a very little amount of the solution in the crack tip region was absorbed by the indicator paper owing to capillary effect and this changed the colour of the tip of the indicator paper stripe.

(2) Microelectrode Method

A Sb/Sb_2O_3 microelectrode (diameter of the head < 0.5mm) was used as working electrode and a Ag/AgCl electrode was used as the reference electrode. In this exteriment, a very fine piece of lens tissue was placed in front of the propagating crack. As the crack tip reached the tissue, a very little volume of solution was absorbed from the crack tip, and meanwhile the microelectrodes were placed on the wet tissue and the potential difference between both electrodes was measured by a pH-meter (Fig. 1) and recorded. The ΔE v.s. pH characteristic curve of this electrode couple was calibrated by using a set of standard solutions. It has been observed that measurements in bulk solution and on tissue wetted by a small drop of standard solution gave two ΔE v.s. pH curves with slightly different slopes. This difference may be the result of the surface tension of the electrolyte in the latter case and will become important in measurement for steels because the pH value of the solution in SCC crack tip region of steels may be about 3 ~4 [8].

The experimentally measured results are compiled in Table 2. Results by two methods are in good agreement with each other. These results are also in good agreement with

the results on Ti-8Al-1Mo-1V by Brown with fast freezing method[7].

Table 2: pH values of the solution in the crack tip region of Ti Alloys during SCC

Materials	Method	
	Indicator	Microelectrode
Ti-5Al-2.5Sn	2.0	1.8
Ti-5Al-4V	2.0	1.7

b. In situ observation of the undercritical crack propagation of SCC

One suface of the 65 x 45 x 6mm specimens was first polished for metallographic examination, the specimens were then fatigue-precracked, wedge-loaded and put into nearly neutral solution of 3.5% wt NaCl with their polished surface remained exposed to air. Owing to the capillary effect, the crack tip of the surface layer was still filled with the solution. The development of the plastic zone and cracking were followed with a metallograph.

As a typical example, Fig. 3 shows the observed undercritical cracking process of SCC of a Ti-5Al-2.5Sn sample. At the start, a small plastic zone A was formed in front of the crack tip just after the sample was being loaded (Fig. 3(a)). After 70 hours, the plastic zone had grown slightly, and near the plastic-elastic border, a fine crack had been formed at B and another fine crack had been forming at C (Fig. 3(b)). After 120 hours, crack B propagated backward to meet the main crack at F, and extended forward to connect with C, and a new crack had been formed at D (Fig. 3 (c)). These processes were repeated and the SCC was thus advanced.

c. Determination of the formation of hydride on SCC fracture surface by TEM and XRD.

Several fine samples were cut from fractured SCC samples, further thinned by double jet electrolytical polishing with a mixed electrolyte (methyl alcohol : n-butyl alcohol : perchloric acid = 10 : 6 : 1) and then investigated with TEM. In all samples cut from SCC fracture surface fine precipitates, that could not be seen with any optical microcope, were observed. Using selected region electron diffraction it was determined that these fine precipitates were TiH_2 with fct lattice (a_o=4.44 Å, C_o=4.18Å) and metalstable hydride with bcc lattice (a_o=3.32Å). No hydride precipitate has been found in samples cut from the parts far from SCC fracture surface.

The characteristic X-ray diffraction peaks of above mentioned fct hydride have been obtained on relatively smooth area of the SCC fracture surface by carefully selecting scanning speed and time constant.

d. Determination of H distribution on SCC fracture surface by SIMS

Relative hydrogen content on the SCC fracture surface along the longitudinal middle line was measured by SIMS just after the fracture of a Ti-5Al-2.5Sn sample. Argon ion beam with energy of 15 KeV was used. The beam diameter was about 133 μm and the mean distance between measurement points was about 0.6mm. At each point a pre-sputtering of about 60 seconds was carried out in order to eliminate the interference from the adsorbed layer.

The measured intensity of the second hydrogen ion tream seemed, however, unregular from point to point because of the geometry effect of the fracture surface. The intensity of hydrogen ion stream was consequently normalized to the intensity of total second ions stream. The normalized intensity of hydrogen ion stream reflect the relative hydrogen content on the fracture surface. These results were shown in Fig. 4. One can see that there is a peak at the point about 2 mm from the fatigue crack tip that was about the position of the plastic-elastic border in front of the crack.

e. Fractography of Titanium Alloys in SCC by SEM

The SCC fracture surfaces of Ti-5Al-2.5Sn and Ti-5Al-4V were investgated by SEM. Typical fractographs are shown in Fig. 5 and Fig. 6 respectively. The SCC fractographs were brittle in appearance with many cleavage facets and secondary cracks, while the fracture surfaces of the same alloys by fast tear in air show typical ductile fractographs with dimples. What interesting is that there is an intergranular fracture zone of ca. 100 μm in width between the fatigue-crack and SCC fracture surfaces, some corrosion products are visible on the intergranular facets as shown in Fig. 7. One can also see some small round holes on the corrosion products. These may be formed through some gas bubbles that arose during the corrosion in the initiation stage of SCC. At the end of this intergranular cracking band many fine secondary cracks have been observed.

III. Discussion

a. Incubation of SCC of Titanium Alloys

At the fatigue-crack tip (or any other surface microcrack in practical cases) the concentrated stress caused local plastic deformation in front of the crack tip (Fig. 3 (a)). During such plastic deformation a great amount of dislocations moved out of the alloy and formed slip steps at the crack tip surface. The surface passive film at these slip steps was damaged and the bare metal was exposed to the electrolyte leading to local active titanium dissolution. The crack was very narrow and its path was zigzag so that formed an occluded cell with the crack tip as the anode and the crack wall away from crack tip as the cathode. In anode region (at the crack tip) titanium dissolved as Ti^{3+} and the latter reduced the pH value of the local solution through the hydrolysis reaction:

$$Ti^{3+} + 3H_2O \rightarrow Ti(OH)_3\downarrow + 3H^+$$

This reaction, in fact, led to the measured low pH value of the crack tip electrolyte and finally controlled it. The hydrogen evolution then occurred locally in the vicinity of the crack tip. The cathodic reaction first consumed the dissolved oxygen in the crack electrolyte and this resulted in the hydrogen evolution as cathodic reaction. Increasing concentration of Ti^{3+} and H^+ at the crack tip region built up a electric field in the crack. Under the potential gradient of the electric field Cl^- diffused from outside to the crack tip and enriched there. All above mentioned processes taking place in the crack tip electrolyte (acidification, oxygen depletion and Cl^--enrichment) inhibited the self-repairing of the passive film at the crack tip surface and kept the metal to be bare and the dissolution of titanium to continue. This is a selfcatalyzed process. The active path for the anodic dissolution in titanium alloys was proved to be grain boundaries as shown in Fig. 7. The atomic hydrogen evolved at crack tip has two ways to go: one is to combine with each other to form hydrogen molecules and then to escape as hydrogen bubbles leaving the traces as can be seen in Fig. 7; another way is to be absorbed into the metal and to cause local embrittlement so that many fine secondary cracks were observed at the end of the intergranular incubation band of SCC of titanium alloys.

In the case of pure titanium the radius of the fatigue-crack tip under load is always too big (in the magnitude of 0.1~0.5mm)to cause a high stress concentration and to form occluded cell as a result of its low strength. Therefore, like other pure metals, pure titanium dose not suffer from SCC.

b. The role of hydrogen in SCC of titanium alloys

After penetrating into the metal, hydrogen diffused to the region of high, three-axial stress at the plastic-elastic border in front of the crack tip owing to the stress gradient. The final hydrogen distribution on the SCC fracture surface shows a very obvious

similarity to the stress distribution in front of the crack according to fracture mechanics[9](Fig. 4). The enriched hydrogen precipitated out as hydrides on their habit planes. In the case of α-titanium alloy they are mainly {0001}[10]. In the case of (α+ß)-titanium alloy hydrides usually precipitate at the α/ß-phase boundaries on the α-phase side. Titanium hydrides are brittle phases, their fracture strain are only 1~2% at 150°C[11]. The phase boundary between hydride precipitates and titanium matrix is an unstable interface with very high energy because of the much higher specific volume of hydrides. Therefore, both of them are easy to be cleft to initiate microcracks. Stress was concentrated at such microcrack tip too, and enriched hydrogen assisted the growth of such microcracks at their two tips. This is the reason for the observed discontinuous undercritical crack propagation of SCC (Fig. 3) and the brittle fracture morphology with many cleavage facets and secondary cracks of SCC (Fig. 5 and Fig. 6).

c. Polarisation as a method to distinguish mechanisms of SCC ?

From the discussion above one sees a comprehensive mechanism of SCC of titanium alloys. In the initiation stage APC mechanism plays a major role and Cl^--attack is an important condition of APC, while HE mechanism plays a very important role in the undercritical crack propagation of SCC. However, there is a prevalent opinion that one can use polarization as a method to distinguish mechanisms of SCC: those, which can be inhibited by anodic polarization, must be HE; while those, which can be inhibited by cathodic polarization, must be APC[12]. But, in some cases, this principle seems to be too simple. One should be careful to use the polarization method. For example, cathodic polarization will certainly evolve hydrogen at the surface of titanium alloys, but, at the same time, the pH value of the electrolyte near the surface (including the crack tip electrolyte) will be rapidly raised[13]. The Cl^--concentration near the surface will be rapidly reduced, the surface passive film will be then repared. The highly stable impermeable film[14] on the surface will resist the entrance of hydrogen into titanium alloy. This is why cathodic polarization can, under some conditions, inhibit the initiation and undercritical propagation of SCC but this not can be used as a argument to reject the HE mechanism for SCC of titanium alloys.

IV. Conclusion

SCC of titanium alloys in nearly neutral chloride aqueous solution is quite a complicated process. At some fine surface cracks the concentrated stress and the occluded cell effect can change the chemical and electrochemical conditions at the crack tip, including the acidification of the crack tip electrolyte, oxygen depletion and Cl^--enrichment at the crack tip. These changes finally initiate SCC through intergranular

APC. The atomic hydrogen, that is evolved during APC process of the SCC incubation stage, will be absorbed into titanium alloy and be enriched through diffusion in the region of high, three-axial stress in front of the crack tip to form hydride precipitates. The latter consequently leads to the discontinuous undercritical crack propagation of SCC through HE mechanism.

References

[1] H. P. Leckie: Corrosion, 23 (1967) 187.
[2] T. R. Beck: J. Electrochem. Soc., 114 (1967) 551.
[3] I. L. Rosenfield et al.: EUROCO'77 (1977) 485.
[4] T. R. Beck: in "the Theory of SCC in Alloys", (1971) 64.
[5] D. T. Powell and J. C. Scully: Corrosion, 24 (1968) 151.
[6] H. G. Nelson: in "Hydrogen in Metals", ASM, (1974) 445.
[7] B. F. Brown et al.: J. Electrochem. Soc., 116 (1969) 218.
[8] J. C. Scully: in "Localized Corrosion", NACE-3, (1974) 144.
[9] G. R. Irwin: Proc. of Sagamose Ordnamoce Materials Research Conf., IV, (1961) 63.
[10] J. D. Boyd: Trans. ASM, 62 (1969) 977.
[11] P. E. Irving and C. J. Beevers: J. Met. Sci., 7 (1972) 23.
[12] M. G. Fontana: Corrosion Engineering, 3rd Edition, (1987) 109.
[13] L. C. Covengton: Corrosion 35 (1979) 378.
[14] O. W. Johnson et al.: J. Appl. Phys., 46 (1975) 1026.

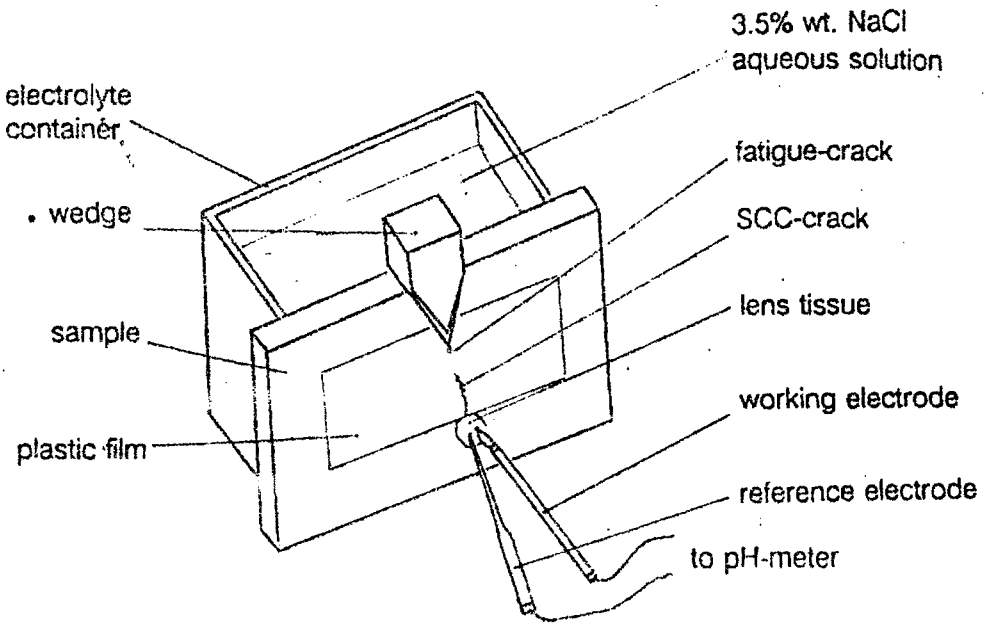

Fig. 1 Schematic diagram of the experimental set-up for the measurement of pH value of the crack tip electrolyte during SCC of titanium alloys.

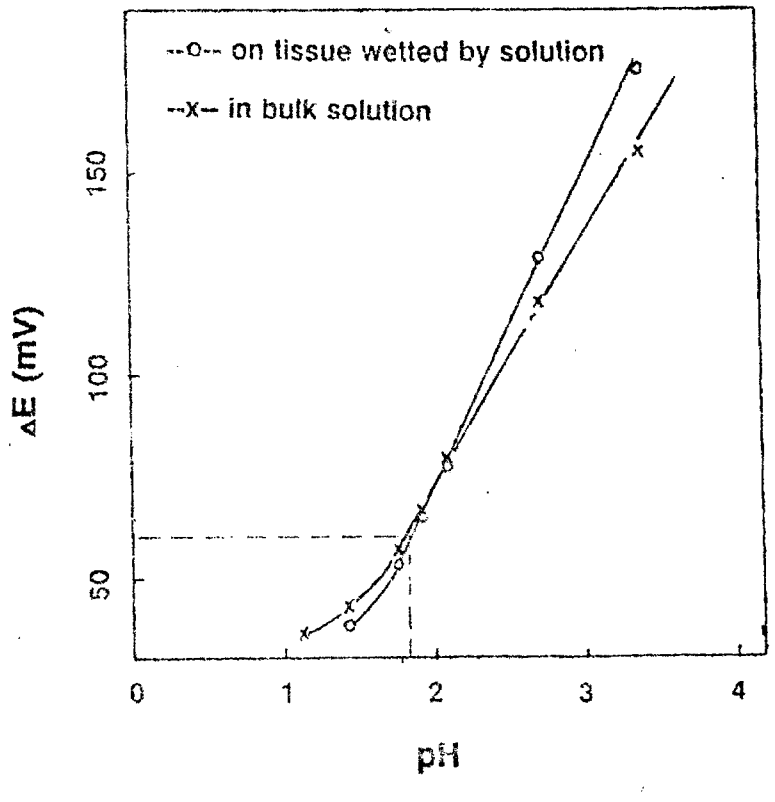

Fig. 2 The characteristic ΔE ~pH curves of Sb/Sb_2O_3 and Ag/AgCl microelectrode couple.

(a) t = 0

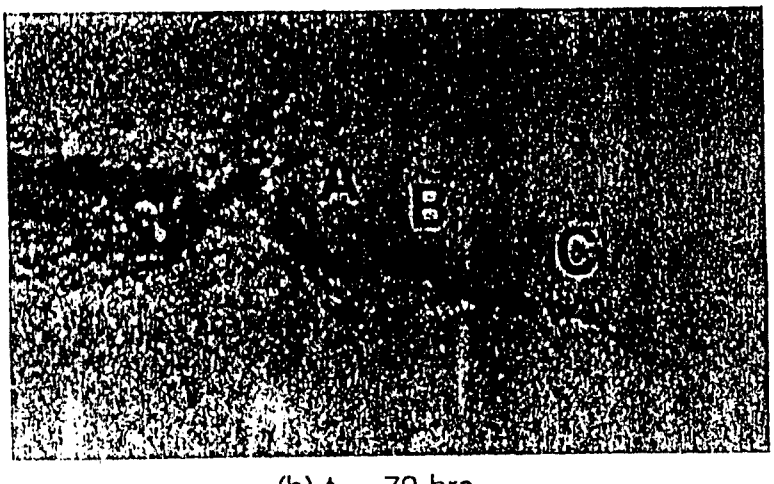

(b) t = 70 hrs

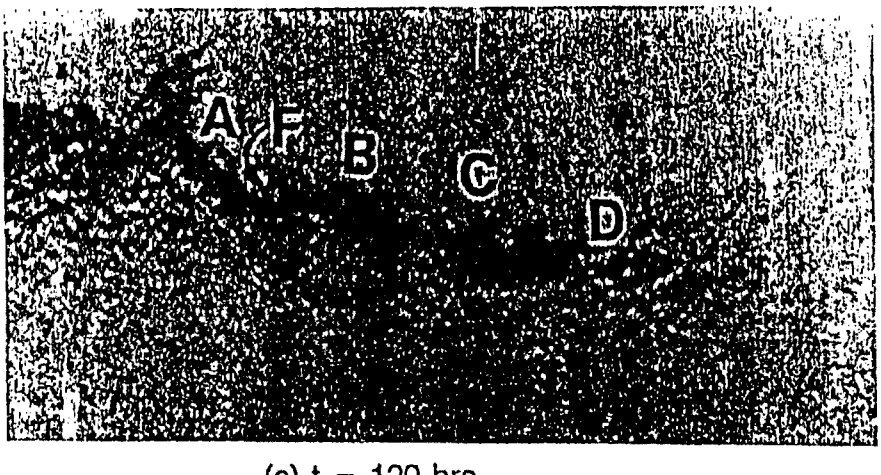

(c) t = 120 hrs

Fig. 3 Undercritical crack propagation of SCC of Ti-5Al-2.5Sn in nearly neutral 3.5%wt NaCl solution. (64x)

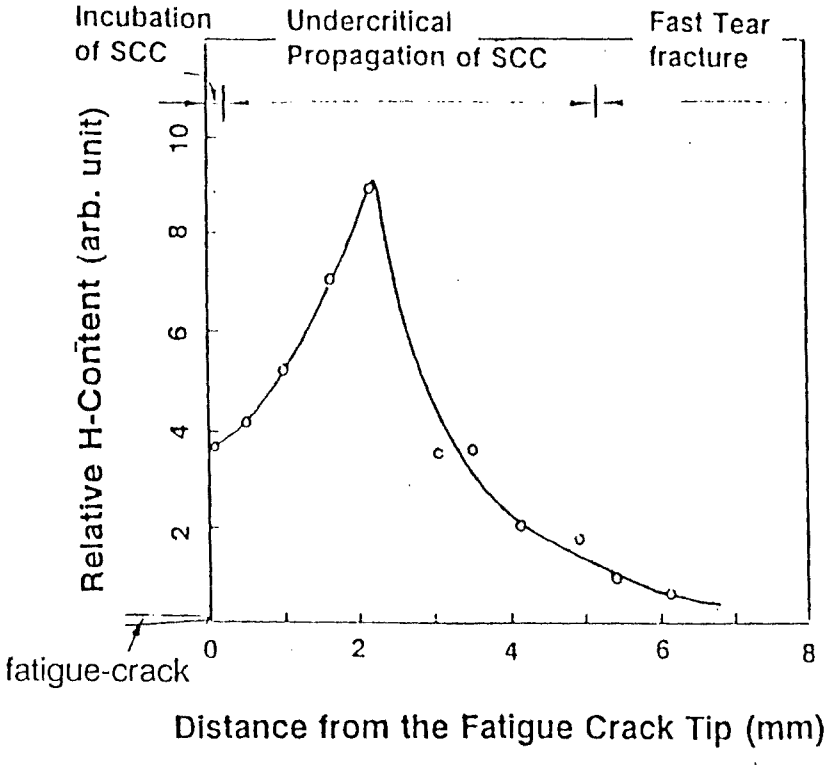

Fig. 4 Hydrogen distribution on the SCC fracture surface of a Ti-5Al-2.5Sn sample in nearly neutral 3.5%wt NaCl solution determined by SIMS.

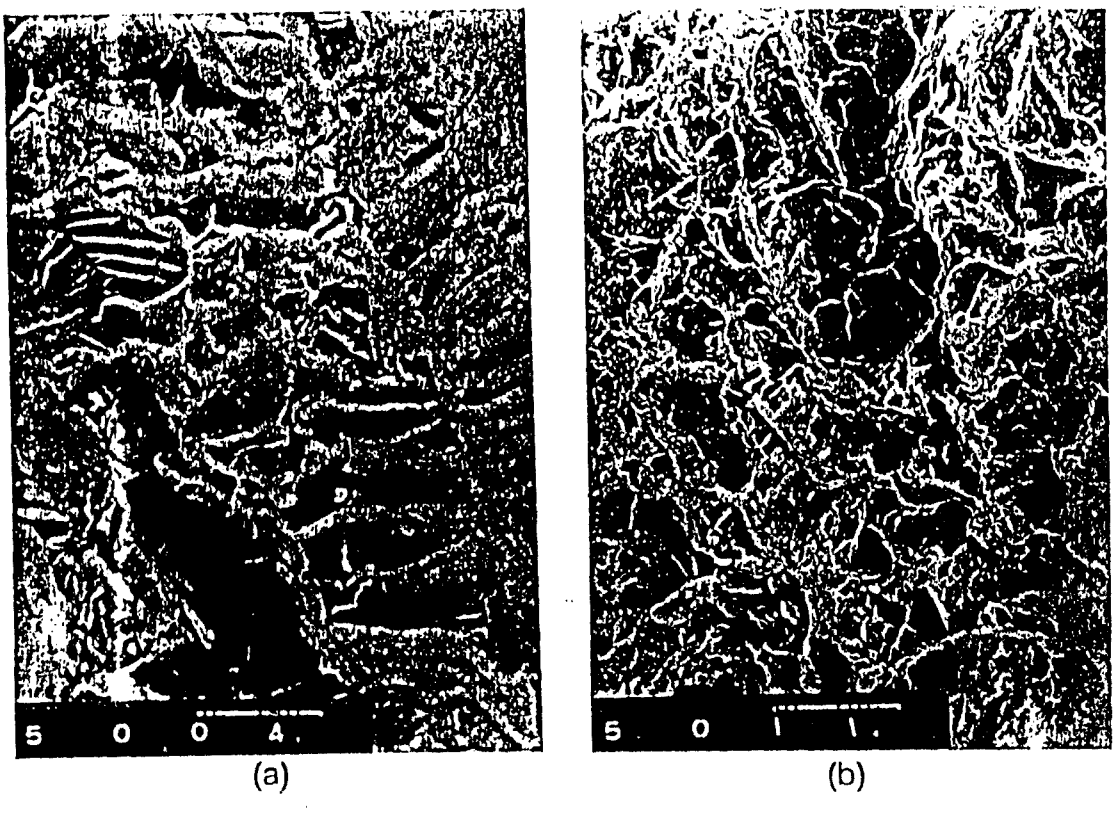

Fig. 5 Miro-morphology of SCC fracture surface (a) and fast tear fracture surface (b) of a Ti-5Al-2.5Sn sample by SEM. (720x)

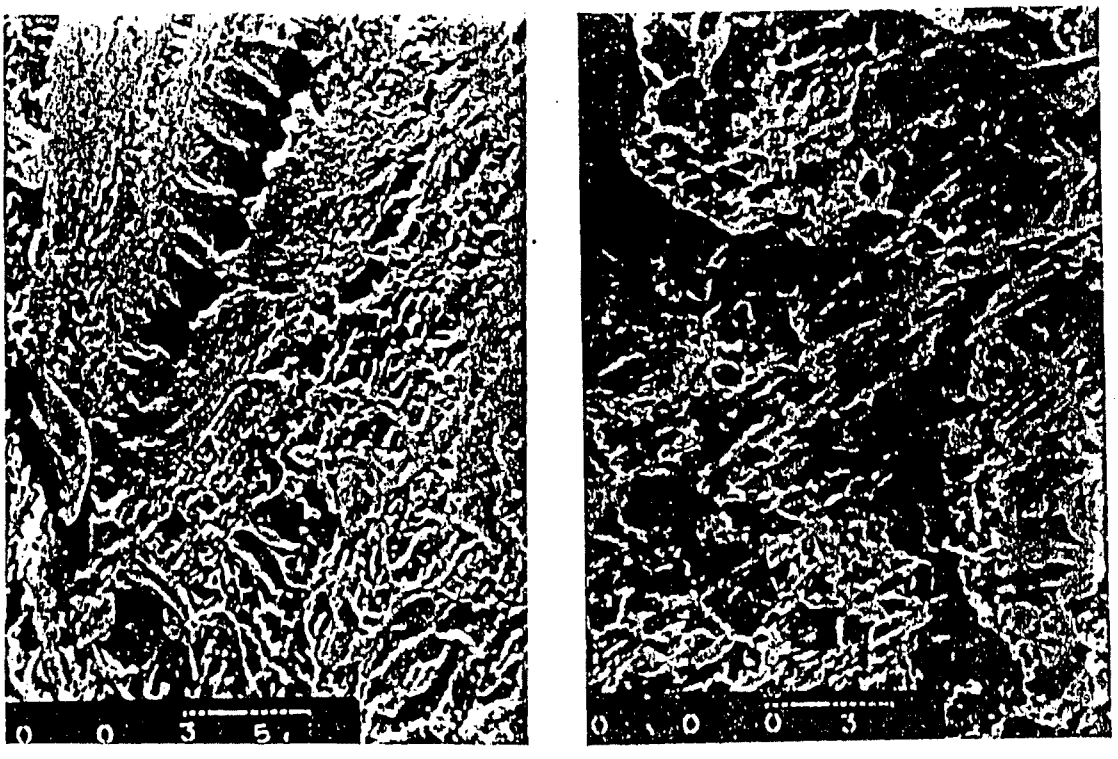

(a) (b)

Fig. 6 Miro-morphology of SCC fracture surface (a) and fast tear fracture surface (b) of a Ti-5Al-4V sample by SEM. (1200x)

Fig. 7 Mico-morphology of the incubation band of SCC of a Ti-5Al-4V sample by SEM. (1200x)

CREEP DAMAGE OF CATALYST TUBE AND PIGTAIL OUTLETS IN STEAM REFORMER FURNACE OF HYDROGEN MANUFACTURING UNIT

Mr.Narong Sukapaddhi

Thaioil Co.,Ltd.

Abstract

The paper describes the premature failur of a steam reformer tubes, material HP alloy 25Cr/35Ni Nb in a short period of 20,880 hours. The damage is due to creep, leading to eventaul rupture. Based on the investigation at plant S/D in 1991, failed and not yet failed tubes were found to have microstructure transformation in the regime of temperature range of 950-1,000° C. This can well be attributable to the accelerated creep damage to the pigtail outlets of material incoloy 800 H. The failure analysis will be given and discussed in more detail.

CREEP DAMAGE OF CATALYST TUBE AND PIGTAIL OUTLETS IN STEAM REFORMER FURNACE OF HYDROGEN MANUFACTURING UNIT.

NARONG SUKAPADDHI

1. SUMMARY

The paper describes the premature failure of a steam reformer tubes, material HP alloy 25 Cr/35 Ni Nb in a short period of operation of 20,880 hours. The damage is due to creep, leading to eventual rupture. Based on the investigation at plant S/D in 1991, failed and not yet failed tubes were found to have microstructure transformation in the regime of temperature rage of 950−1,000 C. This can well be attributable to the accelerated creep damage to the pigtail outlets of material Incoloy 800 H. The failure analysis will be given and discussed in more detail.

2. INTRODUCTION

The hydrogen manufacturing unit is equiped with a steam reformer furnace, where hydrogen gas is produced for hydrocracking unit. The radiant section consists of a single cell top fired combustion chamber with 4 rows of tubes hanging in vertical by spring suspension with 32 tubes in each row, total of 128 tubes (Fig.1).

Two adjacent rows of catalyst tubes are connected to one of two manifolds underneath the furnace floor by the so−called pigtails which are made of Incoloy 800 H tube material of 24.3 mm.in ID and 4.7 mm.thick. The two subheaders are centrifugally cast in material grade 20 Cr/33 Ni Nb.

Since it was commissioned only a few minor problems were encountered. In February 1991, the unit was shutdown to repair a leaking drain nozzle on the boiler, downstream of the reformer. On restart it was noticed that there were some tubes in the reformer which were significantly hotter than the rest (i.e. the skin temperatures were significantly higher than normal). ICI Catalysts were contacted to ask their advice as to what action to take. Thai Oil were adviced as to run the reformer at a very high steam ratio, as it was felt that the cause may be due to carbon laydown. Thai Oil operated the reformer on steam only 8 hours, but when feed was re−introduced, the number of hot tubes had increased by 2 or 3 from the initial apparent two tubes in January 1991, and there had been no improvement in the appearance of the existing hot tubes.

Only onstream skin temperature were measured and observed. As well as pigtails were seen red hot (Fig.2) through insulation gaps.

On 13rd August 1991 the catalyst tube C−2 was found leaking and blue flame impingement at four tubes in the row "B"was observed. The life of the refromer furnace was 20,880 hours on the day of leaking. The crack tube was isolated by nipping inlet and outlet pigtails on stream on 14th August 1991. This tube was remained in leaky condition for about 40 hrs. At the turnaround November 1991, this tube was removed from pigtails. Their remained pigtails were capped by seal weld. Up to this turnaround, the reformer tube had been in the furnace for about 23,040 operating hours.

During a maintenance shutdown of the HMU inspection of the outlet pigtails of the HMU furnace revealed that bulging had occured in the first section of tube in a large number of locations as shown in Fig.1.

Measurements indicated that diameters had increased by up to 10% but that after the first weld diameters were nominal.

Microstructual evaluations indicated that the cause of bulging was creep damage.

Further investigation were then undertaken in more detail in article 5.0, since the furnace had only been in operation for approximate 3 years and creep damage should not have occured.

It was noted here that the D−19, one of hot tube (919C) after completed first weld joint was broken off at the reducer, which was resulted from excessive bending to align it to the second weld preparation. It was then cut and plugged as same as C−2 (burst tube).

The samples were sectionally cut from D−9 at three different locations, including its reducer for further metallurgical investigation and future reference. Findings were given in detail of articles 4.1.4 and 4.1.5.

3. DESIGN AND OPERATING CONDITIONS

Reformer Tube Materials		:	ASTM A−297 HP 25 Cr/35 NiNb	
Dimensions Outside Dia.		:	123.8	mm.
Inside Dia.		:	100.0	mm.
Minimum Sound Wall thk.		:	11.9	mm.
Length		:	12260	mm.
Design Condition of Catalyst tube	Temperature	:	925	
	Pressure	:	27.2	Barg.
Operating Condition of Gas	Inlet Temp	:	550	C
	Pressure	:	26.95	Barg.
	Outlet Temp	:	875	Barg.
	Pressure	:	24.2	Barg.

4. FAILED CATALYST TUBE INVESTIGATION

The failure of C−2 occured at about 1/5 of total length from the top (endothermic zone) and it exhibited longitudinal splitting which numerous microcrystalline cracks orientating in the same direction. Bulging was found in burst area, resulting in diameter growth or creep damage of 10.2%. The dimension of tube was 138.6 mm. In OD, 111.5 mm. In bored ID (see sketch in Fig.3). Wall thickness at bulging was 12.54 mm. against 13.5 mm. at opposite side, because of plastic yielding from hoop stress.

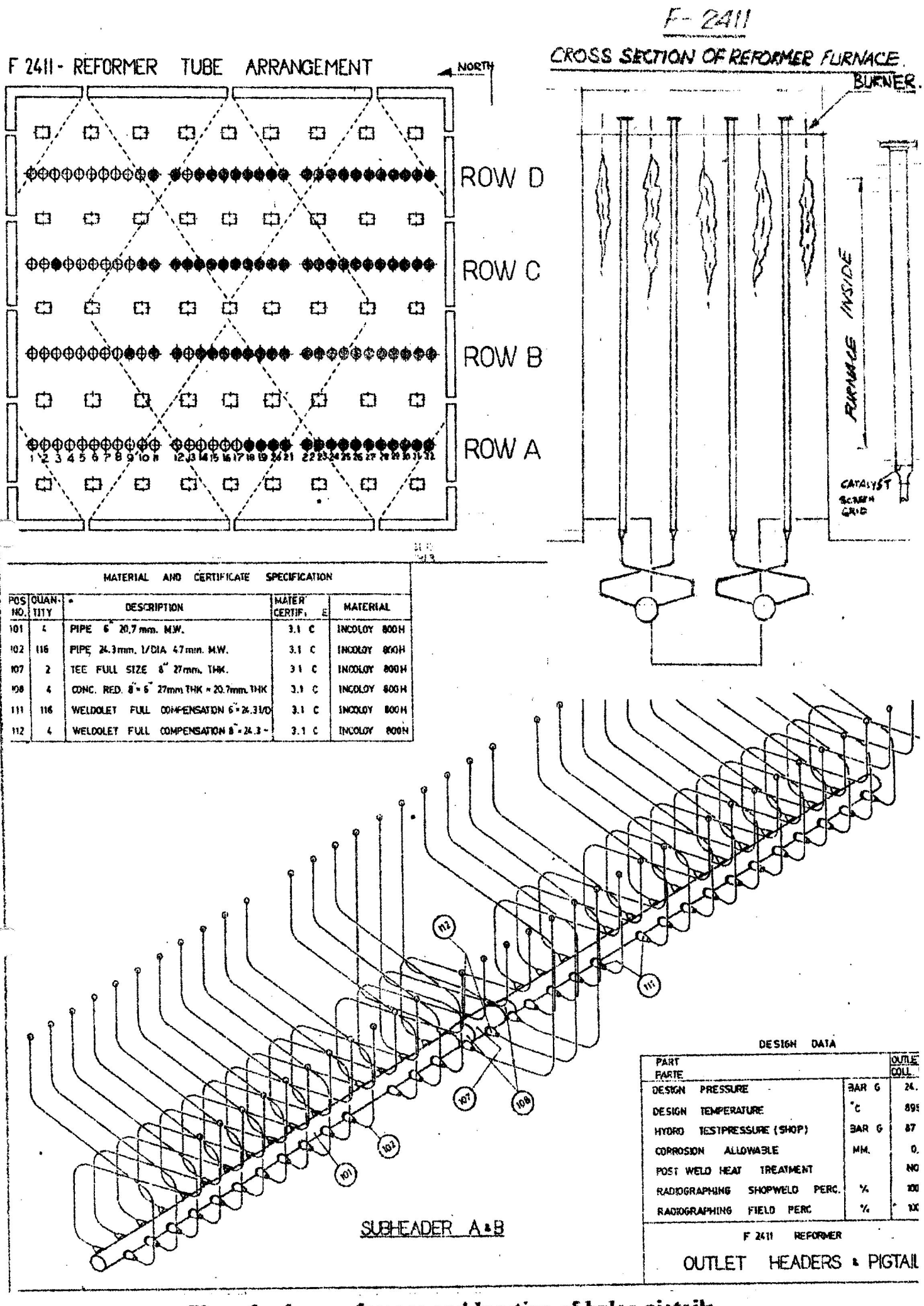

Plan of reformer furnace and location of bulge pigtails.

Fig.1 Hydrogen plant reformer furnace.

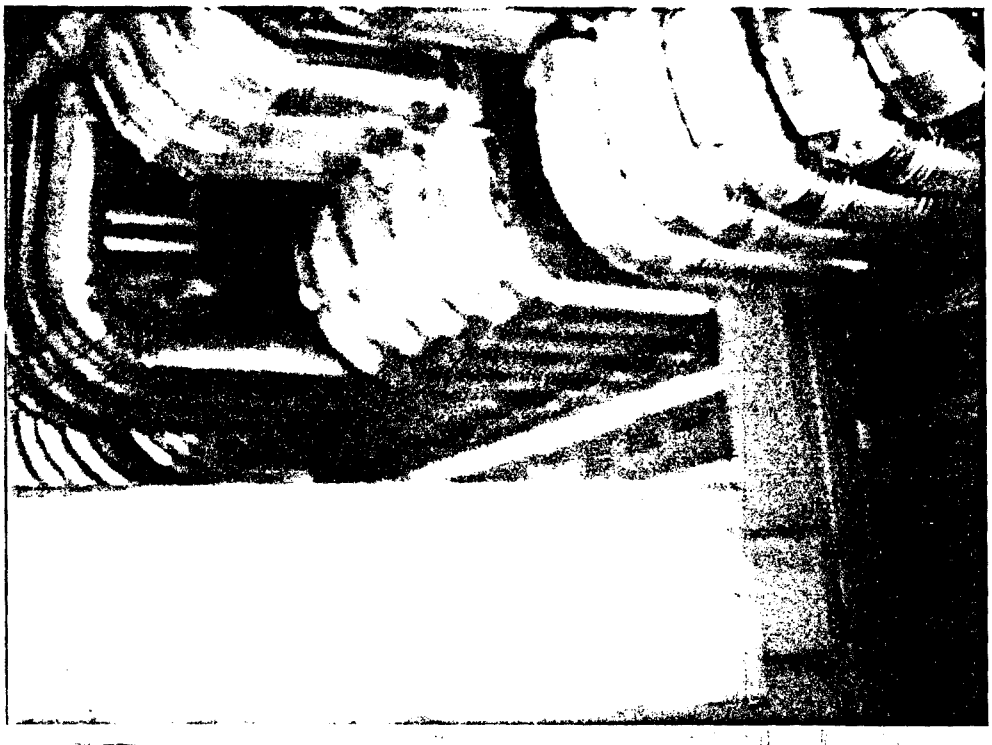

Fig.2 Red hot pigtails observed at insulation gap.

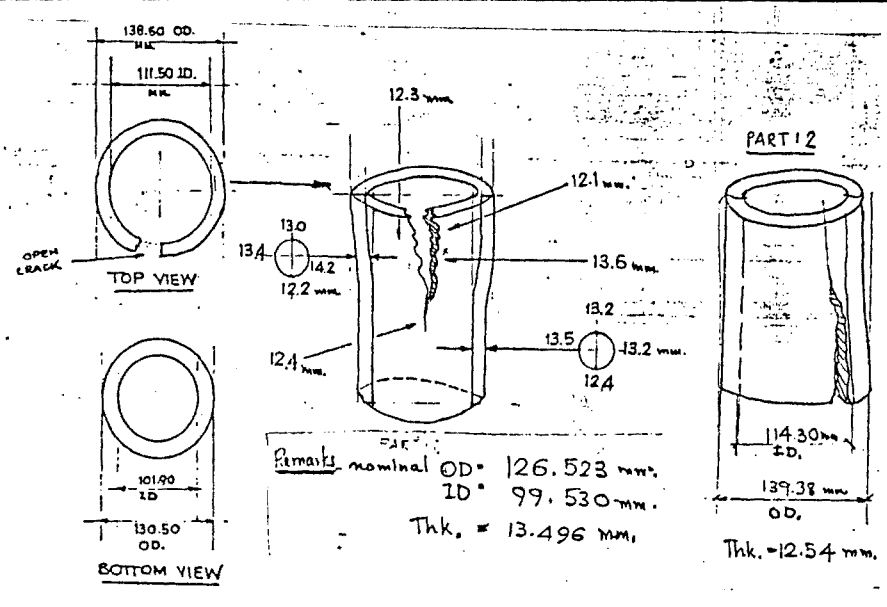

Fig.3 Sketch of the rupturing reformer C–2.

Three sections of burst reformer tube C–2 were investigated, namely the top part, burst area and the bottom prior to the catalyst screen grid, to represent the different thermal gradiants.

The original tube was made of centrifugal casting technique from HP alloy of the chemical composition as shown in table 1 which complied with relevant standard.

TABLE 1 CHEMICAL COMPOSITION OF C–2 TUBE

C = 0.2456	Si = 1.6252	S = 0.0077	P = 0.0085
Mn = 1.0269	Ni = 41.161	Cr = 23.755	Mo = 0.0559
Cu = 0.2005	Al = 0.0187	Nb = 2.1473	Ti = 0.0084
V = 0.0515	W = 0.1285	B = 0.0008	

The following paragraphs gave description of metallographic examination of the sample of crack tube.

4.1 METALLURGICAL EXAMINATION

4.1.1 RUPTURE SPECIMENS

The metallographic structure of the base material, in the vicinity of the fracture surface (Fig.4), was characterised by the presence of interdendritic phase with some secondary carbide in austenitic matrix.

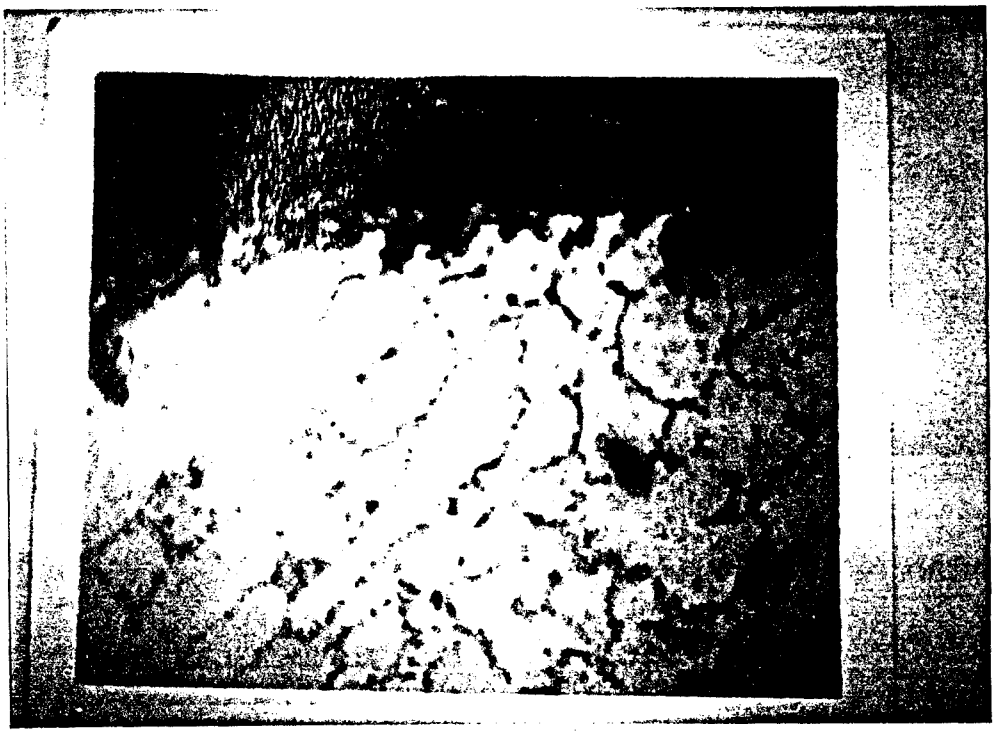

Fig.4 Microstructure at fracture surface 200x. Marakumi Etchant.

There was an evidence of fusion zone (Fig.5) due to excessive skin temperature, (local remelting/or plasticization of the material) at rupture surface, Fig.6 demonstrated severe internal oxidation of metal matrix at crack surface. Fissuring extending from oxidized surface was observed in Fig.7 having creep voids developing at eutectic carbides in Fig.8.

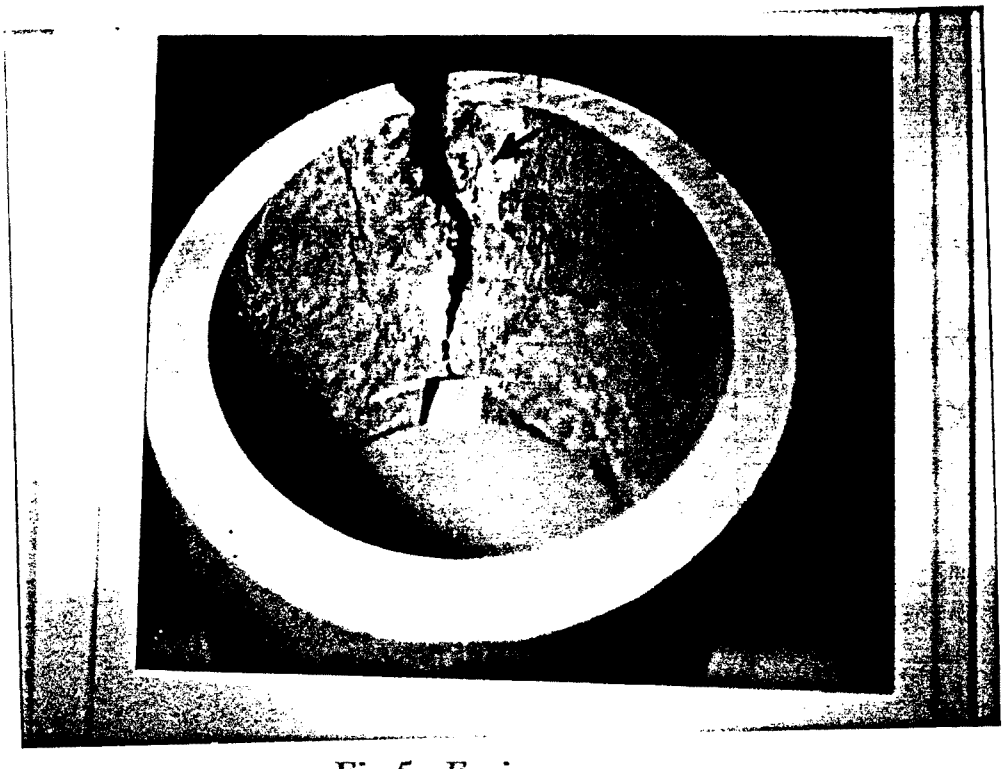

Fig.5 Fusion zone

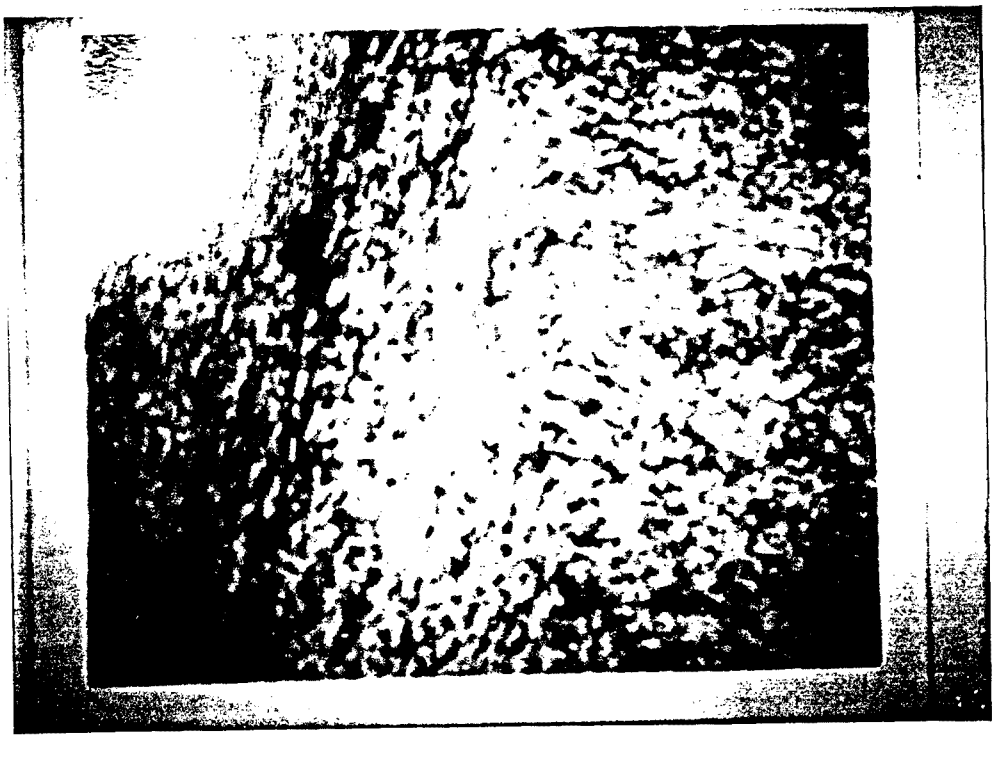

Fig.6 Internal oxidation

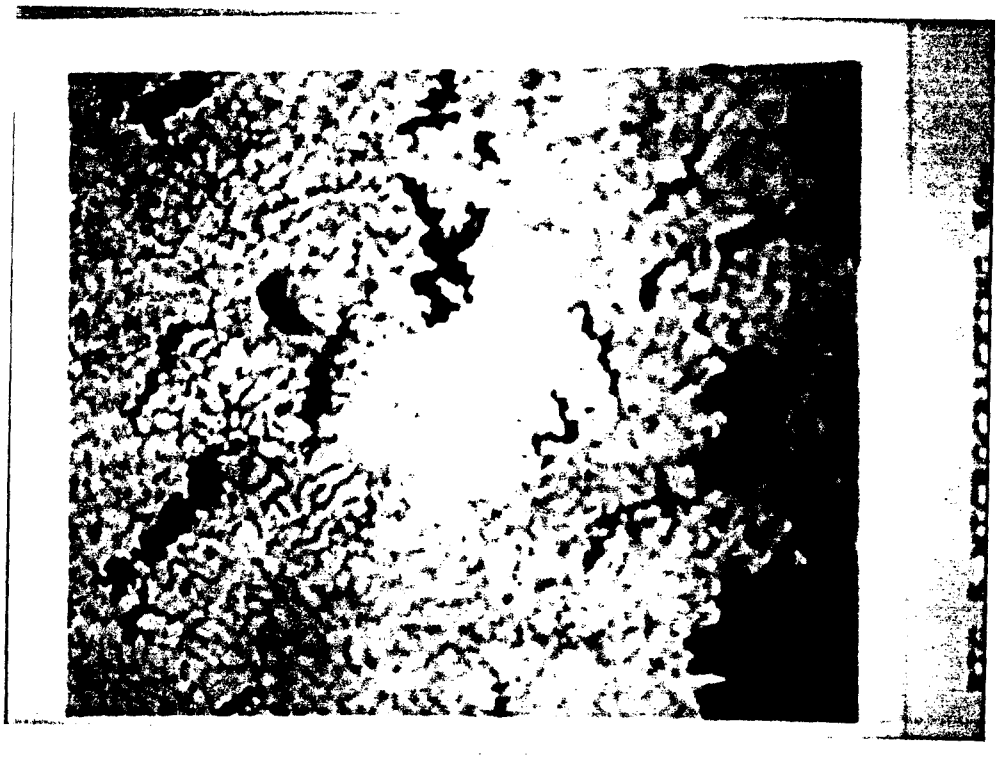

Fig.7 Microcracking of fissuring at grainboundaries and oxidation. 50 x.

Fig.8 Oriented cavitation at eutectic carbides, Murakami Etchant. 1000 x.

Microstructure at the proximity of cracked tip (Fig.10) consisted of similar phases as mentioned above but eutectic carbide coarsening and carbonitride were present in Fig.11 and 12 at higher magnification, meanwhile secondary carbide in grain was very few but coalesced as seen in Fig.13 and 14. This was due to the resolution of carbide at elevated temperature in survice,creep voids were occasionally developed in the eutectic carbides at the advancement of crack tip.

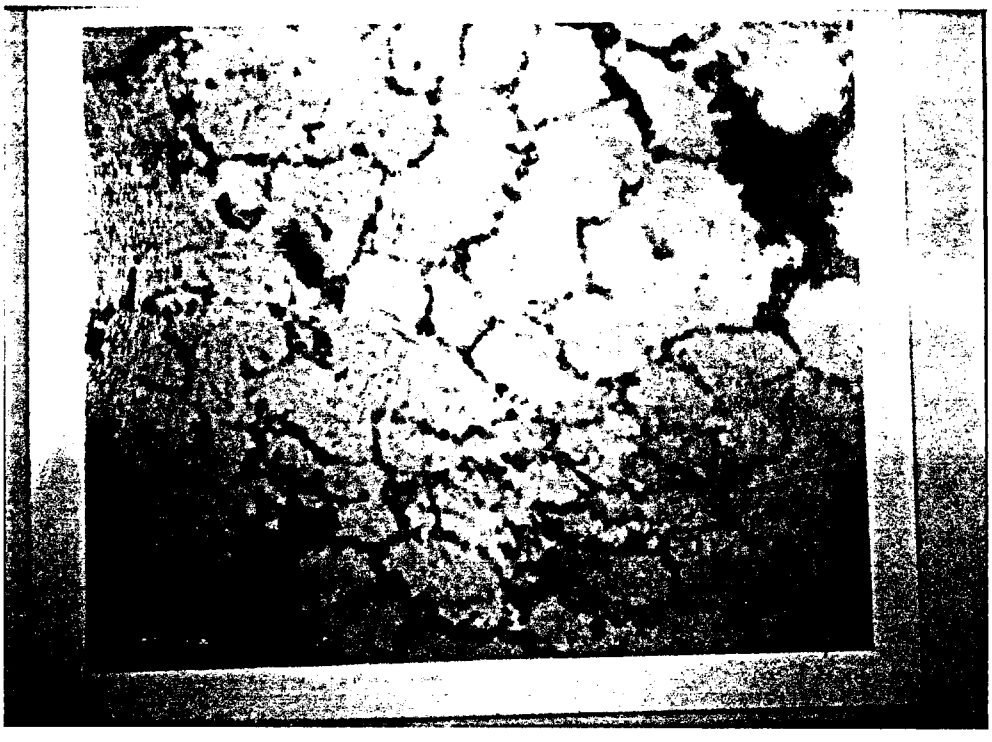

Fig.9 Microstructure at crack tip showed eutectic carbide network and carbonitride. 200 x Murakami Etchant.

Fig.10 Carbide coarsening with isolated voids and carbonitrides. 400 x.

Fig.11 Same as Fig.10 but at 400x showed carbonitride platelets.

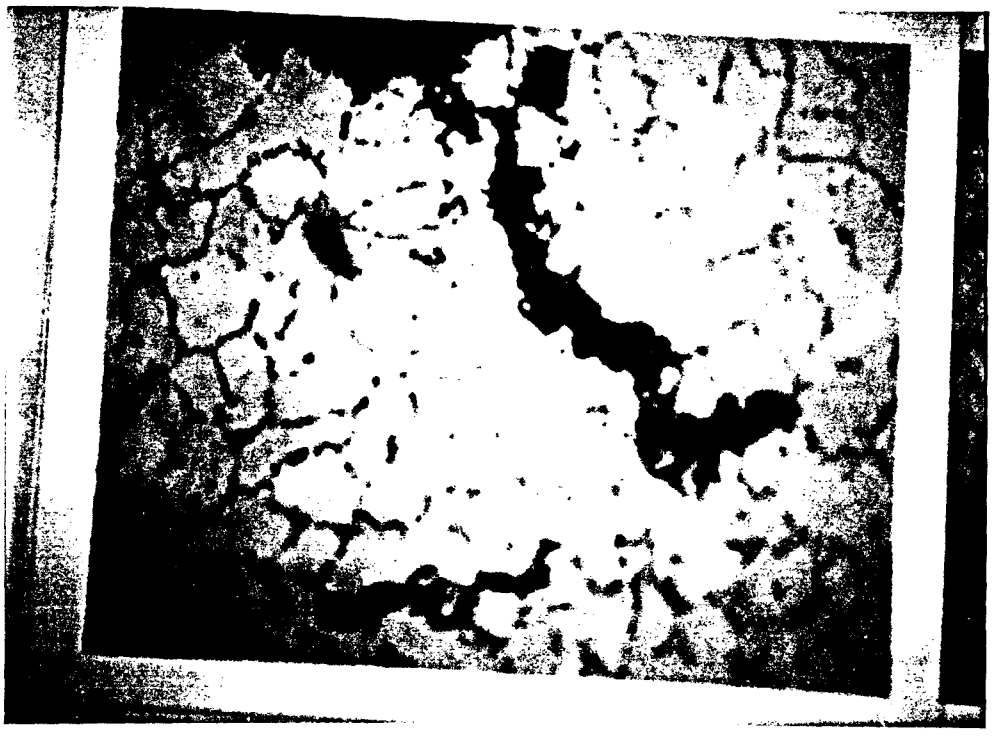

Fig.12 Crack tip area showed few secondary carbides. 200 x.

Fig.13 Some coalesced carbide and voids surrounded by carbides. 1000 x.

Microstructure at diametrically opposed part to rupture (Fig.14) shows massive eutectic carbide and coalescence of secondary carbide due to resolution. Sigma phase could be faintly visible in eutectic carbide patches at higher magnification in Fig.15 (faint grey).

Fig.14 Microstructure of diametrically opposed to rupture. 400 x.

Fig.15 Sigma phase at eutectic. 1000 x.

4.1.2 TOP PART SPECIMENS

Investigation of microstructure at the top part suggested that the skin temperature had been around 900 C as continuous carbide networks were present (Fig.16), some eutectic carbides were partially decomposed (Fig.17). The result of nipping had increased skin temperature of failed tube to this range.

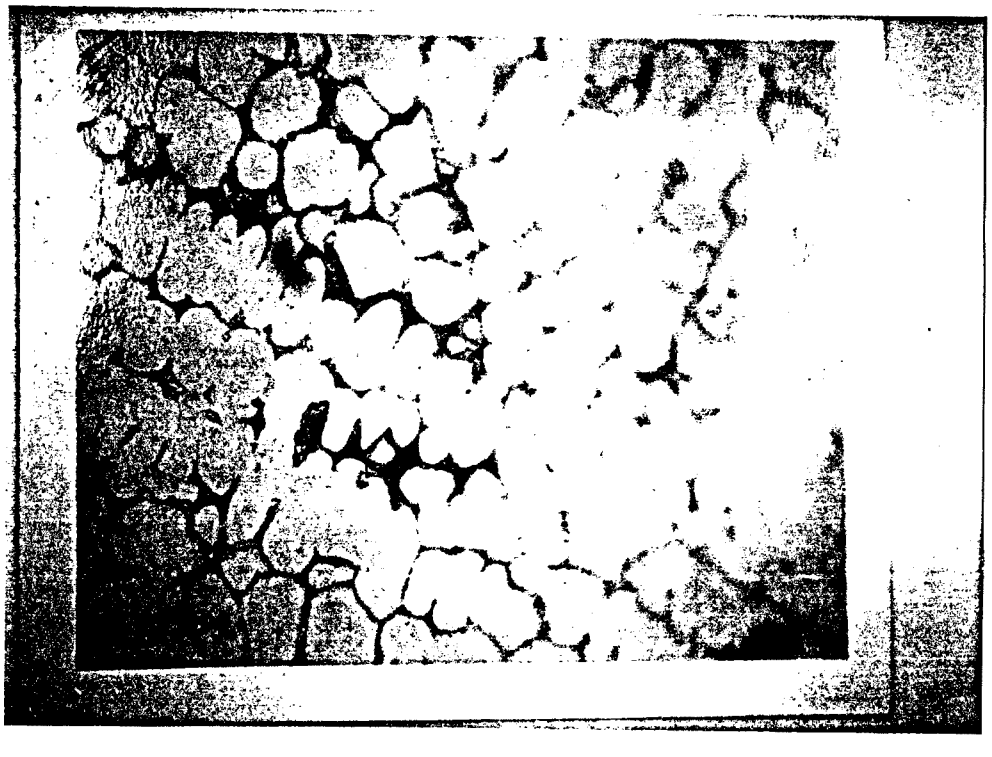

Fig.16 Microstructure of top part showed continuous carbide networks 200 x. Villela Etchant.

Fig.17 Same as Fig.16 but at 1000x showed partially decomposed eutectic carbide island.

4.1.3 BOTTOM PART SPECIMENS

Fig.18 showed microstructure of reformer tube specimen cut from the bottom part diametrically opposed to each other. Thick continuous grainboundary carbide networks were evident and coalesce carbides in austenitic were numerous. But voidage was not yet developed (Fig.19). This part was assumed to be in the temperature range at the area opposite to the crack.

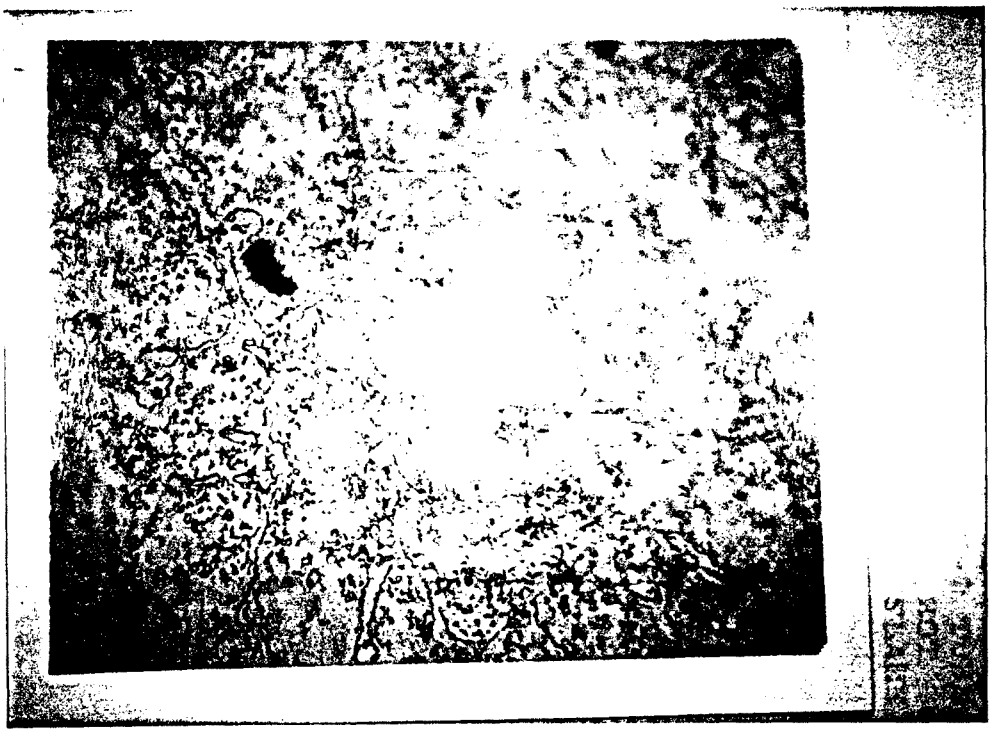

Fig.18 Showed microstructure of reformer tube at bottom part diametrically opposed showed coarsening of eutectic carbide and coalescence of secondary carbide. 400 x.

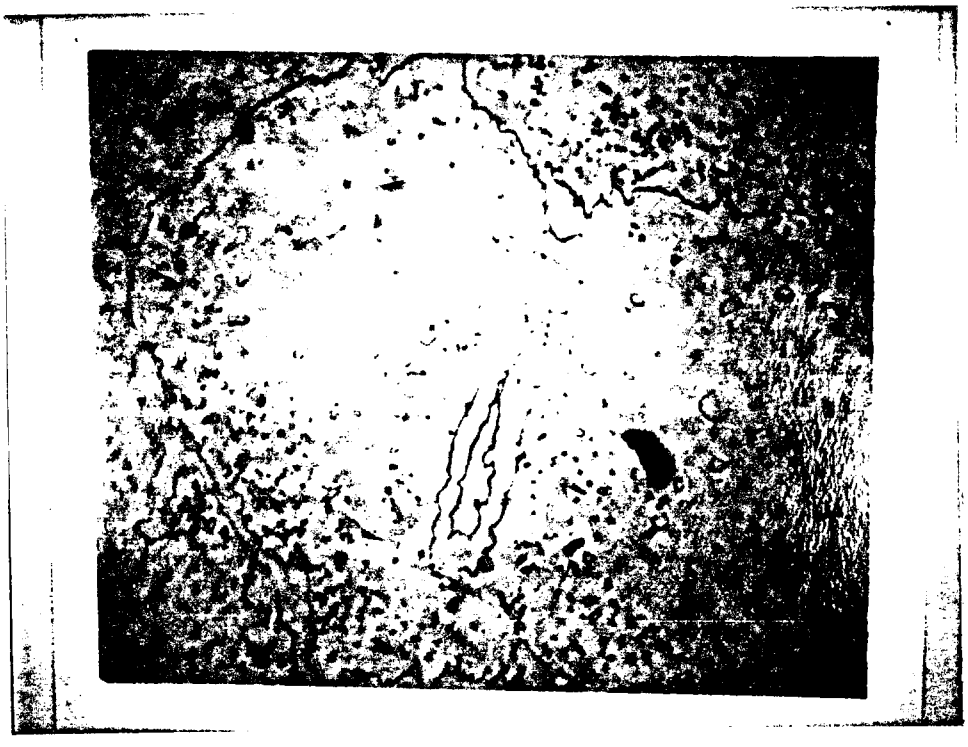

Fig.19 Same as Fig.18 but at 1000 x.

4.1.4 REFORMER TUBE NO.D–19

This was one hot tube which was removed from the furnace due to broken reducer from mechanical adjustment of pigtail welding. Three sections were investigated.

1. At lowest temperature zone of the top section which microstructure consists of eutectic carbide network and very fine secondary carbide precipitated in the austenitic matrix (Fig.20).
2. At the middle section, entering hotter zone, temperature was recorded to be about 919 C, structure consists of interdendritic carbide network and more secondary carbide precipitates in the austenitic matrix (Fig.21).
3. Bottom section microstructure was similar to the middle one, but with carbide agglomeration at grainboundaries more heavily and coalescing in continuous stretches (Fig.22).

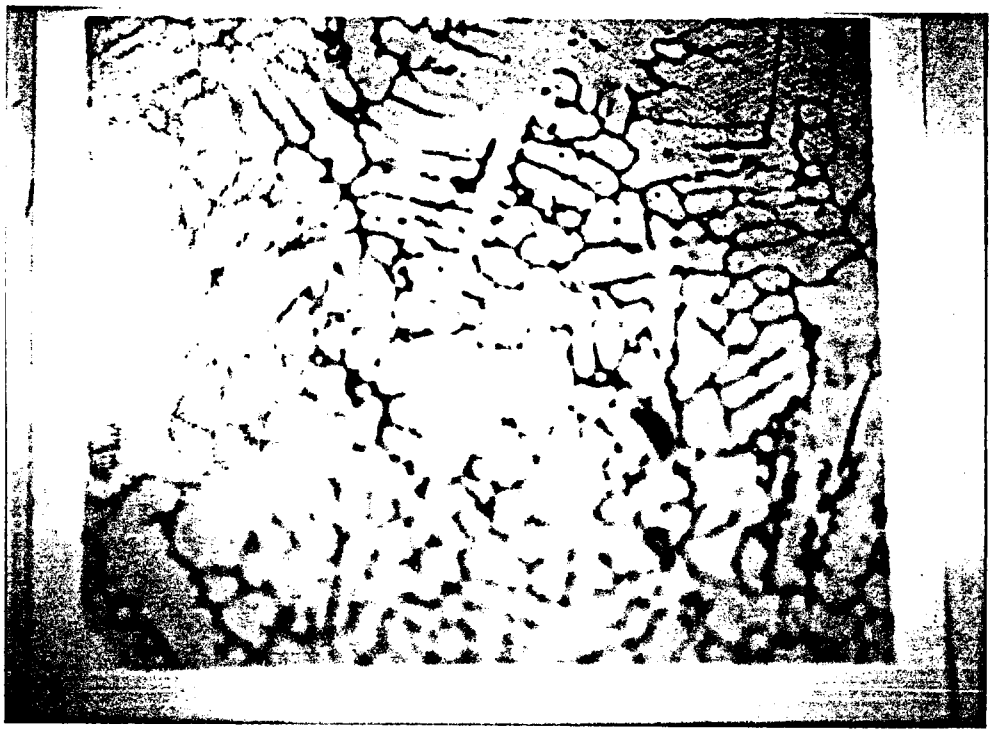

Fig.20 Top section of catalyst tube No.D–19 microstructure. 100 x.

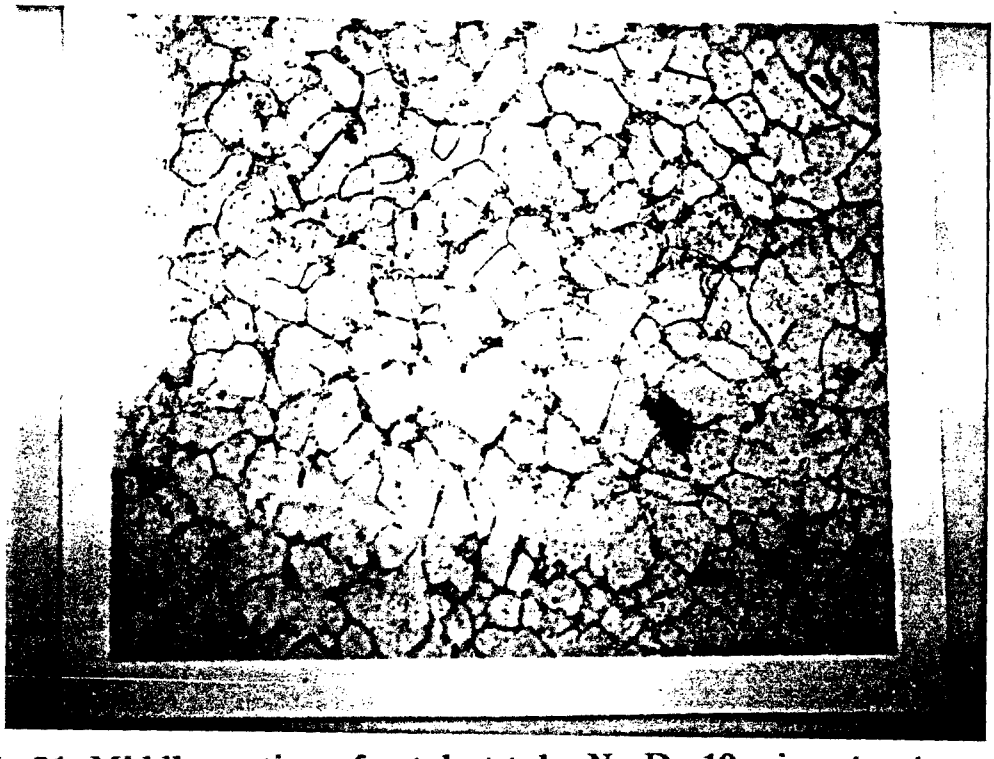

Fig.21 Middle section of catalyst tube No.D−19 microstructure. 100 x.

4.1.5 BROKEN REDUCER OF PIGTAIL JOINT NO.D−19

1. Crack around circumferential partially close to weldjoint fracture surface was brittle.
2. Microstructure revealed crack path was along interdendritic phases which consisted of sigma, ferrite and carbide. Some isolate creep voids were present (Fig.23).

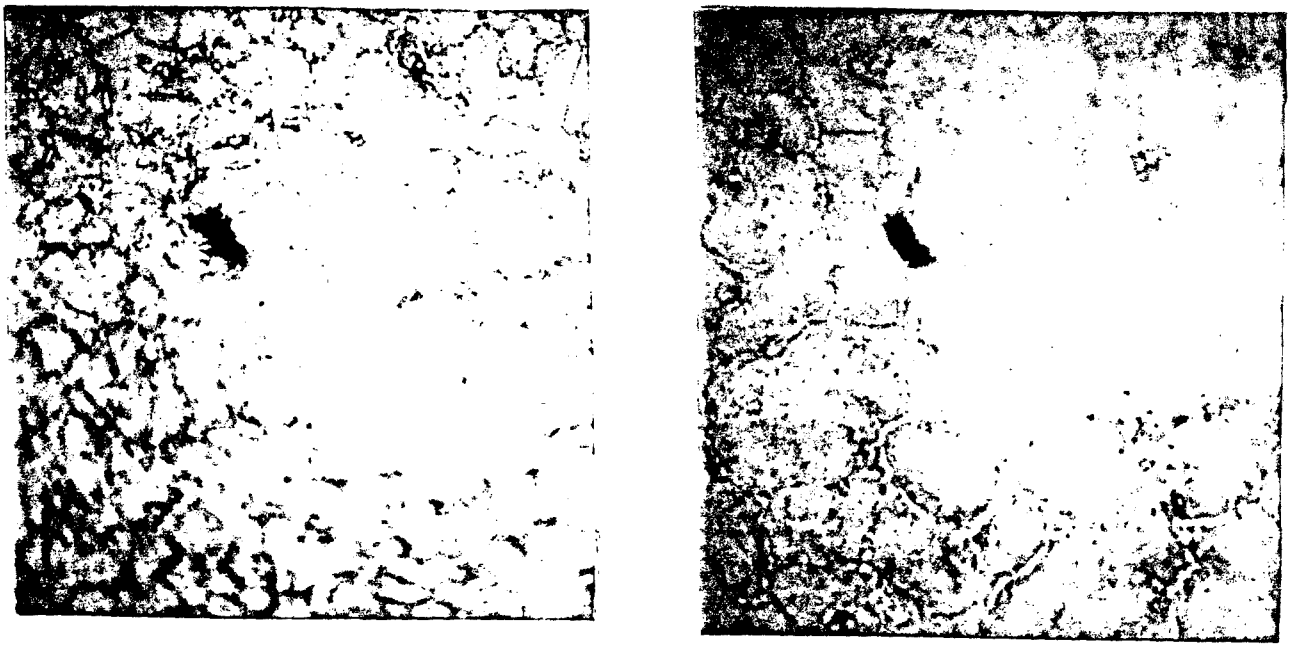

100 X

200 X

Fig.22 Bottom section of D−19 reformer tube of the hottest zone. Structure consists of eutectic carbide agglomeration at grainboundaries with secondary carbide coalescence in grains.

Fig.23 Microstructure of crack reducer of reformer tube No.D−19. 200 x.

5 EVALUATION OF CREEP DAMAGE IN HMU PIGTAILS

5.1 PHYSICAL EXAMINATION

The bulging was confined to the first 300 mm. section of the tubes which had been supplied with the catalyst tubes during the construction of the plant, however the degree of bulging was variable ranging from zero to more than 10% at different locations in the furnace, the general trend being that the south end had suffered more.

The remaining pigtail material (immediately below the weld) did not show any deformation in any of the tubes.

Samples were therefore cut from tubes exhibiting varying degrees of bulging, from the main pigtail tubing showing no bulging and also from both spare (unused) tubes from the original supply and from spare tubes purchased from Kubota prior to the shutdown.

5.2 MICROSTRUCTUAL EVALUATION

5.2.1 UNEXPOSED PIGTAILS

The structures of new tube original material was considered to have grain size too small, as shown in Fig.24 instead of No.3−5 as specified in ASTM standard.

5.2.2 EXPOSED PIGTAILS

This nipped C−2 tube exhibited a structure as shown in Fig.25, which contained some carbide precipitation, also at grainboundaries, and was considered normal for this type of material in this application. The grain size was some what larger than the straight portion material.

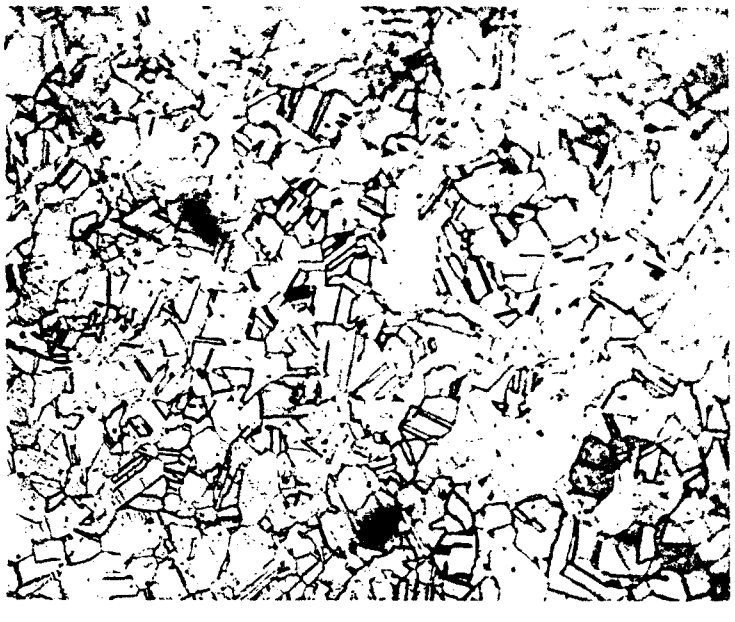

Fig.24 Microstructure of unexposed spare tube pigtail outlet at straight portion. Original material 800 H. 100 x.

TABLE 2 CHEMICAL COMPOSITION OF PIGTAIL OUTLET SAMPLES INCOLOY 800H IN WEIGHT PERCENT.

ELEMENTS/ SAMPLE	C %	Si %	S %	P %	Mn %	Ni %	Cr %	Mo %	Cu %	Ti %	Al %	OTHERS	Ti + Al	Ti / C	Fe
C2 < 1% CREEP	0.0786	0.5128	0.0018	0.0047	0.4882	30.257	20.274	0.0921	0.2076	0.5661	0.6133	W = 0.1083 V = 0.0790 Nb = 0.0190 B = 0.0009	1.1794	7.2	46.695
C31 6.7% CREEP	0.0837	0.3684	.0015	0.062	0.3869	33.973	15.958	0.0581	0.2205	0.3188	0.4827	W = 0.1055 V = 0.0558 Nb = 0.0130 B = 0.0009	0.8015	3.8	47.961
D19 10.2% CREEP	0.0523	0.4190	0.0020	0.157	0.6467	32.363	19.364	0.0555	0.2149	0.3201	0.3673	W = 0.0980 V = 0.0604 Nb = 0.0015 B = 0.0008	0.6874	6.1	46.004
STANDARD ASTM B-407 UNS N08810	0.05 0.10	1.0 MAX.	0.01 MAX.		1.5 MAX.	30.0- 35.0	19.0- 23.0		0.75 MAX.	0.15- 0.60	0.15- 0.60			MIN 5	39.5 MIN

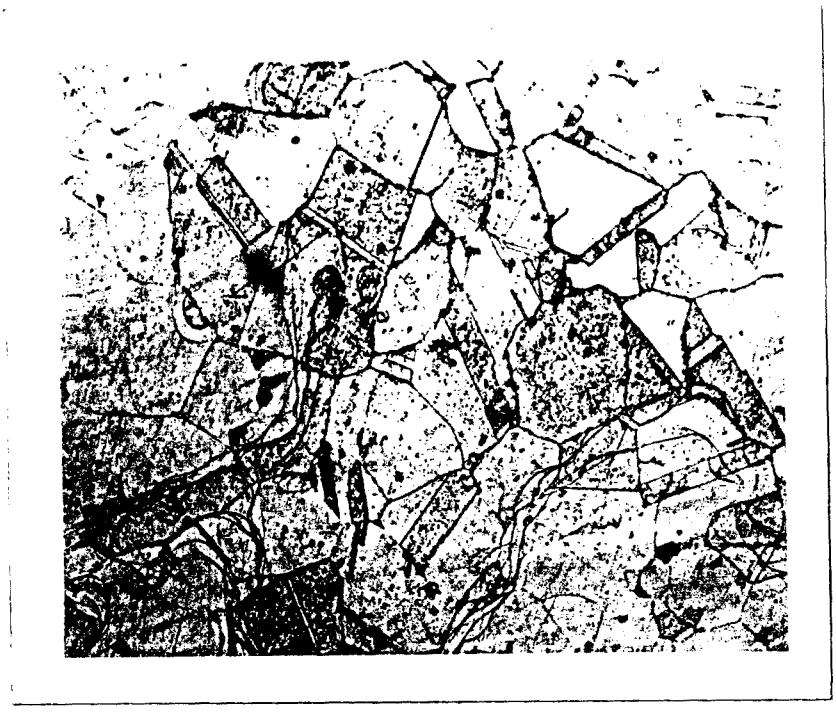

Fig.25 Microstructure of pigtail C−2 straight portion outlet exposed tube. Which did not yet significantly bulge. 100 x.

In all cases the grain size was consistent with that of the unused original stock material, however the structure varied from carbide precipitation at grainboundaries, in tubes that had suffered no distortion, Fig.25, to large carbide islands in conjuction with creep voiding and surface fissuring, in tubes that had suffered the most severe bulging (Fig.26).

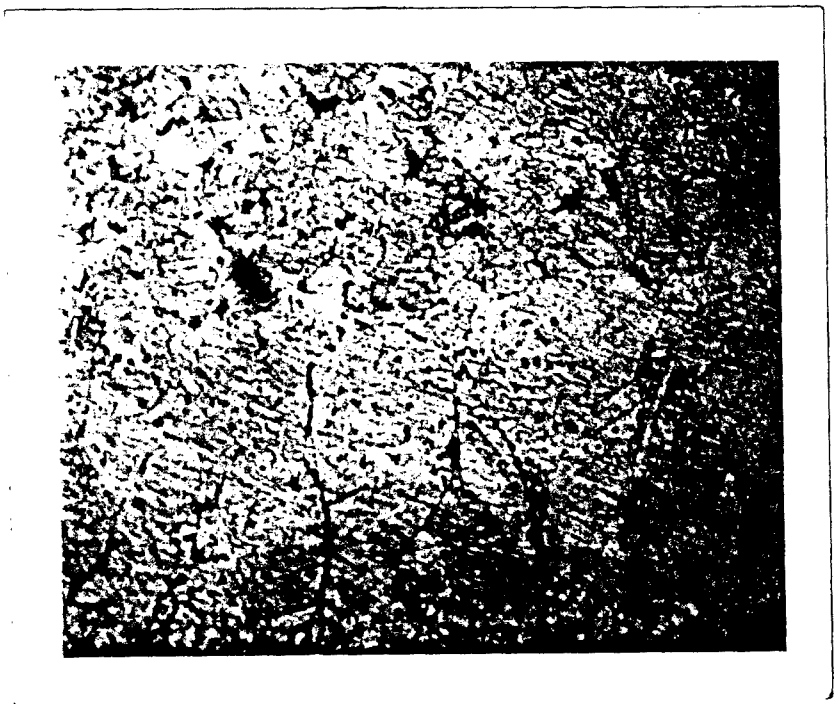

Fig.26 Microstructure of pigtail No.D−21 which crept about 10.7%. Showed external intergranular oxidation/fissuring/voids. 400 x.

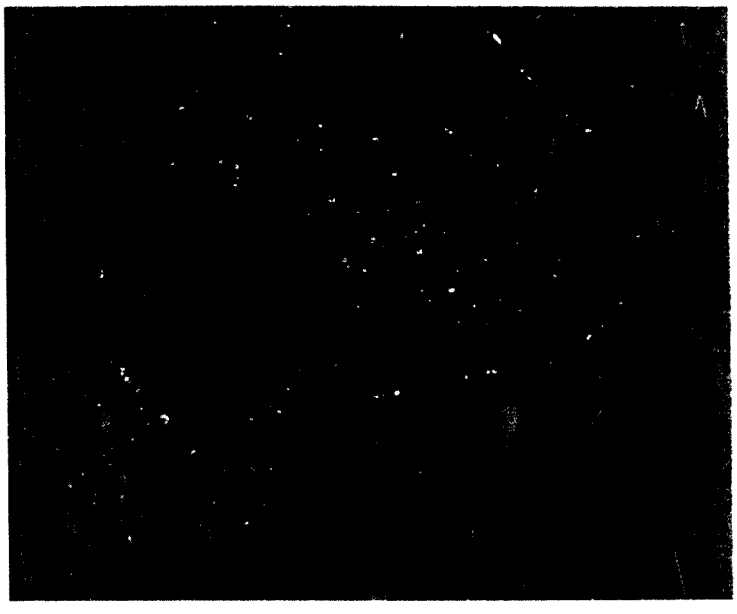

Fig.27 Microstructure of pigtail No.C−2 at bend portion which crept less than 1%. Dark−field micrograph showed −precipitates. 400 x.

6. DISCUSSION AND CONCLUDING REMAKRS

Life assessment according to creep damage accumulation rule was executed at the period prior to failure, by using Larson−Miller parameter formula, it revealed that, with tube temperature fluctuation in the range of 875−950 C, and exposure period as indicated in Table 3, estimate consumed life were only 0.4 and 0.2% for minimum and average creep strength respectively. It was also demonstrated by the calculation, theoretically, if the tubes were exposed to temperature beyond the design, let us say 1,000 C as shown in Table 4 the life would be shortened by 6−13%, therefore, no creep failure in this regime of operating temperature, until November when the unit is due to be shutdown and the catalyst changed, and also that the reduced life of the tube may not be too much of problem as the units is likely to be mothballed at the end of next year.

The appearance of hot tubes in the period prior to tube split had indicated the malfunction of catalyst. From plant observation not only hot tube developed but there were also giraffe necking tubes. The latter is the term used to describe a tube showing a number of uneven hot zones.

At the catalyst renewal, considerable amount of fine and carbon accumulation were found. Either of both accumulation is extensive enough to restrict the flow of gas through the tube, the tube will become overheated as a whole or localised unevenly.

TABLE 3 REMAINING LIFE OF REFORMER TUBE F-2411
OPERATING PERIOD UPTO PRESENT (14-6-91)

PERIOD	OP.PRESS (bar)	TUBE TEMP. (C)	DURATION (y)	FRACTION (min)	FRACTION (avg)
1	26.95	875.00	0.41667	0.00023	0.00011
2	26.95	875.00	0.25000	0.00014	0.00006
3	26.95	875.00	0.58333	0.00033	0.00015
4	26.95	930.00	0.02740	0.00027	0.00013
5	26.95	925.00	0.03562	0.00027	0.00013
6	26.95	920.00	0.00822	0.00005	0.00002
7	26.95	950.00	0.09589	0.00251	0.00118
8	26.95	875.00	0.01644	0.00001	0.00000
9	26.95	950.00	0.00548	0.00014	0.00007
10	26.95	925.00	0.00822	0.00006	0.00003
11	26.95	875.00	0.02740	0.00002	0.00001
12	26.95	930.00	0.00000	0.00000	0.00000
	ACCUMULATED DAMAGE ---->			0.00403	0.00188

TABLE 4 PREDICTION OF DAMAGE IF TEMPERATURE INCREASING AT VARIOUS LEVELS UNTIL S/D (6 MONTHS).

OP.PRESS (bar)	TUBE TEMP. (C)	DURATION (y)	FRACTION (min)	FRACTION (avg)
26.95	935.00	0.50000	0.00630	0.00294
26.95	940.00	0.50000	0.00806	0.00377
26.95	945.00	0.50000	0.01027	0.00482
26.95	950.00	0.50000	0.01308	0.00616
26.95	955.00	0.50000	0.01661	0.00785
26.95	960.00	0.50000	0.02106	0.00998
26.95	965.00	0.50000	0.02666	0.01267
26.95	970.00	0.50000	0.03367	0.01605
26.95	975.00	0.50000	0.04245	0.02029
26.95	980.00	0.50000	0.05342	0.02561
26.95	985.00	0.50000	0.06709	0.03226
26.95	990.00	0.50000	0.08413	0.04057
26.95	995.00	0.50000	0.10529	0.05093
26.95	1000.00	0.50000	0.13155	0.06381

The microstructure feature of failed tube confirmed this because it exhibited high temperature transformation at different ranges. The most deteriorious effect was at the rupture area. Only short period of about 40 hrs, this area was subjected to cooling when syn gas leak through crack aperture at the surface prior to nipping, after that it was heated up to a very high temperature far beyond 1,000 C due to no more gas flow. The prolongation in service after nipping for more than 2,000 hrs had changed the microstructure at this zone completely different from the top and bottom section, by the amount and distribution of secondary carbide coalescence.

It can be explained that at around 1,000 C secondary carbide precipitation was complete, accompanied by sigma phase transformation, and considerable coalescence had occured when burst tubes were in service without flow after nipping for another 2,160 hrs. Thereafter solutizing of the secondary carbides in the austenitic matrix occured. After thousand service hours some precipitated carbides was completed; the microstructures consisted of only massive eutectic carbides in an austenitic matrix. The eutectic carbides tended to coarsen quite rapidly and in many thousand hours had become massive and had taken on a definite gray cast indicative of conversion to a carbonitride. At the zone near the rupturing, there was completely solubilized carbide phase (temperature > 1,000 C) but in the vicinity adjacent to the crack surface, there was platelet carbonitride, which is more stable than chromium carbide (Cr 23−C6). In contrast to above, numerous coalesce carbides indicating the lower range of transformation (1,000 C). The similarlity was the primary carbide or eutectic carbide was massive, which confers brittleness. This accounted for low creep ductility as measured by wall thinning of 7.1% only. This alloy can have deformation upto 50%. It has been fully documented in the literature (1) that this type of structure is prone to creep failure which is characterised by cavities and crack associated with carbide particles situated along grainboundaries.

Carbide networks at grainboundaries are generally undersirable. They usually occur in very high carbon alloys or in those that have cooled slowly through the high temperature ranges where excess carbon in the austenitic is rejected at grainboundaries rather than that as dispersed particles. These networks confer brittleness in proportion to their continuity. Carbide networks also provide paths for oxidation attack by hot gas. Those remains hot tubes would have similarly deteriorated microstructure as exhibited by tube D−19.

Associated with hot tube development was the extensive bulge was observed in several pigtail outlets and embrittling effect of sigma phase in reducer as revealed by microstructure in Fig.23. This had led us to investigate their microstructural transformation. Micrograph in Fig.24 showed that the original fine grain austenitic and twinning with fine secondary carbides matrix, revealing material is mill-annealed instead of solution annealed. Meanwhile the pigtail portion beyond the first weldjoint i.e. at the elbow, grain sizes were larger in Fig.27 and were finely distributed and homogeneously nucleated γ' -precipitates. This microstructure indicated the proper heat-treatment and exhibited higher creep resistant than the straight portion. The solution annealing temperature is illustrated by Thomas Anderson (6) that affects the number and distribution of both M23-C6 and γ' higher solution temperature resulting coarse grain size of alloy 800H and low creep rate property is gained.

With the chemical composition shown in Table 2, Chromium content of tube No. C-31 was lower than the specification, and the other tended to have minimum values which affected the resistance of oxidation and intergranular attack. Anderson had further pointed out that the second type of phase transformation is the precipitation of the intermetallic compound γ', i.e. Ni3(Al,Ti) can have influence on precipitation hardening and thereby lower the creep rupture ductility. The amount of γ'-precipitation is controlled primarily by the (Ti+Al) content but is also influenced by the carbon and nickel content as well as by the heat treatment (7). For C 0.050-0.080% and Ni 30-32%, the critical amount of (Ti+Al) is 0.7% which our pigtails had this amount up to 1% for the case of less creep damage.

Therefore the following remarks could be drawn as follows.

1. A catalyst tube experienced creep failure due to localized uneven hot zone because of catalyst was broken and carbon deposit

and 2. The bulging damage of pigtail outlets is considered to be attributable to accelerated creep rate of inferior creep property resulting from improper heat-treatment.

REFERENCES

1. V.GUTTMANN and R. RURGEL; the Creep Behaviour of HK40 & Alloy 800H in a Carburizing Environment, paper presented at the Symposium Petten, the Netherlands, May 13–14, 1980.

2. P.G. STONE et al; J.B. NuCl. Energy Soc, 14 (1975), 25–34.

3. PH. BERGE et al; MEM SCI, Rev, Me't; 72 (1975), 836–857.

4. R.H. COOK; Creep and Corrosion of Alloy 800 in Simulated High Temperature Reactor Helium at 600 C to 800 C; HTMP report No.7, Sept 1972.

5. L, EGNELL. N.G. Person, Creep–Rupture Ductility of Alloy 800; paper presented at the 18 eme Collogue the Metallurgic–d' Alliage, Saclay, June 23–25, 1975.

6. THOMAS ANDERSON; Effects of Composition, Heat Treatment and Cold Work on Structure and Properties of Alloy 800. R & D Center Steel Division, paper presented at 21–e'mes Journies des Aciers Spicioux, France, April 27–28, 1982.

7. L.EGNELL, N.G PERSON; Creep–Rupture Ductility of Alloy 800; Paper presented at the 18 e'me Colloque the Metallurgic–d'allige, Saclay, June 23–25, 1975.

Creep Rupture Strength Curves

KHR35C

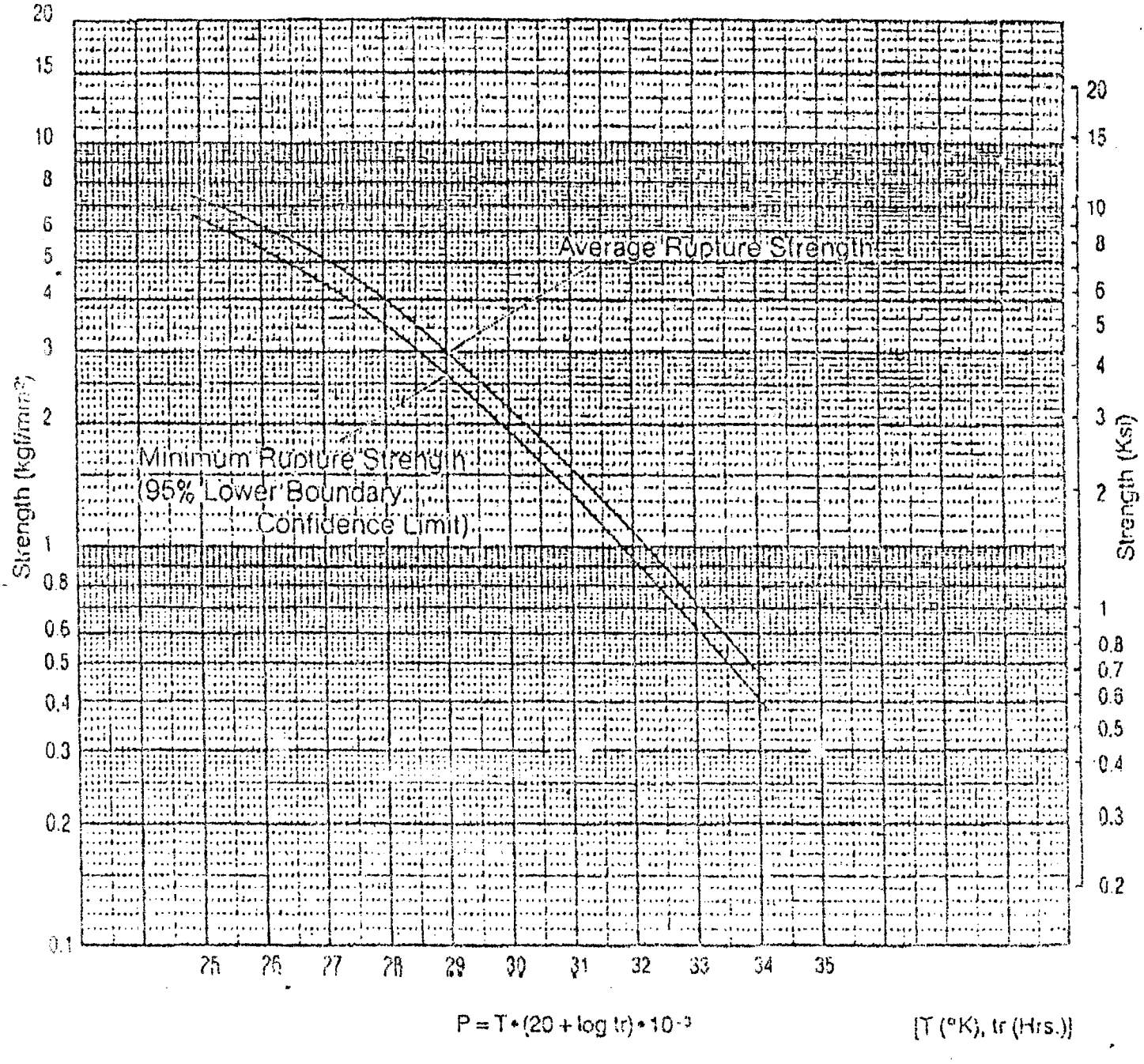

Fig. 5-1

Recent Progress in Scanning Microprobe Systems for Electrochemical Corrosion Measurement

T. Shibata

Department of Materials Science and Processing,
Faculty of Engineering, Osaka University,
2-1 Yamadaoka, Suita, 565 JAPAN

ABSTRACT

Localized corrosion is more important than uniform corrosion in corrosion failure, and the exact information on the rate at the localized sites and their distribution are necessary for a quantitative evaluation. However, it is not easy to measure the exact rate at the localized corrosion sites and distribution, although electrochemical methods have become popular and used widely in laboratories or fields.

Then we have developed several scanning microprobe systems, including a scanning vibrating electrode technique (SVET), a scanning pH probe (SPP), a scanning micro impedance probe (SMIP) and a scanning laser enhanced eleqtrochemical microscopy (SLEEM) for measuring corrosion rate and its distribution.

SVET which can measure the distribution of corrosion current density at controlled or free corrosion potential, is applied for mapping current distribution at generated pits and at cracks during corrosion fatigue and SCC.

SPP uses a fine Sb tip for a pH censor and scans over corroded surface, providing pH distribution which is produced by reduction of oxygen.

SMIP can measure the distribution of chemical impedance on the coated steal at the controlled potential and evaluate degradation of coatings.

SLEEM is the most recent developed method for detection of localized corrosion susceptibility of stainless steels. Focussed laser irradiation raises the surface temperature which enhanced electrochemical reaction. Response current to laser irradiation is different at each site and its scanning image displays a susceptible corrosion path.

Basic principles of each technique and application examples to localized corrosion will be presented.

SCANNING MICROPROBE SYSTEMS FOR THE ELECTROCHEMICAL CORROSION MEASUREMENT

Shinji FUJIMOTO, Toshio SHIBATA and Yoshio TANAKA

Department of Materials Science and Processing,
Faculty of Engineering, Osaka University.
2-1 Yamada-oka, Suita Osaka, 565 Japan.

ABSTRACT

Scanning micro probe systems, including a scanning vibrating electrode technique (SVET) and a scanning micro impedance probe (SMIP), have been developed in order to measure two dimensional distribution of localized corrosion or defects in corrosion resistant materials in solutions under in-situ condition. SVET, which can measure the distribution of corrosion current density, was applied for observation of pitting, stress corrosion cracking, corrosion fatigue and others under both open circuit and potentio static conditions. SMIP displays the distribution of chemical impedance, with which the corroding surface can be characterized with less damage and less disturbance for the specimen surface than the potentiostatic SVET. SMIP has been applied to observe polymer coated steels for revealing the distribution of their defects. Characteristics and capability of these micro probes were examined and discussed.

KEYWORD

Scanning vibrating electrode technique, scanning micro impedance probe, in-situ electrochemical measurement, localized corrosion, pitting, stress corrosion cracking, corrosion fatigue, intergranular corrosion.

INTRODUCTION

There are many electrochemical measurement techniques which provide information about corrosion behavior of metals and alloys in solutions. These techniques, however, can not usually give electrochemical parameters about localized corrosions, because these provide averaged information about the materials examined. The scanning micro electrode probes[1], several types of which are now being developed by some authors[2], can measure the distribution of electrochemical variables. The advantage of these techniques is the in-situ quantitative local corrosion characterization and the display with a computer assisted visual media. In this study, two types of scanning micro electrode techniques will be presented. The scanning vibrating electrode[3], which can measure the distribution of corrosion current density, is applied for pitting corrosion and corrosion fatigue of carbon steel, stress corrosion cracking of stainless steel and intergranular corrosion. The scanning micro impedance probe, which displays distribution of chemical impedance, has been applied to characterize a epoxy

Proc. 11 th International Corrosion Congress vol.5, p.511,1990.

coated steel to reveal the distribution of localized corrosion. Characteristics and capability of the scanning vibrating electrode and the scanning micro impedance probe were examined and discussed.

SCANNING VIBRATING ELECTRODE

Principle and apparatus

Localized corrosion accompanies local current flow, which causes a potential gradient, because the solution has a finite conductivity. In the vibrating electrode, a sinusoidal vibration is applied mechanically, and the detected potential change results in an AC signal related to it. This weak signal is amplified by a lock-in amplifier, being converted to a DC output proportional to the amplitude[4]. Figure 1 shows the block diagram of the apparatus. The electrode probe tip is made of an electrolytic polished Ag wire with a few to several hundred um in diameter coated with resin except the top of the tip. This electrode is attached to a audio speaker to be vibrated vertically. The two dimensional scan is provided by a X-Y stage driven by pulse motors. A microcomputer controlled the X-Y stage and recorded the out put of the lock-in amplifier with X-Y stage position. The details of the probe, the amplitude of vibration, and other experimental conditions will be given in the following application.

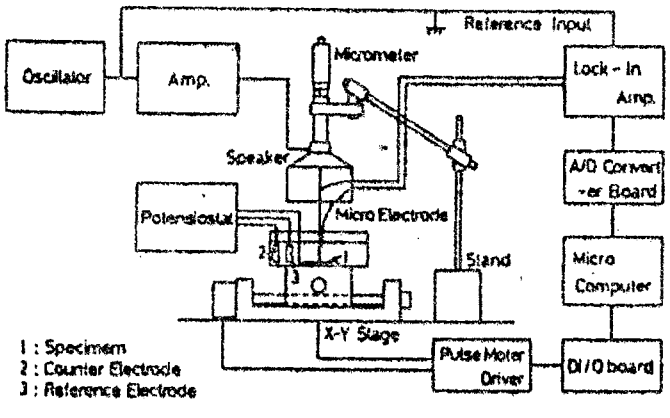

Fig.1 Schematic diagram of the scanning vibrating electrode.

Examples of application

Pitting corrosion on a steel --- Figure 2 shows current density map for a high strength steel(HT-50) in synthetic sea water, in which corrosion pits are developing. In this experiment, the diameter of electrode is about 500 μm and the amplitude of vibration 300 μm, the frequency being about 150 Hz. This figure shows that positive currents are anodic and negative cathodic. The anodic peak at the left corner of Fig.2(a) corresponds to the generation of a pit. This peak is strengthened with time as shown in Fig.2(a) to (f), and the cathodic current increases all over the rest of the specimen. It is noticeable that a localized cathodic current, in some cases, could be also observed, as shown in Fig.2(c).

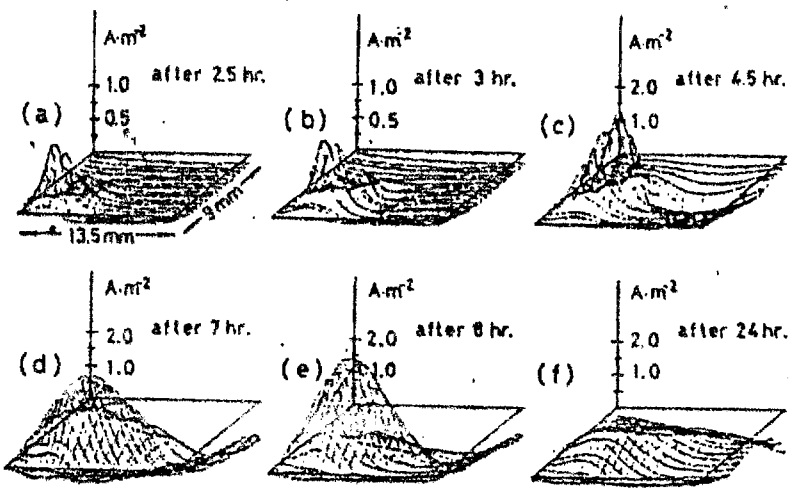

Fig.2 Changes in the distribution of current density with time, showing growth of a corrosion pit on high strength steel in synthetic sea water.

Corrosion fatigue —— Corrosion fatigue tests were conducted[5] for high strength steel(HT-50) and ferritic stainless steel(Type410) in synthetic sea water. The Schenck type fatigue testing machine operating at 1750 rpm was employed, the specimen and corrosion cell being shown in Fig.3. The distribution of corrosion current was measured by the scanning vibrating electrode at intervals of 30 to 100 min during the interruption of fatigue test, the time for the measurement being about 5 to 6 min. Figs.4 and 5 show the changes in the distribution of

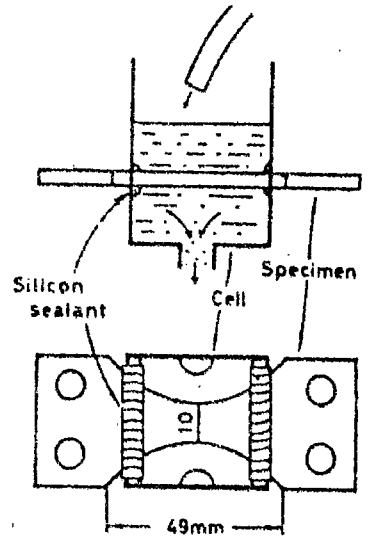

Fig.3 Corrosion fatugue specimen and test cell.

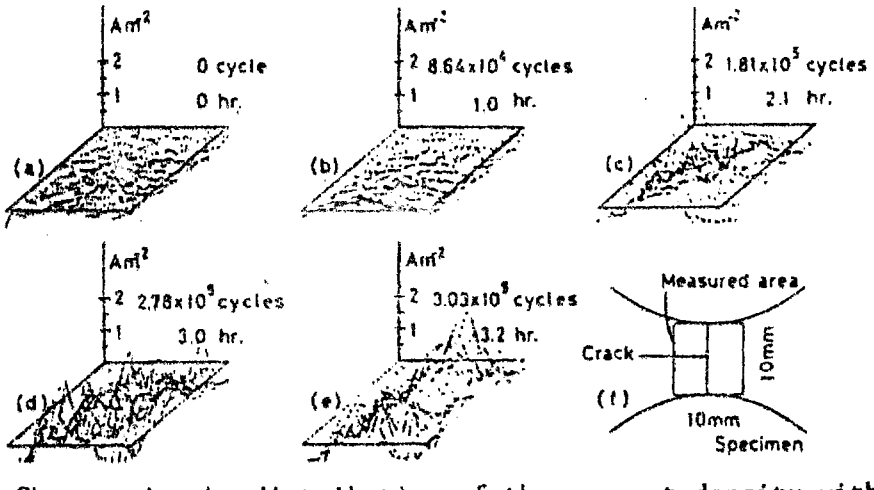

Fig.4 Changes in the distribution of the current density with time during the corrosion fatigue test for high strength steel in synthetic sea water.

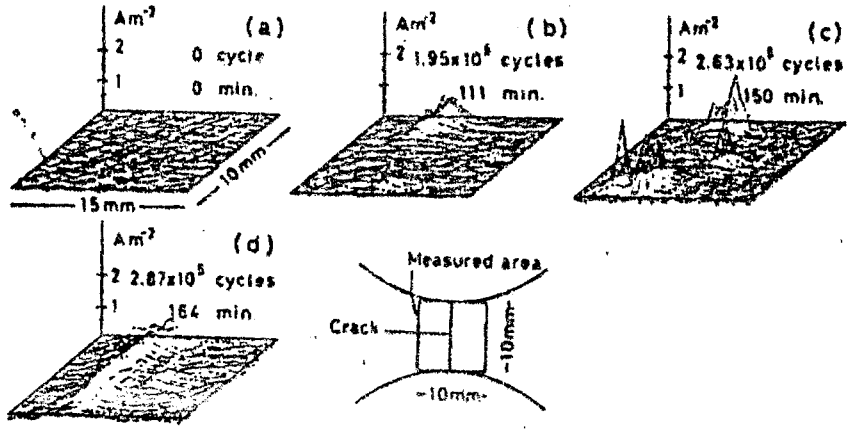

Fig.5 Changes in the distribution of the current density with time during corrosion fatigue test for SUS410 stainless steel in synthetic sea water.

current density with time during the corrosion fatigue test for HT-50 and Type410, respectively. It is found that local anodic current is observed around the main fatigue crack. However, most of anodic current are observed in the area covered by corrosion products, under which many small pits associated with micro cracks are found for HT-50. On the other hand, the apparent anodic peak is observed at the fatigue crack for Type410, the extension of the crack with time being observed distinctly. No corrosion product and no sub-crack were visible on the Type410 specimen. The corrosion fatigue behavior of carbon steel and stainless steel are found to be different.

SCC --- Stainless steel tensile test specimens, 0.2 mm thickness, were sensitized at 750°C for 30 min and 650oC for 24 hr. Constant load SCC test was conducted at 250MPa in 20 wt% $MgCl_2$ + 10^{-3} mol/l $Na_2S_2O_3$ solution at 80°C. The distribution of corrosion current was measured by SVET. Figure 6 shows the change in the distribution of current density with time. It is observed that SCC initiated at the edge of the specimen just after immersion,

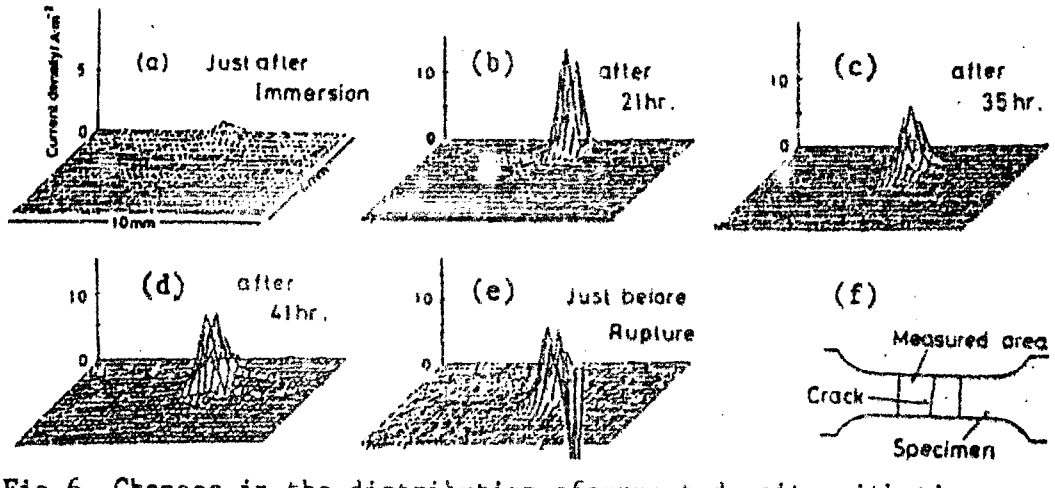

Fig.6 Changes in the distribution ofcurrent density with time. SSC initiates and extends for sensitized SUS304 at 80oC in 20% NaCl + 10^{-3}M $Na_2S_2O_3$, 250MPa.

and extended with time. This specimen was ruptured after 43 hr, when the SCC crack had been extended to around the center of the specimen, and the remained part ruptured by a mechanical fracture.

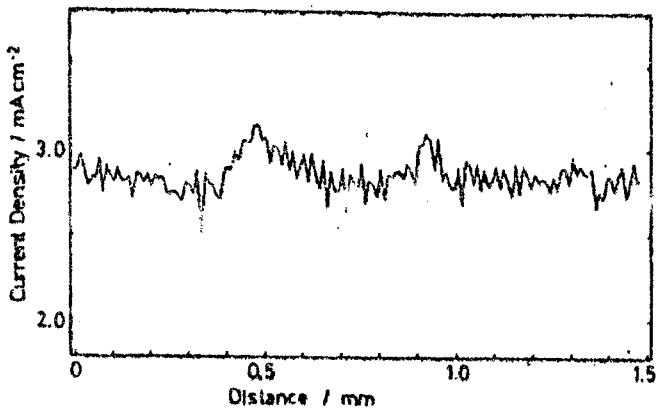

Fig.7 Current distribution on sensitized SUS304 in 0.5M H_2SO_4 + 0.01M KSCN, showing intergranular corosion current.

Intergranular corrosion -- The scanning vibrating electrode can identify fine structures of localized corrosion, for example intergranular corrosion. The dimension of micro electrode, the amplitude of vibration, and the distance between the electrode and the specimen have to be sufficiently small to distinguish the difference in the current density at the grain boundaries, the width and interval of which are very narrow. In this study, it was attempted to detect the intergranular corrosion current of sensitized stainless steel. Type304 stainless was solution annealed at 1150 ℃ for 200 h, resulting in grain growth to large grains of up to few hundred um, and then sensitized at 750 ℃ for 30min and 650 ℃ for 24hr. In order to accelerate the intergranular corrosion, the EPR (Electrochemical potentiokinetic reactivation) method was applied with some modification. The specimen was potentiokinetically polarized from corrosion potential to a passive potential via. an active region, and the applied potential was returned to a constant potential in the active region, in order to accelerate selective dissolution at the chromium depleted zone formed by sensitization. Very fine electrode system was used for this measurement, the diameter of the tip being about 10 μm, the amplitude of vibration 10um, and the distance between the electrode and specimen about 5μm. Figure 7 shows the distribution of current density which was obtained by averaging 3 times for line scanning across the specimen area. It is confirmed that the position of current peaks corresponds to the grain boundary by microscopic observation after the measurement.

SCANNING MICRO IMPEDANCE PROBE

Principle and apparatus

Isaacs et al[6], and Leidheiser et al[7] have been reported the idea for measurement of impedance distribution by a scanning micro electrode. An

electrochemical impedance measurement system was equipped with a micro probe and X-Y pulse stage, a block diagram of the system being shown in Fig.8(a). The micro probe shown in Fig.8(b) is newly designed, which consists of a small counter electrode and a micro reference electrode contained in a

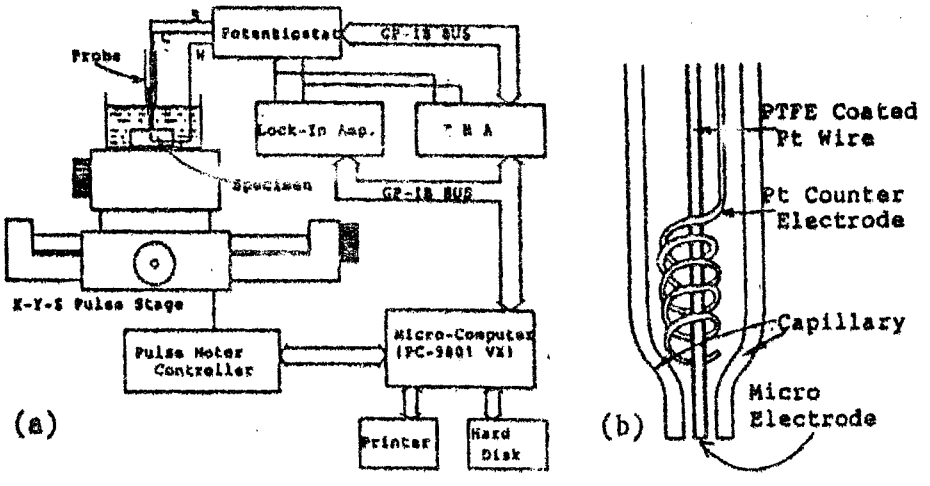

Fig.8 Schematic drawings of (a)the scanning micro impedance probe system and (b)the micro probe.

capillary. The micro reference electrode is made of platinum wire coated with PTFE tubing except the top end cross section. The top end of the electrode tip is located at the center of the open end of the micro probe capillary. The micro probe, including the reference electrode, is scanned near the surface. Since ion current flows through the capillary, the measured impedance corresponds to some restricted area. In the newly developed system, the top end of the capillary is contacted directly to the specimen to limit strictly the measured area, so that the measured value just corresponds to the area confined. The examples shown below were measured with this system. The electrochemical impedance was measured at a single

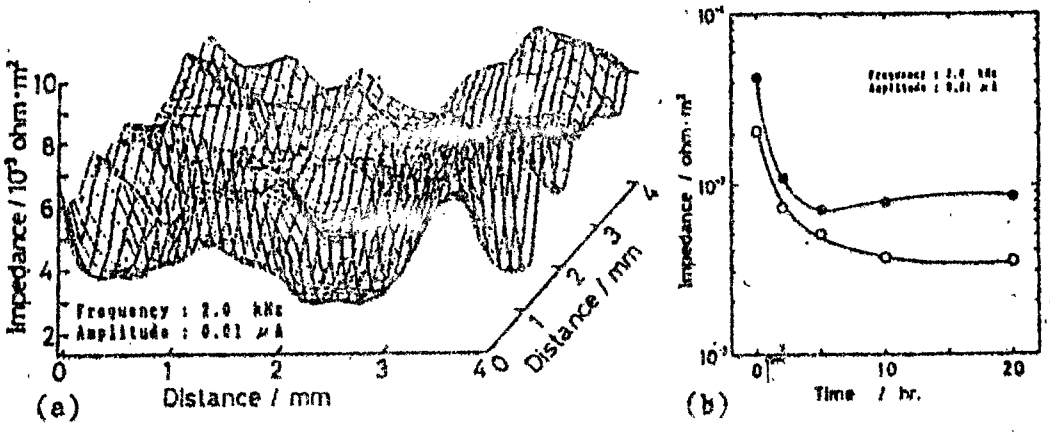

Fig.9 (a)Impedance distribution on epoxy coated zinc galvanized steel in 1% NaCl after 20 hours immersion. (b)Impedance changes with immersion time for (●)no corrosion and (○)localized corosion site.

frequency for one measurement site, because the usual impedance measurement for wide frequency range need very long time. Both the potential and current modulation were also tried and the following result were obtained.

Distribution of impedance on epoxy coated zinc galvanized steel

A zinc galvanized steel coated with epoxy resin was immersed in 1 % NaCl solution, and the distribution of impedance was measured during about 20 hours. An example of the impedance distribution using 2 kHz is shown in Fig.9(a). Some sites at which impedance was lower than the others were detected and were confirmed to correspond to defects on the coating. Figure 9(b) shows the change in impedance with time at both the deteriorated and the not deteriorated sites. Initially, almost a similar equally decrease in impedance is observed for both sites, that corresponds to the process of the initial uniform degradation, and then the impedance at the specified sites decreased with time due to local degradation.

DISCUSSION

Function of SVET

The sensitivity and the resolution of SVET are affected by the dimension and function of the probe system. The higher resolution is attained by decreasing the magnetude of the next three factors as small as possible ; the dimension of electrode, the amplitude of vibration, and the distance between the probe and the specimen. The higher sensitivity, however, is obtained by the larger amplitude of vibration, and a good S/N ratio is achieved by using the larger electrode tip. Therefore, not only the small electrode, but also stable vibration driver and precisely controlled scanning stage are required in order to maintain the small constant vibration and the small and fixed clearance between the probe and the specimen. The examples of pitting, corrosion fatigue, and SCC, described before, used not so fine probe system. Measurements in the solution with such a high conductivity generate small amplitude of potential, because high conductivity gives small IR drop. Moreover, these measurement seemed to be not needed such high resolution of less than 1 mm. Thus, the dimension of the probe and the amplitude of vibration used for the examples was order of few hundreds um. Finer probe system was needed for measurement of intergranular corrosion. It seems that the higher resolution has been attained by using of the smaller electrode tip and the more stable vibration driver. For the precise measurement, it was also proved that the electrode vibration must be controlled strictly vertical direction. Ion currents consist of both vertical and horizontal components. Thus, if vibration contains horizontal component, the signals derived from both vertical and horizontal currents are overlapped resulting in an inaccurate current distribution. Therefore, the stable and precise vibrating driver is needed when the measurement is conducted for the high resolution.

Change in local impedance

In the scanning micro impedance probe, a single high frequency is preferable for a quick measurement of impedance map. Thus, it seems that the measured impedance is mostly contributed by solution resistance. The deteriorated sites on high corrosion resistance material, however, can be detected and/or distinguished by the distance between these sites and the probe, because solution resistance proportional to the distance. Therefore, the scanning impedance probe is suitable for detection of local corrosion sites or defect of corrosion protection coating on metal or alloys, for example, polymer or ceramic coating. The advantage of the scanning impedance electrode is that specimen is scarcely damaged during sampling, because only small AC modulation is applied for the measurement.

CONCLUSION

The scanning micro probe systems is suitable for characterizing the distribution of corrosion and/or defects sites on metals and alloys in-situ and on real time, the measured value being displayed in visual media. The scanning vibrating electrode can indicate the distribution of corrosion current quantitatively with high lateral resolution under potentio static or natural immersion condition. Thus, this technique is suitable for observation of initiation and extension of localized corrosion, for example pitting, SCC, galvanic corrosion, and others. On the other hand, the scanning micro impedance probe can detect the localized corrosion or defect sites with little damege on the specimen, and is favorable for characterization of high corrosion resistive coating, like paint, plating or ceramic coating.

REFERENCES

1) H.S.Isaacs and B.Vyas, Electrochemical Corrosion Testing, ASTM STP727, (1981), p.3.
2) S.Fujimoto and T.Shibata, Corrosion Engineering(Boshoku Gijutsu) Allerton Press, 36, 729(1987).
3) Y.Ishikawa and H.S.Isaacs, Presented at Conf. on Corros. and Exploitation of Aluminum Alloys, Cranfield, England(April, 1983).
4) L.F.Jaffe and R.Nuccitelli, J.Cell Biology, 63, 614(1974).
5) T.Shibata and S.Fujimoto, Boshoku Cijutsu, 35, 566(1986).
6) H.S.Isaacs and M.W.Kendig, Corrosion, 36, 269(1980).
7) J.V.Standish and H.Leidheiser, Jr., Corrosion 36, 390(1980).

NEWLY DEVELOPED SCANNING LASER ELECTROCHEMICAL MICROSCOPY TO DETECT INTERGRANULAR CORROSION

T. Shibata, S. Fujimoto and T. Shono
(Department of Materials Science and Processing,
Faculty of Engineering, Osaka University,
2-1 Yamadaoka, Suita, 565, Japan.)

ABSTRACT

Scanning laser enhanced electrochemical microscopy(SLEEM) has been developed in order to detect intergranular corrosion. A focused laser beam generated from a semiconductor laser of AlGaAs (wave length: 830 nm, out put power:40 mW) was scanned across a grain boundary of sensitized Type 304 stainless steel which was kept at a constant potential within the active region in a H_2SO_4+KSCN solution. The enhanced dissolution current at the grain boundary due to a temperature rise induced by the laser irradiation was found to produce the clear boundary image. The scanning operation and data acquisition were totally controlled by a microcomputer and integrated into the system called SLEEM. The details of SLEEM and optimum conditions for the operation such as radiation frequency and applied potential were discussed.

INTRODUCTION

Various kinds of electrochemical methods have been applied to study corrosion and proved to be essentially important for evaluating the corrosion resistance of materials, or analyzing the corrosion mechanism, but the electrochemical parameters obtained are mainly concerned with an average value over the whole surface area examined. Localized corrosion which distributes either uniformly or at random over the surface needs the more exact evaluation on distributed sites and their corrosion rate.

Scanning probe techniques[1] including, scanning vibrating electrode, scanning electrochemical impedance have been proved to be useful to identify the position and to measure its corrosion rate quantitatively in situ for pit formation[1], grain boundary corrosion[2,3], crack propagation in SCC[5] or corrosion fatigue[4], degradation of coated steel[5], selective corrosion of welded part[6], and so on. The above methods, however, have a limit in spatial resolution because spatial distribution of ionic current induced by corrosion was not sharp, so that small corrosion current occurring at a narrow grain boundary region was hardly detected.

Then, we had proposed a scanning laser enhanced electrochemical microscopy(SLEEM)[7] for detecting localized corrosion, especially for intergranular corrosion. Laser beam probe does not need any direct contact on the specimen and fine spot as small as its wave length will provide an improved spatial resolution for detecting intergranular corrosion.

EXPERIMENTAL

1. Scanning laser enhanced electrochemical microscopy

Instrumentation of SLEEM was illustrated in Fig.1. SLEEM consists of

---

Proc. 7th Asian Pasific Corrosion Controll Conference, p.188, 1991.

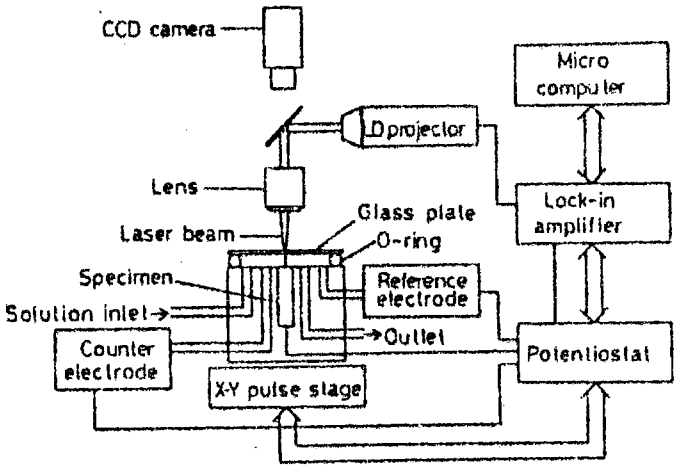

Fig.1 Schematic illustration of SLEEM

three main parts; the first is a laser irradiation part including a laser with power source and optics, the second a small electrolytic cell integrating small steel specimen with a scanning stage, and the third a microcomputer which could control the scanning stage, data acquisition and display a scanning image. As the specimen, the small square bar having a cross sectional area of 1.5 mm x 1.5mm was used and molded into epoxy region. The surface of the specimen was covered with a rubber o-ring of 7.5 mm in inner diameter and a thin glass plate of 0.15 mm, so that the volume confined over the specimen surface was 60 mm^2. The solution which was preliminary deaerated with purified nitrogen gas was circulated to the confined volume over the specimen surface through inlet and outlet fine tubes. Another two tubes attached to the cell were connected with a Pt counter electrode and a Ag/AgCl reference electrode, so that potential of the specimen was controlled by a potentiostat. A semiconductor laser(type: AlGaAs, output power:40 mW, wave length:830 nm) was used as a laser source and is highly possible to cause only thermal effect on the electrochemical reaction because its wave length is too long to produce holes by photochemical excitation. Laser beam emitted from the laser was focused through the objective lens and irradiated into the specimen surface. The effective laser power irradiated on the surface was estimated to be about 10 mW with a focused spot of 10 um as stated later. The irradiated surface can be monitored with a CCD camera as illustrated in Fig.1.
Laser irradiation with modulated frequency onto the specimen which was kept at a constant potential at room temperature produced a modulated current response which was measured by a lockin amplifier, separated from the steady current. Such laser irradiation was continuously scanned over the surface of the specimen which was moved by an X-Y stage operated by the microcomputer, and then the image of the laser response as a function of the X-Y position was stored in the microcomputer and displayed in CRT or a plotter.

2. Specimens and solutions used

Type 304 stainless steels and a series of Fe-Cr alloys were used and their chemical composition was shown in Table 1. In addition to the above alloys, diffusion bonded alloys were also prepared to simulate the boundary. For 304 stainless steel, solution annealing with grain growth at 1423 K for 100 hrs followed by water quenching was accomplished, and then final heat treatment at 773 K for 24 hrs was applied for sensitization. Almost all solution used in the experiment was 0.5kmolm^{-3} H_2SO_4, but another solution of 0.5kmolm^{-3} H_2SO_4 +

$0.01 kmolm^{-3}$ KSCN was used to intensify grain boundary dissolution for revealing grain boundary image, because it is used for electrochemical polarization for reactivation(EPR) to measure intergranular corrosion susceptibility of stainless steels.

Table 1 Chemical composition of alloys

	C	Si	Mn	P	Ni	Cr	Ti	Al	N	Mo
304	0.05	0.55	0.98	0.026	0.008	9.38				0.12
Fe-8Cr	0.028	0.28	0.30	0.003	<0.01	8.23	0.31	0.14	0.0049	
Fe-18Cr	0.025	0.30	0.30	0.003	<0.01	18.59	0.30	0.17	0.0064	

RESULTS AND DISCUSSION

1. Determination of the spot size of the irradiated laser beam

In Fig.2, an example of laser enhanced current image was demonstrated, which was obtained by line scanning of 1 um steps for 304 stainless steel maintained at 1020 mV in 0.5 $kmolm^{-3}$ H_2SO_4 solution at room temperature. Laser beam modulated by 10 Hz frequency was scanned just over the boundary between resin and Type304 steel from the left to the right. As can be seen in Fig.2, no current increase was observed on resin located in the left side, but steep increase started at the boundary, approaching to a steady current in the right side. The width of transition in the enhanced current profile located at the boundary provides the radius of the laser beam and was found to be ca. 10 um. Then current density could be calculated by dividing observed enhanced current increase by the area irradiated, i.e., $S = (3.14)(5\times10^{-6}\ m)^2 = 7.85\times10^{-11}\ m^2$, and the converted unit for current density was shown in the right vertical axes in Fig.2. It should be emphasized that current density is rather large in the order of Am^{-2}, although observed current is quite small in the range of nA.

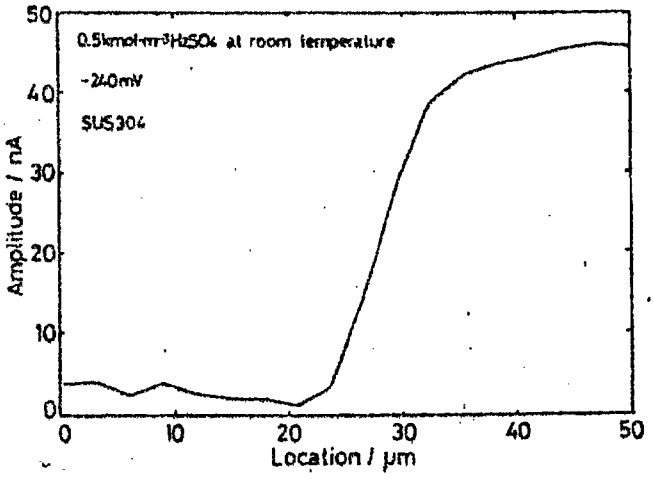

Fig.2 Line profile of laser enhanced current across the boundary between resin and Type304 steel.

2. Effect of modulation frequency on the laser enhanced current

Fig.3 shows the effect of modulation frequency of laser on the enhanced current which was observed for Type304 stainless steel kept at the constant potential indicated in the figure both in 0.5 $kmolm^{-3}$ H_2SO_4 solution and in 0.5 $kmolm^{-3}$ H_2SO_4+0.01$kmolm^{-3}$KSCN solution. From Fig.3, it is concluded that the lower the modulation frequency,

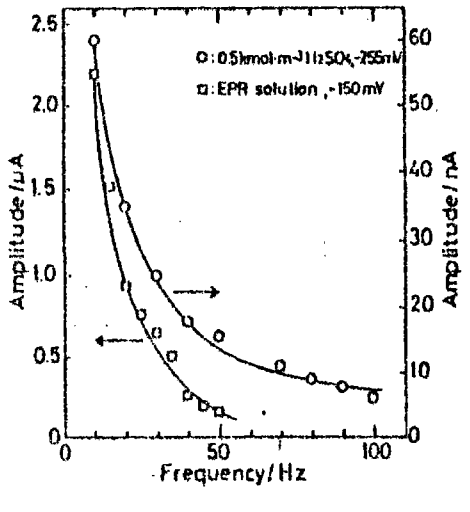

Fig.3 Effect of modulation frequency on laser enhanced current.

the higher enhanced current was observed for both cases. It is reasonably explained that the longer time exposed to laser irradiation at the lower frequency causes the higher temperature increase at the irradiated surface compared to the shorter time at the higher frequency. The higher temperature at the surface accelerates the anodic reaction, resulting to the larger enhanced current.

3.Effect of potential and alloy composition on the laser enhanced current

Fig.4 is the polarization curves of Fe-8Cr, Fe-18Cr, and 304 stainless steel in 0.5kmolm^{-3} H_2SO_4 solution and Fig.5 is the laser enhanced current density depending on applied potential for the same alloys in

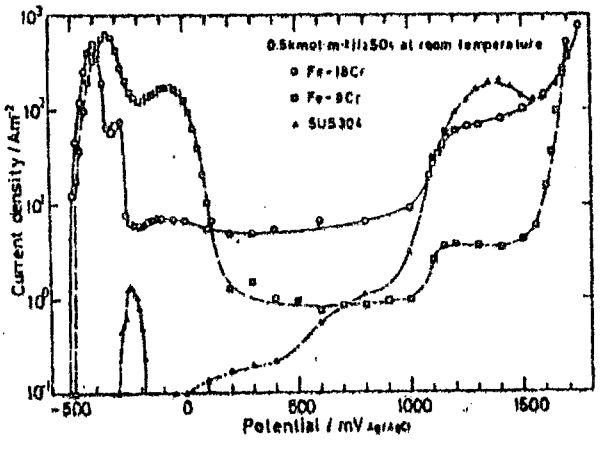

Fig.4 Polarization curves of Fe-8Cr, Fe-18Cr, and 304 steel in 0.5 kmolm^{-3} H_2SO_4.

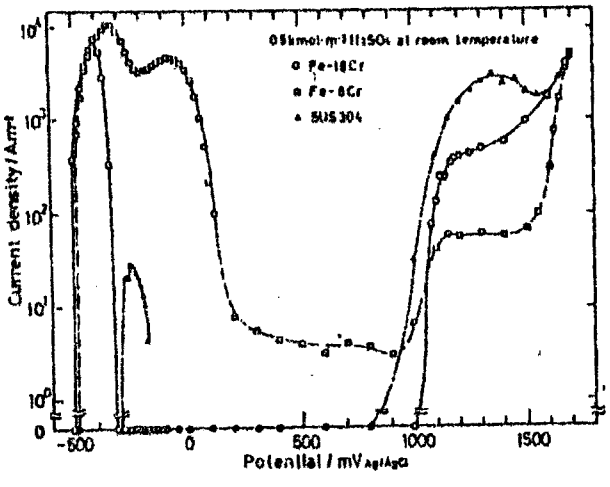

Fig.5 Laser enhanced current for the same alloys in the same solution as Fig.4.

the same solution as Fig.4. It is interesting to note that a similar potential dependence of laser enhanced current density as the polarization curves is observed for all alloys examined. That is, the higher laser enhanced current was observed both in the active potential region and in the transpassive region. It should be noticed

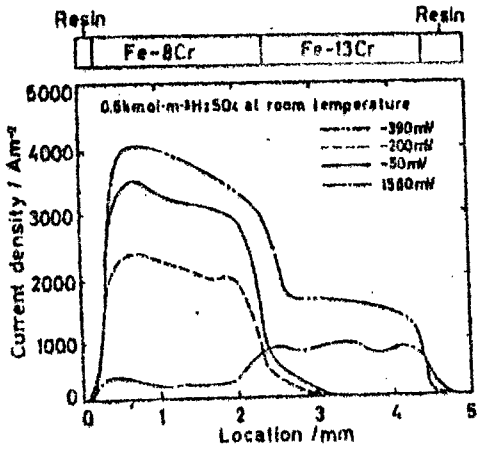

Fig.6 Line profiles across the boundary between Fe-8Cr and Fe-13Cr.

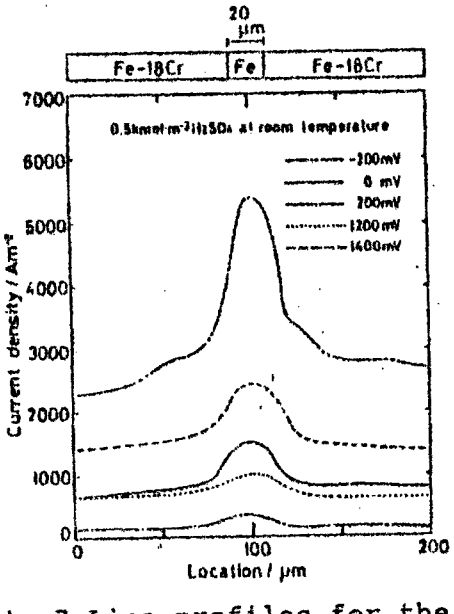

Fig.7 Line profiles for the sandwiched boundary of Fe.

that no laser enhanced current for Type 304 steel and Fe-18Cr was admitted in the passive potential region between -100 mV and 800 mV, while Fe-8Cr showed the large response to laser irradiation in the same region, especially at around -100 mV. This fact suggests that the selective response of chromium depleted zone to laser irradiation will be expected in this potential region.

4. Line profiles across the simulated boundary

Fig.6 shows line profiles of laser enhanced current across the boundary of Fe-8Cr and Fe-13Cr diffusion bonded joint which was kept at various potentials in 0.5kmolm^{-3} H_2SO_4 solution. The large laser enhanced current for Fe-8Cr was recorded at -390 mV, -200 mV and -50 mV, but the large difference between two alloys was obtained at -50 mV because Fe-13Cr shows no response at this potential. Another example of a simulated boundary consisting of Fe-18Cr/Fe/Fe-18Cr was shown in Fig.7. In this case, the larger laser enhanced current was observed at -200 mV at the thin Fe layer of 20 um in thickness, which is sandwiched between two Fe-18Cr. Thus, SLEEM can detect easily composition change in 20 um thickness. It should be emphasized that the Cr depleted zone could be detected in the active or the less noble passive potential region, but a Cr enriched zone could be detected in the transpassive potential region[7].

5. Detection of inter granular corrosion of 304 stainless steel

Fig.8 shows a comparison of laser enhanced current at grain boundary and within grain of Type 304 stainless steel to its polarization curve in the EPR solution. In this solution, the large lasor enhanced current was observed around a potential showing the critical passivation current density in the active region. A definite difference in laser enhanced current between grain boundary and grain itself can be seen in the whole potential region examined as shown in Fig.8. Thus, any potential in this active region can be used for detecting the Cr depleted zone at grain boundary, but lower dissolution current is preferable because surface change due to dissolution should be avoided as far as possible. Then, -210 mV was chosen as the setting potential for detecting intergranular corrosion. Fig.9 is a line profile across grain boundary of sensitized 304 stainless steel which was kept at -210 mV in the EPR solution.

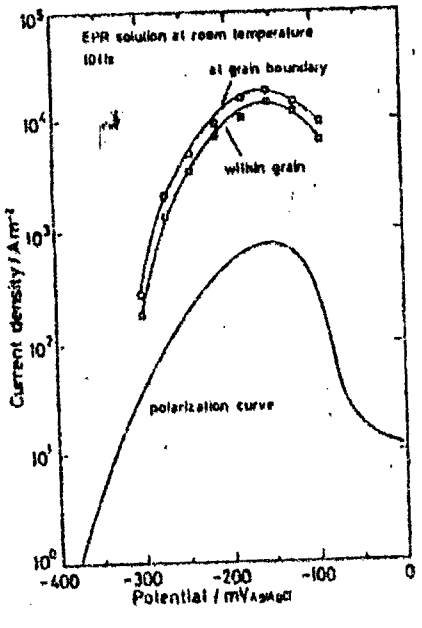

Fig.8 Laser enhanced current at grain boundary and within grain of sensitized Type 304 stainless steel with polarization curve in the EPR solution.

Clear peaks at two boundaries were seen and confirmed to correspond to boundaries at this position by CCD camera attached in SLEEM.

6. Further development and applications

In this study, the laser beam was emitted from the AlGaAs semiconductor type laser which is small in shape and low output power, so that the laser irradiation system is compact and not so expensive. Further development of the semiconductor laser to achieve the more high output power will be expected and then the much higher laser enhanced current of SLEEM will be attained to provide the higher resolution.

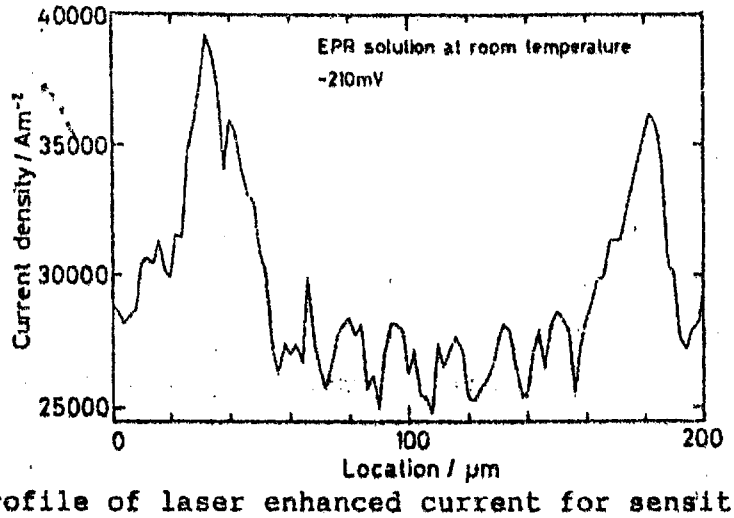

Fig.9 Line profile of laser enhanced current for sensitized Type304 stainless steel kept at -210 mV in the EPR solution, giving the grain boundary image.

The most important factor to achieve the high resolution, however, is the laser beam diameter which is now ca. 10um. The laser beam is possible to be focused theoretically to the same size as its wave length, giving resolution power of the same order. Now we are planning to use an Ar laser which emits much higher power beam and is possible to be focused below few um. The high irradiation power beam with the fine spot could provide the improved resolution which might detect the grain boundary image even in passive potential region. The high power beam with the fin spot could be used for selective dissolution and deposition which is another important application fields of SLEEM in future.

CONCLUSION

Laser enhanced electrochemical microscopy(SLEEM) using semiconductor laser of AlGaAs was proposed to identify intergranular corrosion. The lower modulation frequency the higher laser enhanced current was obtained. Spot size of laser was 10 um, which gave a high spatial resolution. Two potential regions, active and trans-passive potential region, for obtaining the high laser enhanced current were found. The active potential region was suitable to detect Cr depleted zone. Line profile of grain boundary was obtained for sensitized 304 stainless steel in 0.5kmolm-3+0.01kmolm3KSCN solution at -210 mV.

This work was supported by the Grant-in-Aid for Scientific Research no. 63850153 from the Japanese Ministry of Education, Science and Culture.

REFERENCES

1. H. S. Isaacs and B. Vyas: "Electrochemical Corrosion Testing", ASTM STP 727, p3.(1981).
2. T. Shinohara, K. Ozaki and S. Tsujikawa: Boshoku Gijutsu, 39(1990), 688.
3. K. Minoshima, S. Ogawa and K. Komai: Zairyo, 39(1990), 350.
4. S. Fujimoto and T. Shibata: Boshoku Gijutsu, 36(1987), 812.
5. S. Fujimoto and T. Shibata and Y. Tanaka: Proc. 11th Int. Corros. Cong., Vol.5, p.511(1990).
6. T. Shibata, T. Haruna and S. Fujimoto: Boshoku Gijutsu, 39(1990), 303.
7. S. Fujimoto, T. Shibata and T. Shono: Corros. Sci.,to be published.

SCANNING LASER ENHANCED ELECTROCHEMICAL MICROSCOPY FOR CHARACTERIZING LOCALIZED CORROSION

Shinji FUJIMOTO, Toshio SHIBATA and Tomoryo SHONO

Department of Materials Science and Processing,
Faculty of Engineering, Osaka University
2-1 Yamada-oka, Suita OSAKA 565 Japan

Abstract -- A newly developed Scanning Laser Enhanced Electrochemical Microscopy (SLEEM) has been applied for corrosion studies. A focused infra-red laser beam was scanned over a metallic specimen which was polarized at a constant potential. Increase in the anodic current accelerated by a localized temperature rise was detected as a function of position. The image of enhanced anodic current distribution was successfully obtained for the two phase stainless steel polarized at an over-passive potential.

INTRODUCTION

In recent years, the electrochemical micro probe techniques with the scanning focused laser irradiation have been developed by some authors(1-3) in order to characterize passive films as a function of position, in terms of the semiconductive property. In those techniques, the laser light mainly contributes to excite electrons from the valency band to the conduction band, resulting in the photo current. The other important effect of laser is local heating on a surface, which may accelerate the electrochemical reactions including dissolution and deposition(4). In this study, an infra-red laser has been introduced in order to detect localized corrosion at in-situ condition. The focused infra-red laser beam was scanned over a specimen polarized at an anodic potential, in order to get a map as the response of anodic current which is accelerated by the temperature increase.

APPARATUS AND EXPERIMENTAL PROCEDURE

A block diagram of the Scanning Laser Enhanced Electrochemical Microscopy (SLEEM) is illustrated in Fig.1. A semi-conductor laser diode (AlGaAs), wave length and maximum power of which were 830 nm and 40 mW, respectively, was used as light source, which was focused by X20 optical microscope, the work distance being approximately 10 mm. The laser beam can be focused to ca.10 μm diameter with 10 mW output power at operation, so that the power density was calculated to be approximately 1.3×10^{4} W/cm^{2}. The specimen was cut into a small bar of 1x1 mm cross section, mounted in an epoxy resin, and polished. The mounted specimen was covered with a synthetic rubber O-ring of 7.5 mm internal diameter, and a glass plate of 0.15 mm thickness was placed on the O-ring. An electrolyte was filled in the closed space. The thickness of the solution layer was 1.85 mm, and hence the volume of the confined space was 61 mm^{3}. The test solution was stored and deaerated by nitrogen gas in another vessel, and was circulated with flow rate of 50 mm^{3}/min. The micro cell thus assembled was provided with an

---

Corrosion Science, 32, 669(1991).

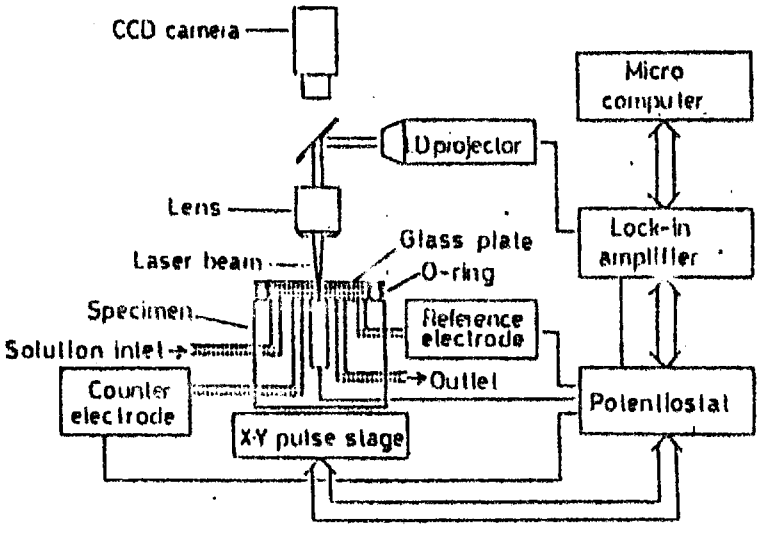

Fig.1 Schematic drawing of SLEEM.

Ag/AgCl reference electrode and Pt counter electrode connected through PTFE capillaries. The specimen in the micro cell was scanned by an X-Y stage driven by stepping motors. The surface optical image and reflection of the laser beam were able to be monitored at the same time by a CCD (Charge Coupled Device) camera. The laser could be switched on and off at a frequency of 10 Hz. The small cyclic current synchronizing with the modulated laser irradiation was observed overlapping on a steady current, and was separated and amplified with a lock-in amplifier (NF Electric Instruments, model 5610).

RESULTS AND DISCUSSION

The response in the anodic current to laser irradiation was demonstrated in Fig.2 for Type304 stainless steel polarized at an over-passive potential in 0.5 kmol/m^3 H_2SO_4. Laser spot was scanned linearly across the boundary between the specimen and the epoxy resin in which the specimen was mounted. Increase in the current by laser irradiation, which is proportional to the

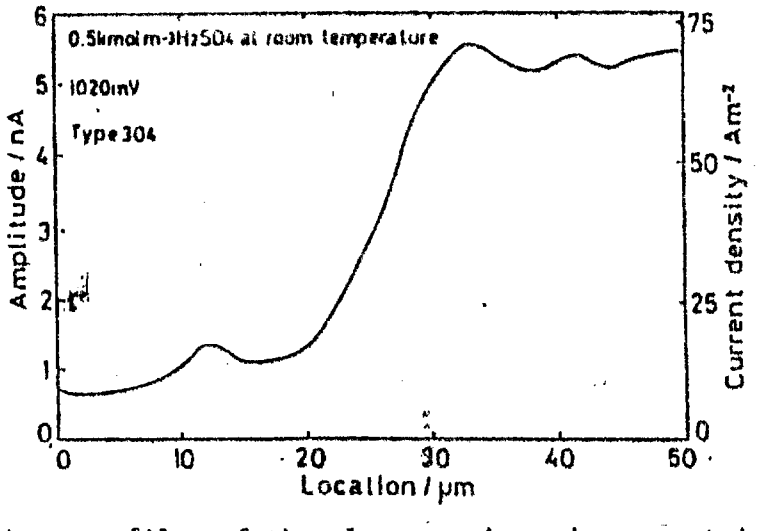

Fig.2 Line profile of the laser enhanced current image scanned across the boundary between resin and Type304 stainless steel polarized at 1020 mV in 0.5 kmol/m^3 H_2SO_4 at room temperature.

amplitude of current oscillation synchronizing with laser modulation, was plotted versus position. As demonstrated in this figure, almost no current response, is observed for the laser irradiation on the resin, while steep increase starts as the laser beam irradiates the stainless steel, then reaches to a steady level. The width of the transient region from the back ground to the increased steady level is approximately 10 μm, which corresponds to the size of the laser beam. Thus, the laser activated current can be converted to current density by dividing the increased current by the spot area, as indicated in the figure.

The laser spot was scanned across the diffusion joined boundary of Fe-8Cr and Fe-18Cr alloys, which were kept at various applied potentials in 0.5 kmol/m^3 H_2SO_4, as shown in Fig.3. The laser activated current was found to depend on the chromium content and the applied potential. This figure shows that the larger enhanced current was observed for the lower chromium content alloy of Fe-8Cr in the active potentials of -390 and -200 mV, whereas the higher chromium alloy of Fe-18Cr shows the larger enhanced current at the over passive potential of 1600 mV. At the passive potential of 250 mV, however, a slight enhanced current is only observed for the Fe-8Cr alloy, while not any for the Fe-18Cr alloy. It is concluded that the laser enhanced current is roughly proportional to the current without laser irradiation, which could be measured in polarization curve, with the factor of several tens changing as a function of the potential and the alloy composition. Thus, a difference in the chromium content in the grain boundary or in the different phase, that are responsible for localized corrosion attack, could be detected by using SLEEM.

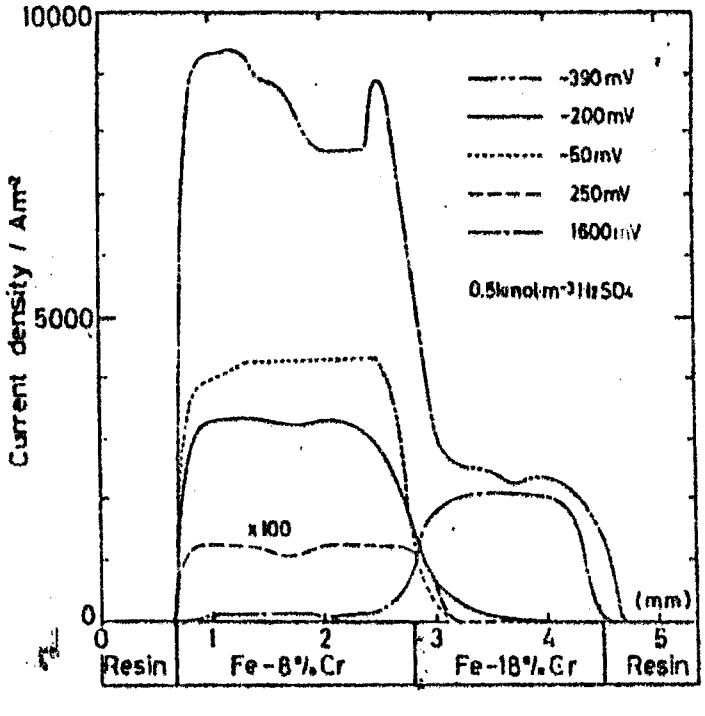

Fig.3 Line profile for the current imaging across the boundary between Fe-8Cr and Fe-18Cr alloys kept at various applied potentials.

Figure 4 shows the scanning laser enhanced electrochemical microscopy image obtained for a two phase stainless steel, the chemical composition being ; Cr:25.35, Ni:7.35, Mo:3.15, C:0.022, Si:0.42 (mass %), and Fe:bal. Figure 4(a) illustrates the difference in anodic current for each grains of the two phase steel in 0.5kmol/m^3 H_2SO_4 at the over-passive potential of 1070 mV. As observed in the figure, the ferritic phase, which appears as dark grains in Fig.4(b), exhibits the larger activated current.

The resolution power of SLEEM described here will be improved to be up to few μm, because the laser beam is possible to be focused theoretically to the same order as its wave length. It has been already achieved that the intergranular attack of sensitized Type304 stainless steel is successfully detected with SLEEM, which will be described elsewhere. In conclusion, the current imaging with laser beam scanning will be promising technique to evaluate the localized corrosion susceptibility at the in-situ condition.

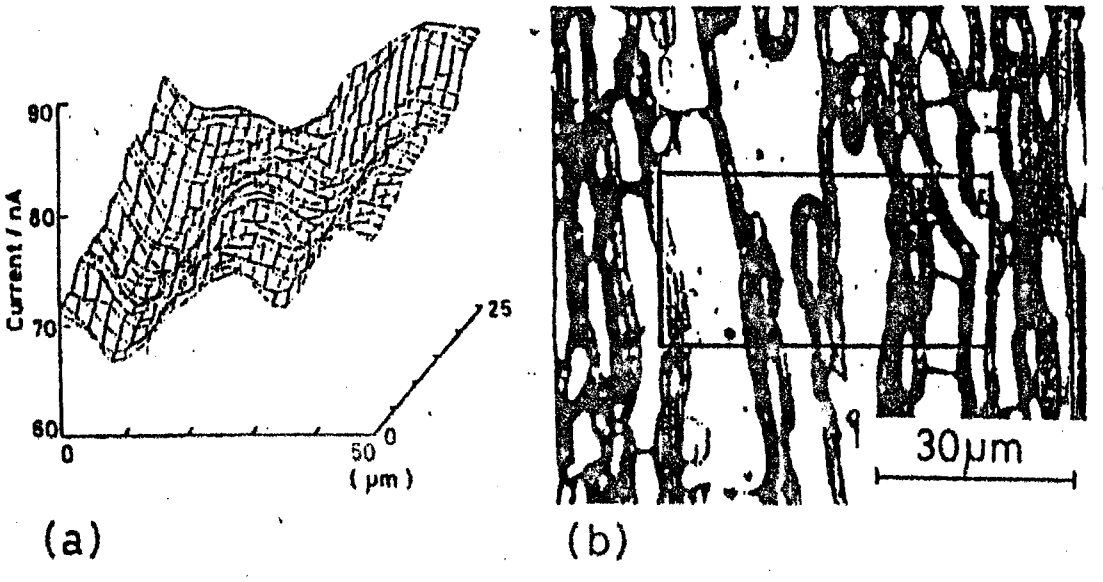

Fig.4 (a): SLEEM image on two phase stainless steel polarized at the over-passive potential of 1070 mV, and (b): Photograph of the corresponding area. The square indicates the scanned area shown in (a).

REFERENCES

1. M.A.Butler, J.Electrochem.Soc. 130, 2358 (1983).
2. D.Shukla, T.Wineg, and U.Stimming, J.Electrochem.Soc. 134, 2086 (1987).
3. M.R.Kozlowski, P.S.Tyler, W.H.Smyrl, and R.T.Atanasoski, Corrosion 46, 505 (1990).
4. R.J.von Gutfeld, E.E.Tynan, R.L.Melcer, and S.E.Blum, Appl.Pys.Let. 35, 651 (1979).

STRESS CORROSION CRACKING ON SOME COMPONENTS USED IN OIL INDUSTRY (*)

A.D. Wiyono, H. Sunandrio, E. Sumarsono, A. Partowiyatmo

UPT-LABORATORIUM UJI KONSTRUKSI
BPP-TEKNOLOGI, PUSPIPTEK
SERPONG, INDONESIA

A B S T R A C T

Stress corrosion cracks (SCC) is a general term describing stressed alloy failure that occur by the propagation of cracks in corrosion environments. The requirement for SCC to occur are the presence of tensile stress, either residual, applied or a combination of both, and the presence of a specific corrodent.

In the present study, two damaged components used in oil industry were examined which indicated stress corrosion cracking (SCC).

The two components under studied were : 1) weld area between backing plate and diapraghm, and 2) tube sheet stud-bolt of recycle combined feed exchanger on the Hydrocracking Plant.

Examination used in this study included metallography, fractography, chemical composition analysis and mechanical test.

The results of investigation showed that the SCC on the two mentioned components were caused by chlorides.

(*) Presented for Seminar/Workshop on Corrosion and Protection, held in Thailand, June 30-July 2, 1992.

I. INTRODUCTION

The oil industry is a major contributor to modern technical civilization as supplier of energy and raw materials for the manufacture of many chemical from carbon black and ammonia through alcohols and glycol to synthetic rubber, man-made fibers and plastics.

A large variety of corrosive conditions is encountered in different facets of this industry from oil production through transportation to processing and storage of oil and petrochemical streams.

Stress corrosion cracking is one of several typical corrosion problems encountered in oil industry.

Stress corrosion cracking (SCC) is an interaction between tensile stress and corrosion, which results in localized cracking. SCC is a progressive type of failure that produces cracking at stress levels are well below those of a material's tensile strength. Therefore, the wrong combination of environment, material and minimum tensile strength will produce SCC in any metal or alloy : steel, stainless steel, nickel-based alloy, aluminium and titanium.

SCC has a characteristic appearance, which in many cases it easy to identify. One of the most outstanding features is the black corrosion deposit that exists on the fracture surface. When viewed from the outside surface, a fracture caused by SCC generally is jagged, which is due to the fact that the origin results from the combination of a number of cracks that are not directly in line with each other.

SCC are generally found in cluster; the cracks surrounding the primary crack are reffered to as secondary cracks. Rather than a single crack, a whole network of fine, feathery, branched cracks will form. The break or fracture appears brittle, with no localized yielding, plastic deformation or elongation.

Pitting is frequently seen, and will often serve as a stress concentrator to initiate cracking. One or more cracks will grow from the pit, eventually leading to failure.

Many of these failures occurs only under the most severe laboratory conditions and in the past were usually not encountered in the field. However, such conditions now found commercially with greater frequency as oil production, oil refining, petrochemical-processing, power plants are using higher pressures and temperatures to increase efficiencies.

This paper discusses are two cases of failures caused by stress corrosion cracking (SCC) on some components used in oil industry, namely :

1. SCC on backing plate and diapraghm of recycle combined feed exchanger,
2. SCC on tube sheet stud-bolt of recycle combined feed exchanger,

In many cases, the cause of failure is not what it appeared to be, and identifying the actual cause can be very helpful in determining when the next failure will occur and what additional measures should be taken to prevent failures.

II. CASE HISTORY NO.1

Stress corrosion cracking (SCC) of backing plate and diaphragm of recycle combined feed exchanger in Hydrogen Plant.

2.1. INFORMATION

A. Exchanger Specification Sheet.

Size / type	: 31"-240"/D-E-U
Shell per Unit	: 4
Surface per Unit	: 848,4 m^2
Surface per Shell	: 212,1 m^2

B. Performance of one Unit

	Shell side	Tube side
Fluid circulated	HCBN + H_2	HCBN + H_2
Total fluid entering, Kg/cm^2	60,849	60,849
- vapor, Kg/cm^2	14,142	37,409
- liquid, Kg/cm^2	46,707	23,440

	Shell side	Tube side
Fluid vaporized or condensed, Kg/cm^2	442	16,380
Temperatur in / out, ^oC	148 / 360	405 / 211
Operating pressure, Kg/cm^2	191,47	179,01
C.Construction.		
Design pressure, Kg/cm^2	201	188,9
Design temperature, ^oC	388	427
Material	2¼ Cr-1Mo	304 SS

Material for other component :

- Shell cover 2¼ Cr-1Mo
- Channel 2¼ Cr-1Mo lined w/321 or 347 SS
- Channnel cover 2¼ Cr-1Mo
- Backing plate 347 SS
- Diaphragm 347 SS
- Tube sheet-stationary 304 SS
- Baffles/Tube Supports 304 SS

During the operation some fluid was leak in the area of backing plate and diaphragm in the position of bottom side of exchanger (see figure 1).
At the time of failure, the unit of exchanger had been in service for about eight years.
The section received for laboratory investigation was removed from the inner side joint between backing plate and diaphragm (see figure 2).

Information and detail data on composition of hydrocarbon, flow-chart of hydrocraking processing and maintenance history were not available.

2.2. MACROSCOPIC EXAMINATION.

The inside surface of backing plate which is in contact with a diaphragm and adjacent to welding area was found to reveal a number of cracks and pitting corrosion (see figure 3).

Also, the outside surface of backing plate showed the same cracks and pittting corrosion (figure 4).

The inside surface of diaphragm which is in contact with a backing plate revealed a crack and showed no evidence of a deformation area (figure 5). On the contrary, the outside surface of diaphragm revealed a crack and showed evidence of a deformation area (figure 6).

The specimens which were taken in the longitudinal section on both of backing plate and diaphragm showed cracks starting from both of the inside surface, especially near the circumference of welding area (figure 7). The cracks exhibit typical branching as a characteristic appearance of SCC. This typical crack were encountered more on the diaphragm than on a backing plate, and initiating from the inside surface (figure 8).

2.3. MICROSCOPIC EXAMINATION

The cracks typically exhibit some branching and transgranular propagated from inside to outside surface of diaphragm (figures 9 and 10). Microstructure of diaphragm consists of austenite and showed no evidence of sensitization.

On the backing plate, transgranular SCC initiated adjacent to HAZ from inside to outside surface (figures 6 and 11). Microstructure of backing plate also consists of austenite and elongated carbides in direction with rolling orientation is still clearly distinguished (figure 12).

2.4. HARDNESS TEST

The results of hardness test of the backing plate and diaphragm has average value about 164 BHN (85 HRB) and 176 BHN (88 HRB).

2.5. CHEMICAL COMPOSITION

The qualitative result of analysis on the sludge which taken

from recycle combined feed exchanger is summarized in Table 1. Some quantitative analysis on corroded elements caused by SCC was also carried out, and the results are shown in Table 2.

2.6. DISCUSSION

We conclude from the macroscopic, microscopic observation and chemical analysis that the cracks of the backing plate and diaphragm is typical stress corrosion cracking (SCC) initiated from inside surface and propagated to outside surface of the both components.

Based on the some references about SCC on stainless steel could be occurred as resulting by;

a. Polythionic Acid Cracking [1)]

The technological problem encountered in the petroleum industry is essentially as follows. Stainless steel components are used at operating temperatures that may be high enough to sensitize the material. On subsequent shutdown of a refinery unit, polythionic acid ($H_2S_xO_6$, where x = 3, 4 or 5) may form by the interaction of sulfur compounds, moisture, and air at low temperatures, and attack the chromium depleted boundaries.

b. Chloride Cracking [2)]

Without doubt, the most common stress corrosion cracking agent is the aqueous chloride ion (SCC is an electrochemical process, and water is necessary to allow electron flow; completely dry chloride compounds are not normally cracking agents). Common in brackish river water, sea water and coastal atmospheres, the chloride ion can cause SCC of austenitic stainless steel even at extremely low concentrations. Failures have been reported in steam condensate having as little as 0,5 ppm chlorides. Such low levels are not normally dangerous to stainless. However, in spots where evaporation and concentration raise the local level of chloride-such as

crevice, deposits and liquid-vapor interfaces cracking can still take place. Under these conditions, the only safe level of chlorides is zero.

Chlorides cracking usually adopts a transgranular path, with some segments of the crack following the slip planes of the austenite lattice.

C. Caustic cracking [1,2)]

Caustic environments many also crack stainless steel, and are perhaps the second most common cause of unexpected SCC failures. The austenitic stainless steel find many uses in such environments at temperatures below 150°C. Above that temperature, however, cracking can take-place.

The use of austenitic alloys in heat exchanger or in conventional boiler technology that boiling and steam blanketing at heat transfer surfaces can give rise to very high local concentrations of caustic. The extent to which caustic can concentrate, at equilibrium conditions, as a function of the temperature difference between the bulk environment and a thin film of liquid at the heat transfer surfaces.

We conclude that SCC in caustic environment should be occured more on the tube surfaces.

According to reference[2)], stainless steel (347 type) has been found not resistant in environment containing chlorides as showed in table 3.

Based on the above mentioned discussion in conjunction with chemical composition of sludge, we suspected that the stress corrosion cracking agents in recycle combined feed exchanger which cause of SCC on the material 347 SS of the backing plate and diaphragm is chlorides.

2.7. CONCLUSION

From this failure analysis on stainless steel 347 type for components of backing plate and diaphragm of recycle combined

feed exchanger, several conclusions can be drawn.

1. Cracks occurred on the backing plate and diaphragm is typically chlorides stress corrosion cracking.
2. Chlorides as stress cracking agents were contaminated in the sludges. The chloride can raise their concentration in crevice between backing plate and diaphragm.
3. Cracking is observed in the base material of both components adjacent to weld areas.
4. Plastic deformation (induced the residual compressive stress) on the outside surface of diaphragm may give contribution to the rise of subsurface residual tensile stresses on the inside surface. However, SCC was found to occur more pronounce on the diaphragm (This may be necessary to be proved by X-ray difraction).
5. Backing plate and diaphragm were made from austenitic steel type 347 which is according to standard ASTM A 213-7913 (They have a Brinell hardness not exceeding 192 or Rockwell B 90).

III. CASE HISTORY NO.2

Stress corrosion cracking (SCC) on tube sheet stud-bolt of recycle combined feed exchanger.

3.1. INFORMATION

From 36 pieces of stud-bolt as fastener tube-sheet on the shell exchanger, during inspection were found 6 pieces was broken. The broken stud-bolts in between to the 5 to 7 o'clock position of the tube sheet. Stud-bolt has diameter 37,50 mm and 188 mm in length, made of a material according to specification SA 213 TP304H.
Whereas exchanger specification is the same with point 2.1. as has been described in the case history no.1.

At the time of failure, the unit of exchanger had been in service for about eight years. Three from six broken stud-bolts have been taken for laboratory examination (see figure 13).

Information and detail data on about composition of hydrocarbon, flowchart of hydrocarbon processing and maintenance history were not avalaible.

3.1. MACROSCOPIC EXAMINATION

From macroscopic examination it was found that some black corrosion deposit was existed on the fracture surface at the both of broken stud-bolt (see figures 14 and 15).
The fracture surface generally exhibit jagged or rough to coarse grained, coated and no deformation.
The cracks were also found to appear in thread surface areas of stud bolt (under main fractures) that progress linearly, branched with mostly negligible uniform surface corrosion (figures 16 and 17).

3.2. MICROSCOPIC EXAMINATION

The cracks generally originate from one of the thread root (figure 18) with transgranular path and a whole network of fine cracks was characterized as stress corrosion cracking (figure 19). They often branch off in clusters (figures 20 and 21).
The microstructure of stud-bolt consists of austenitic with fine carbides to disperse throughout the microstructure (figure 22).

3.3. DISCUSSION

Based on the references that had been described in point 2.6. we conclude from these macroscopic and microscopic observations that the cracks of a stud-bolt is typically chlorides stress corrosion cracking.

3.4. CONCLUSION

The result failure analysis on stud-bolt of recycle combined feed exchanger can be concluded as follows :

1. Stud-bolt with material SA 213 TP304H is susceptible to chloride environtments.
2. Chloride as cracking agents was found to contain in the sludge and these sludge contaminated on the stud-bolt to the 5 to 7 o'clock position.

ACKNOWLEDGMENTS

The authors wishes to acknowledge the help of Dr.Ir. D.N. Adnyana as a senior scientist BPPT for their valuable discussions, review of the manuscript and comments.

REFERENCES

1). A.John Sedriks,"Corrosion of stainless steel", John Wiley & Sons, 1979, p.55,95,172.

2). D.R. Mc Intiry,"How to prevent stress corrosion cracking in stainless steel, I & II", Chemical Engineering, 7 April 1980,p.107-112.

3). James L.Gossett, "Stop stress corrosion cracking", Chemical Engineering, 15 November 1982, p.143-146.

4). Z.A. Foroulis, " Corrosion and Corrosion inhibitor in the petroleum industry", Verlag Chemie GmbH, 1982, p.121-131.

Table I.

Qualitative chemical analysis of sludge*)

A. Sludge-I (taken under tube-bundle).

Ca	S	Se	As	Sb	Te	Sn	Si	Ag	Ni	Fe	Cl^-	NO_3^-
+	+	-	-	-	-	+	+	-	+	+	+	-
Al	Mn	Zn	Au	Cr	Mg	Bi	P	B	Co	Na	K	Cs
+	+	+	-	+	-	-	+	+	-	+	-	+
V	W	Pt	Sr	Ti	Ba	In	Cu	Pb	Mo	Zr		
-	-	-	+	-	-	+	+	-	+	-		

B. Sludge-II (taken in the area of backing plate & diaphragm).

Ca	S	Se	As	Sb	Te	Sn	Si	Ag	Ni	Fe	Cl^-	NO_3^-
+	+	-	-	+	-	+	+	-	+	+	+	-
Al	Mn	Zn	Au	Cr	Mg	Bi	P	B	Co	Na	K	Cs
+	+	+	-	+	-	-	-	+	-	+	-	+
V	W	Pt	Sr	Ti	Ba	In	Cu	Pb	Mo	Zr		
-	+	-	+	-	-	+	+	-	+	-		

Note : Kation detected by ICP (Inductively Couple Plasma Spectrophotometer).

Anion detected by HPLC (High Performance Liquid Chromatography).

*) These chemical analysis had been conducted by Laboratory of Metallurgy Laterite - LIPI.

Table 2.
Quantitative chemical analysis of sludge**)

Element	Concentration, % weight		Methods
	Sludge - I	Sludge - II	
Cl^-	< 0,162	0,33	Volumetric
S_{total}	21,44	20,63	Volumetric
NaOH	0,30	1,63	Ion chromatography

**) These chemical analysis had been conducted by Laboratory of Applied Chemistry - LIPI.

Table 3.
Aqueous environment that can cause SCC in stainless steel.

MATERIAL	Environment					
	Cl^-	OH^-	S^{2-}	S^{2-}/Cl^-	S_4O_6	NH_3
304	5	4	2	5	3	1
304L	5	4	2	5	3,4	1
318	5	4	2	5	3	1
316L	5	4	2		3,4	1
321	5	4	2	5	1	1
347	5	4	2	5	1	1

Code : 1 Resistant
2 Resistant unless cold-worked or hardened
3 Resistant unless sensitized
4 Resistant except at high temperatures and concentrations
5 Non resistant

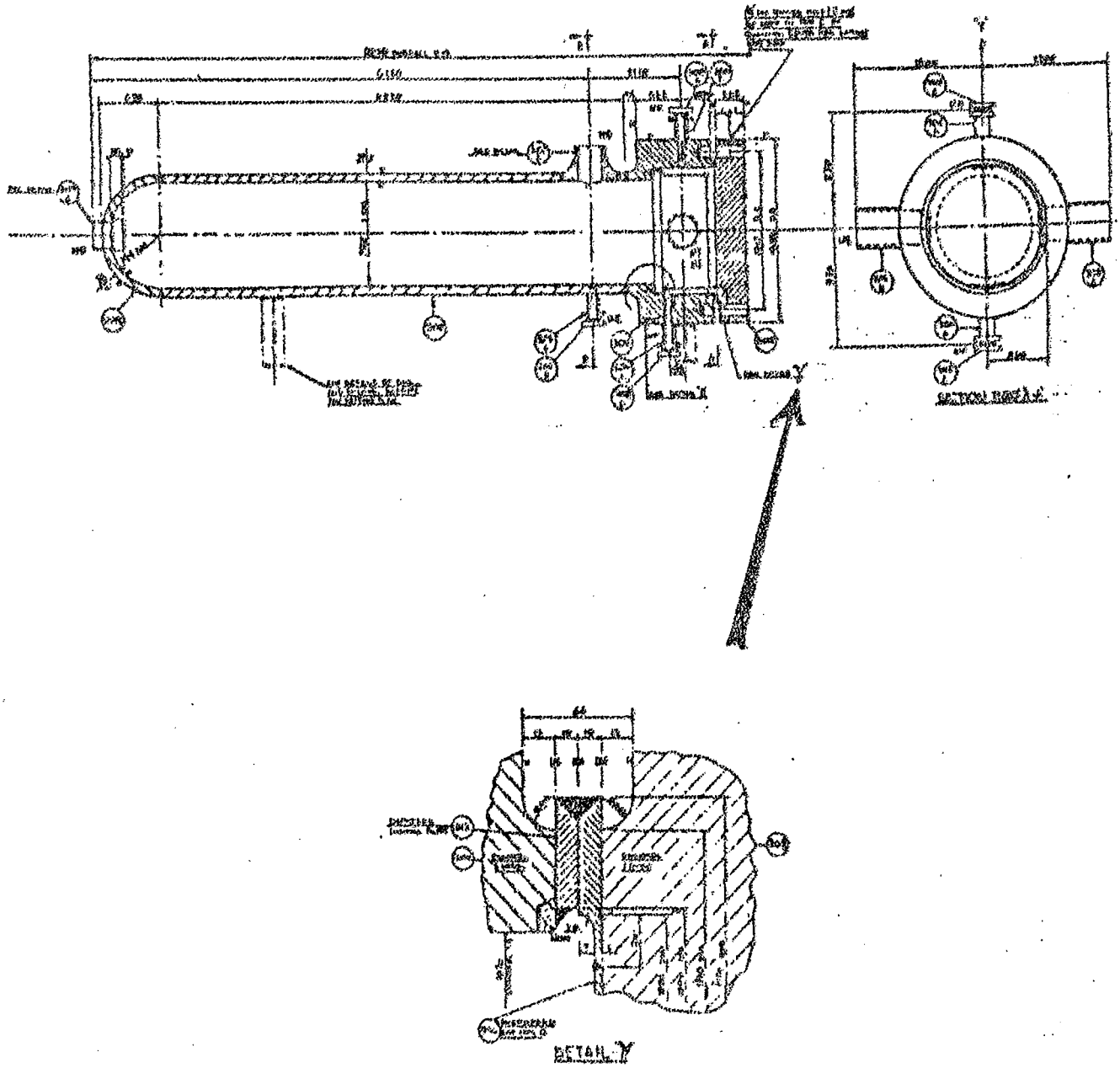

Figure 1. Schematically recycle combined heat exchanger and sample position was taken at bottom side (detail-Y).

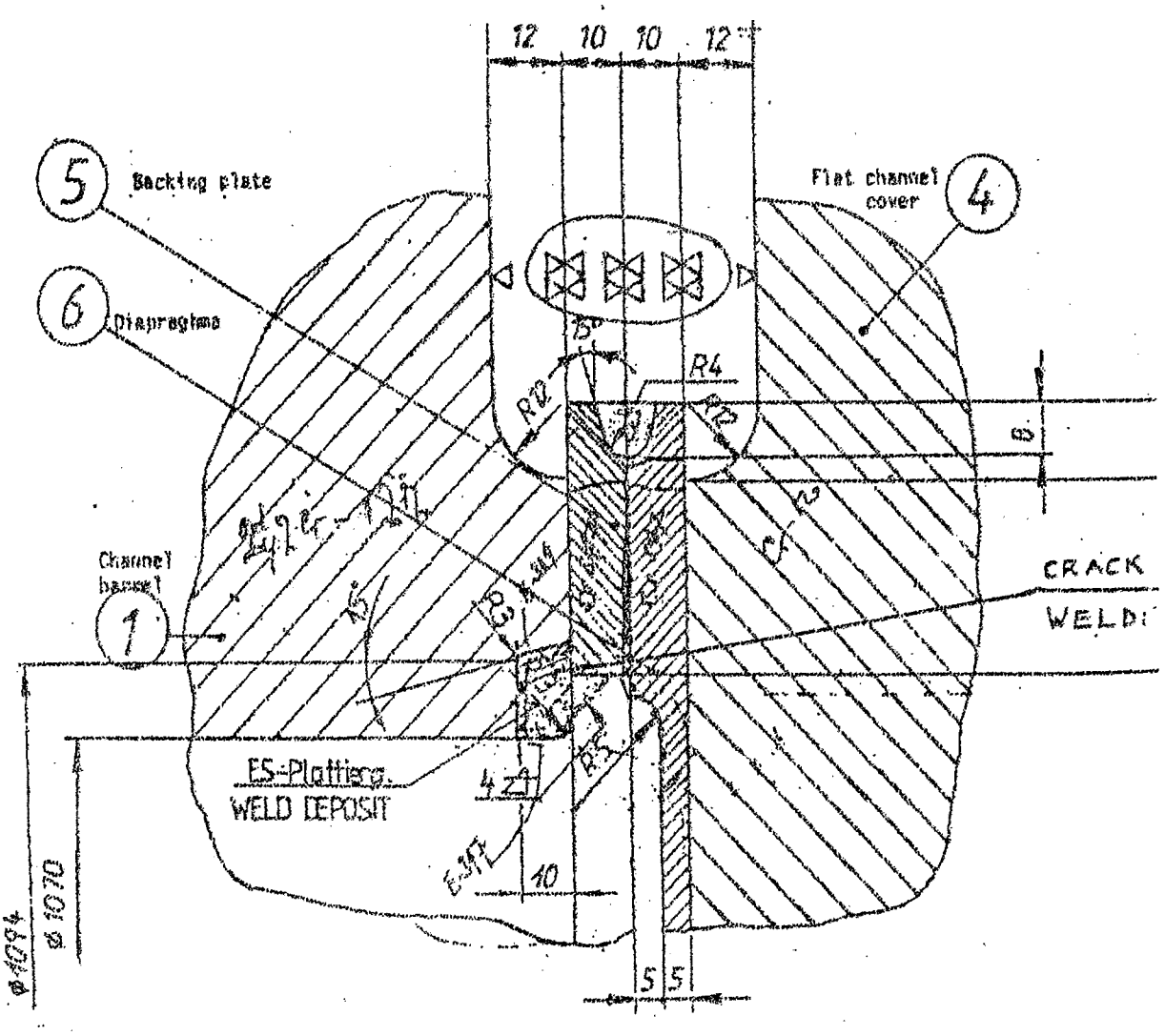

Figure 2. Sample section was taken from backing plate and diaphragm for laboratory examination.

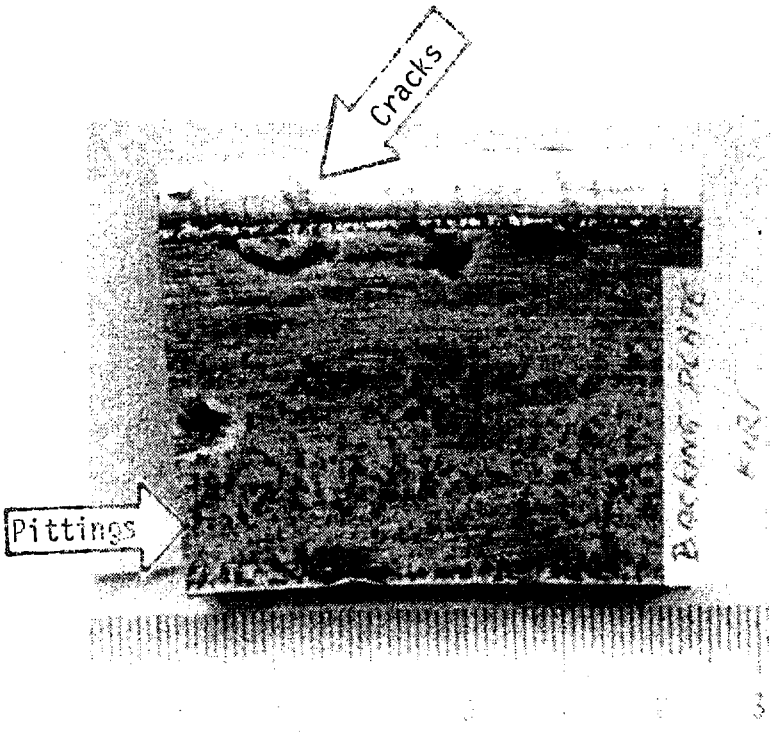

Figure 3. Inner surface of backing plate revealed a cracks adjacent weld area (top) and some pittings corrosion (1,5 X).

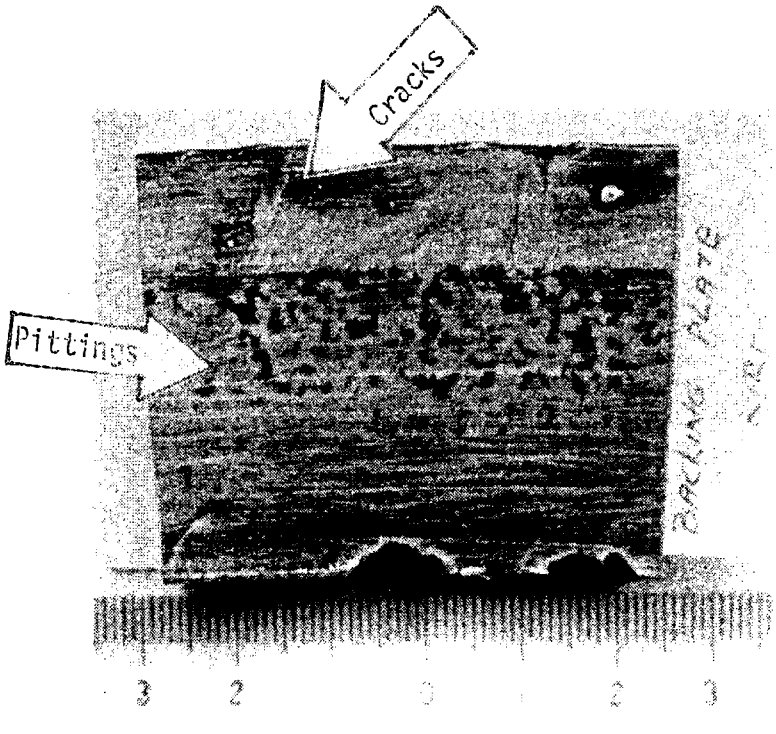

Figure 4. Outer surface of backing plate also revealed some cracks and pitting corrosion (1,5 X).

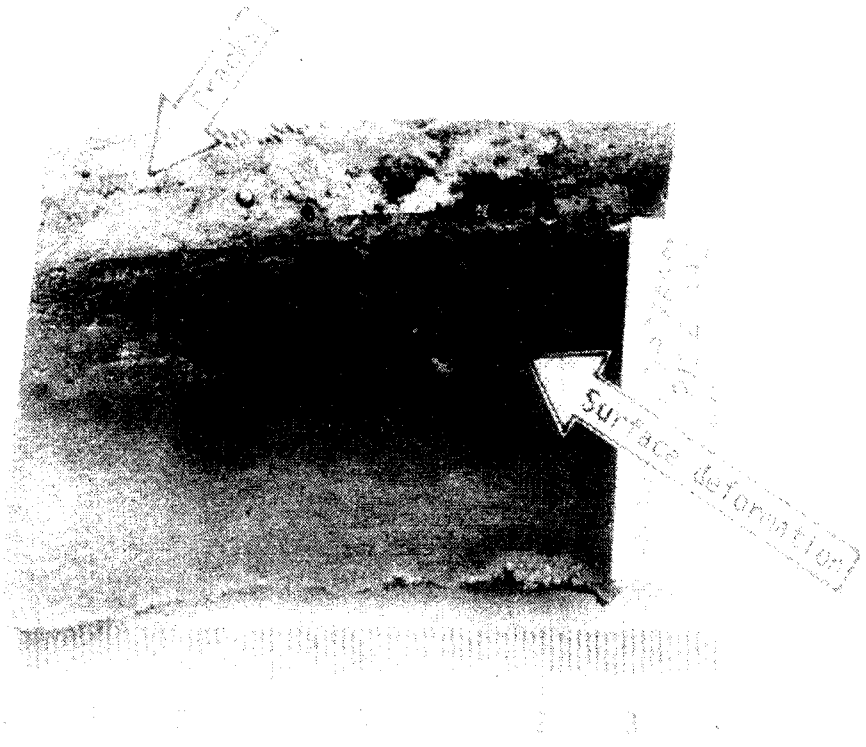

Figure 5. Outer surface of diaphragm revealed some cracks close to the weld zone and surface deformation (1,4X).

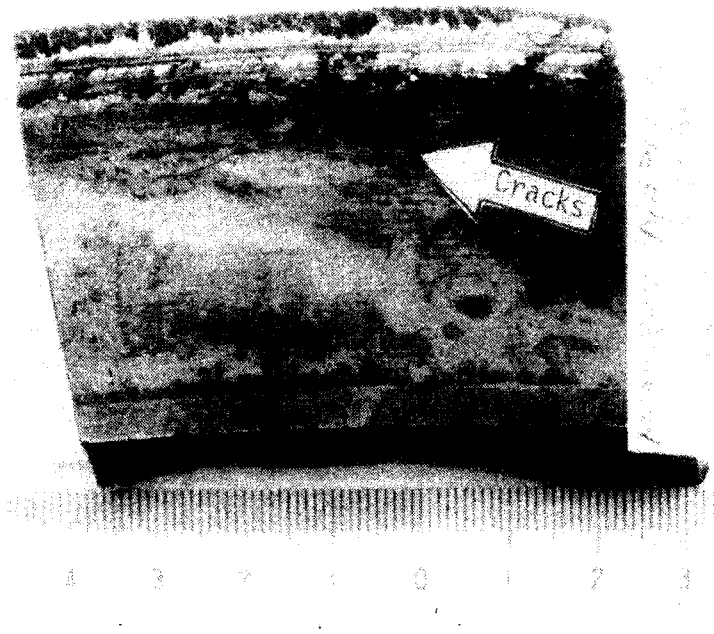

Figure 6. Inner surface of diaphragm also showed some cracks (1,4X).

Figure 7. Specimens section was taken through backing plate (left side) and diaphragm (right side).

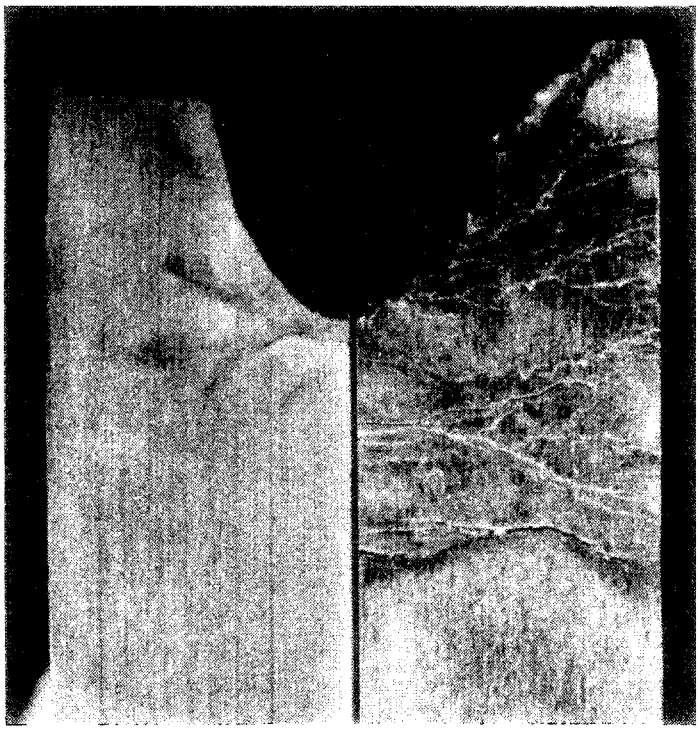

Figure 8. Branched cracks initiated from inner surface of the both components and propagation to the outer surfaces (12 X).

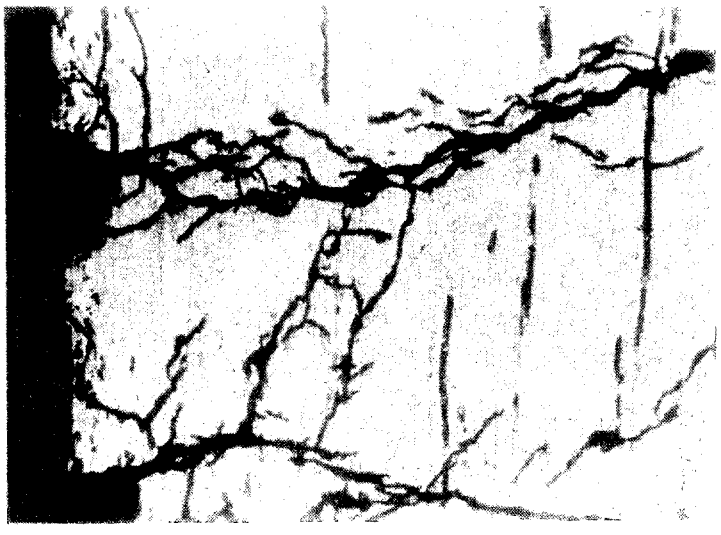

Figure 9. Branched cracks with transgranullar propagation as a characteristic appearance of SCC starting from inner surface of diaphragm (left side), 100 X magnification, Kalling's etched.

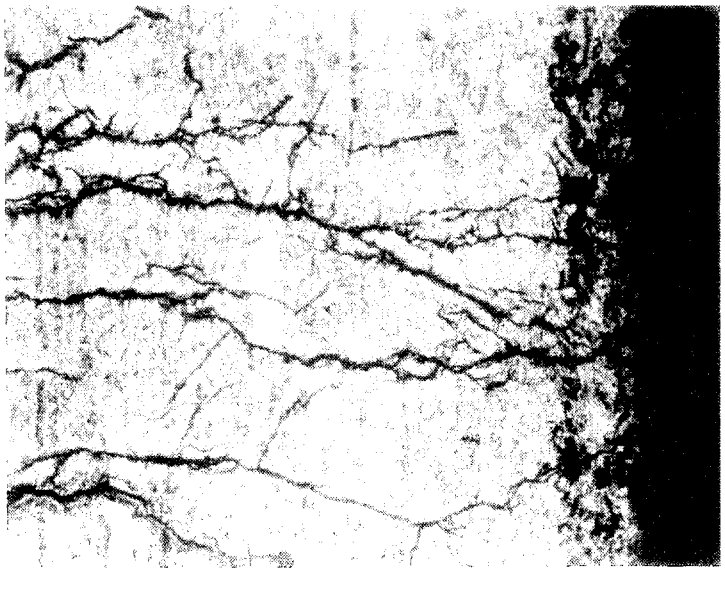

Figure 10. The end of branched cracks lead to the outer surface of diaphragm which it was revealed some pittings corrosion (100X, Kalling's etched).

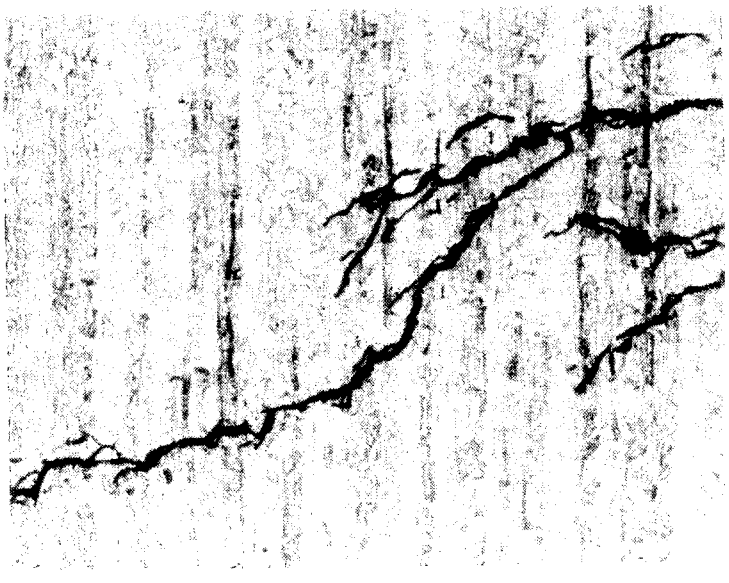

Figure 11. SCC on the backing plate initiated from inner surface (right side) and propagated to the outer surface (left side), 200 X magnification and Kalling's etched.

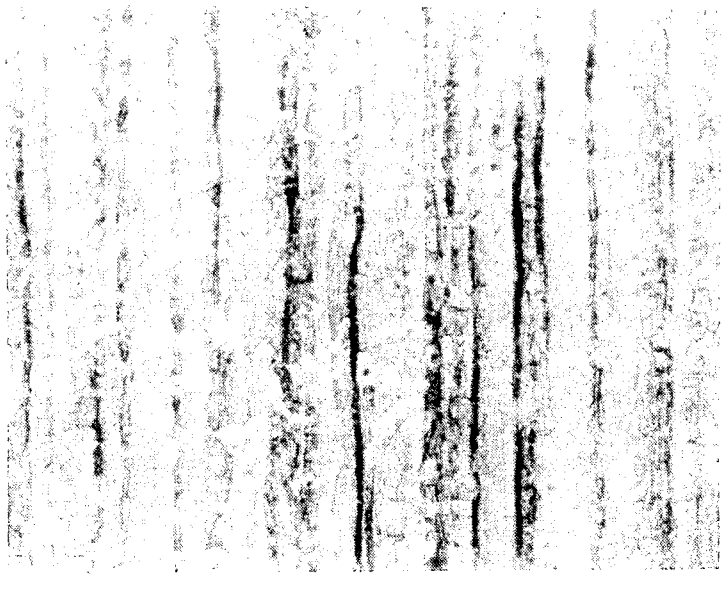

Figure 12. Microstructure of backing plate consists of austenite with elongated carbides (200X, Kalling's etched).

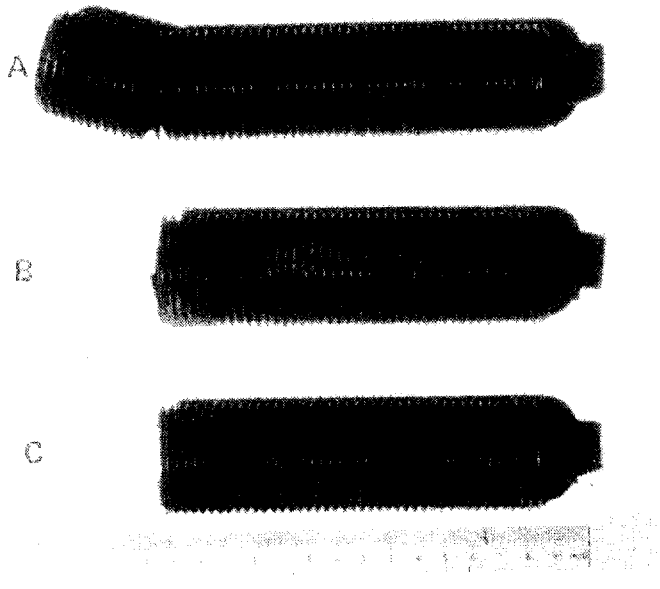

Figure 13. Three from six broken stud-bolt of tube sheet at recycle combined feed exchanger was sent to the laboratory for failure analysis.

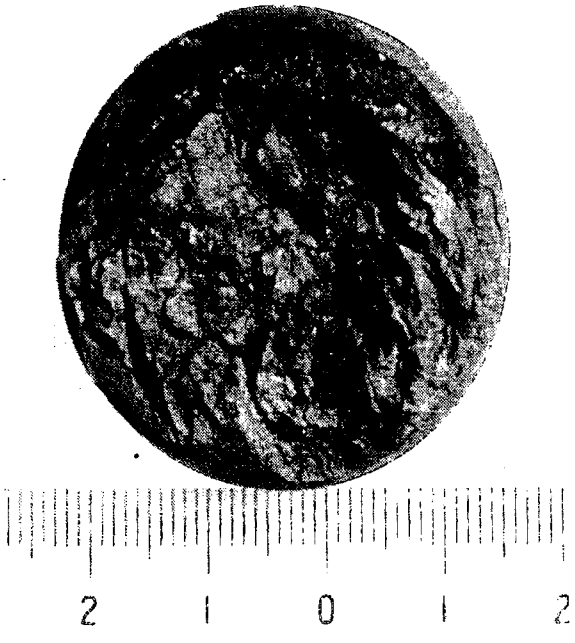

Figure 14. Fracture surfaces of stud-bolt-B revealed brittle, jagged and coated with corrosion deposit (2 X).

Figure 15. Fracture surfaces of stud-bolt-C also showed the same appearance as above (2X).

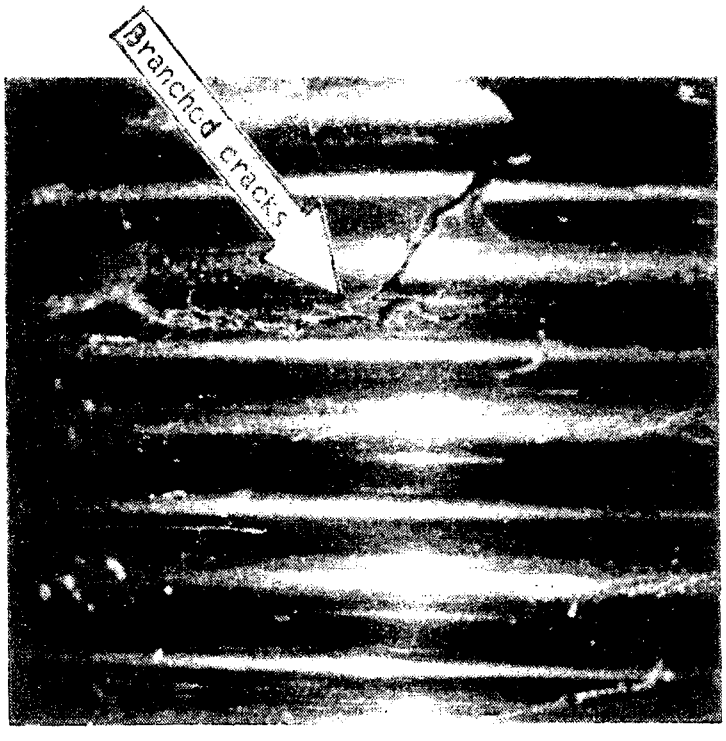

Figure 16. Branched cracks also revealed on the thread surface of stud-bolt-B under the main fractures (12 X).

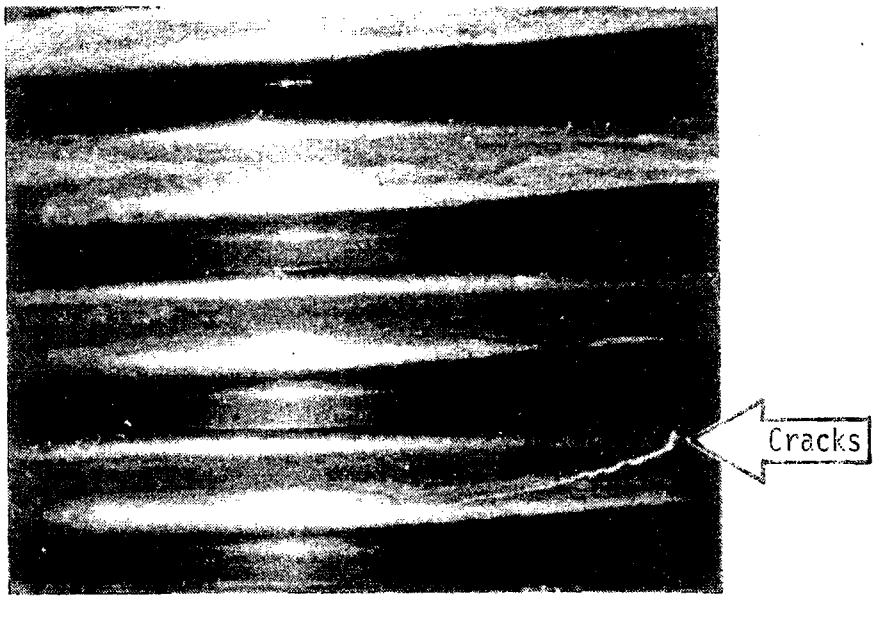

Figure 17. SCC still found at another thread surface of stud-bolt-B under the main fractures (12 X).

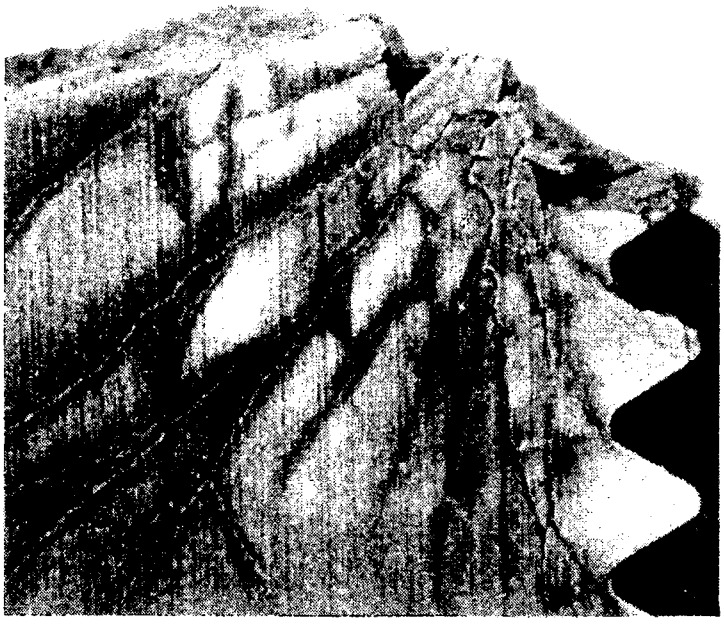

Figure 18. Longitudinal section through the stud-bolt-B showing of branched cracks initiated from one of the thread root (6 X, Kalling's etched).

Figure 19. Cross section of stud-bolt-B also showing of branched crack forms (6 X, Kalling's etched).

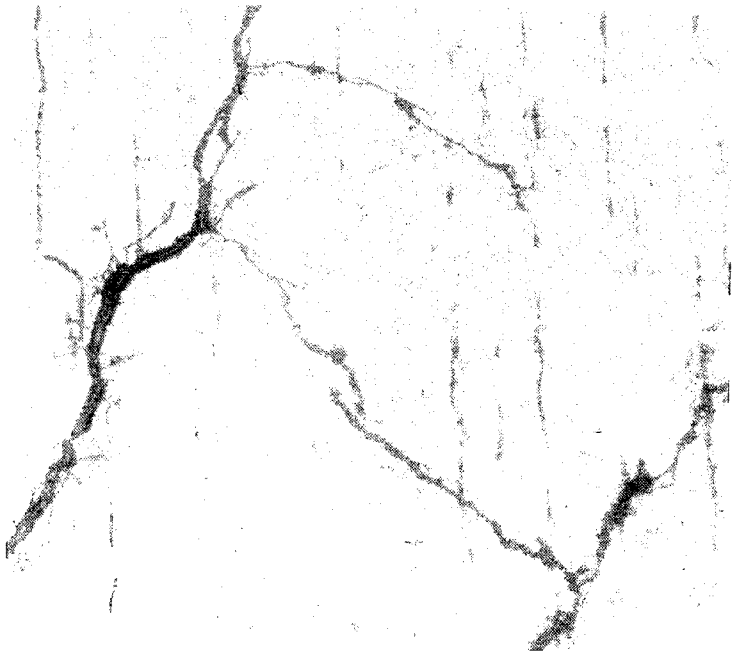

Figure 20. Branched cracks as characteristic of SCC was propagated transgranular (200X, Kalling's etched).

Figure 21. SCC was found in cluster (200 X, Kalling's etched).

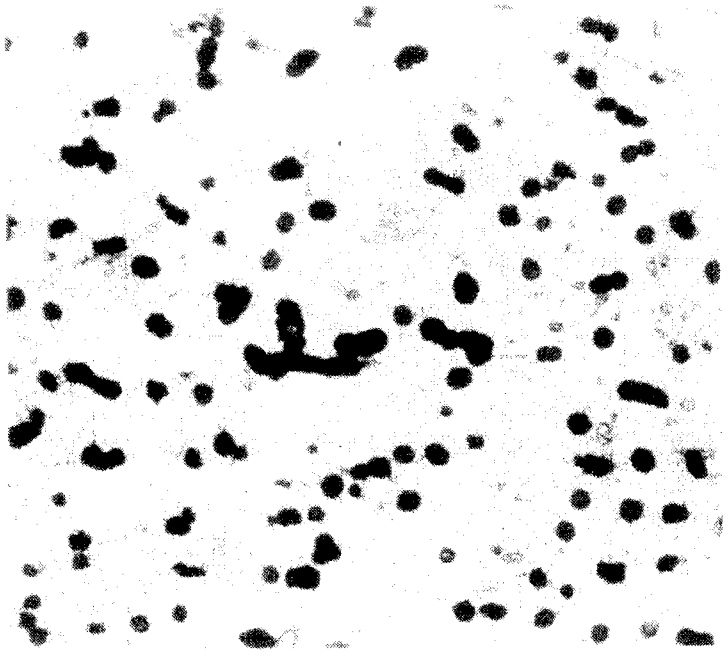

Figure 22. Microstructure of stud-bolt consists of austenite with spheroidize carbides disperse throughout of microstructures (500X, Kalling's etched).

CORROSION PERFORMANCE OF DEFORMED GALVANISED COATINGS

DR. JAMALIAH IDRIS
FACULTY OF MECHANICAL ENGINEERING
UNIVERSITI TEKNOLOGI MALAYSIA

Introduction

In most corrosion work reported in the literature, flat sheet samples have been used. However it should be appreciated that a larger proportion of galvanised steel sheet is used in the profiled form. In order to assess the corrosion performance of deformed commercial coatings in this study and accelerated salt spray corrosion test was carried out on three sets of samples. The samples were chosen as an extension of the study initiated by a previous worker, Wall (1985). He found worsening corrosion resistance with increasing bending strain for commercially galvanised samples. The corrosion performance of flat sheets of Galfan coatings showed protective actions approximately the same as the commercially produced minimised spangle coatings. However, Galfan deformed by bending showed less deterioration in corrosion tests compared with galvanised steel. In the present work, two sets of commercially produced minimised coatings with coating weights of 275 and 350 g/m^2 together with a set of commercial Galfan samples having a coating weight of 280 g/m^2 have been salt spray tested. The results of coating performance are expressed in terms of time to the appearance of first red rust for a range of samples of different bend strain. Although the samples are deformed around a fixed mandrel, for example 20mm radius, the amount of maximum surface strain will differ slightly as the samples have different thicknesses. Hence it is more appropriate to assess the first red rust appearance against the calculated strain value for each sample as shown in Table 1.

Results

Salt Spray Tests on Deformed Minimised Spangle Samples

The data for deformed sheets of both sets of coatings as expressed in terms of hours to first red rust in the deformed region against bend strain is illustrated in Fig. 1. Both types of coating from different coating weight show an increase in protection as the bend strain is reduced. The corrosion resistance of heavily deformed (1 to 6 mm radius) 275 g/m^2 samples was less than that of the 350 g/m^2 material. For example for a 2mm bend, red rust was detected after about 250 hours for the 275 g/m^2 sheet while the 350 g/m^2 sheet remained rust-free for a further 100 hours. Once the red rust formed it spread very rapidly along the bent area, as seen in Figs. 2 and 3.

At larger bend radii (up to 16 mm) the initial red rust appears at longer times in the range 430 to 500 hours exposure time. A small change in bend strain for these radii has little effect in altering the corrosion protection of both types of coatings. However, at 18 and 20mm bend radius, the deformed samples with 350 g/m^2 show a more resistant nature to salt spray mist that the 275 g/m^2 coating. The corrosion attack remained concentrated around the deformed region rather than on the faces. In order to compare the behaviour of the galvanised coatings with the Galfan coating, the former were left in the corrosion cabinet for extended periods beyond the first appearance of rust. After 900 hours (Fig. 4), it can be seen that the 350 g/m^2 coating displays far less damage for bend radii of 1, 2, 3, 4, 5, 6, and 8mm than the corresponding bends in 275 g/m^2 material.

Salt Spray Test on Deformed Galfan Samples

The time to first red rust on all deformed Galfan samples is three times longer than the minimised regular spangles. As shown in Fig. 5, the rate of corrosion of Galfan samples dropped

sharply as bend radius increased above about 4mm (6% surface strain). Further decreases in bend strain produced proportional increases in corrosion resistance. An example of Galfan samples exposed after 1400 hours is shown in Fig. 6. The samples show evidence of red rust on the formed area close to the apex of the bend.

Discussion

The Effect of Bend Strain on The Corrosion Performance of Minimised Coating

There is a clear indication that the 350 g/m^2 coating provides better protection than the 275 g/m^2 coating. There are two factors that might have caused this to happen. The heavier coated steel has more zinc metal to protect sacrificially both the intermetallic layer and steel beneath it. This layer corrodes uniformly at a rate proportional to its thickness and in this case it favours the coating with 350 g/m^2 coating weight. It has also been observed during microscopic examination of deformed samples (Figs. 7 to 12) that the 275 g/m^2 sample showed a greater tendency to display cracks after bending than the 350 g/m^2 coating has smooth shiny spangles compared with the 275 g/m^2 coating for which the coating is slightly frosty and grooved. Although both types of coatings have relatively high basal texture and similar spangle size, a slightly lower corrosion resistance is expected on those frosty samples with minor grooves. In other investigations (Helwig 1988) it is claimed that there is a direct relationship between corrosion resistance and impurity levels. The alloying metals on the surface which tend to concentrate at the frosty spangles, produced galvanic cells that made the surface more susceptible to staining and general corrosion.

Apart from the effect of coating compositions and surface topography the major factor in determining the corrosion performance of deformed samples is bend strain. With increasing strain more of the steel substrate will become exposed as a

result of cracking. In the presence of an aggressive electrolyte, a corrosion cell will be set up in which the zinc coating will act anodically (i.e. sacrificially). The larger the exposed region the larger will be the cell current and thus the faster will be the rate at which zinc is used up.

The Corrosion Performance of Galfan Coating

The deformed samples of Galfan coating showed protective action about three times that for minimised galvanised sheet of relatively similar coating weight. The influence of bend strain on time to first red rust shows a similar relationship to that for galvanised samples. That is, there is a steep increase in time to first rust in the range 10 - 50mm but at smaller bend radii the reduction in corrosion resistance is not so pronounced. Undoubtedly the better corrosion resistance of Galfan is the result of a combination of less cracking and also a smaller (although still protective) corrosion current. The latter means that the durability of the coating will be greater, all other things (crack size and distribution, for example) being the same. It should be noted that the relationship between the corrosion resistance of Galfan and galvanised material found in the current study is in accordance with work reported elsewhere and detailed in Table 2 (Galfan Technical Resource Centre, 1988). This data refers to flat sheet samples and is therefore more directly comparable to the corrosion performance of the large bend radius samples tested in this study. However, in general, a durability ratio of about 2:1 or 2.5:1 in favour of Galfan seems to hold.

Conclusion

Corrosion Evaluation

The corrosion tests were carried out to provide answers to a series of simple questions:

(i) does bend severity influence corrosion performance?

(ii) does coating weight influence corrosion performance on bent samples?

(iii)does Galfan outlast galvanised in tests on deformed samples?

The answer to all these questions, not surprisingly, was 'yes'. Increasing bend severity does reduce the time to first red rust as might be expected from a knowledge of the way in which more cracks form in more severely bent material. The answer to question (ii) was not so obvious because it was felt that a thicker coating might crack more than a thinner coating and thus some of the benefits of increased coating weight might be lost. This proved not to be the case even though there is some evidence from the bend tests that cracking is more prevalent when the coating is thicker (compare Fig. 8 with Fig. 12).

Finally, the tests on Galfan confirmed the claims of the producers. Its salt spray resistance was approximately three times that for conventionally galvanised samples with pro rata reductions after bending. This is associated with two factors: a smaller corrosion current and a lesser tendency to cracking.

References

Helwig L.E., Effect of Crystallographic Orientation and Surface Composition on Humid - Storage - Strain Resistance of Chromated Galvanised Sheet, Zinc Inst. Galvanisers Committee Meeting, 27th April 1981, Montreal Canada.

Galfan Galvanising: 1988, Galfan Technical Resource Centre, ILZRO.

Wall N.J., Ph.D. Thesis University of Wales, Cardiff, 1985.

Coating Type	Minimised (HDG)	Minimised (HDG)	Minimised (Zn-5%Al, Galfan
Coating Weight g/m^2 Top side/Total	135/275	175/350	140/280
Sheet Thickness (mm)	0.60	0.55	0.70
Bend Radius (mm)	Bend Strain ε_1		
20	0.015	0.014	0.017
18	0.016	0.015	0.019
16	0.018	0.017	0.021
14	0.021	0.019	0.024
12	0.024	0.022	0.028
10	0.029	0.027	0.034
8	0.036	0.33	0.042
6	0.048	0.044	0.055
5	0.057	0.052	0.065
4	0.070	0.064	0.080
3	0.091	0.084	0.104
2	0.130	0.121	0.149
1	0.231	0.216	0.259

Table 1 : Calculated bend strain, ε_1, for samples tested in the salt spray cabinet

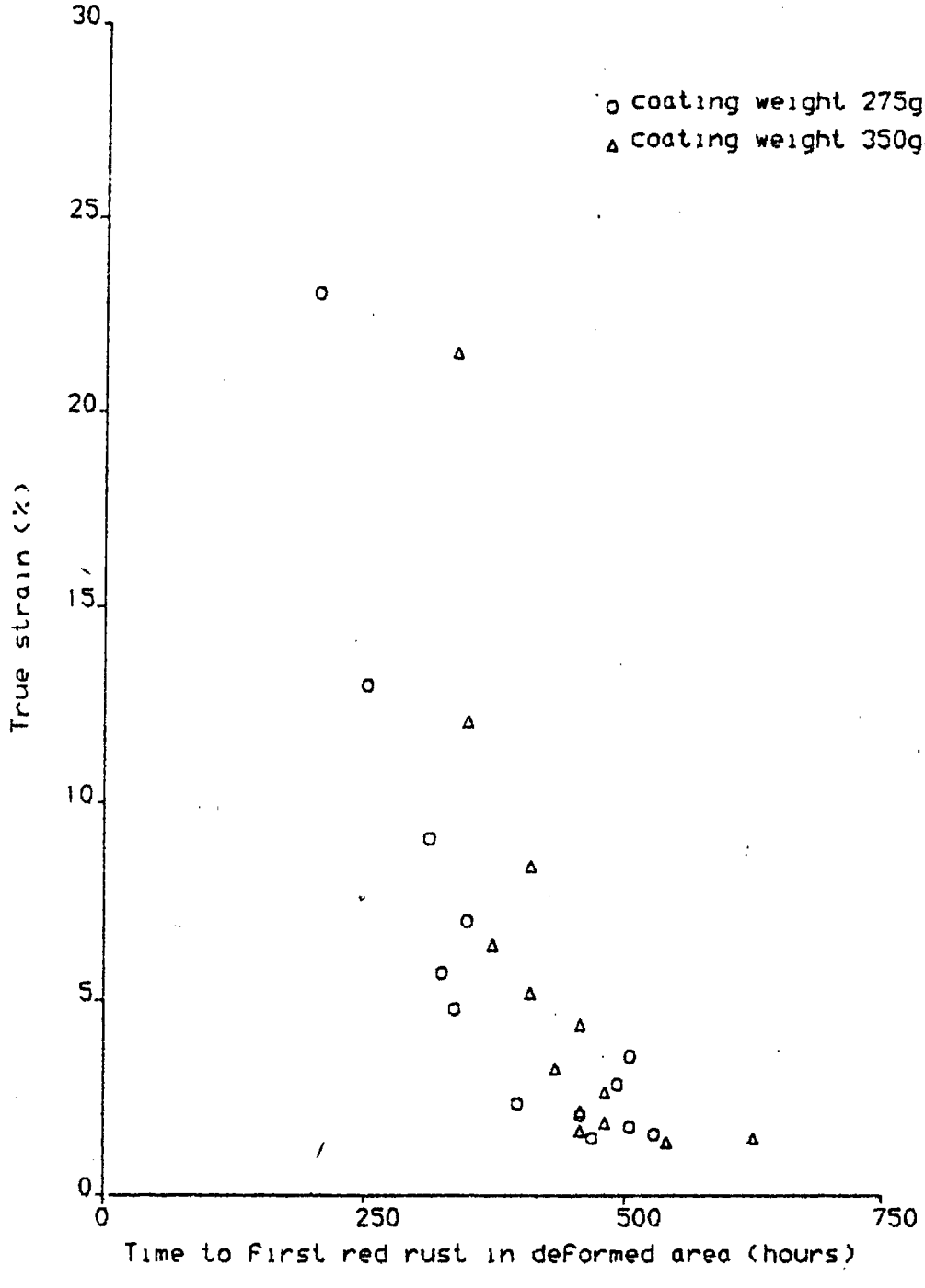

Figure 1 : Results of salt spray tests on deformed minimised sheet

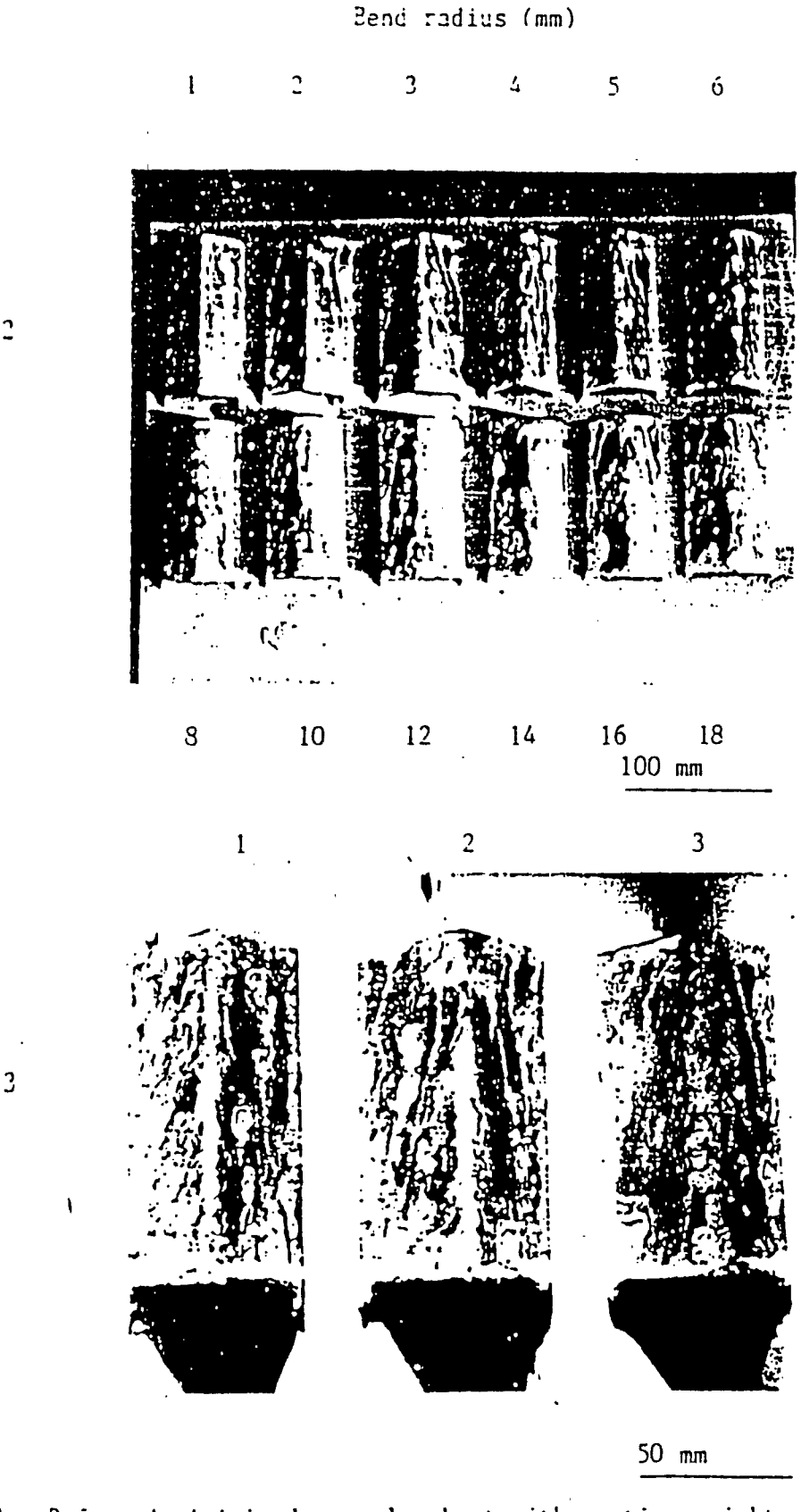

Fig. 2: Deformed minimised spangle sheet with coating weight 350 g/m², exposed for 400 hours.

Fig. 3: Close examination of 1, 2 and 3mm bend radii, showing red rust appearance on the deformed area.

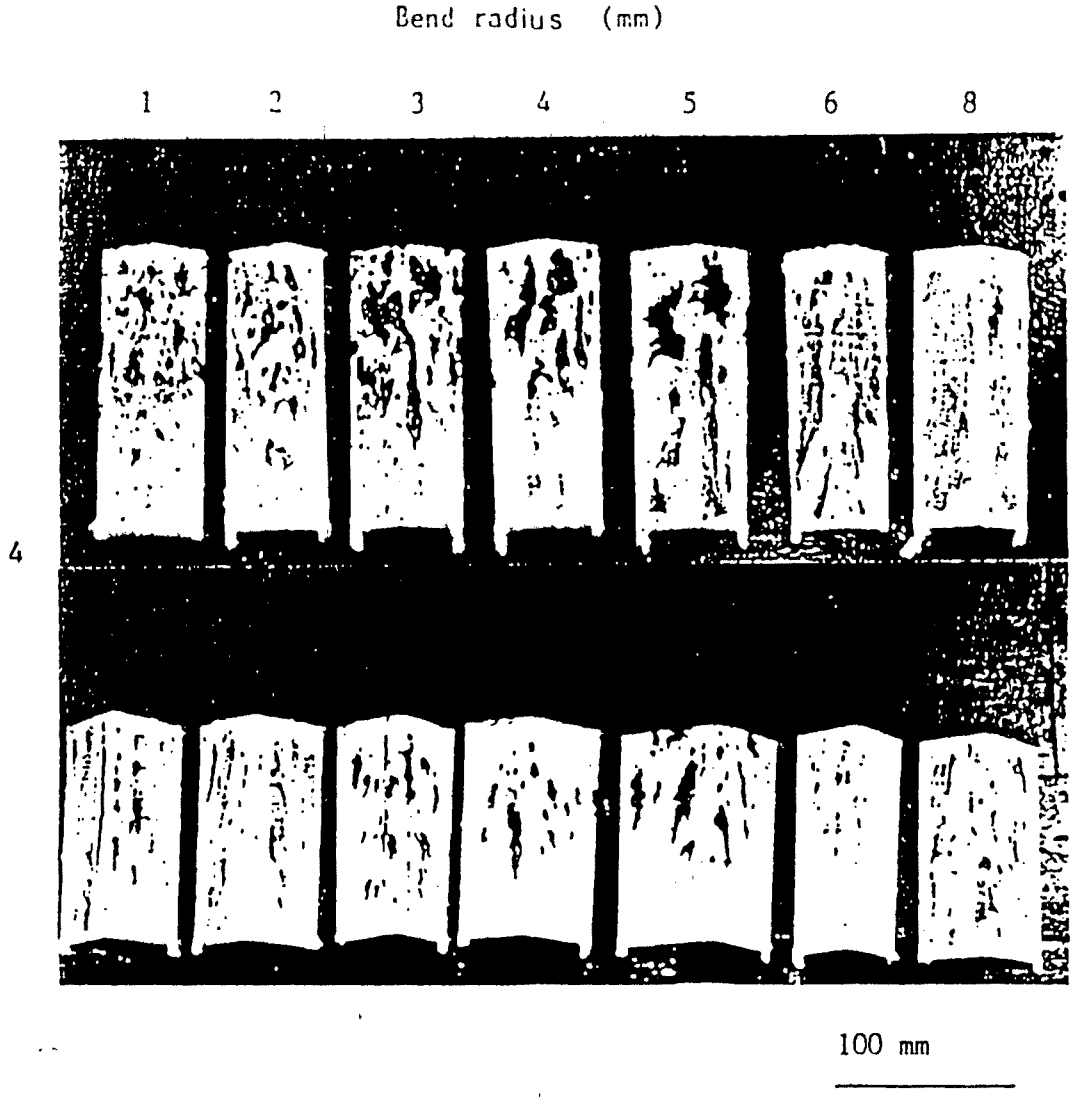

Fig. 4: Comparison between red rust formation on minimised sheets deformed around 1, 2, 3, 4, 5, 6 and 8mm bend mandrels, exposed for 900 hours.
Top row, materials coating weight 273 g/m² (both sides).
Bottom row, materials coating weight 330 g/m² (both sides).

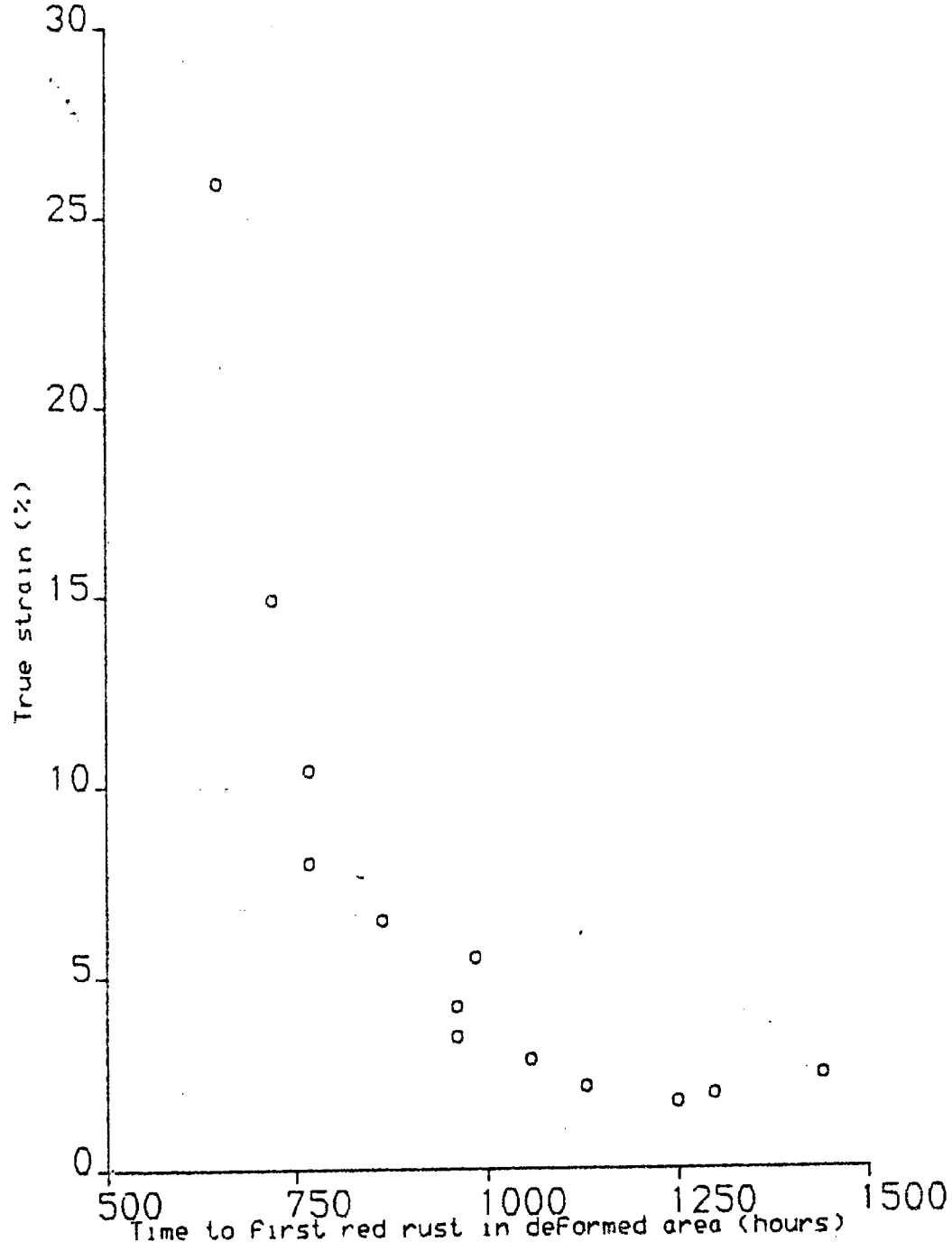

Figure 5 : Results of salt spray tests on deformed Galfan coating

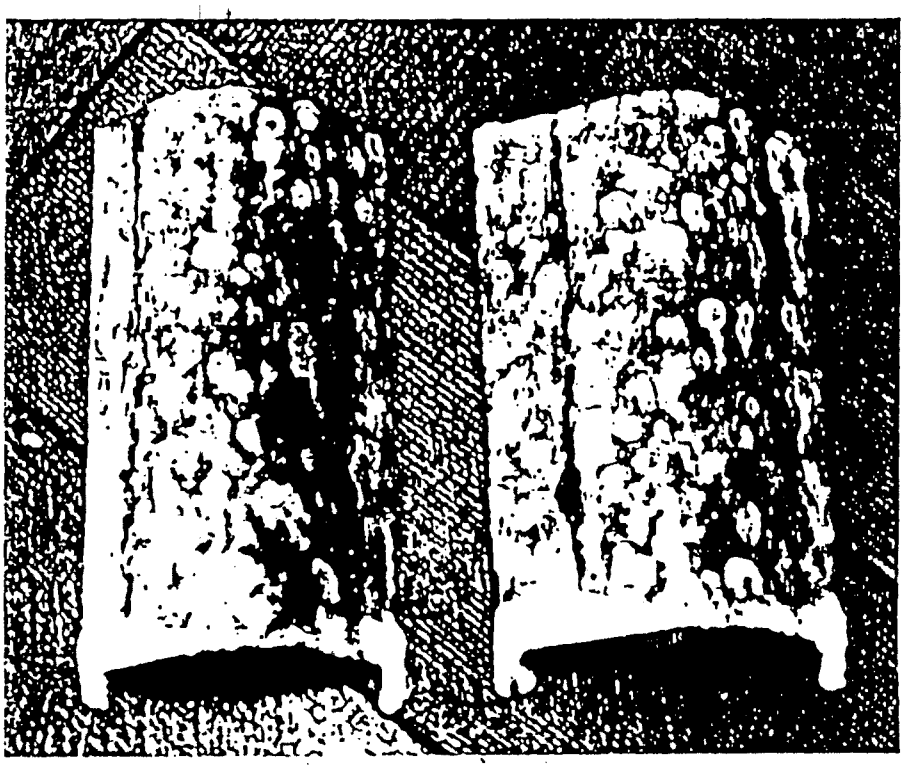

50 mm

Fig. .6: Red rust appearance on Galfan material deformed around 18 and 20mm bend mandrels, exposed for 1400 hours.

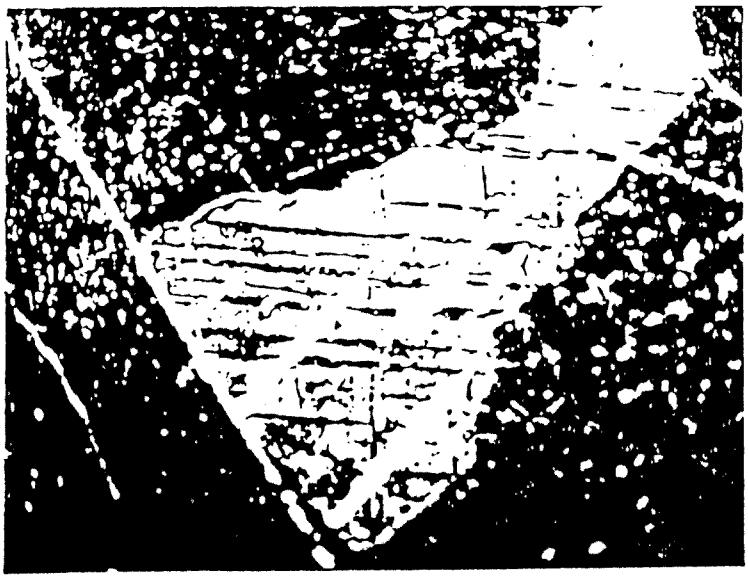

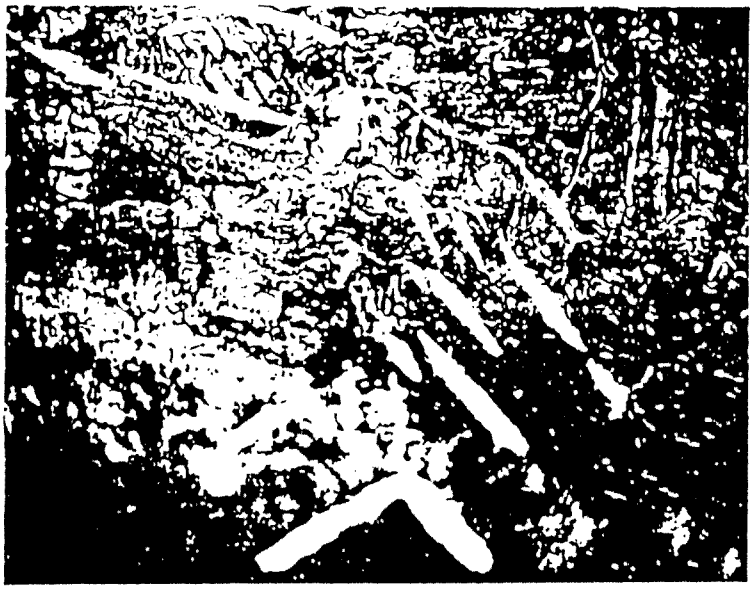

100 μm

Fig 7: Polarised light micrograph showing cracks in minimised spangle material, deformed around a 6mm bend mandrel, coating weight 175 g/m^2 (top side).

Fig 8: Polarised light micrograph showing cracks in minimised spangle material, deformed around a 4mm bend mandrel, coating weight 175 g/m^2 (top side).

Bending axis in east-west direction unless indicated.

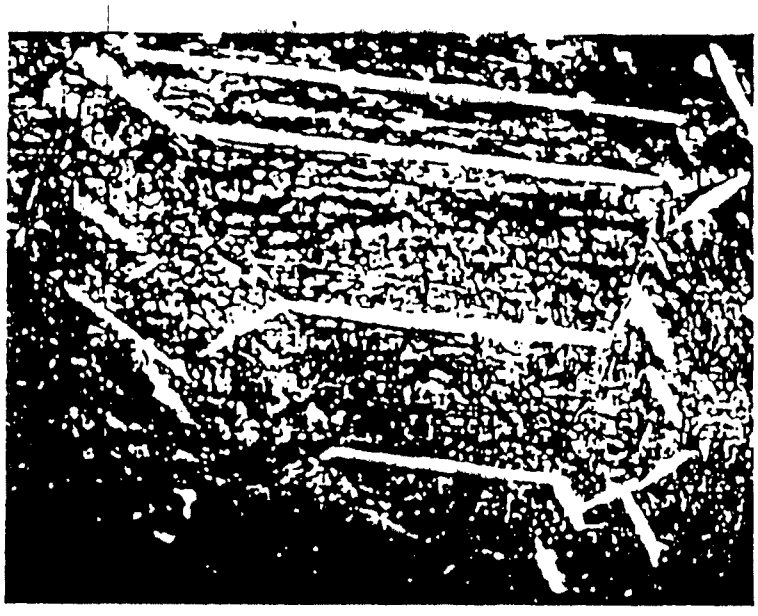

100 μm

Fig 9: Polarised light micrograph showing cracks in minimised spangle material, deformed around a 2mm bend mandrel, material coating weight 175 g/m^2 (top side).

Fig 10: Polarised light micrograph showing extensive cracks in minimised spangle material, deformed around a 1mm bend mandrel, material coating weight 175 g/m^2 (top side).

Bending axis in east-west direction unless indicated.

11

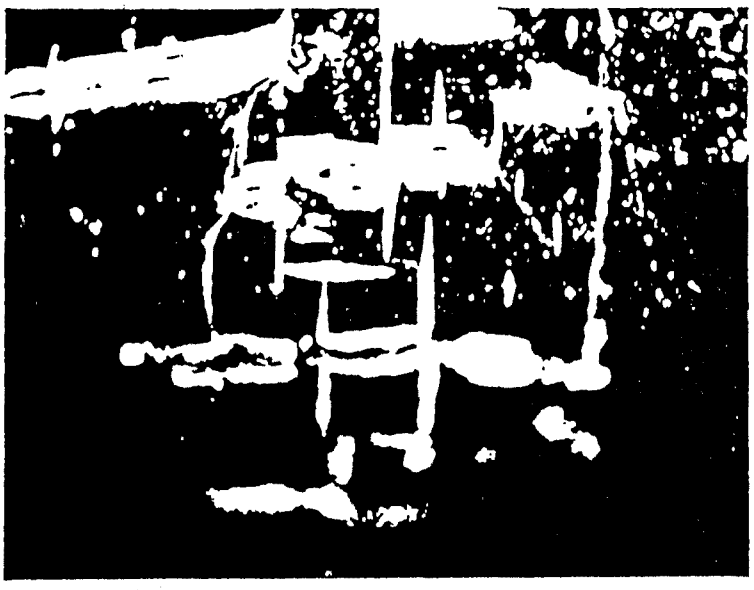

12

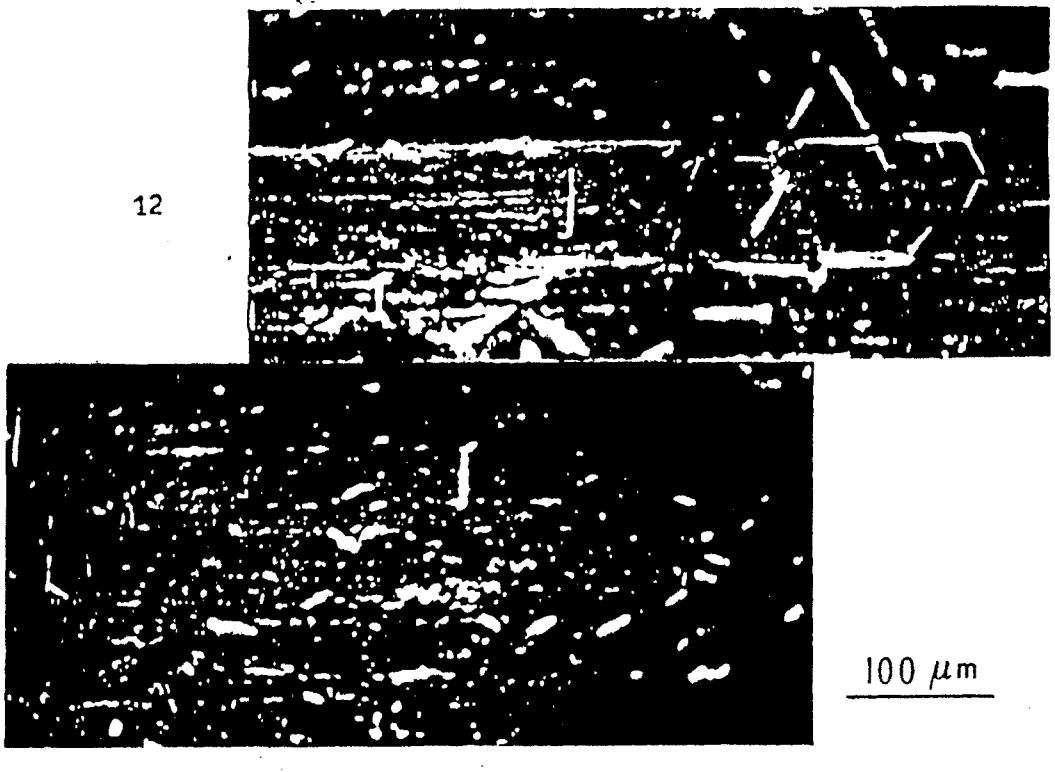

Fig 11: Polarised light micrograph showing a large increase in crack width along the bend axis in a minimised spangle material, deformed around a 1mm bend mandrel, coating weight 175 g/m² (top side).

Fig 12: Polarised light micrograph showihg cracks produced in basal grains of minimised spangle material, deformed around a 3mm bend mandrel, coating weight 137 g/m² (top side). Grain A shows near-equilateral triangle crack orientation whilst cracks in grain B are less evident, but are also paired at 60° to each other.

Bending axis in east-west direction unless indicated.

Salt Spray Test, Hours to Initial Red Rust			
Sample Coating wt g/m^2	Galvanised	Galfan	Sources
50	100	250	Nisshim
100	200	500	Steel
150	350	1000	
260 (Edge: Sealed)	-	800	
260 (Edge: Not Sealed)	-	800	
288 (Edge: Sealed)	330	-	Kawasaki Steel Corporation
288 (Edge: Not Sealed)	330	-	

Table 2 : Comparison of corrosion data reported for Galfan and galvanised coating (Galfan Technical Resourse Centre, 1988)

Evaluation of Corrosion Protective Properties of Coated Steels after Chemical Conversion Treatments by AC Impedance Measurement and Scanning Vibrating Electrode Technique

I. Sekine*, M. Yuasa*, K. Tanaka* M. Fuke*,
and L. Silao**

*Department of Industrial Chemistry,
Faculty of Science and Technology,
Science Unversity of Tokyo,
2641 Yamazaki, Noda, Chiba 278, Japan

**Chemical Engineering Department,
De La Salle University,
2401 Taft Avenue, Manila, Philippines

Abstract

The corrosion protective properties of the steels coated with various polymer resins after chemical conversion treatment of molybdate-various phosphate systems were evaluated by AC impedance measurement and scanning vibrating electrode technique (SVET). The steels were chemically treated with Na_2MoO_4 and various phosphate compounds such as $Na_6P_4O_{13}$, $Na_5P_3O_{10}$, $CH_8P_2O_7$ (HEDP), H_3PO_3 and H_3PO_4, and were coated with epoxy resin (EP), poly(vinyl chloride) resin (VC) and fluoro resin (F). The most efficient solution for the chemical conversion treatment of steel plate was found to be a 0.5 M Na_2MoO_4-10% $Na_6P_4O_{13}$ aqueous solution with a pH of 10, and the immersion times were 6 hours. The corrosion protective property of steel plate coated by F resin paint was most excellent compared with that in a blank (no treatment) solution or even in a 0.5 M Na_2CrO_4 aqueous solution. The film resistance (R_f) from AC impedance measurement and the current density (i) from SVET were correlated with each other. It was found that the corrosion protective property of paint film could be evaluated by SVET.

1. Introduction

In previous papers,[1-2] the corrosion protective properties of various coating films have been evaluated in acetic acid solution or NaCl solution by AC impedance method and scanning vibrating electrode technique (SVET) as the electrochemical measurements. However, no detailed study by such methods has been reported on the effect of chemical conversion treatment of steel plate before coating.

In this paper, in order to find the most effective solution for the chemical conversion treatment, investigations were done on the film resistance (R_f) obtained by AC impedance measurement and the current density (i) obtained by SVET under various conditions of the chemical conversion treatments. The molybdate solution was chosen as a solution for the chemical conversion treatment because molybdate is non-toxic.[3] It was reported that the chemical conversion treatment of molybdate-phosphate (Na_2MoO_4-H_3PO_4) was effective.[4-6] To find a more effective treatment, various phosphates were added to the molybdate solution.

2. Experimental

2.1 Materials and Preparation of Coated Steel Plates

The specimen used was cold rolled steel plate (JIS G3141 SPCC/SB, Nippon Test Panel, 7 x 15 x 0.08 cm). This plate was first polished with emery paper #1200 for five minutes before degreasing by immersing in tetrachloro-ethylene for 10 minutes and then in ethanol for 10 minutes. The specimens were grouped into two, according to whether these plates were chemically treated or not. Those treatments of steels by chemical conversion (Table 1) were further classified into those treated with Na_2MoO_4, Na_2MoO_4 and various phosphate compounds such as $Na_6P_4O_{13}$, $Na_5P_3O_{10}$, $CH_8P_2O_7$ (HEDP), H_3PO_3 and H_3PO_4, and Na_2CrO_4 for comparison. Aqueous solutions used for such chemical conversion treatment were prepared by adding NaOH to 0.5 M Na_2MoO_4 with and without various phosphate compounds to make pH 10. The polished steels were immersed in these 1000 cm^3 solutions at room temperature for 6 hours. The paints used were epoxy resin (EP), poly(vinyl chloride) resin (VC) and fluoro resin (F) (Fig. 1). Each plate was coated with paint to a thickness of 0.02 mm by using a barcoater. The coated steel plate was then baked for 10 minutes at 150^{o}C. The prepared specimens after shielding were immersed in various NaCl solutions for different lengths of time before electrochemical measurements.

2.2 Electrochemical Measurements

1) AC Impedance Measurement

The coated plate was further coated all around (both sides) by paraffin wax except a circular area of 2.0 cm^2 which was enclosed by a plastic O-ring. This area was exposed to a 3% NaCl solution at 30°C and became the measurement area of the working electrode. The measurement cell was composed of the counter and reference electrodes together with the working electrode. The counter electrode was a platinum plate (40 cm^2) and the reference electrode was a saturated calomel electrode (SCE).

The AC impedance measurement (Fig. 2) was conducted at the open circuit potential by the use of a potentiostat (Toho Technical Research, Model P/G-2000) and a frequency response analyzer (NF Electronic Instrument, Model 5020) in the frequency range from 20 kHz to 10 mHz. The reference signal voltage of the sinusoidal wave was 9 mV (RMS).

2) SVET

The coated steel plates (7 x 15 x 0.08 cm) in thickness of 0.02 mm were cut to a size of 5 x 5 cm for SVET. The edge and reverse side of the specimen were shielded with paraffin wax except for the measurement area (7.07 cm^2; diameter = 3.0 cm) which was enclosed by a plastic O-ring. Paint films of the specimens were artificially cut to the length of 0.5 cm at the center of the measurement area by a

cutter in conformity with a method of the cross cut test regulated by Japanese Industrial Standard (JIS).

The apparatus used for the scanning vibrating electrode technique is the NF Electronic Instrument, SVET-1000 (Fig. 3). The measurements were carried out for speciments immersed in 100 ppm NaCl solution at room temperature for various times (6 to 100 hours). The measurements were also conducted at 441 points on the area of 1 x 1 cm. where both X and Y coordinates were divided into 20 parts. The potential gradient produced from a lock-in amplifier was displayed on a three-dimensional map. The vibrating electrode was a platinum needle, and the conditions of measurement were as follows: the vibrating frequency; 221 Hz, amplitude; 0.15 mm and the distance between center of amplitude and coated steel surface; 0.15 mm.

3. Results and Discussion

In the chemical conversion treatment, the effective i) immersion time, ii) pH of solution and iii) concentration of molybdate were i) over ca. 6 hours, ii) more than 7 and iii) 0.5 M, respectively. In various chemical conversion treatments of molybdate systems, the AC impedance spectra of the steel plates treated chemically were measured in a 3% NaCl solution at 30°C. The charge transfer resistance (R_{ct}) values of the steel plates

treated chemically were determined by analyzing the Cole-Cole plots, equivalent circuit models and their curve fitting. The R_{ct} values were ca. 10 - 20 kohm. The better solutions for chemical conversion treatments were Na_2MoO_4-$Na_6P_4O_{13}$ and Na_2MoO_4-H_3PO_4.

Figures 4a, b and c show the loci of typical complex plane impedance plots and equivalent circuits for steel plate coated with EP after chemical conversion treatment in a 0.5 M Na_2MoO_4 solution. The curve until 12 hours at early immersion time (Fig. 4a) was not described in the shape of semicircle, but as a part of a large semi-circle because the paint film resistance (R_f) is fairly high. After 24 hours immersion, it represents a partial capacitive semicircle. The R_f value decreases with increasing immersion time which suggests that the film is wet-swelled or deteriorated. Specifically, the R_f values reflect the variation of mobility and concentration of ions in the paint film, so higher values represent better isolation. Since these paint films are in a comparatively good condition, the interfacial model of coated steel-solution can be represented by an equivalent circuit (film resistance; R_f, film capacitance; C_f and solution resistance; R_s) as shown in Fig. 4a. In the case (Figs. 4b and c) of longer immersion times, the water layer between the steel and the EP paint is formed. The loci of

complex impedance plane plots show the double capacitive semicircles with different time constants because of the degradation of the paint film. It is thought that the semicircles on the higher frequency side in Figs. 4b and c reflect the R_f and C_f as well, as shown in Fig. 4a, while those on the low frequency side in Figs. 4b and c are ascribed to the charge transfer resistance (R_{ct}), double layer capacitance (C_{dl}) and Warburg impedance (Z_w) which is based on diffusion, at the paint film-metal substrate interfaace as an equivalent circuit shown in Fig. 4c. Therefore, this equivalent circuit represents the deterioration of paint film.

The variation of film resistance (R_f) vs. immersion time for various coated steel plates without chemical conversion treatment of metal substrate is shown in Fig. 5. It can be seen that the R_f value is highest for the F coated steel up to 300 hours but goes down to almost same R_f values as the EP coated steels at 600 hours immersion time. Although the EP paint film started with an R_f as high as F paint film, its value decreased faster than that of F paint film. The VC paint film showed a resistance lower than that of EP even from the start of its immersion and in this paint film, some blisters appeared after immersion for 24 hours. Consequently, the R_f values of these

paint films were low in an order of F > EP > VC.

Figure 6 shows the variation of R_f with immersion time of steel plates coated by VC after various chemical conversion treatments. The R_f values of coated steel after 6 hours immersion in a 0.5 M Na_2MoO_4 solution were higher than those of blank (no chemical conversion treatment), and lower than those of a 0.5 M Na_2MoO_4-10% H_3PO_4 or 0.5 M Na_2MoO_4-10% $Na_6P_4O_{13}$ type aqueous solution. The chemical conversion treatment in a 0.5 M Na_2MoO_4-10% $Na_6P_4O_{13}$ solution was observed to be effective in the corrosion resistance of paint film. It is thought to be ascribed to the prompt formation of passive film, and the promotion of adhesion between the paint film and substrate, by the polyphosphate, $Na_6P_4O_{13}$.[7,8] Comparing the effect of the chemical conversion treatments in a 0.5 M Na_2MoO_4-10% $Na_6P_4O_{13}$ solution and in a 0.5 M Na_2CrO_4 solution, it was found that the R_f values of molybdate-polyphosphate were higher than those of chromate (Na_2CrO_4) until about 500 hours immersion, but became lower than those of chromate (Na_2CrO_4) after 500 hours immersion. From these results, the corrosion protective effect of molybdate-polyphosphate is not as long lasting as that of chromate.

Figure 7 exhibits the relation between the R_f values and the immersion time of steel plates coated

by F resin after various chemical conversion treatments. These R_f values of F resin paint were generally further enhanced than those by VC resin paint as shown in Fig. 6, and the values until about 500 hours were ca. 10^9 ohm. In this case, the chemical conversion treatment in 0.5 M Na_2MoO_4–10% H_3PO_4 or 0.5 M Na_2MoO_4–10% $Na_6P_4O_{13}$ solutions was was found to be more effective compared with that in a 0.5 M Na_2CrO_4 solution throughout the measuring times.

Figure 8 shows the typical three-dimensional SVET maps after immersion for 6 and 24 hours of steel plates coated by VC resin paint without chemical conversion treatment. The artificial cut and non-cut (coated) parts become a local anode (peak part) and a local cathode (flat part), respectively. Local corrosion proceeds on a metal surface when a local anode and a local cathode are separated from each other, where the ionic current flows through a solution between two local electrodes. The potential distribution is established in the vicinity of a metal surface due to the ohmic drop in a resistive solution. Consequently, the measurement of potential distributions makes it feasible to evaluate the corrosion behavior of a metal.[9]) Since a potential gradient (E) corresponds to the current density (i),

it is possible to analyze the local corrosion behavior by measuring the two-dimensional distribution of E on corroding metal surface. To evaluate the degradation of paint film, the degree of growth of the anodic part is given by the difference of potential gradient (ΔE) as follows;

$$\Delta E = E_a - E_c \qquad \text{(Eq. 1)}$$

where E_a is a mean value of the top 3 potential gradients at anodic (peak) part and E_c is a mean of potential gradients at cathodic (flat) part. The ΔE in Fig. 8 increased with increasing immersion time, because the cathodic area of metal substrate was enlarged by the deterioration of the paint film.

The variation of current density with immersion time of steel plates coated by various paints is shown in Fig. 9, The i values increased with increasing immersion time by the wet-swelling of coating films, and then became constant after about 50 hours. These values in steady state decreased in an order of VC > EP > F reflecting the corrosion protective property of each paint film. It is thought that the corrosion resistance of the film increases as the i value decreases. The i value of VC with chemical conversion treatment in a 0.5 M Na_2MoO_4-10% $Na_6P_4O_{13}$ solution became smaller compared to that of VC without treatment.

Figure 10 shows the relationship between the R_f value by AC impedance measurment and the i value by SVET of steel plates coated by various paints after immersion for 72 hours with or without chemical conversion treatments in a 0.5 M Na_2MoO_4-10% $Na_6P_4O_{13}$ solution. These data give an approximately straight line except the plot of VC with chemical conversion treatment. From this figure, it can be seen that the more the i value decreases, the more the R_f value increases. Since the R_f from AC impedance and the i from SVET were correlated with each other, it was found that the corrosion protective property of paint film could be evaluated by SVET.

4. Conclusion

The efficient solutions for chemical conversion treatment of steel plate were investigated. After their chemical conversion treatments, the corrosion protective property of steel plates coated by various paints was evaluated with AC impedance measurement and SVET, and the following conclusions were obtained.

1) The most efficient solution for the chemical conversion treatment of steel plate was found to be a 0.5 M Na_2MoO_4-10% $Na_6P_4O_{13}$ aqueous solution with a pH of 10 and the immersion times were 6 hours.

Since the film resistance (R_f) value for fluoro resin (F) paint after such a chemical conversion treatment was about 10^9 ohm until ca. 500 hours after immersion, the corrosion protective property of steel plate coated by F paint was most excellent.

2) Both the R_f from AC impedance measurement and the current density (i) from SVET were correlated with each other. It was found that the corrosion protective property of paint film could be evaluated by SVET.

References

1. Sekine, K. Moriya, and M. Yuasa, Proc. Symp. on Advances in Corrosion Protection by Organic Coatings, ed. by D. Scantalebury and M. Kendig (Electrochemical Society Proc. Volume), Vol. 89-13, p.218, Electrochemical Society, Pennington (1989).
2. M. Yuasa, M. Ichikawa, K. Moriya, I Sekine, T. Mukumoto, H. Mizuki, and T. Murakami, Denki Kagaku, 57, 1061 (1989).
3. A. von Koeppen, G. A. Emerie, K. Nishio, and B. A. Metz, Materials Protection and Performance, 12 23 (1973).
4. K. Kurosawa and T. Fukushima, Nippon Kagaku Kaishi, 1987, 1822.
5. K. Kurosawa and T. Fukushima, Corrosion Sci., 29, 1103 (1989).
6. K. Kurosawa and T. Fukushima, Corrosion Sci., 32, 893

(1991).

7. G. Hatch, Ind. Eng. Chem., 44 1774 (1952).

8. J. Lamb and R. Eliassen, J. Am. Water Works Assoc., 46, 445 (1954).

9. S. Fujimoto and T. Shibata, Boshoku Bijutsu, 36, 812 (1987).

Table 1 Coated steel plates without or with chemical conversion treatment.

①	No treatment(Blank) + Paints(VC, EP, F)
②	0.5M Na_2MoO_4 + Paints(VC, EP, F)
③	0.5M Na_2MoO_4 + 10% H_3PO_4 + Paints(VC, EP, F)
④	0.5M Na_2MoO_4 + 10% $Na_6P_4O_{13}$ + Paints(VC, EP, F)
⑤	0.5M Na_2CrO_4 + Paints(VC, EP, F)

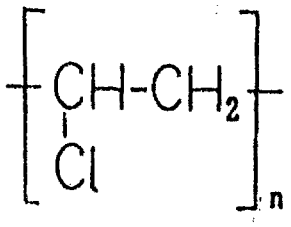

Polyvinyl chloride resin(VC)

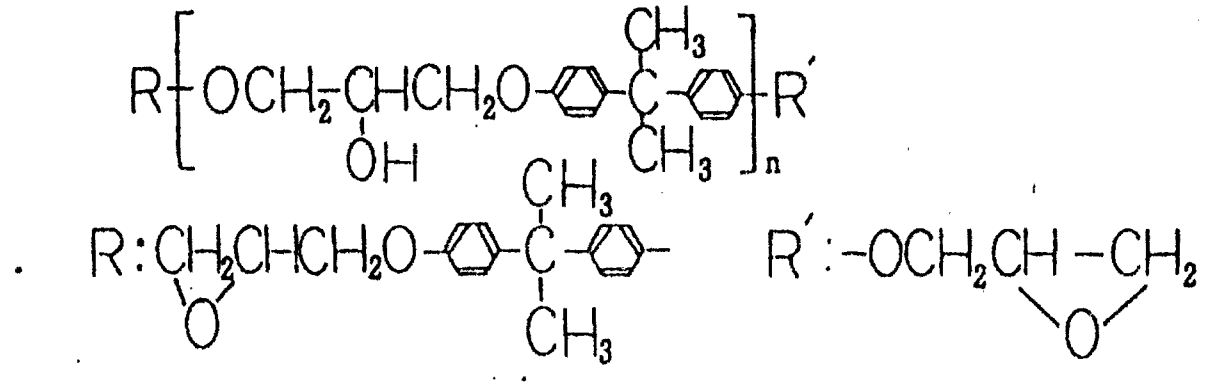

Epoxy resin(EP)

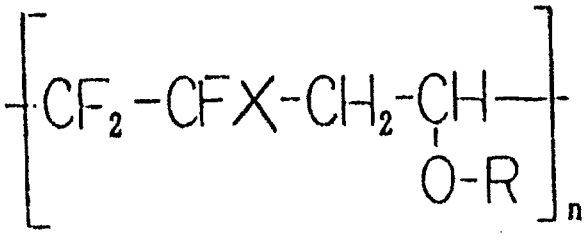

X: F, CF_3, Cl R: CH_{2n+1}, CH_{2n}-COOH, CH_{2n}-OH

Fluoro resin(F)

Fig.1 Structural formulas of various resins.

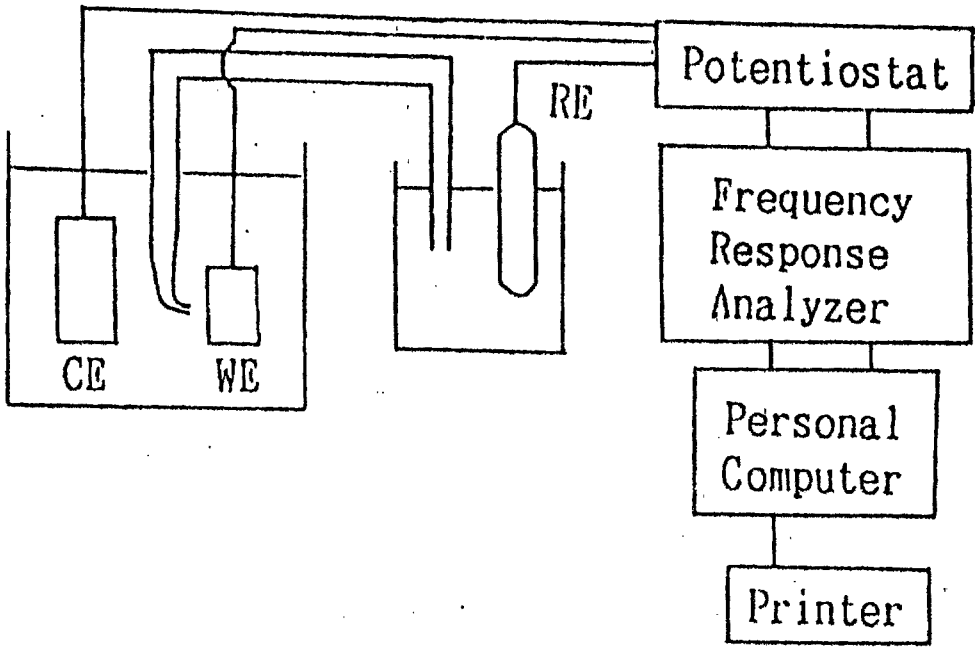

Fig. 2 Block diagram of electrochemical impedance measurement.

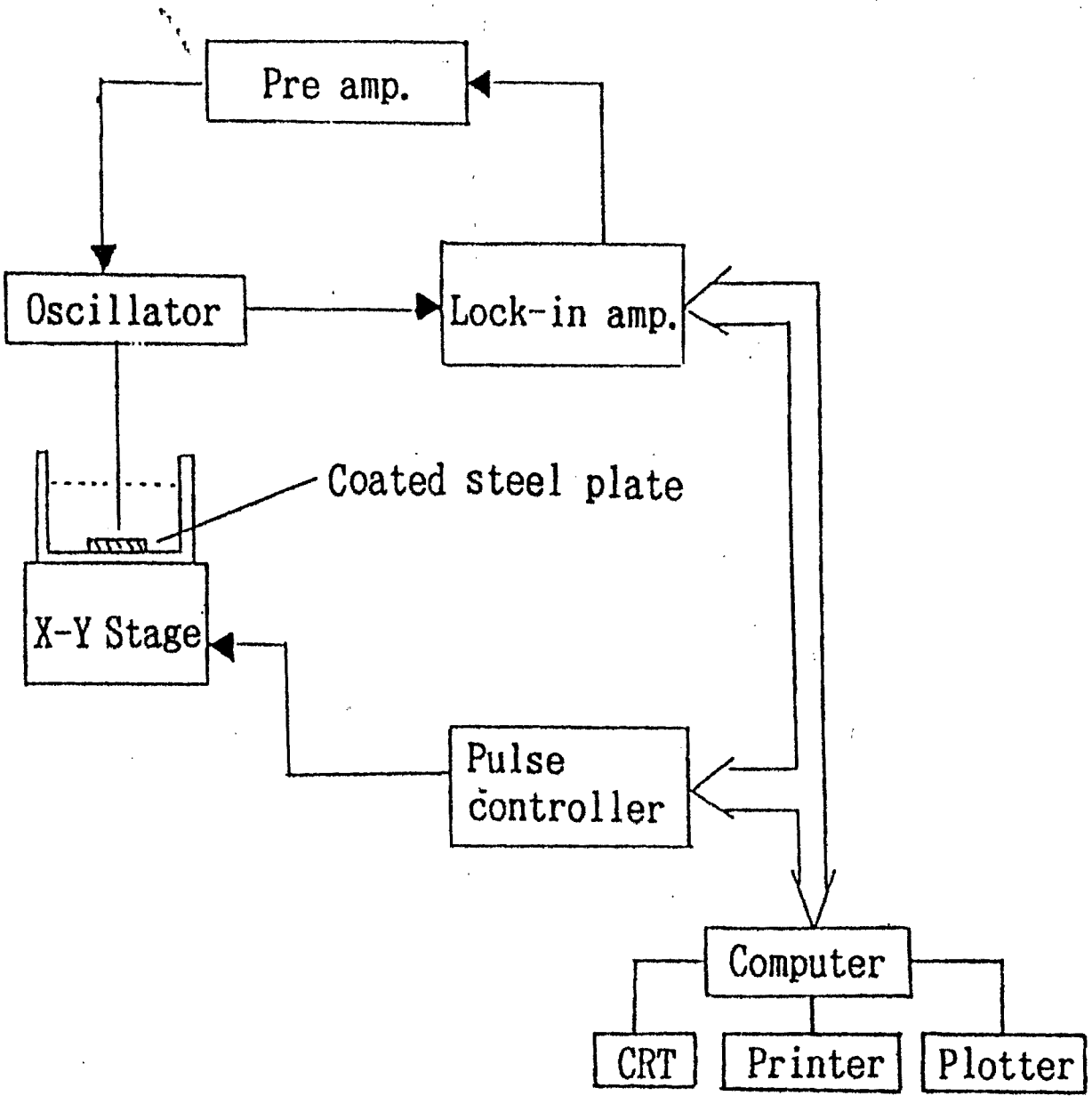

Fig. 3 Block diagram of scanning vibrating electrode technique.

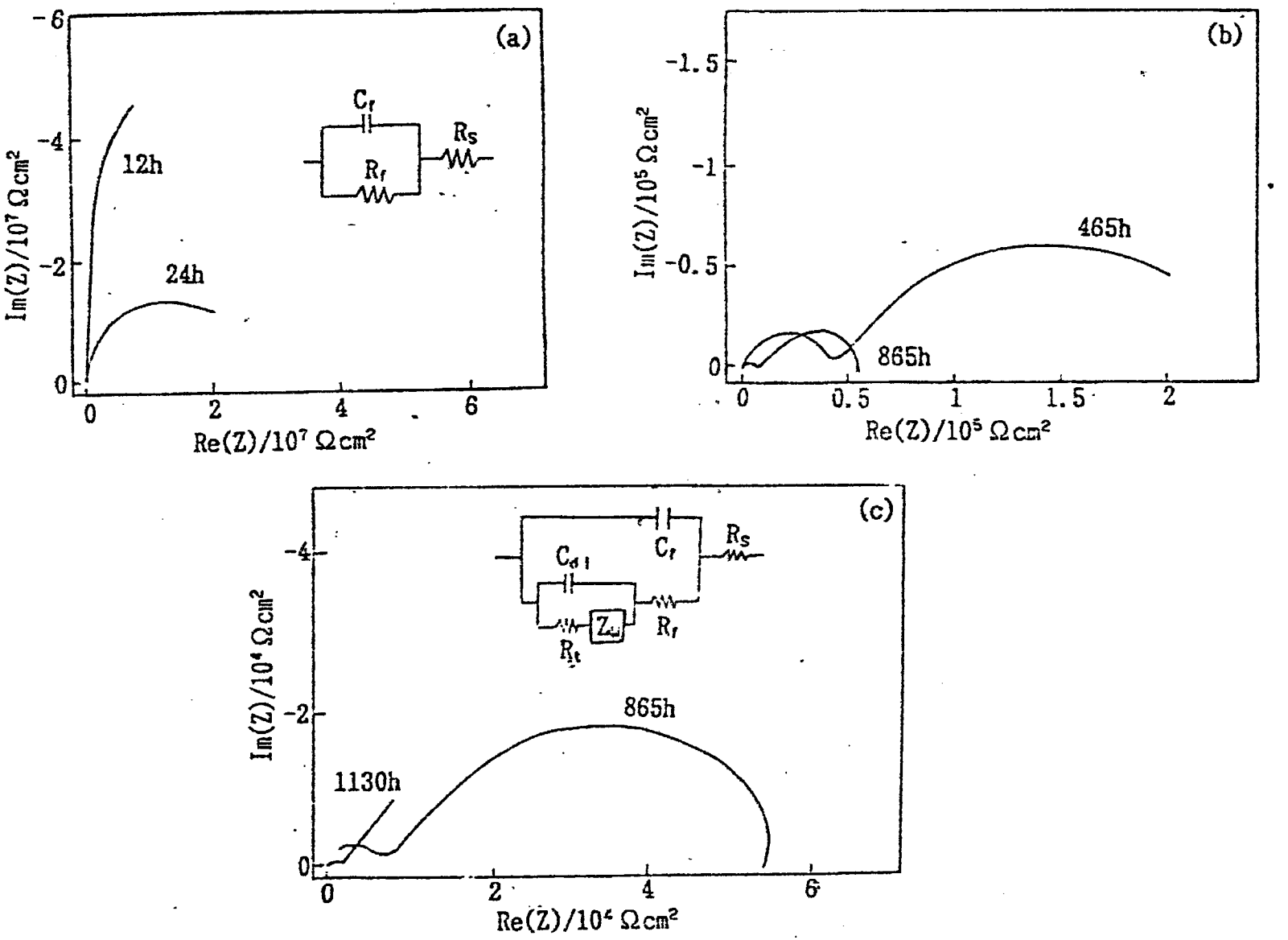

Fig. 4 Complex impedance plane plots and equivalent circuit for steel plate coated with EP after treatment in 0.5M Na_2MoO_4 solution.

(a):at early immersion for 12 and 24h

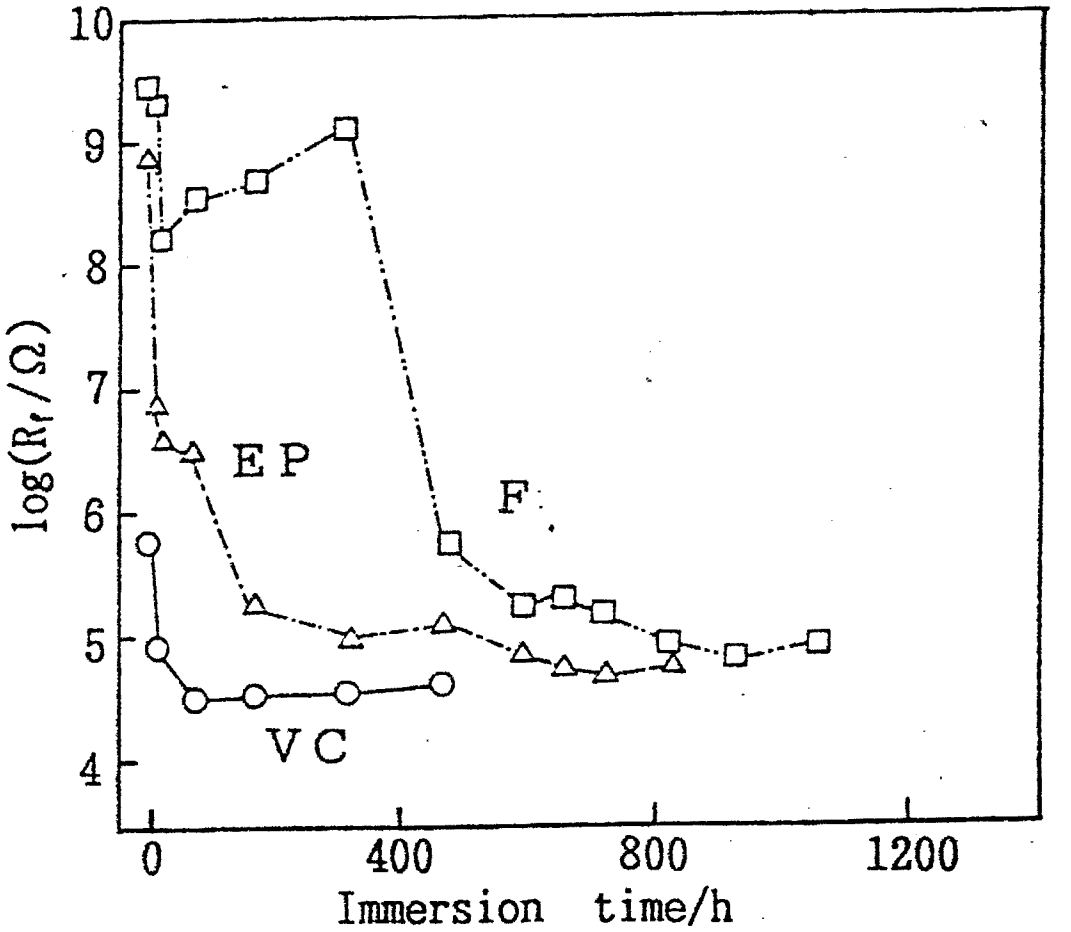

Fig. 5 log R_f vs. immersion time curves of steel plates coated by various resins in 3%NaCl solution at 30℃ without chemical conversion treatment.

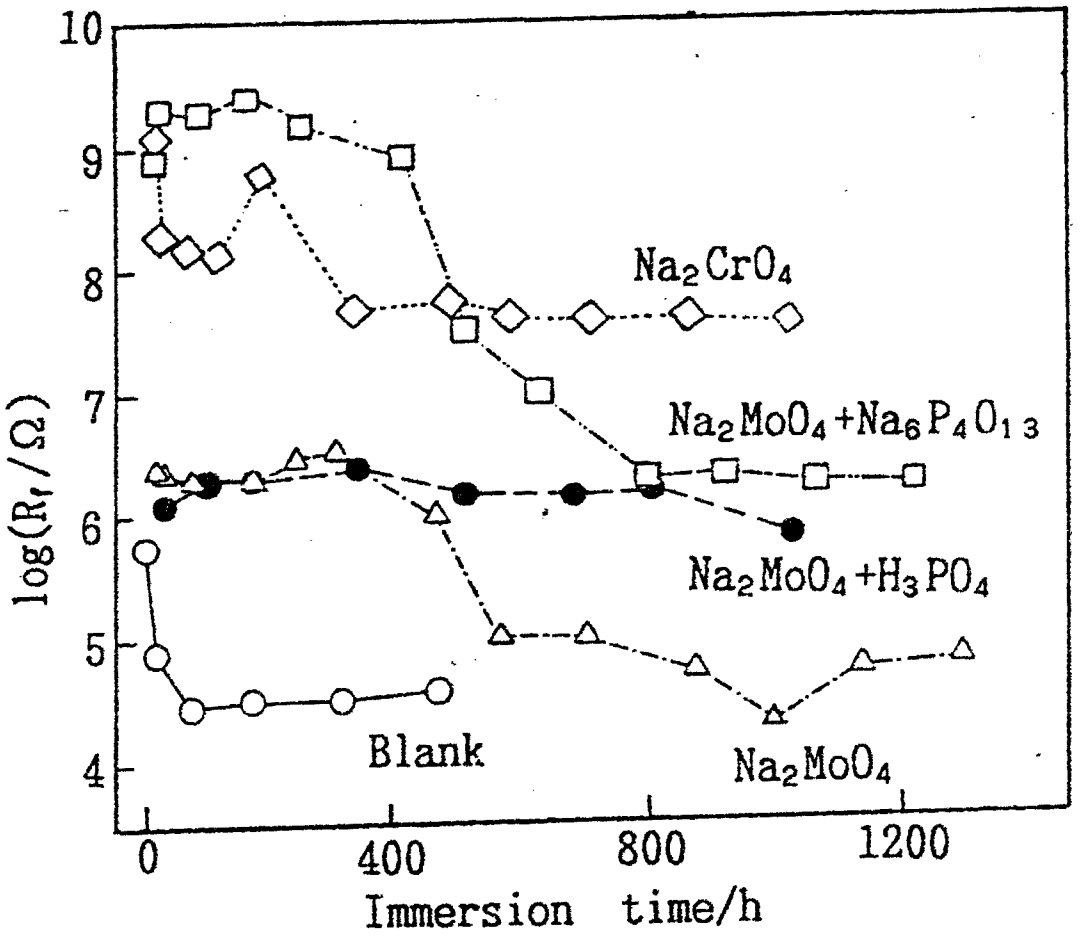

Fig.6 log R_f vs. immersion time curves of steel plates coated by VC in 3%NaCl solution at 30℃ after various chemical conversion treatments.

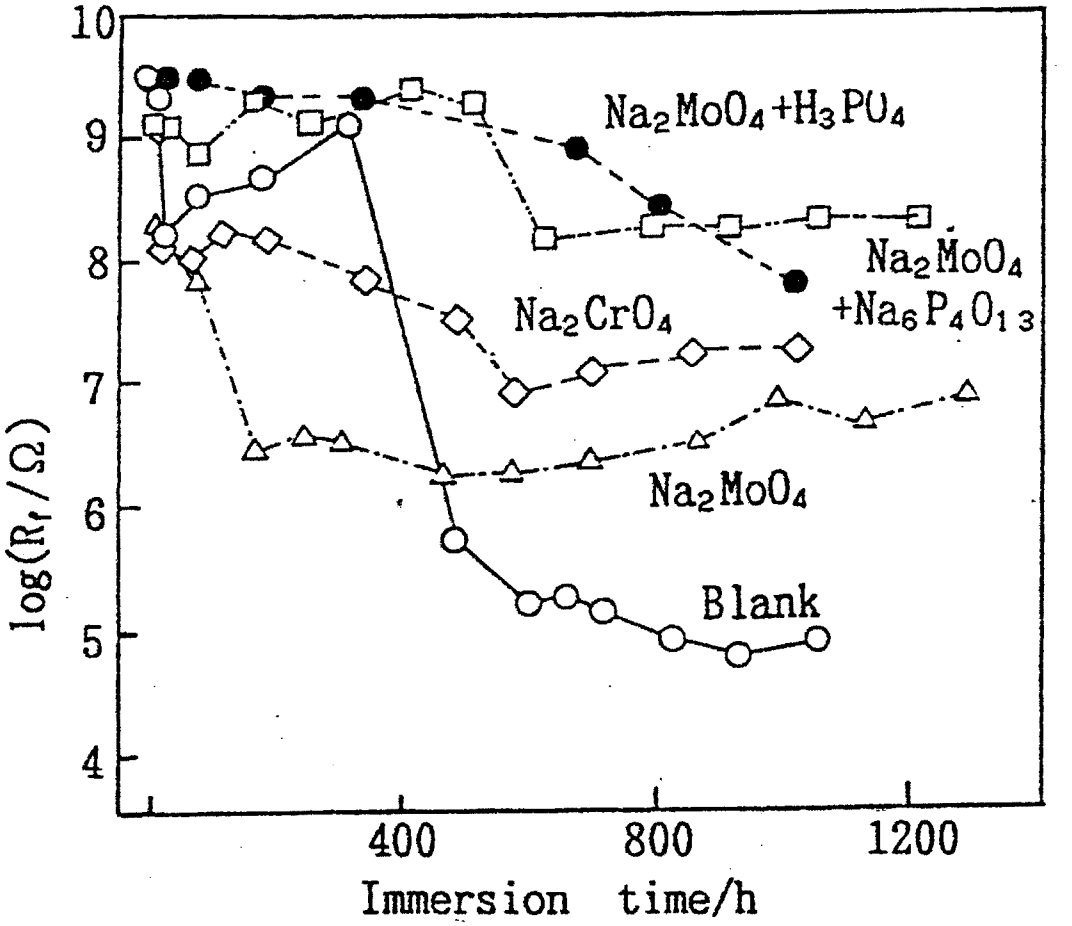

Fig. 7 log R_f vs. immersion time curves of steel plates coated by F in 3%NaCl solution at 30℃ after various chemical conversion treatments.

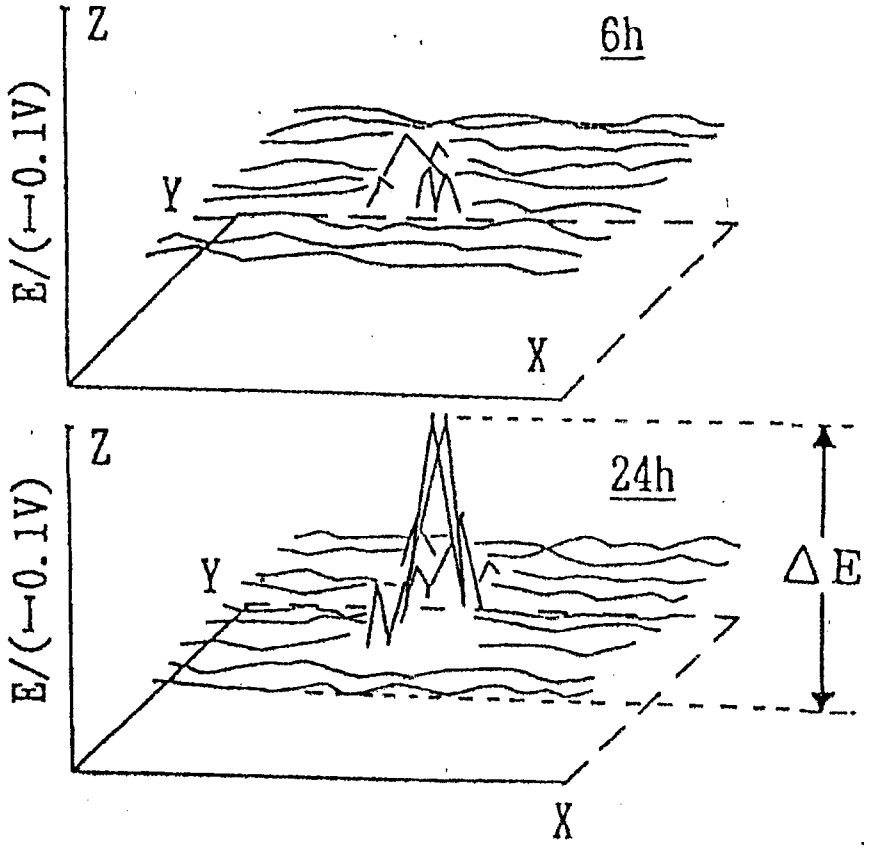

Fig. 8 SVET maps of steel plate coated by VC in 100ppm NaCl solution at room temperature without chemical conversion treatment.

ΔE (potential gradient) $\propto$ i (Current density)

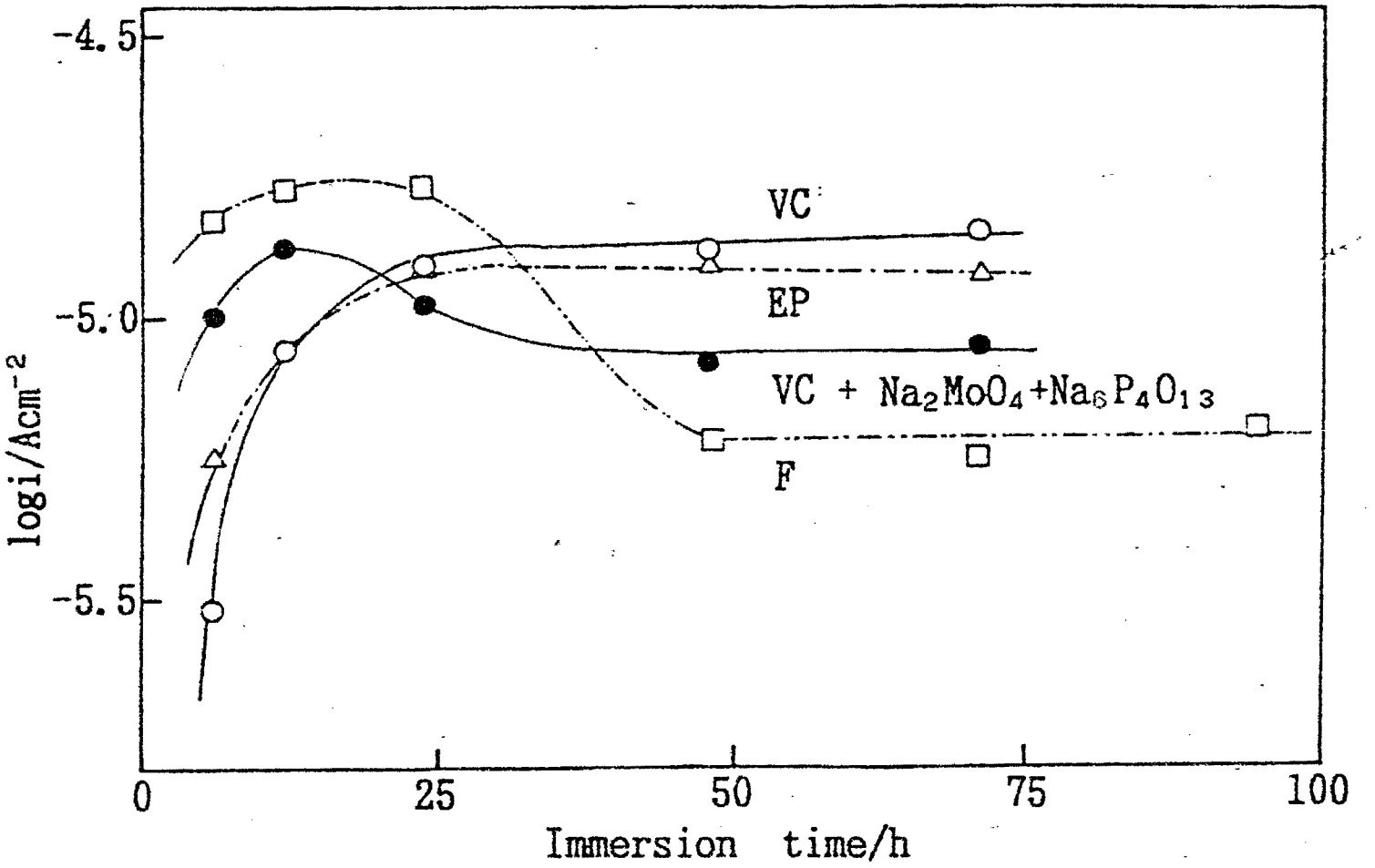

Fig. 9 log i vs. immersion time curves of steel plates coated by various paints in 100ppm NaCl solution at room temperature with or without chemical conversion treatments.

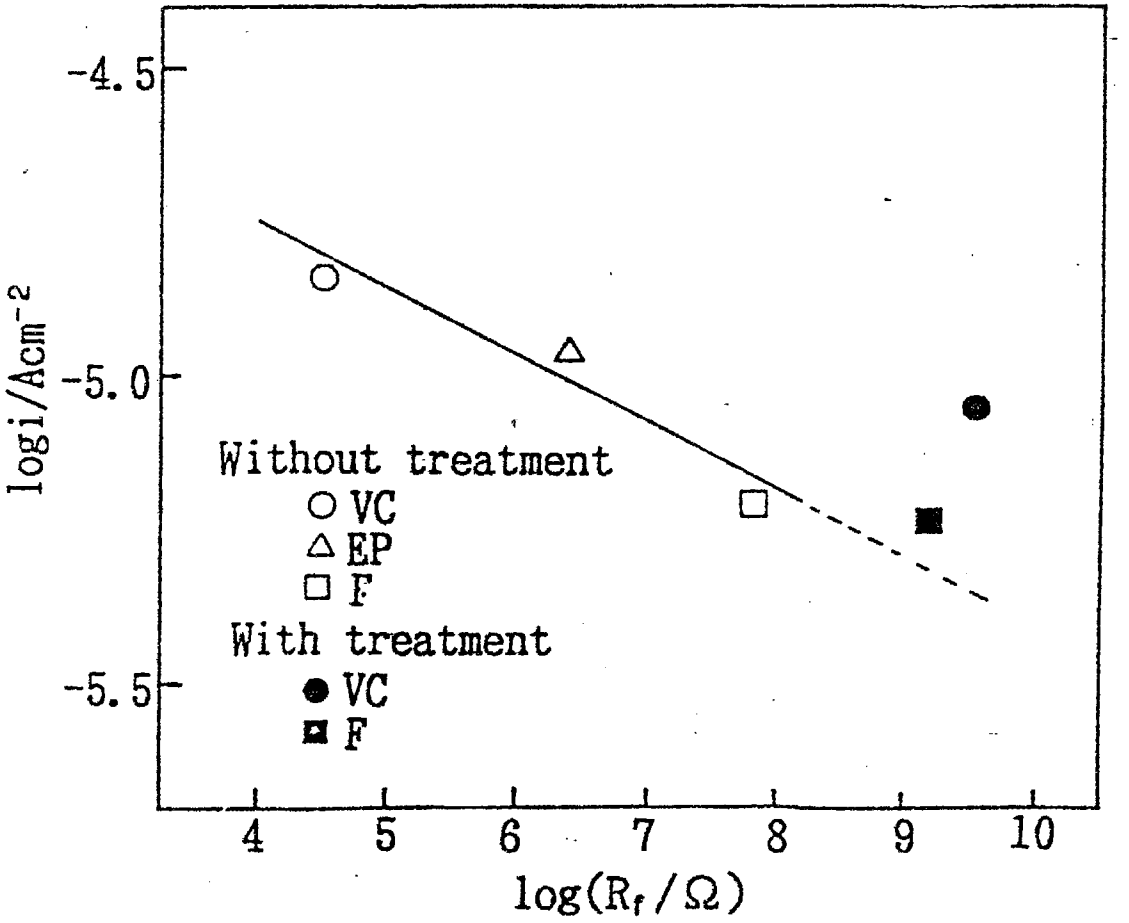

Fig. 10 Relation between R_f and i of steel plate coated by various paints after immersion for 72h.

CORROSION TEST OF PLATED PRODUCT FOR THE STUDY OF SERVICE LIFE

SERMKIAT JOMJUNYONG
* * *
M. FUJITA , S. YOKOYAMA , S. MATSUMOTO
Faculty of Engineering, CMU Chiang Mai Thailand.

Abstract

Steel panels plated with nickel of various thicknesses were subjected to a cyclic corrosion test. Times to failure (service lives) of the panels were analyzed by using reliability techniques. The testing procedure and analytical result showed that service life of the nickel plated steels at which a specified portion have failed, at various stress levels, could be quantitatively estimated.

Introduction

In metal finishing research field, there are many studies on the corrosion of plated products which are mainly on corrosion rate and corrosion mechanism.[1-3] However, in recently the study on predicting service life of plated products has come to an interest and necessity. Many research works on this topic had been reported.[4-7] Result of the studies, life prediction, had been recognized as essential to the improvement of products' quality, material selection and system development. In general, it is agreed that making quantitative service life prediction of plated products exposed to its intended operating conditions is a difficult task. Difficulties in making the prediction are probably due to various factors (Fig.1.) which have effects on the service life of plated products such as large number of environment conditions, atmospheric pollution constituents, quality of basis metal, plating procedure and variation in plating quality which vary from factory to factory ..... etc.

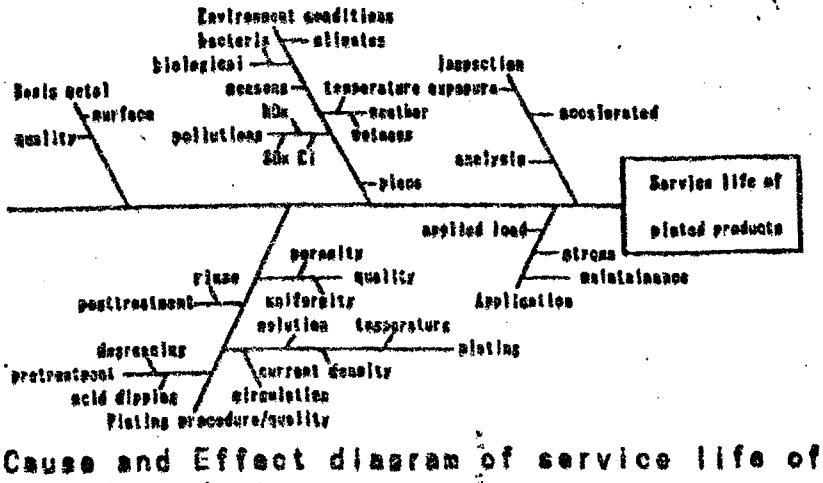

Fig. 1 Cause and Effect diagram of service life of plated products.

* Musashi Institue of Technology, Tokyo Japan.

Because of these difficulties, even though many prediction techniques such as correlative analysis, multi regression analysis, statistic of extreme ...etc. had been applied to the study on predicting service life of plated products, but the results have not been entirely satisfactory. Among many prediction techniques , reliability theory has been found widely used in many science and engineering fields in predicting service life of materials, components and system.[8-11] Reliability theory has an advantage in analysis wide variation of time to failure and representing service life as a distribution rather than a mean. Compare to another prediction technique such as correlative analysis which is an inexact and relatively incentive, reliability analysis seems to be more effective. However, only few reports on the predicting service life of plated products by using reliability technique have been found. Using reliability theory and life testing analysis is a systematic, probabilistic procedure designed for the purpose of making quantitative service life predictions. As for these reasons, the authors applied this technique in the study of predicting service life of plated products.

In this research, reliability theory and life testing technique were applied to the prediction service life of nickel plated steels. Artificial sea water corrosion test were designed and used for life testing method. Data obtained from the test were analyzed by using reliability technique.[12] From the analytical results, P-S-T diagram (Probablity of failure - Stress - Time to failure) was constructed and used for the prediction of service life of nickel plated steels.

Analysis and prediction of service life by using Reliability technique

Reliability is the probability that a device or a system will perform its function adequately for the period of time intended under the operating conditions encountered. Such probability is also referred to as the probability of survival. In general, a reliability prediction is obtained by mathematically combining probabilistic events.

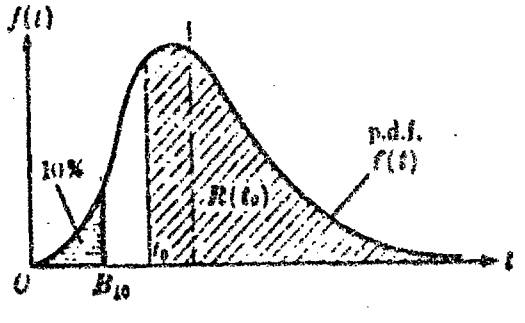

$$R(t_0) = \int_{t_0}^{\infty} f(t)\,dt \qquad [1]$$

$$F(t) = 1 - R(t) \qquad [2]$$

Fig. 2. Failure distribution diagram

In Fig.2, probability density function f(t) was plotted as a function of time. Reliability $R(t_0)$ is the probability of survival in which a device will not fail prior to time t_0. $F(t_0)$ is the probability of failure at time t_0, and B10 represent

the point that 10% of devices are expected to have failed.

The prediction of service life by using reliability technique is started from conducting a life testing. The service life which is defined as the time at which the specimen has failed was investigated.

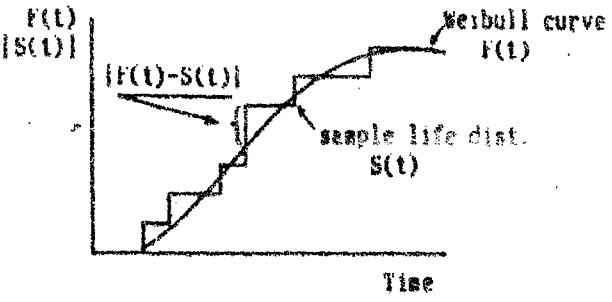

Fig.3 Schematic diagram of sample life distribution (superimposed with Weibull distribution curve).

Weibull distribution :

$$f(t) = \frac{m}{\eta}\left(\frac{t-\gamma}{\eta}\right)^{m-1} e^{-\{(t-\gamma)/\eta\}^m} \qquad (t \geq \gamma) \qquad [3]$$

$$= 0 \qquad (t < \gamma)$$

$$R(t) = \exp(-(t-\gamma)/\eta)^m \qquad [4]$$

where m = shape parameter
η = scale parameter
γ = location parameter

Times to failure of the specimens were arranged in ordered. In Fig. 3 a sample life distribution was constructed by plotting the ordered time to failure with the cumulative failure probability of the specimens. Weibull distribution curve was superimposed on the sample life distribution and test of fitness was performed by employing Kolmogolov-Smirnov method. Weibull shape, scale, location parameters were calculated by using the maximum likelihood method and iteration technique.[8,15] The obtained parameters were used to estimate failure times or service lives of the specimen instead of observed failure times.

In reliability analysis, the maximum service life is defined as the time beyond which a specified portion(λ) have failed. A portion which is designated as a service life of products is usually a function of safety, accessibility and warranty costs. For a manufacturer in order to minimize his warranty cost a portion of 10% (B10 life) is normally used as a service life. From the Weibull distribution curve, maximum service lives were computed by solving the reliability function in equation (4).

$$t_{s\ell} = \eta(-\ln(1-\lambda)^{1/m}) + \gamma \qquad [5]$$

where $t_{s\ell}$ = maximum service life
λ = a specified portion of specimens

The obtained maximum service lives were plotted as a function of temperature which was referred as a P-S-T diagram. From the P-S-T diagram, service life of plated articles at which a specified portion(λ) have failed, at various temperature, can be quantitatively estimated.

Application to the service life prediction of nickel plated panels were carried out as the following :

Let t represent service life of nickel plated steel and t is a function of plating thickness , quality level of plating and environmental conditions. This relation can be simply expressed as the following :

$$t = G(d, Q, S) \quad [6]$$

where t = service life of nickel plated steel
d = plating thickness
Q = quality level of plating
S = stress of all inclusive factors

In the artificial sea water test, temperature was selected as just an only one variable stress since it seems to fit with Chemical Reaction model and can be varied, controlled over a wide range in the experimental process. Thus, if other variables are constant life testing time t' can be expressed as the following :

$$t' = g(d, Q, T) \quad [7]$$

where T = temperature

If the corrosion modes in service conditions and in the accelerated corrosion test are not much different and the acceleration factor is known, then

$$t = k\, t' \quad [8]$$

where k = acceleration factor

By combining expressions [6],[7] and [8],the following expression is obtained

$$g(d, Q, S) = k\, G(d, Q, T) \quad [9]$$

From [9]: If thickness and quality level of plating represented by d_o and Q_o are constant.

$$g(d_o, Q_o, S) = k\, G(d_o, Q_o, T) \quad [10]$$

Therefore S is a function of T and in the accelerated corrosion test stress level can be classified by temperature levels of the test.

Test panels, nickel plated with various thicknesses, were subjected to the artificial sea water test at three different temperatures(3 levels of T). Failure times of the test panels were investigated and sample life distributions were constructed. To each sample life distribution Weibull distribution curves were fitted. Test of fitness was conducted and Weibull parameters were estimated . For each thickness, at each temperature, maximum service lives were calculated and these calculations were plotted as a function of temperature(P-S-T diagram). From this diagram, quantitative service lives of nickel plated steels at which a specified portion has failed, at various temperatures, were able to be estimated.

In an exposure test ,service life (B10) of 5 μm Ni plated panel was determined. This service life was plotted in the obtained P-S-T diagram and the temperature level of artificial sea water which corresponding to the same stress level of exposure test was determined. From this temperature level the service lives of nickel plated steels for different thicknesses of nickel plating in exposure test can be quantitatively predicted.

Experiment

Test specimens were prepared by using low carbon steel panels with size of 195mm x 180mm x 0.3mm. Prior to plating, pre-treatments of panels were conducted by a process consisting of brushing, electrolytic cleaning (anodically) and acid dipping (10% HCl). Between each step panels were rinsed with tap water

and delonized water. Subsequently water-free break test was performed to assure that clean surface panels had been obtained.

Watts' bath, compositions and plating condition as shown in Table 1, was used for plating. Panels were plated with nickel of 4 different thicknesses 5,10,15,20 μm for which plating time, determined by preliminary test, were 11.0,22.0,33.0,44.0 minutes respectively. Plating area on each panel was 150mm x 100mm. After plating, panels were stored in desiccator to prevent from corrosion.

The plated panels were randomly selected for each test. Sets of 15 panels of each thickness were used for thickness test. Plated area on each panel was sectioned into 15x10 matrix square blocks, thickness at the center of each block was measured by using coulometric method. Besides measurement of thickness, panels were subjected to ferroxyl test for measurement of porosity. The compositions of ferroxyl test solution and operating conditions were shown in Table 2.

In preparation of the panels for cyclic corrosion test, except testing area of 100mm x 50mm, the back and edges of the panels were masked with durable commercial resistance tape and coating. The experiment was conducted at three different temperatures of 25°C, 40°C, 55°C. Testing bath contained with 3% NaCl solution were aerated 30 minutes before the immersion of the test panels in order to saturate oxygen. The test panels were immersed in testing bath for a period of 18 hours. After the immersion, the panels were rinsed, dried and kept at room temperature for the total of 6 hours. During the rinse period, corrosion products were removed (procedure recommended by ISO).[13] The test solution was renewed when it was contaminated by corrosion products, usually every cycle at the beginning and once every two or three cycles later on.

The quantitative evaluations of corroded area were performed during the drying period by placing a transparent grid over each test panel. The grid was sectioned into 20 x 40 matrix of square blocks. For each evaluation, number and size of protective defects in each block were investigated for every panels. The panels were determined to have failed when their percentage of corrosion areas reach 0.1% and 0.25%. The panels with percentage corrosion area exceed 0.25% were terminated from test.

Additional experiment of an out-door exposure test was carried out. Panels from the same lot as above were placed on an exposure rack with the exposed angle of 45 degree. The test rack was set facing to the south on the roof top of building No.10 at Musashi Institute of Technology for conducting the exposure test.

Table 1. Watts bath constituents & operating conditions

$NiSO_4.7H_2O$	250	g/l
$NiCl_2.6H_2O$	45	g/l
H_3BO_3	35	g/l
pH	4-5	
current density	3	A/dm^2
temperature	55	°C

Table 2. Ferroxl solution & operating conditions.

$K_4Fe(CN)_6.3H_2O$	10	g/l
$K_3Fe(CN)_6$	10	g/l
NaCl	60	g/l
NH_4OH	5-10	g/l
time	5	mins
testing area	>10	cm^2

Results and Discussion

The plots in Fig. 4 showed distributions of thickness on plated panels. The distributions were found to be in U-shape with comparative thick in edge area and symmetrically decreased to the center. Plated area at the center(100mm x 50mm) with least dispersion was used as a significant area for corrosion test. From the analysis of variance, the results showed that there were no significant at 95% confidence interval in thickness different of 15 panels in each set.

The results of ferroxyl test showed that the average number of defect points per unit area in 5,10,15,20 μm Ni plated panels were 0.018, 0.008, 0.047, 0.009 pts./cm^2 respectively. According to Japanese Industrial Standard,[14] all of these figures were in accepting limit. For individual panel, number of defect points per unit area of thicker panels were found, sometime, higher than thinner panels. This is probably due to the variation in plating quality resulted by unexpected factors in plating process.

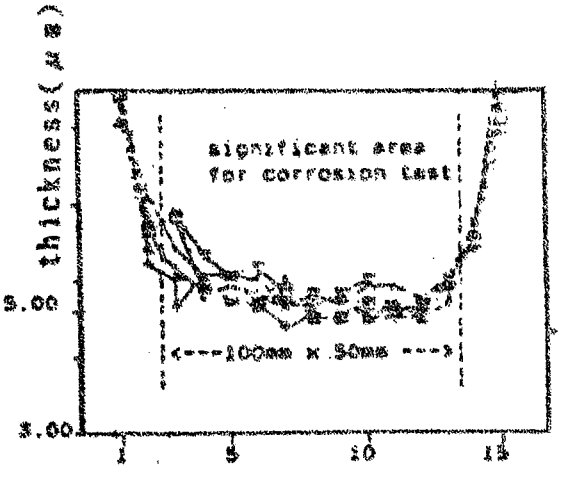

Fig. 4 Distribution of Ni plating on test panel 5 μm.

$\bar{X}$ and s.d. of significant area for each thickness.

categories	$\bar{X}$	s.d
5 μm	5.6	0.1
10 μm	11.7	1.6
15 μm	17.3	1.7
20 μm	23.7	2.5

In Fig.5 change in percent area of corrosion for each panel were plotted as a function of immersion time. From this figure, it could be observed that change in percent area of corrosion were varied increasingly with the increasing of immersion time. For some individual panels, change in percent corrosion area sometime showed a temporary decreased. This is probably due to variation in determining defect sizes and type of defects. Pin hole corrosion, type of defect on cathodic metallic coating, were found randomly on testing area of each panel.

Evidence in Fig. 5 also showed that the panels of the same thickness when subjected to the test at different temperatures times to failure were decreased with the increasing of temperature. The panels of different thicknesses when subjected to the test at same temperature, times to failure were increased with the increasing of Ni thickness. These tendencies were all the same for all thicknesses.

It was observed that the variation in change of percent

area of test panels in which some panels with thicker Ni plating may be found to have shorter failure times than thinner panels or the panels with the same thickness of Ni plating when subjected to different stress level failure times at lower stress level were found, sometime, shorter than at higher stress level . This occurrence could be explained as the same phenomenon which was found in the ferroxyl test.

For the panels in the same category, there are always one or two panels which have failure rate much greater than the others. These can be referred as the early failure cases which may be caused by some defective products.

Sample life distribution of each thickness were constructed by plotting the ordered time to failure as shown in Table 3 with the cumulative probability of failure. To each sample distribution life Weibull distribution curve were fitted and test of fitness were conducted by using Kolmogorov-Smirnov method. The results of test in Table 4 showed that Wiebull distribution curve were fitted to all of the sample life distributions.

Weibull parameters shape, scale and location were estimated and were tabulated in Table 5. In Fig. 6, 7 Weibull scale and location parameters were shown to be related nearly

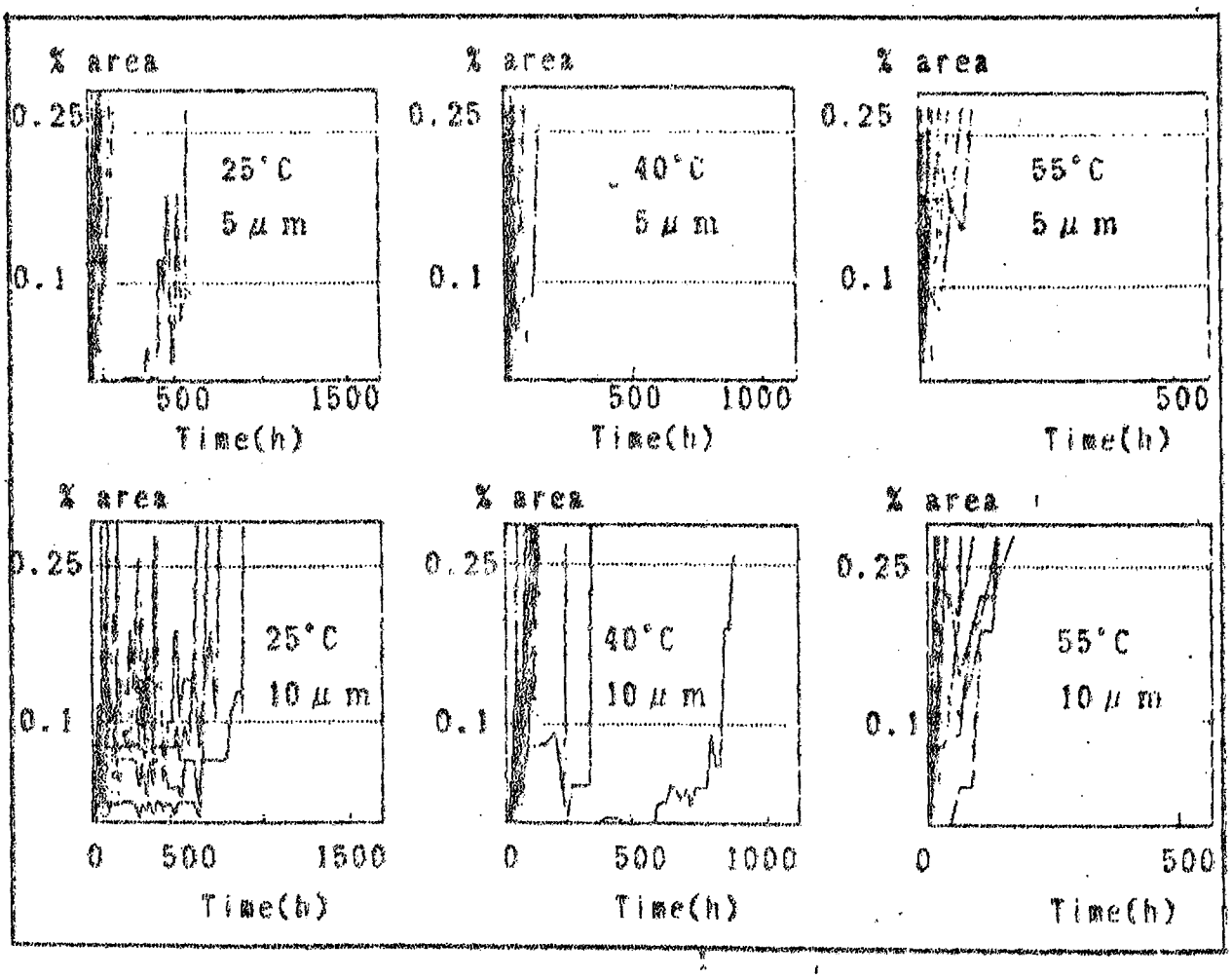

Fig. 6 Change in percent area corrosion of nickel plated steel panels subjected to the artificial sea water test at 25°C, 40°C, 55°C

Table 3. Times to failure of nickel plated steel panels (10 μm) subjected to artificial sea water corrosion test at 25°,40°,55°C

Unit : hour

temperature (°C)	25°		40°		55°	
failure criterion (% area)	0.1	0.25	0.1	0.25	0.1	0.25
ordered time to failure index						
1	85.1	100.8	38.2	46.6	4.7	12.6
2	90.0	133.6	51.8	85.3	4.9	13.1
3	126.9	148.0	52.0	86.7	5.8	14.5
4	137.7	154.3	59.2	94.1	7.2	18.0
5	139.4	155.5	60.3	100.6	7.6	19.3
6	144.9	199.8	65.0	103.5	7.6	22.1
7	188.1	214.6	66.4	107.1	12.2	29.9
8	202.0	216.0	76.7	110.3	12.2	29.9
9	262.4	321.3	93.8	111.2	14.2	30.6
10	363.1	409.9	94.1	125.5	14.2	56.5
11	399.1	414.0	96.3	136.3	16.4	66.6
12	504.9	641.3	102.4	141.8	21.4	108.0
13	660.8	691.6	222.3	248.4	30.6	115.0
14	674.5	748.4	343.4	347.4	55.8	116.1
15	828.0	891.4	833.2	882.0	79.2	126.0
No. of panel test	15	15	15	15	15	15
No. of panel fail	15	15	15	15	15	15
Maximum exposure time	828.0	891.4	833.2	882.0	79.2	126.0

Table 4 Results of Kolmogorov-Smirnov test of fitness.

$D^*n = \max |F(t)-S(t)|$

Temperature °C categories (μm)		25	40	55
5	a	0.156	0.093	0.075
.....	b	0.183	0.109	0.093
10	a	0.105	0.332	0.092
.....	b	0.187	0.225	0.210
15	a	0.147	0.186	0.129
.....	b	0.154	0.206	0.167
20	a	0.158	0.188	0.235
.....	b	0.208	0.216	0.222

Critical value for the Kolmogorov-Smirnov test

$D^*n\ (0.025, 15) = 0.33759$

a) failure criteria 0.1% b) failure criteria 0.25%

Table 5 Weibull parameters estimated by Maximum Likelihood Method :

Temperature level(°c)		25				40				55			
Thickness of nickel/μm		5	10	15	20	5	10	15	20	5	10	15	20
No of test panel		15	15	15	15	15	15	15	15	15	15	15	15
No of panel fail		15	15	15	15	15	15	15	15	15	15	15	15
Shape parameter	a.	.57	1.05	0.75	0.68	1.04	.67	.72	.68	.80	.70	.82	.61
(m)	b.	.74	1.13	.65	.71	1.05	.75	.65	.58	.84	1.09	.80	.52
Scale parameter	a.	33.8	260.1	414.0	475.8	27.8	81.3	178.9	298.5	7.8	12.01	114.3	113.9
(η)	b.	62.4	301.0	459.9	751.0	40.9	114.8	178.7	311.8	21.5	47.0	143.2	168.6
Location	a.	13.2	85.4	124.8	150.6	1.8	38.0	68.0	79.8	0.8	4.6	8.8	13.6
parameter	b.	24.0	75.0	157.2	199.8	5.2	48.6	105.4	112.4	2.0	6.0	14.2	25.4
(γ)			* a. failure criteria 0.1%			b. failure criteria 0.25%							

TABLE 6 Linear Regression Coefficients for regression lines of Weibull scale and location parameters with reciprocal absolute temperature via arrhenious model.

	Weibull scale parameter $\log \eta = a + b(1/T)$			Weibull location parameter $\log \gamma = c + d(1/T)$		
thickness, failure criterie	a	b	r(correlation)	c	d	r(correllation)
1) 5 , 0.1 %	-5.21	2.03	0.91	-14.01	4.28	0.97
2) 10 , 0.1 %	-12.08	4.33	0.89	-10.54	3.72	0.94
3) 15 , 0.1 %	- 3.54	1.90	0.38	-14.12	4.68	0.93
4) 20 , 0.1 %	- 4.03	2.00	0.97	- 9.08	3.37	0.96
5) 5 , 0.25%	- 3.23	1.50	0.97	-10.48	3.53	0.99
6) 10 , 0.25%	- 5.21	2.16	0.99	-10.72	3.73	0.93
7) 15 , 0.25%	- 5.21	2.20	0.99	- 8.97	3.36	0.92
8) 20 , 0.25%	- 4.03	2.14	0.99	- 7.34	2.89	0.96

linear with the reciprocal absolute temperature. These relationships were fitted with Arrhenius model. The linear regression coefficients were tabulated in Table 6. These relationship are probably implied that the corrosion rate on test panels were the same, at least over the range of testing temperature. In Fig. 8, shape parameters were plotted with temperature and they were found to be almost constant. This replied that failure rate of test panels are almost the same.

From Weibull distribution function, the maximum service lives for each thickness and at each stress level were computed For example, from table 5 the panels with 5 micron thickness at 0.1% failure criteria m=.57, η=33.6, γ=18.2 replace these values in equation [5] and the maximum service life can be obtained tal=19.9 hrs.

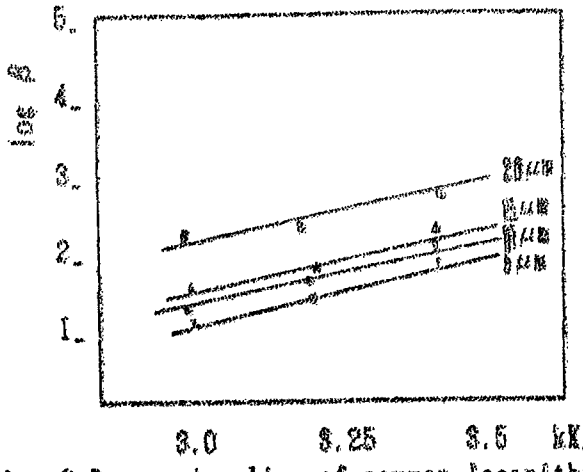

Fig. 6 Regression line of common logarithm of Weibull scale parameter vs. reciprocal absolute temperature.

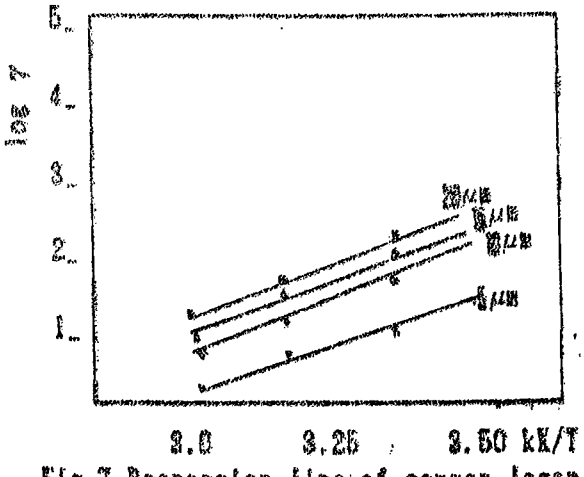

Fig.7 Regression line of common logarith of Weibull location parameter vs. reciprocal absolute temperature.

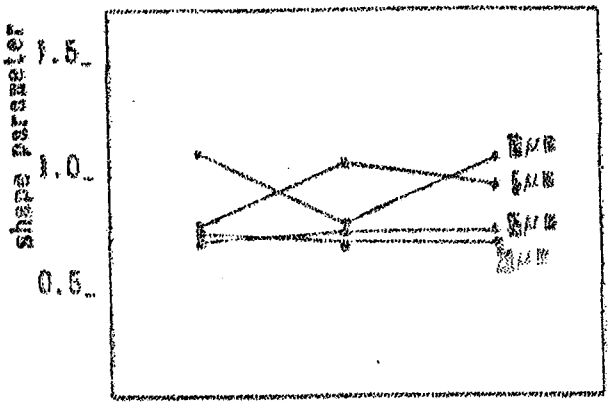

Fig.8 Weibull shape parameter vs. temperature

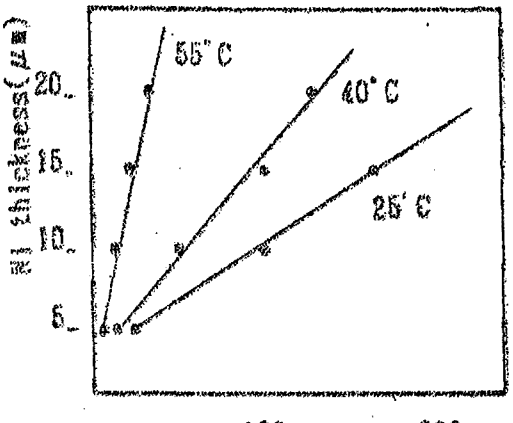

Fig.9 Ni thickness vs. service life

In Fig. 9, thickness of nickel were plotted with the obtained service life. From this diagram, the minimum thickness of nickel which could stand with out failure for the required testing time, at different temperature levels , can be estimated.

In Fig.10, a P-S-T diagram was constructed by plotting the computations of maximum service lives on log scale with reciprocal absolute temperature. From the P-S-T diagram, service lives of nickel plated steels at which a specified portion(λ) of panels have failed, at various temperature, were able to be estimated.

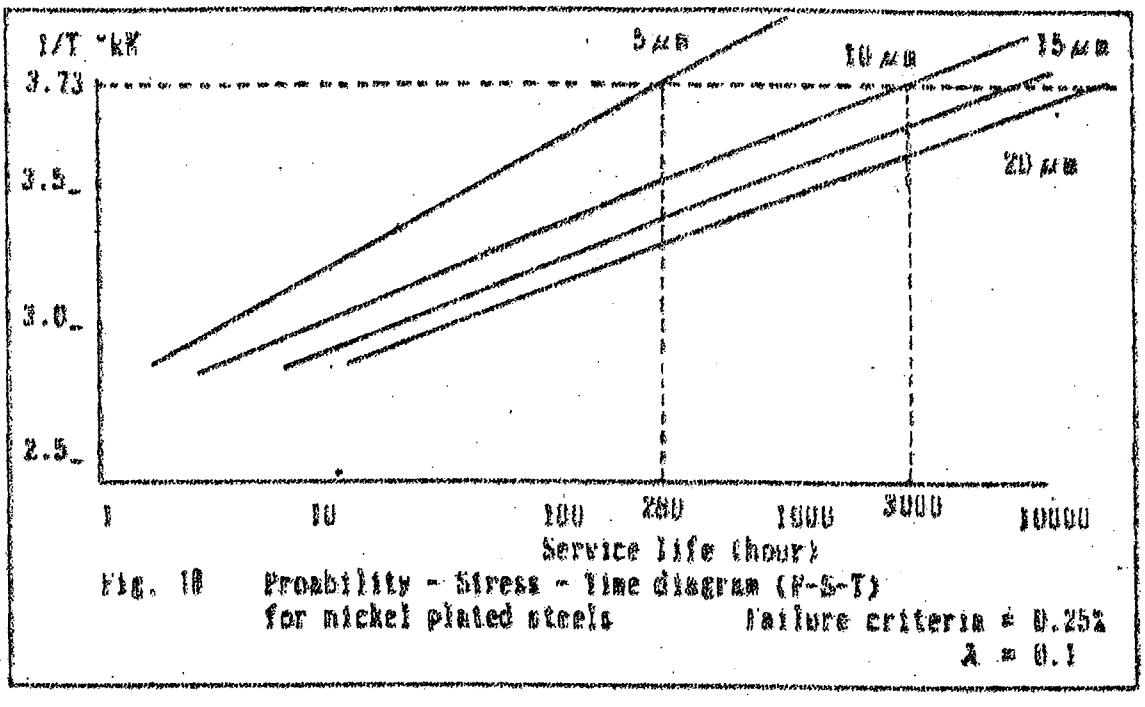

Fig. 10 Probability - Stress - Time diagram (P-S-T) for nickel plated steels Failure criteria = 0.25%
λ = 0.1

The results of this P-S-T diagram were used to predict service life of nickel plated panels in the exposure test by obtained service life (B10 life) of 5μmNi plated panels from field data first. For example, the service life of5μmNi plated panels subjected to the additional exposure test at Musashi Institute of Technology was found to be 280 hours. This value was plotted in the above P-S-T diagram and from the corresponding curve stress level of artificial sea water at -5°C was found to be equivalent to the stress level of exposure test. The extrapolation was made to predict the service life of 15μm Ni plated panels which was 3000 hours and was found to be nearly the same as the results which was obtained directly from the exposure test.

Conclusion

The application of reliability and life testing analysis technique to the study of service life prediction of nickel plated steel panels was demonstrated in this paper. Results of the study were concluded that plating characteristics of test panels were appropriate for the corrosion test. Sample life distribution of test panels were found to fit with Weibull distribution curve. Scale parameter and location parameter of Weibull distribution were found linearly related to the reciprocal absolute temperature and were fitted with Arrhenius model. Shape parameter was found to be almost constant.

Service life of nickel plated steels subjected to artificial sea water at which a specified portions(λ) have failed, at various temperature, could be quantitatively predicted. The minimum thickness of nickel plated on steels which will survive for the required testing time, at each temperature, could be quantitatively estimated. From the P-S-T diagram, the prediction service life of nickel plated steels in other stress conditions such as exposure stress could be made.

This testing procedure and the analytical results demonstrated a possibility of the prediction service life of plated products which is generally agreed to be a difficult task. The confidence in applying this procedure could be significantly improved if more experiments are conducted and more data available for further analysis.

References

1. Tadeusz Bieniek," Comparative corrosion testing of 6 system of electrodeposited Ni/Cr and Cu/Ni/Cr coating on steel", Surface technology,21,283-294 (1984)

2. Yasuchito Togawa,"Atmospheric Test of some Metallic Coatings" Journal of Metal Finishing Soc. Japan,32,(7),336-343(1981)

3. Roger L. Saur et al.," Correlation of EC and CASS tests to Service Using Duplex Nickel system", Plating, 320-325 March (1986)

4. Hirayuki Tsuge," Life estimation of corroded materials by using the statistic of extreme",Jap Soc. of corrosion Engineer, January (1986)

5. Yuichi Ishikawa,"A probabilistic approach to pitting corrosion life prediction"Jap Soc. of Corrosion Engineer,28,278-284(1977)

6. "Service Life Prediction of Plant Material- Experience and Practice" proceeding of the 73th Corrosion Engineering symposium, Jap Soc. of Corrosion Engineer,March 9,1988 Tokyo

7. Martin,J.W. and Mc Knight,M.E.,"The Prediction of the service Life of Coating on Steel,Part1,2" Journal of Coating Technology, 57,(724),31-49(1985).

The Chlorination of Selected Commercial Alloys at High Temperature

M.J. McNallan
Faculty of CEMM, University of Illinois at Chicago, U.S.A.
and
S. Thongtem
Faculty of Science, Chiang Mai University, Thailand.

Abstract

Chlorine contaminated environment can cause corrosion of alloys at high temperatures by the formation of both volatile and nonvolatile products. The corrosion of the selection of commercial alloys in the environment containing chlorine was studied at the temperature of 1000 ^{o}C. It was found that the susceptibility of each alloy to the corrosion process is controlled by the temperature, chlorine potential and the composition of the alloys.

Introduction

The presence of chlorine contamination is a promoting factor to accelerate the corrosion of materials in industrial environments[1,2] Naturally, chlorine can diffuse into alloy matrix[3,4] and form liquid metal salt deposits which are easily volatile even at low temperature[5,6]. To improve the understanding of high temperature corrosion in environment containing chlorine, the selected alloys were exposed in a gas mixture of 0.25 % Cl_2 - 20 % O_2 - Ar at the temperature range of 700 - 1000 ^{o}C.

Apparatus and Procedures

A furnance consists of a nichrome, a thermocouple, and a fused quartz rack which can support four samples in a fused quartz reaction tube. The samples were approximately 1 cm^2 with 1 to 2 mm thick. The composition of the alloys in this study were shown in Table 1.

Weight and dimension of the samples were carefully determined and hung on the quartz rack. The samples were heated in argon gas until the temperature was stabilized. The gas was replaced with 0.25 % Cl_2 - 20 % O_2 - Ar and the experiment was prolong for 50 hours. At the end of each run, the samples were cooled down to room temperature in argon gas for weighing. The experiment was repeated until the total of 400 hours was attained.

Discussion

Weight Loss

The alloys were exposed in environment containing both oxygen and chlorine at high temperature and their weight loss was shown in Figures 1 - 7. Most of them showed weight loss that fitted to a linear equation of the form

$$\Delta w = at + b \qquad (1)$$

where Δw = weight loss of the samples

t = the experimental time

a & b = constants

For all alloys, the rate of weight loss increased with increasing the test temperature. According to the experiment, alloys C-276 and 188 which contained Mo or W showed the highest of weight loss, ranging from 160 - 300 mg/cm^2 at 1000 ^{o}C. Alloy 600, a nickel base alloy, showed the high rate of attack at 1000 ^{o}C but much slower at low temperature. Iron-base alloys like 310 SS, 800H and 556 showed the lower rate of attack with less than 100 mg/cm^2 even at 1000 ^{o}C. Alloy 214 which contained alumina forming compound showed the least of attack with less than 10 mg/cm^2 at the highest temperature.

Activation Energy of the System

For this system, nickel oxide is the thermodynamically stable condensed phase and nickel chloride is the highest vapor pressure species. Thus the main reaction is

$$NiO(s) + Cl_2(g) = NiCl_2(g) + \frac{1}{2} O_2(g) \quad (5,7,8) \qquad (2)$$

where, $\Delta G^o = 167,078.9 - 134.3T$ joules/mole $(9-13)$ (3)

Slope of each line in Figures 1 - 7 is the corrosion rate(k_v) of reaction (2). The value of $\ln|k_v|$ was then plotted relative to $\frac{1}{T}$ as shown in Figure 8 and the slope of each line would be the activation energy(Q) of the alloy.

Nickel Chloride Controlling Process

For this experiment, it was assumed that the flow of the gases was laminar across the average length of 1 cm samples. Mass transfer of nickel chloride between the corroding surface and the gas phase was assumed to be the controlling process. The theoretical reaction rate is given by (14)

$$k_1 = h_{NiCl2} \frac{A}{RT} P_{NiCl2} \qquad (4)$$

and

$$h_{NiCl2} = 0.664 \frac{D^{2/3}}{\nu^{1/6}} (v)^{1/2} \qquad (5)$$

where h_{NiCl2} = mass transfer coefficient of $NiCl_2$ in gas phase (cm/sec)

A = atomic weight of nickel

R = gas constant (cm^3.atm / ^oK.mole)

T = temperature (^oK)

P_{NiCl2} = vapor pressure of $NiCl_2$ (atm)

D = diffusivity of $NiCl_2$ in Ar (cm^2/sec)

ν = kinematic viscosity of 20 % O_2 - 80 % Ar (cm^2/sec)

v = velocity of gases (1.5 cm/sec).

By using equation (4) and (5) with some parameters calculated from references 15 and 16, k_l can be determined. The values of $\ln|k_l|$ were then plotted against $\frac{1}{T}$ as shown in Figure 8. It was found that nickel chloride controlling process agrees very well with all of the alloys in this experiment.

Conclusions

1. The corrosion rate of all alloys was controlled by the test tempertures, the experimental time and the composition of the alloys.
2. For all alloys studied, iron based alloys are the most stable with the exception of alloy 214 which can form the protective scale to resist the corrosion.
3. Alloys C-276 and 188 which contained high content of Mo or W are corroded at the highest rate.
4. The nickel chloride controlling process agrees very well with the calculated values from the weight loss result.

References

1. A.L. Plumley, W.R. Roczniak : 'Naturally Occuring High Chloride Coal and Superheater Corrosion - A Laboratory Study', Journal of Engineering for Power, Vol.104, 1982, pp.874-884.

2. H.H. Krause, D.A. Vaughan, P.D. Miller : 'Corrosion and Deposits from Combustion of Solid Wastes - Part 2 - Chloride Effects on Boiler Tube and Scrubber Metals', Journal of Engineering for Power, Vol.96, 1974, pp.216 - 222.

3. Y.K. Li and R.A. Rapp : 'Internal Chloridation of Dilute Ni - Cr Alloys', Metallurgical Transactions B, Vol.14B, September 1983, pp.509 - 510.

4. S.N.S. Reddy and R.A. Rapp : 'Internal Fluoridation of Ni - 5.6 Pct Cr Alloy', Metallurgical Transactions B, Vol.11B, September 1980, pp.533 - 534.

5. Y. Ihara, H. Ohgame, K. Sakiyama and K. Hashimoto : 'The Corrosion Behavior of Nickel in Hydrogen Chloride Gas and Gas Mixtures of Hydrogen Chloride and Oxygen at High Temperatures', Corrosion Science, Vol.22, No.10, 1982, pp.901 - 912.

6. Y. Ihara, H. Ohgame, K. Sakiyama and K. Hashimoto : 'The Corrosion Behavior of Iron in Hydrogen Chloride Gas and Gas Mixtures of Hydrogen Chloride and Oxygen at High Temperatures', Corrosion Science, Vol.21, No.12, 1981, pp.805 - 817.

7. K. Hauffe and J. Hinrichs : 'Simultaneous Oxidation and Chlorination of Nickel', Oxidation of Metals and Alloys, ASM, 1970, pp.87-100.

8. P. Elliott, C.J. Tyreman and R. Prescott: 'High Temperature Alloy Corrosion by Halogens', Journal of Metals, Vol.37, No.7, 1985, pp.20-23.

9. O. Kubaschewski and C.B. Alcock : Metallurgical Thermochemistry, Vol.24, 5th Ed., 1979, pp.378-384.

10. L.B. Pankratz : Thermodynamic Properties of Halides, Bulletin 674, U.S. Department of the Interior Bureau of Mines, Director : R.C. Horton.

11. L.B. Pankratz : Thermodynamic Properties of Elements and Oxides, Bulletin 672, U.S. Department of the Interior Bureau of Mines, Section and Process Applications by R.V. Mrazek, 1982.

12. D.R. Stull and H. Prophet : JANAF Thermochemical Tables, U.S. Department of Commerce National Bureau of Standards, NSRDS-NBS 37, 1971, including 1974 and 1982 Supplements.

13. D.R. Gaskel : Introduction to Metallurgical Thermodynamics, Materials Science and Engineering Series, 2nd Ed., McGraw-Hill Book Co., 1981, pp.585 - 586.

14. M.J. McNallan, J.M. Oh and W.W. Liang : 'High Temperature Corrosion of Metals in Argon - Oxygen - Chlorine Mixtures', Proceedings JIMIS - 3, High Temperature Corrosion Transactions of the Japan Institute of Metals, Supplement, Vol.24, 1983, pp.677 - 685.

15. R.J. Fruehan : 'The Rate of Chlorination of Metals and Oxides' Metallurgical Transactions, Vol.3, October 1972, pp.2585 - 2592.

16. J.O. Hirschfelder, C.F. Curtiss and R.B. Bird : Molecular Theory of Gases and Liquids, John Wiley & Sons, Inc., New York, 1954, pp.528-567 and Appendix.

Table 1. Alloys in present study.

Alloy Designation	Nominal Chemical Composition (Weight %) [2,23]											
	C	Fe	Ni	Co	Cr	Mo	W	Si	Mn	Al	Ti	Others
310 Stainless (UNS S31000)	0.047	BAL	19	--	25	--	--	0.5	0.8	--	--	--
Alloy 800H (UNS N08800)	0.08	BAL	33	--	21	--	--	1.0*	1.5*	0.38	0.38	0.75 Cu*
HAYNES Alloy No. 556	0.10	BAL	20	18	22	3	2.5	0.4	1*	0.2	--	0.8 Ta, 0.2 N, 0.02 La, 0.02 Zr
Alloy 600 (UNS N06600)	0.08*	8	BAL	--	16	--	--	0.5*	1*	0.35*	0.30*	0.5 Cu*
CABOT Alloy 214	0.04	4	BAL	--	16	--	--	--	--	4.5	--	0.01 Y
Alloy C-276 (UNS N10276)	0.02*	5.5	BAL	2.5*	15.5	16	4	0.08*	1*	--	--	0.35 V
HAYNES Alloy No. 188	0.1	3*	22	BAL	22	--	14	0.35	1.25	--	--	0.04 La

*Maximum

CABOT, HASTELLOY and HAYNES are registered trademarks of Cabot Corporation.

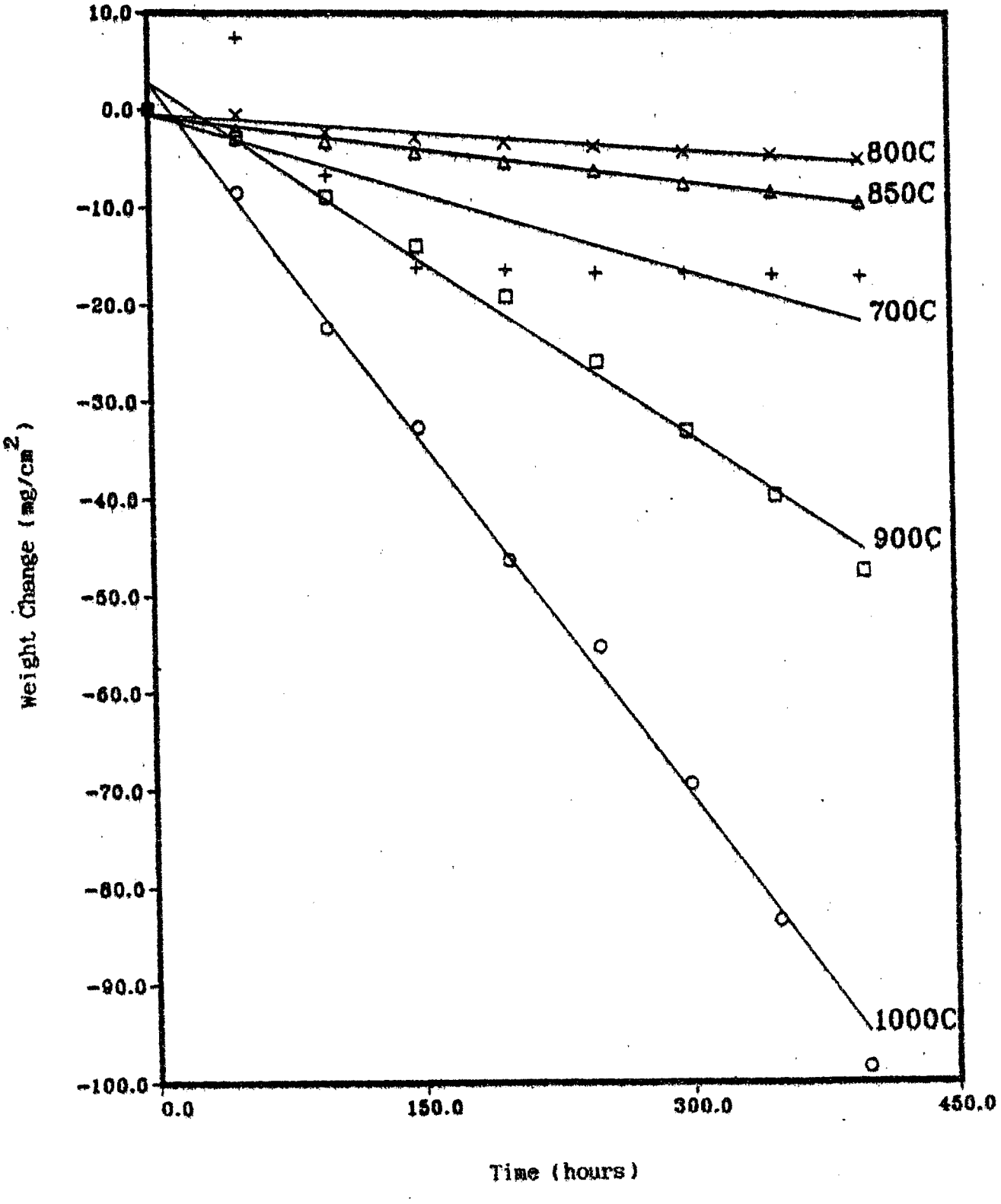

Figure 1. Weight change of alloy 310 with the experimental time.

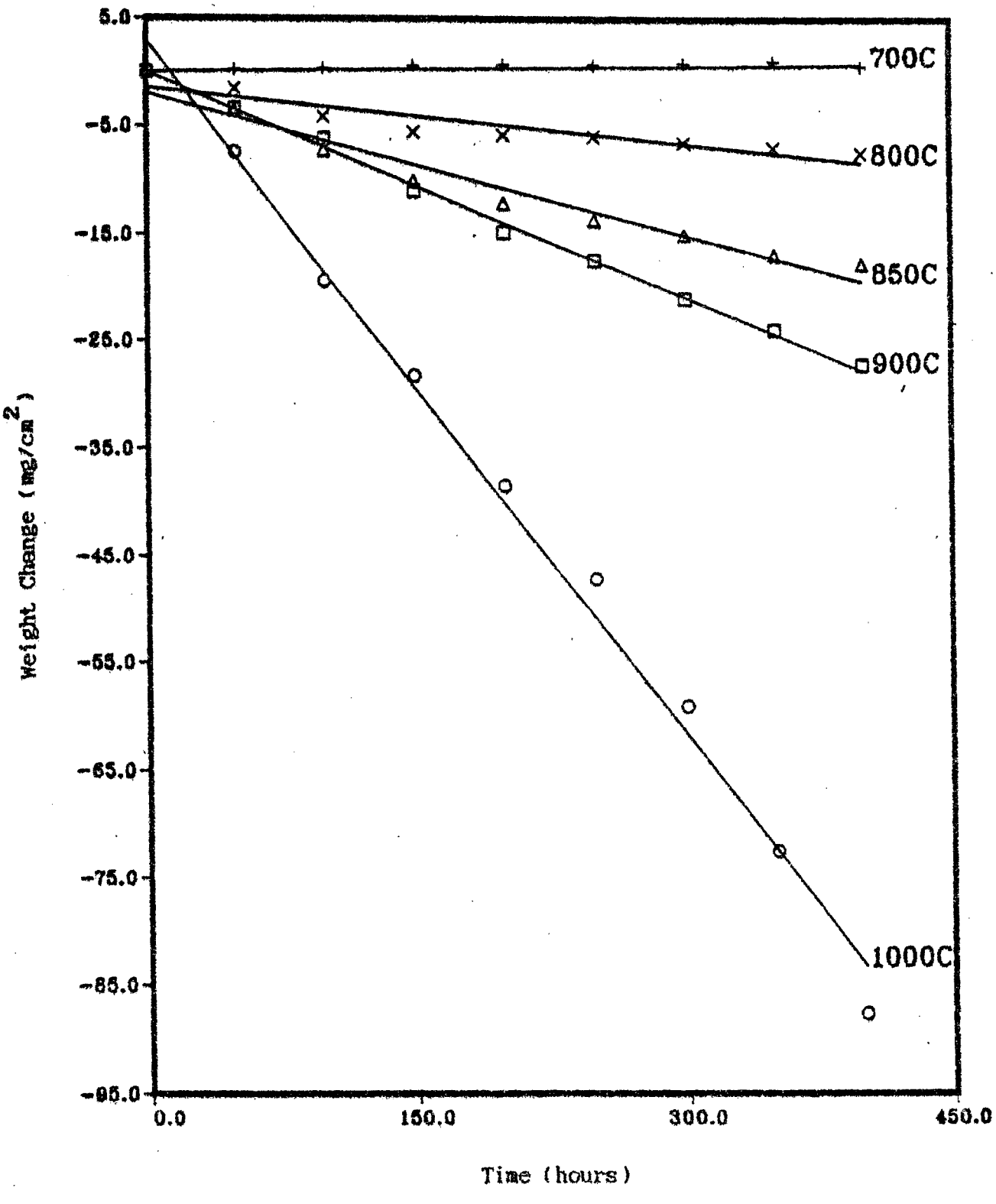

Figure 2. Weight change of alloy 800H with the experimental time.

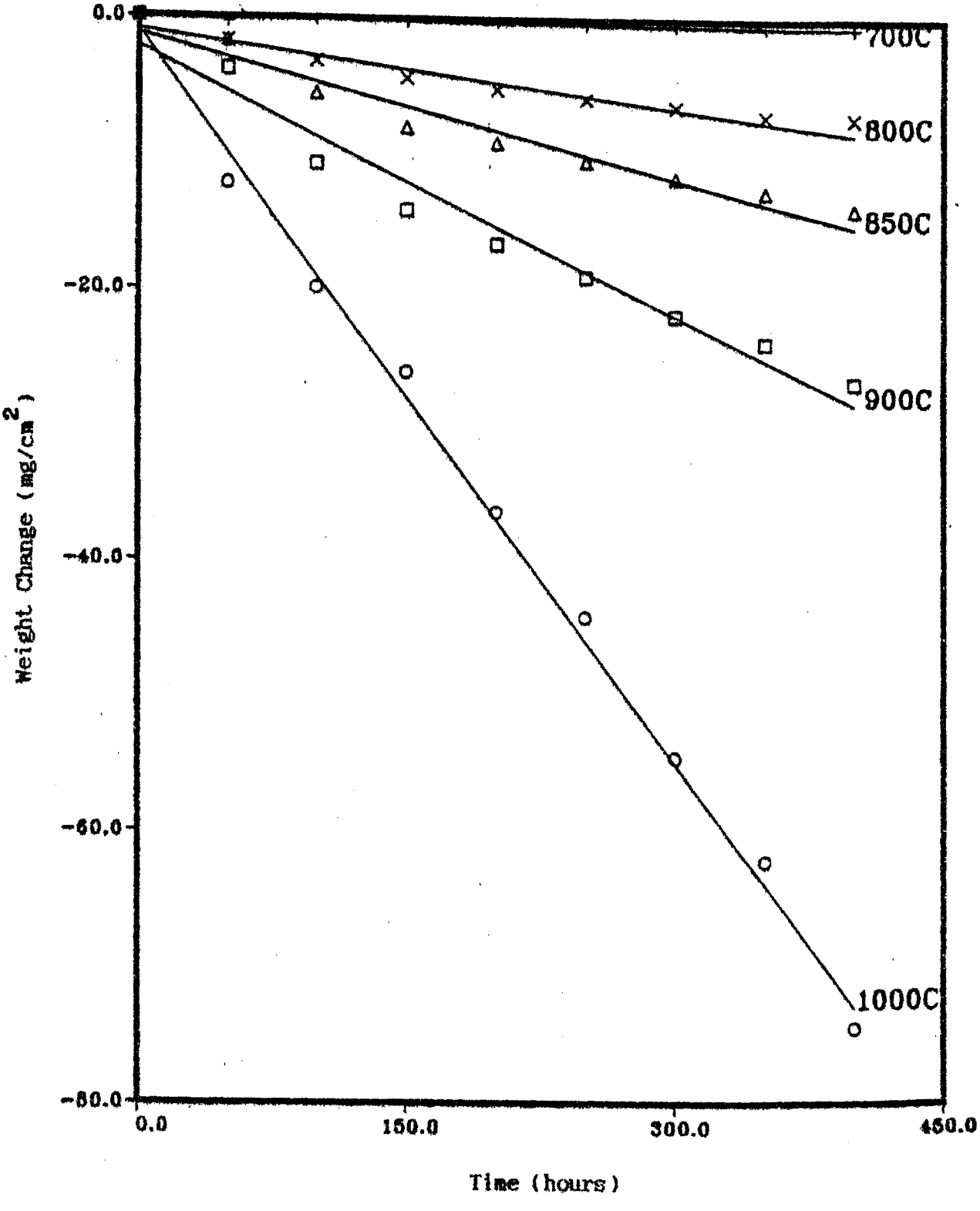

Figure 3. Weight change of alloy 556 with the experimental time.

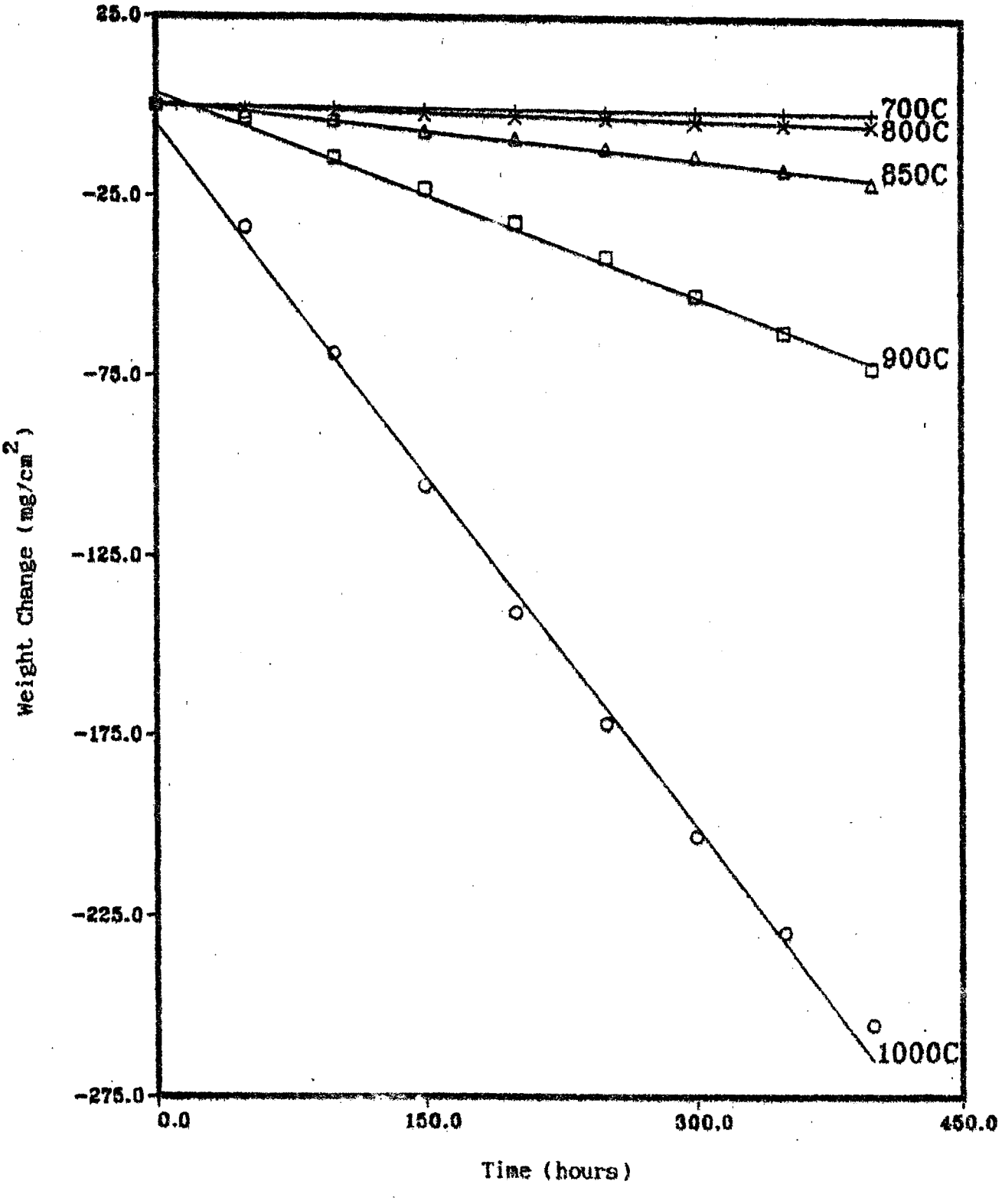

Figure 4. Weight change of alloy 600 with the experimental time.

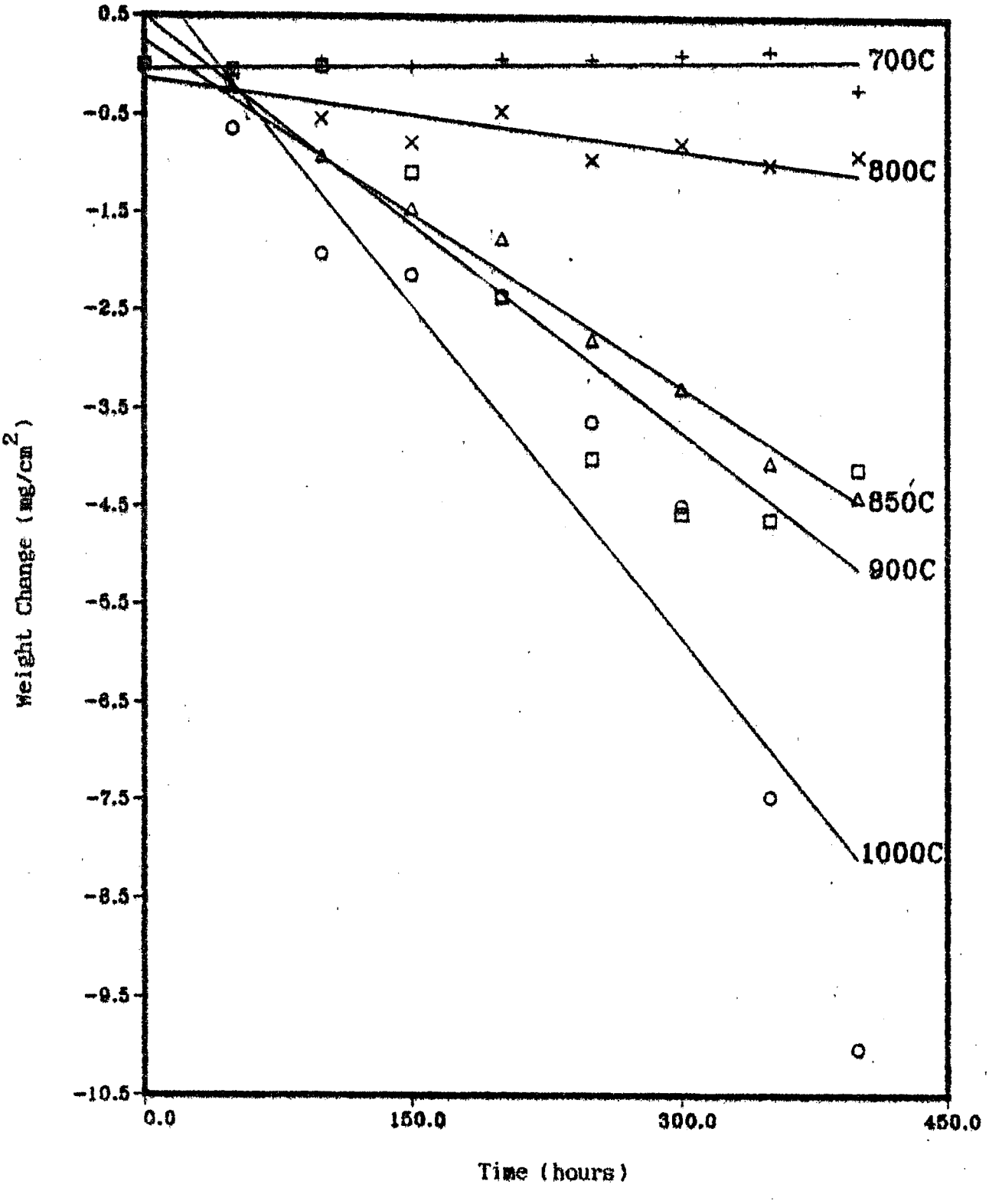

Figure 5. Weight change of alloy 214 with the experimental time.

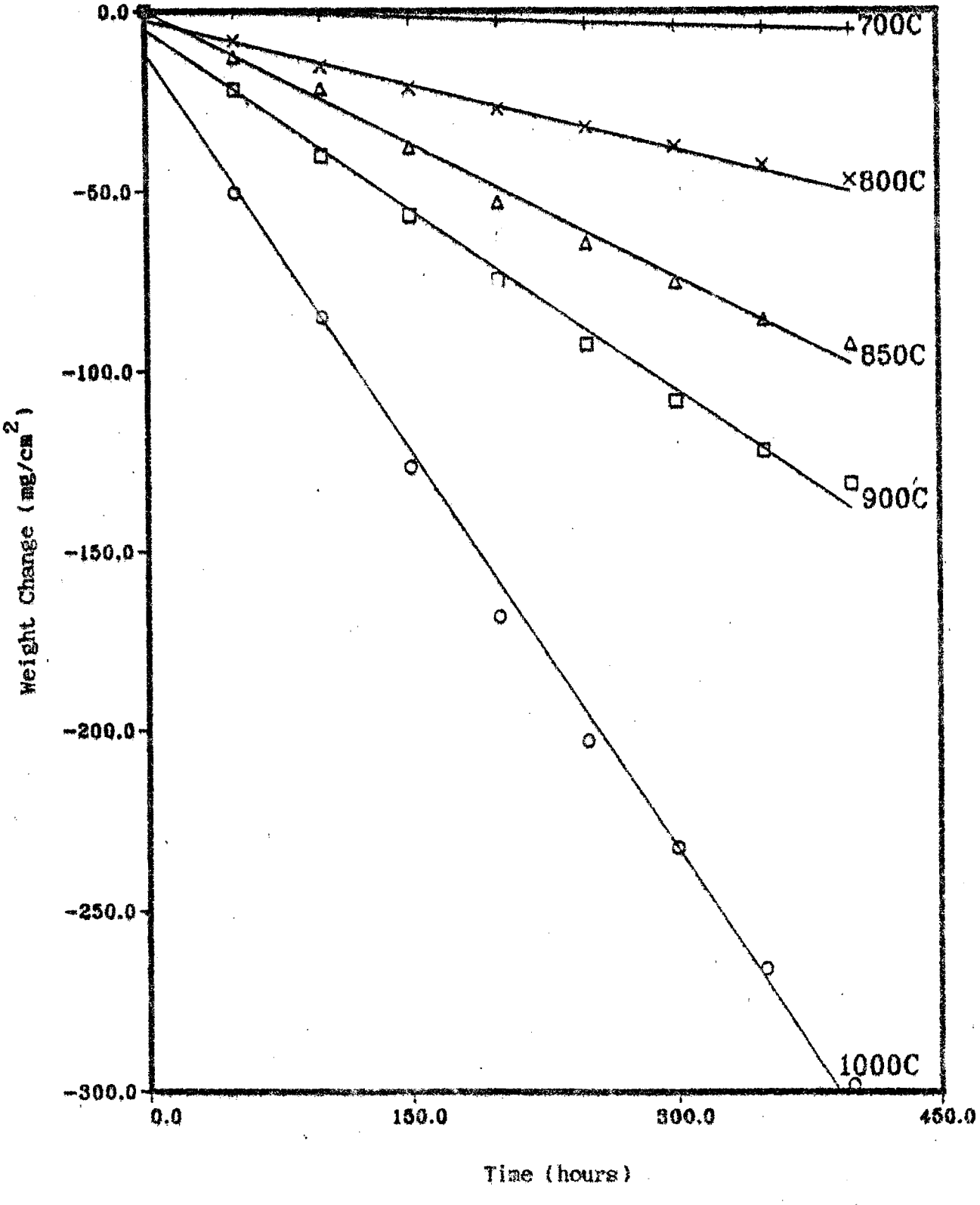

Figure 6. Weight change of alloy C-276 with the experimental time.

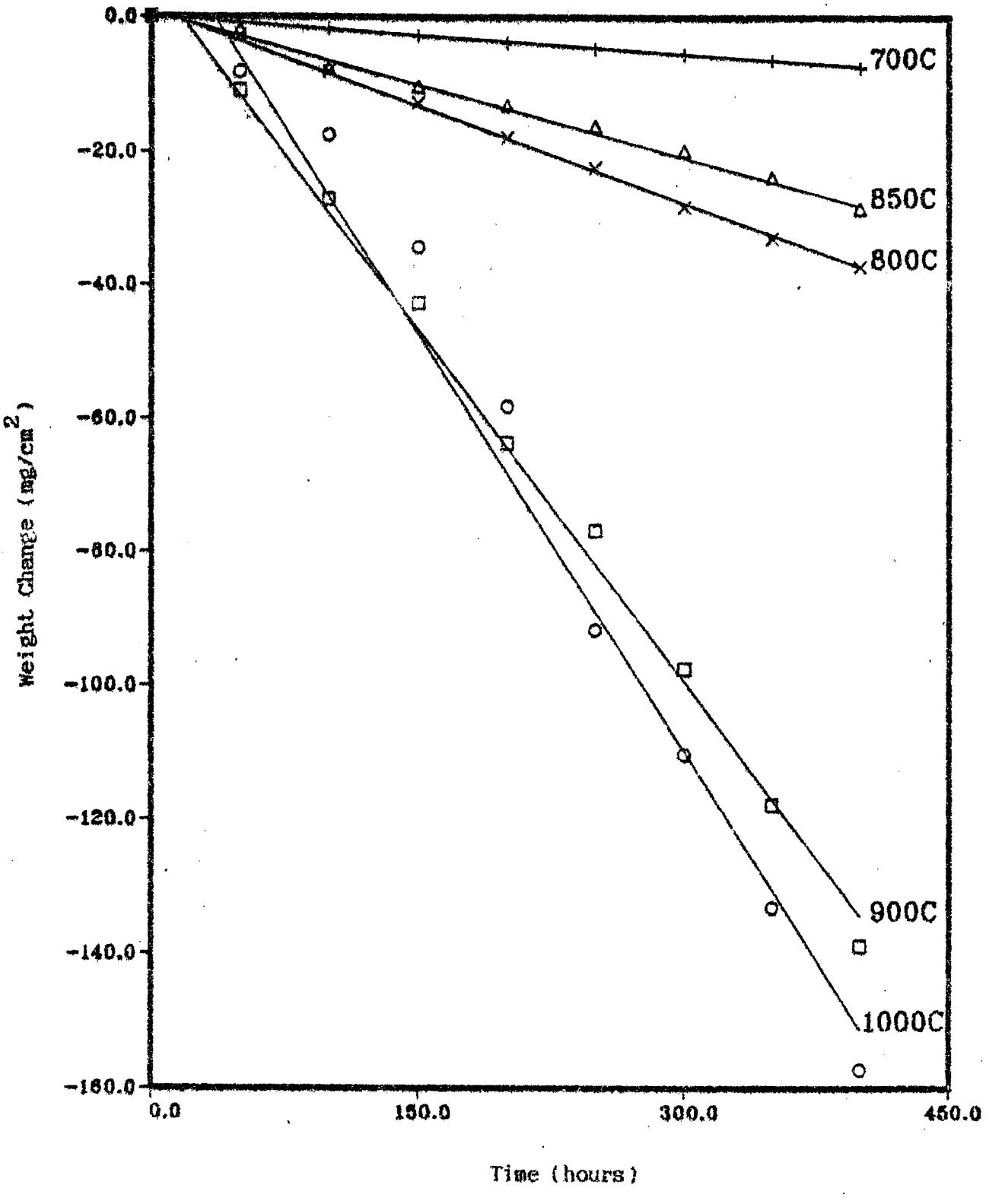

Figure 7. Weight change of alloy 188 with the experimental time.

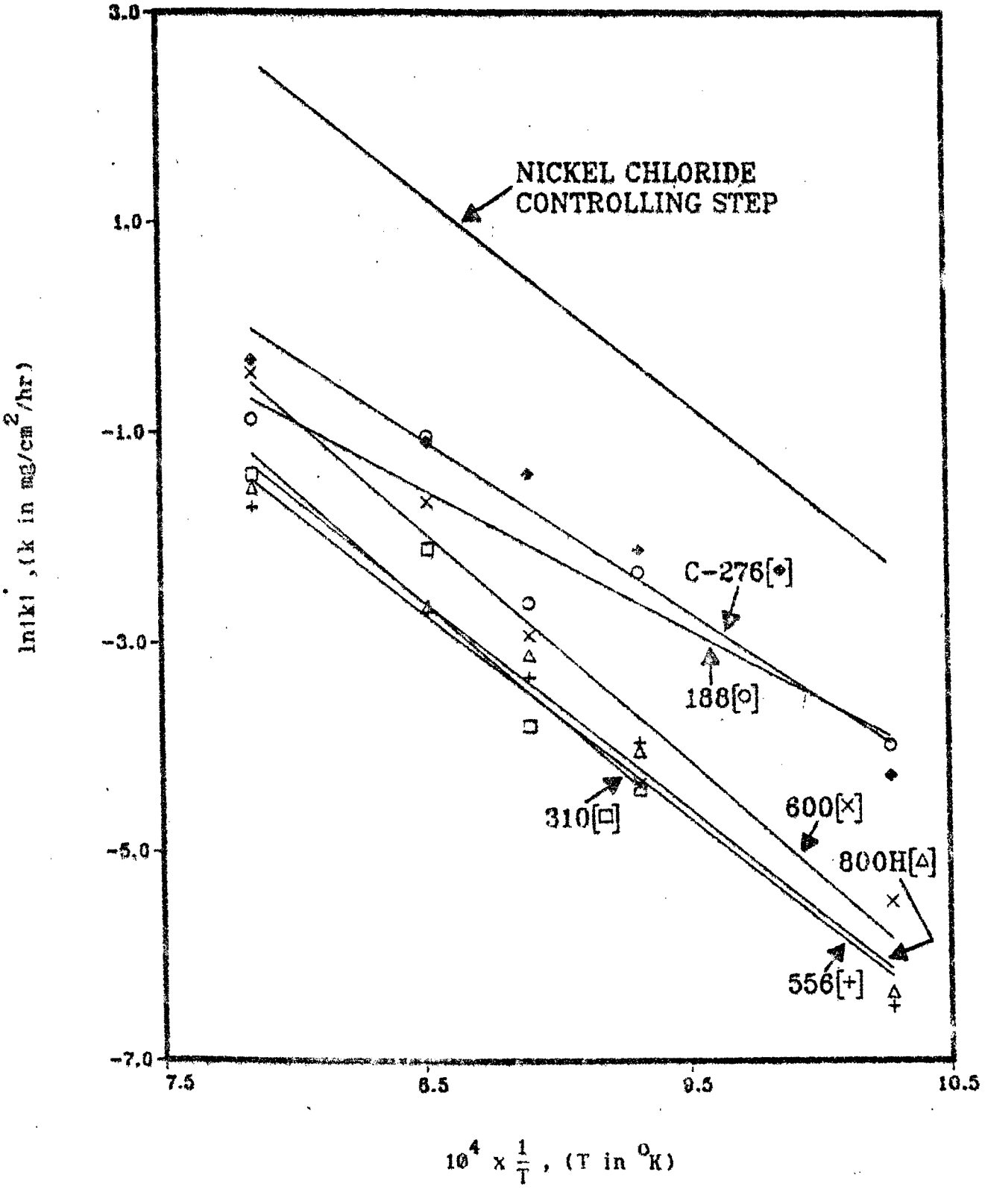

Figure 8. Comparison of the corrosion rates calculated from weight loss result and that from the nickel chloride controlling process.

ELECTROPLATING OF TIN FROM HALOGEN BATHS FOR DECORATIVE AND CORROSION PROTECTIVE PURPOSES

By Dr.-Ing. Faraz Umar
Ir. I. Putu Sutiabudi

Prepared for Seminar on Corrosion and Protection,
Bangkok, Thailand, 30 June - 2 July, 1992

INSTITUTE OF TECHNOLOGY BANDUNG

1992

ELECTROPLATING OF TIN FROM HALOGEN BATHS FOR DECORATIVE AND CORROSION PROTECTIVE PURPOSES

Dr.-Ing. Faraz Umar *
Ir. I. Putu Satiabudi **

Institut Teknologi Bandung (ITB)
Jl. Ganesha No. 10, Bandung 40132, Indonesia
Phone : 022-87809 ; Fax : 022-438338

Abstract

A serie of experiment had been conducted in our Laboratory to study the characteristics of electrolytic tin deposition from halogen baths containing between 21.0 and 52.5 g/l Sn^{2+} (as $SnCl_2$), 51.4 g/l KF, up to 2 g/l gelatin, and up to 4 g/l β-napthol as additives.

The experiments were carried out at solution temperatures between 323 and 353 K, current density between 100 Asm and 700 Asm for 5 - 65 minutes of plating time.

Test results showed that the best tin plating of 29.7 μm, 66 % reflectivity, and 81 % of current efficiency could be achieved at certain electroplating conditions.

Since tin itself is corrosion resistant in atmospheric environment, the quality of the products had been examined by an appropriate porosity test method, which shown that plated-tin was non-porous.

---

* Dr.-Ing. Faraz Umar is Senior Lecturer in ELectrometallurgy at the Graduate Program on Metallurgy and Material Science and Engineering, and Chairman of Technical Committee of Indonesian Corrosion Association (INDOCOR)

** Now at P.T. Bakrie Brothers Steel Industry, Jakarta, Indonesia.

I. INTRODUCTION

The most significance development in the electrodeposition of tin in last three decades has been the introduction of commercial viable baths for the deposition of bright coating (Chapman, 1983).

Tin can be deposited electrolytically from acid as well as alkaline baths. The acids baths include acidic stannous sulphate, stannous fluorides and stannous chloride-fluorides or halogen baths. It's well know that the acid baths is superior compared with alkaline bath in term of brightness of the coating (Anonymous, 1972, Beadle, 1972, Hoare et.al, 1965, and Lowenheim, 1974). Among these, the halogen baths can produce superior bright coatings of excellent appearance and properties (Cuthbertson, 1966, Rajagopalan and Rajam, 1978, and Davies, 1974).

Eventhough, in Indonesia this field of research and development has not yet been conducted intensively to support the industrialization era in coming years. The type of process can be promoted to support the small-to medium -scale industry, so that some technical data must still be explored.

Electrolyte composition, temperature, and cathodic current density determine the physical appearance of deposited-tin, the current efficiency, and energy consumption of the tin deposition process.

Therefore, it is important to understand the characteristics of some variables affecting the tin deposition process in halogen baths.

II. EXPERIMENTAL WORKS

During our study of tin-plating process in halogen baths, the effect of electrolyte concentration, temperature and cathodic current density on current efficiency, macrothrowing power, and surface reflectivity were investigated.

The pure tin were deposited on low carbon steel cathode in plating baths at various temperature between 50 - 80 °C, containing 21.0 - 52.5 g/l Sn^{2+} (as $SnCl_2$), 51.39 g/l KF as shown in Table I, denoted as solution type D, C, B, and A respectively at constant pH-value of 2.7.

Table I : Halogen Baths Composition.

Solution Type	Molar ratio of $KF/SnCl_2$	Concentration of - (g/l)			
		$SnCl_2$	Sn^{2+}	KF	F^-
A	2 (stoichiometric)	83.87	52.5	51.39	16.8
B	3	55.91	35.0	51.39	16.8
C	4	41.93	26.3	51.39	16.8
D	5	33.54	21.0	51.39	16.8

The cathodic current density was varied from 100 Asm to 700 Asm as indicated by Hull-Cell (250 ml) test conducted before. The anode was Banka-tin (99.85 % Sn) of 48 cm^2 and the cathode was low carbon steel (0.2 % C) of 4 cm^2 of effective area. The chemical analysis of the anode can be seen in Table II.

Table II. Chemical Composition of Tin Anode.

Element	Composition (%)
Sn	99.850
Fe	0.010
Pb	0.043
Cu	0.035
Zn	0.001
Ni(+Co)	0.005
Al	0.001
Cd	0.001
As	0.027
Sb	0.006
Bi	0.006

The cathode specimens were polished, cleaned, and degreased in alcohol solution. Thereafter, the speciments were washed in distilled water, pickled in 5 % HCl for 10 minutes, washed again in distilled water, dried and weighted before being electroplated.

The deposited-tin specimens were washed in alcohol and distilled water, dried, and then weighted for current efficiency calculation. Thereafter, the samples were tested for their surface reflectivity by using Toyoseiki Reflectometer.

Since tin itself is corrosion resistance in atmospheric environment, the quality of the products was examined by sulphur-dioxide porosity test method. The SO_2 was produced by reacting sodiumthiosulphate (10 g/l) with certain volume sulphuric acid 0.1 N. The samples were tested in such environment for 24 hours (Carter, 1982).

To support the experimental results, the macrothrowing power of the electrolyte were investigated by using Haring-Blum Cell.

The Hull-Cell test enable an estimate to be made of the current density range, overwhich acceptable appearance of deposited-tin can be produced.

Standard methods for chemical analisis were used mostly by using the Atomic Absorption Spectophotometer (AAS).

III. RESULT AND DISSCUSION

As mentioned before the experimental work were carried out to examine the effect of some plating variables on certain characteristics of electrodeposition tin in halogen baths. Test results can be seen in Figure 1 to figure 12 throughout this paper.

A. The Effect of Electrolyte Composition.

A.1. On Macrothrowing Power.

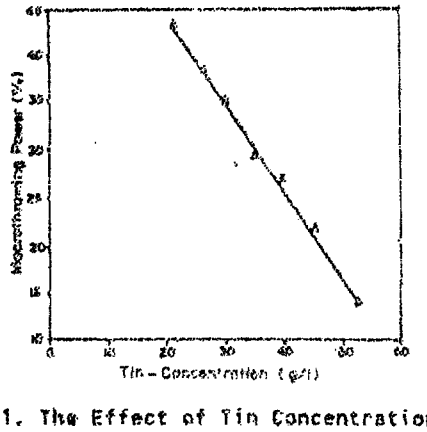

Figure 1. The Effect of Tin Concentration on Electrolyte Macrothrowing Power

As can be seen in Figure 1, by increasing tin concentration from 21.0 g/l to 52.5 g/l in plating bath, the macrothrowing power will decrease from 43.3 % to a value as low as 14 %.

In other words to get good macrothrowing power the molar ratio of KF to $SnCl_2$ must be kept at higher value (solution type C and D).

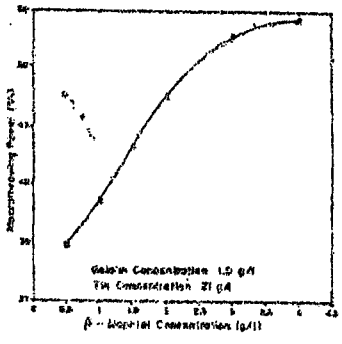

The effect of β-naphtol on macrothrowing power of the electrolyte can be seen in Figure 2.

It's clear that the increase of β-naphtol concentrations from 0.5 g/l to 4.0 g/l can increase remarkably the macrothrowing power of electrolyte in solution type D from 34.8 % to 54.3 %.

Figure 2. The Effect of β-Naphtol Concentration on Electrolyte Macrothrowing Power

A.2. On Specific Conductivity.

Table III shows the effect of tin concentration on specific conductivity of the halogen baths tested.

Table III. Specific Conductivity of Halogen Bath for Various Tin Concentration at 65 °C.

Tin Concentration g/l	Solution type	Specific Conductivity (μmohs/cm)
1. 21.0	D	240,000
2. 26.3	G	210,000
3. 35.0	B	190,000
4. 52.5	A	190,000

By decreasing tin concentration, the specific conductivity can be increased to a certain level, which has a positive effect also to the possibility of tin reduction at the cathode.

A.3. On Tinplate-Surface Reflectivity.

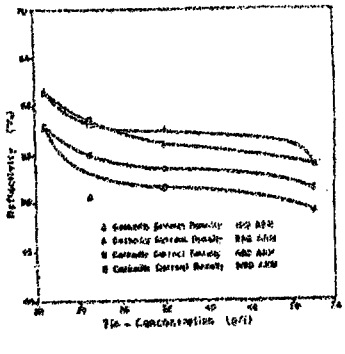

Figure 3 shows the effect of tin concentration on tinplate surface reflectivity.

It's clear that at various current density the tendency is almost the same, that the increase of tin concentration can decrease slightly the reflectivity in the range of 2 % to 13.5 %.

Figure 3. The Effect of Tin Conc. on Tin-Deposit Reflectivity at Several Cathodic Current Density

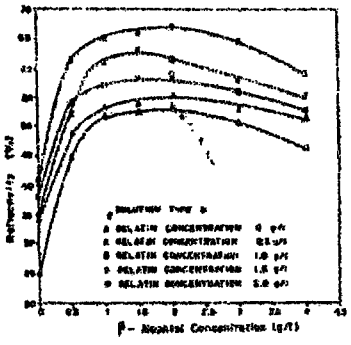

Figure 4. The Effect of ß-Naphtol Conc. on Tin Deposit Reflectivity at Several Gelatine Conc., 250 Asm and 65 °C

Figure 4 shows the effect of ß-naphtol addition on the reflectivity of deposited tin.

It is clear from that figure that maximum points of each curve at various gelatine addition are between 1.5 - 2 g/l ß-naphtol concentration. The maximum combination which can be used is at 1.5 - 2 ß-naphtol and 1.5 g/l gelatine, which resulted surface reflectivity about 67 %.

A.4. On Cathodic Current Efficiency.

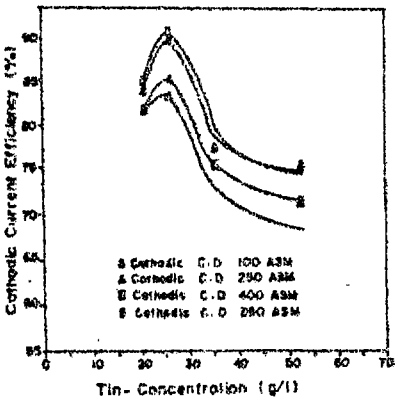

Figure 5. The Effect of Tin Conc. on Cathodic Current Efficiency at Several Cathodic Current Density and 65 °C

The effect of tin concentration on current efficiency has been examined at variuos current density. Test results can be seen in Figure 5.

As expected before, there is a tin-concentration which can cause a maximum on current efficiency, namely around 26.3 g/l Sn (solution type C), for all current density tested. At that condition, due to certain reasons the possibility of hydrogen reduction can be minimized.

The effect of ß-naphtol on cathodic current efficiency is shown in Figure 6.

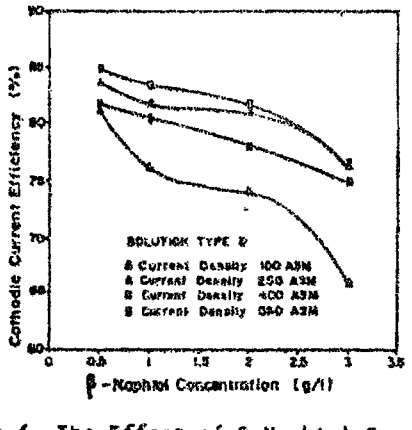

Figure 6. The Effect of ß-Naphtol Conc. on Cathodic Current Efficiency at Several Current Density, 65 °C and for 35 Minutes

The increase of ß-naphtol at all current density can decrease the cathodic current efficiency between 10% to 15%. At lower current density the negative effect of increasing ß-naphtol concentration is higher. It is clear from this figure that the addition of ß-naphtol between 1.5 - 2 g/l can decrease sligtly the cathodic current efficiency.

It has been shown that by increasing tin concentration at 65°C, from 21.0 g/l to 52.5 g/l, the specific conductivity tends

Table IV. The Effect of Tin Concentration on Energy Consumption at 250 Asm.

Tin-Conc. (g/L)	Solution type	Cell Pot. (volt)	Current Eff. (%)	Energy Cons. (khw/kg Sn)
21.0	D	0.25	83.6	0.135
26.3	C	0.53	89.2	0.268
35.0	B	0.27	77.4	0.158
52.5	A	0.32	75.2	0.193

to decrease from 240.000 μmhos/cm to 190.000 μmhos/cm, which means also that cell potential will also decrease. It can be understood if in the same time, the energy comsumption will increase to certain extent, since energy consumption (Ec), calculated using following formula :

$$Ec = (45)\ \frac{(V)}{(\tau)}\ \text{kwh/kg Sn}$$

where : V = cell potential (volt)
τ = cathodic current efficiency (%)

B. The Effect of Cathodic Current Density.

B.1. <u>On Surface Reflectivity.</u>

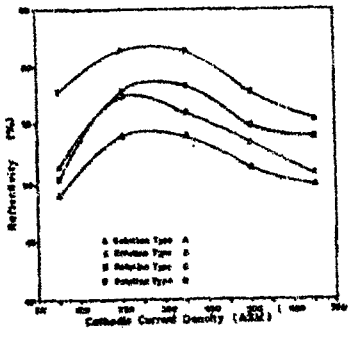

Figure 7. The Effect of Cathodic Current Density on The Reflectivity of Tin-Deposits at Several Tin Concentrations

The effect of current density on the surface reflectivity of plated-tin can be followed in Figure 7.

The experiments were done for all solution types tested, and at solution type D (21.0 g/l tin) the reflectivity values seen to be the highest between, especially at current density between 250 - 400 Asm.

B.2. On Cathodic Current Efficiency.

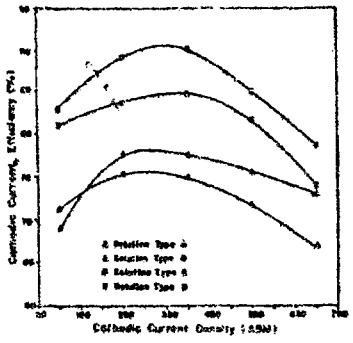

Figure 8. The Effect of Cathodic Current Density on Cathodic Current Efficiency at Several Tin-Concentration

On the otherhand, for current efficiency, solution type C (26.5 g/l tin) shows superior values but still at the same range of current density between 250 - 400 Asm, as can be seen in Figure 8.

B.3. On Energy Consumption.

The effect of cathodic current density on energy consumption can be followed in Table V.

Table V. The Effect of Cathodic Current Density on Energy Consumption at 65 °C for Solution type C and D.

Current Density (Asm)	Energy Consumption (kwh/kg Sn)	
	Solution type C (26.5 g/l Sn)	Solution type D (21.0 g/l Sn)
100	0.076	0.067
250	0.268	0.135
400	0.321	0.224
550	0.351	0.293
700	0.391	0.366

The data in Table V show, that the energy consumption tends to increase by increasing the current density between 100 - 700 Asm for both solution types tested, since by increasing the current density will increase also the cell potential.

C. The Effect of Bath Temperature.

C.1. On Cathodic Current Effiency.

The effect of bath temperature on cathodic current efficiency is shown by table VI.

Table VI. Data on the Effect of Bath Temperature on Cathodic Current Efficiency at 250 Asm and 400 Asm for Solution type D.

Bath Temp. (°C)	Cathodic Current Efficiency (%)	
	at 250 Asm	at 400 Asm
50	78.0	79.2
65	80.8	81.6
80	75.0	75.8

The data show, that at both cathodic current density the increase in bath temperature tends to show a maximum at 65 °C of both current density used.

C.2. On Energy Consumption.

The effect of bath temperature on energy consumption was also studied for solution type D at 250 Asm. The experimental result is shown in table VII.

Table VII. The Effect of Bath Temperature on Energy Consumption for Solution type D at 260 Asm and 400 Asm.

Bath Temp. (°C)	Energy Consumption (kwh/kg Sn)	
	at 250 Asm	at 400 Asm
50	0.214	0.336
65	0.168	0.299
80	0.181	0.310

It can be seen, that the lowest energy consumption can be achieved at 65 °C for both cathodic current density used.

D. The Effect of Plating Time on Tin-Deposit Thickness

Figure 9 shows the effect of plating time on tin-deposit thickness resulted in solution type D, at 250 Asm and 65 °C.

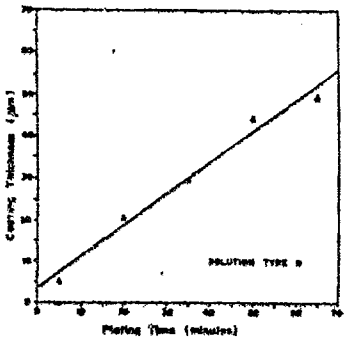

Figure 9. The Effect of Plating Time on Coating Thickness at 250 Asm and 65 °C

It is clear that the increase in plating time tends to increase the thickness of deposited-tin on the cathode.

The resulted thickness of deposited-tin were tested for their porosity and qualitative results can be seen in Table VII.

Table VII. Porosity Test Results and Comparison with Recommendation from Davis.

Thickness of Deposited Tin (μm)	Porosity Test Result	Recommended Thickness VS Service Condition (Davis. 1985, p. 27)	
4.7	good	3.8 - 7.6	modetare; warehouse atmosphere
20.6	very good	12.7 - 25.4	severe; industrial atmosphere
29.7	excellent	25.4 - 127	very severe; seacoast atmosphere
40.0	excellent	25.4 - 127	
49.7	excellent	25.4 - 127	

influenced by tin and additive concentrations, as well as by cathodic current density.
The reflectivity above 65% is good enough in appearance for decorative purpose.

2. The resulted thickness of deposited-tin of 29.7 μm is good enough for atmospheric corrosion protective purpose, since the porosity of tin-coating is excellent.

3. The best condition for tin electroplating from halogen bath, for decorative and cathodic protective purposes can be summarized as follows.

   a. Solution type D, containing 21.0 g/l tin, at pH-value = 2.7 and for 35 minutes.
   b. Cathodic current density at 250 - 400 Asm.
   c. Additives concentration 1.5 g/l gelatine and 1.5 - 2.0 g/l β-naphtol.
   d. Bath temperature : 65 °C.

   At that conditions, the reflectivity is 67 %, current efficiency 81 %, energy consumption between 0.21 - 0.30 kwh/kg tin, whereas the thickness of deposited-tin is 29.7 μm.

Acknowledgment

The authors wish to thank to the Department of Mining Engineering of ITB for providing research fasilities during the implementation of experimental works at the Laboratory of Corrosion and Electrometallurgy. Special thanks are conveyed to Research Institute of ITB, for supporting financially the project, through contract work number 46/LP/OPF-ITB/1990.
We thank also to Mr. Waspodo Martojo for assisting us in finishing the research report.

V. REFERENCES

1. Anonymous : "Chemical Tinplating Process for the Oxidation of Conductive Materials"
   Corrosion Prevention and Control 13(11), 1966, p. 14 - 16.

2. Beadle, J.D. : "Product Treatment and Finishing"
   The McMillan Press Ltd., Hamshire UK, 1972.

3. Carter, V.E.(Ed) : "Corrosion Testing for Metal Finishing"
   Institute of Metal Finishing, Butterworths Scientific, London UK, 1982, p. 77 - 81.

4. Cuthbertson, J.W. in H.W. Detter und J. Elze : "Handbuch der Galvanotechnik", Band II-Carl Hansen Verlag, Munchen, 1966, p. 337 - 338.

5. Davis, P.E. : "Tin and Tin Alloy Coatings: Yesterday, Today and Tomorrow"
   Plating and Surface Finishing No. 12, Dec. 1985, p. 26 - 29.

6. Hoare, W.E, E.S. Hedges and B.T.K. Barry : "The Technology of Tinplate"
   Edward Arnold (Publisher), Ltd., London, 1965.

7. Lowenheim, F.A. : "Modern Electroplating"
   3rd Ed. John-Willey & Sons, Inc., New York, 1974.

8. Rajagopalan, I. and K.S. Rajam : "Tin Deposition from Halogen Baths"
   Metal Finishing No. 4, April 1978, p. 43-48.

9. Steeg, H.J. : "Bright Tin Coating"
   Galvanotechnik 95(1), 1968, p. 55 - 56.

ASEAN-JAPAN COOPERATION PROGRAMME
ON MATERIALS SCIENCE AND TECHNOLOGY

SEMINAR/WORKSHOP ON CORROSION AND PROTECTION IN THAILAND
1992

PRESENT STATUS OF THE METAL PROTECTION AND FINISHING INDUSTRIES IN MALAYSIA

DR. MUSTAZA HJ. AHMADUN

STANDARDS & INDUSTRIAL RESEARCH INSTITUTE OF MALAYSIA
PERSIARAN DATO' MENTERI, SEKSYEN 2
P.O BOX 7035, 40911 SHAH ALAM
SELANGOR D.E, MALAYSIA

ABSTRACT

This paper highlights on the present status of the metal protection and finishing industries in Malaysia, particularly on the problems encountered by the industries and the steps that are planned and implemented to remedy them in view of the present and future challanges.

1984 Malaysia saw the reversal of its industrialization trend from that which was predominantly agricultural to manufacturing. This comes about with the strong emphasis on heavy industrialization, which marked the start of heavy industrialization projects for steelmaking, petrochemicals and automobile manufacturings. It is here that essentially the metal protection and finishing industries play important supportive roles.

INTRODUCTION

By the year 2020, Malaysia can be a united nation, with a confident society, infused by strong moral and ethical values, caring, economically just and equitable, progressive and prosperous, and in full possession of an economy that is competitive, dynamic, robust and resilient. There can be no fully developed Malaysia until we have finally overcome the nine central strategic challenges that have confronted us from the moment of our birth as an independent nation. These are the words and vision of Malaysian Right Honourable Prime Minister, Dato' Seri Dr. Mahathir Mohamad at the inaugral meeting of the Malaysian Business Council in Kuala Lumpur last year (1).

Among the nine mentioned is the challenge of establishing a scientific and progressive society, a society that is innovative and forward looking, one that is not only consumer of technology but also a contributor to the scientific and technological civilisation of the future.

In 1984 Malaysia diverted its industrialization trend from that which was predominantly agricultural to the manufacturing (2); when its manufacturing share in the GDP overtakes the agricultural sector, Figure 1. This comes about from the strong emphasis on heavy industrialization (secondary import substitution) in the Fourth Malaysia Plan, in 1981. As a result of this unprecedented expansion,

the manufacturing sector currently accounts for about 27% of GDP; about 60% of total export; and about 18% of total employment (3).

This signalled the needs of extensive supportive back-up industries, to feed components and provide services to the 'giants' such as the Heavy Industry Corporation of Malaysia (HICOM) and many others; locals and multinationals. The metal protection and finishing industries generally play supportive role, as such they fall into the Small and Medium Industry (SMI). The importance of the role of the SMI in Malaysia has been emphasised under the Second Outline Prospective Plan (1991-2000) as well as in the 6th Malaysia Plan (1991 - 1995).

THE METAL PROTECTION AND FINISHING INDUSTRY IN MALAYSIA

In the context of this seminar/workshop, the presenter will confine to the subject of metallic and polymeric coatings industries in relation to corrosion protection of metals components and structures.

The Electroplating Industry

Typically there are three types of operation practised in Malaysia. The service oriented small scale enterprises, predominantly family owned; solely dependent on jobbing works. Their facilities are rather old and poorly maintained. They do not normally observe any Standards and

limits their quality control to casual visual checks of finished products. However, with stronger emphasis on quality by new sets of multinational clients who can offer much larger volume of works, many are now more willing to upgrade their facilities and invest on basic in-house quality control equipments. The government are encouraging them to adopt the concept of 'Common Wastewater Treatment', which in the long run benefit both the electroplaters and the public at large. As it is, presently most of them are operating in premises that are already overcrowded and do not permit any further expansion to cater for bigger business ventures. Already, a group of them are in the process of relocating themselves to a much more conducive site and a common treatment plant will be a part of the new venture.

The second type comprises of companies cooperating with foreign partners, in the hope of improving product quality and to get better access to export markets. They practice more advanced techniques, have better maintained and more modern equipments.

The level of operations of the third type of companies are close to that of industrialised countries, although with a lower degree of automation. However, their number are small. The second and third types can be found integrated into metal or plastic components production process flows, operating under the same management. They have the

advantage of firm control over quality, pricing and delivery of their own products.

Protective Coatings Industry

In this paper, only the high build organic or protective coatings industry is presented; eventhough the decorative coatings industry is as important. Under this catagory, there are four groupings that play major role; namely the paint manufacturers, the paint applicators, the paint inspectors and the clients. The main clients are mainly from the oil and gas industries, the ship building and repair industries, power generation industries and the industries at large.

At the moment, there is concerted efforts by the 'Protective Coatings Task Force' to sort out grievences between the four groups, and to provide the direction and mechanisms for a healthy future development of the industry. The task force was formed in 1991 as a voluntary and independent body with a representative of the Standards and Industrial Research Institute of Malaysia as the Chairman, and representatives from other organisations as the members.

Separate dialogues with the four groups were held to fully appreciate the problems peculiar to each groups and inter-groups grievances. Five major problem areas emerged from the dialogues; (a) quality, (b) classifications, (c) training, (d) code of practices and ethics, and (e) health,

safety and the environments. At this stage, the task force and representatives from the four groups are formulating strategies and programs that will provide impetus for the strengthening of Malaysian protective coatings industry and associated industries.

TECHNOLOGY DEVELOPMENT

Essentially, the major players in the protective and finishing industry are the entrepreneurs themselves, but it is the clients that actually determine the directions that the industry has to follow in the short and long terms. As in the case of the oil and gas industry the giants multinationals like ESSO, Shell, British Petroleum and others together with the locals such as PETRONAS could play an important role in the setting up of the various codes of practices and conducts; that are to be adopted for the Malaysian environments.

The second grouping is the components and finished products manufacturers; in almost every aspect of the industry. The needs for quality finished products and the important criteria of corrosion protection of the finished products during transport, storage and service are two very important factors that ensure product reliability and business prosperity. The automotive, electronic, electrical, housing, cosmetic and many other types of industries cannot run away from the two factors mentioned earlier.

The Standards and Industrial Research Institute of Malaysia (SIRIM) as the government agency entrusted with the mission to spearhead technological development of the country, are very much involved in formulating national standards to be adopted by the industries at large. On top of that, SIRIM is also actively involved in industrial research and development projects specially to cater both the present and future needs of the industry. Besides these, SIRIM is also involves in rendering advisory and consultory services, testing and evaluation services, training services and many other services needed by the industry. The linkages with the industries is provided directly through frequent interactions with various Industrial Consultative Committees (ICC); which are made up of representatives from various sectors of the industries.

CONCLUSION

It cannot be denied that education is an on-going process for every individual; especially so now that the world market is very lucrative and competitive. The emphasis is on the creation of pools of highly innovative and deligent blue collar as well as white collar workforce that will make Malaysia a truely industrialised and progressive nation. With the strong emphasis on the manufacturing sectors, the protective and finishing industry will have enough supporting to do for the next decade.

REFERENCE

1. Malaysia: The Way Forward, by YAB Dato' Dr. Mahathir Mohamad; Malaysian Business Council Inaugral Meeting, Feb. 28, 1991, Kuala Lumpur.

2. Y.Bhg. Dato' Dr. Hj. Mohd. Mansor Hj. Salleh, The 3rd. Asian Surface Finishing Forum, Sept. 25-27, 1989, Seoul, Korea.

3. Y.B Dato' Hj. A. Ghani Othman, Seminar On The Role of Small & Medium Scale Industries In Industrial Restructuring - Intra-Industry Linkages; 16-17 December,1991, Kuala Lumpur.

Figure 1: **Trends in Industrialization in Malaysia (1970 to 1985)**

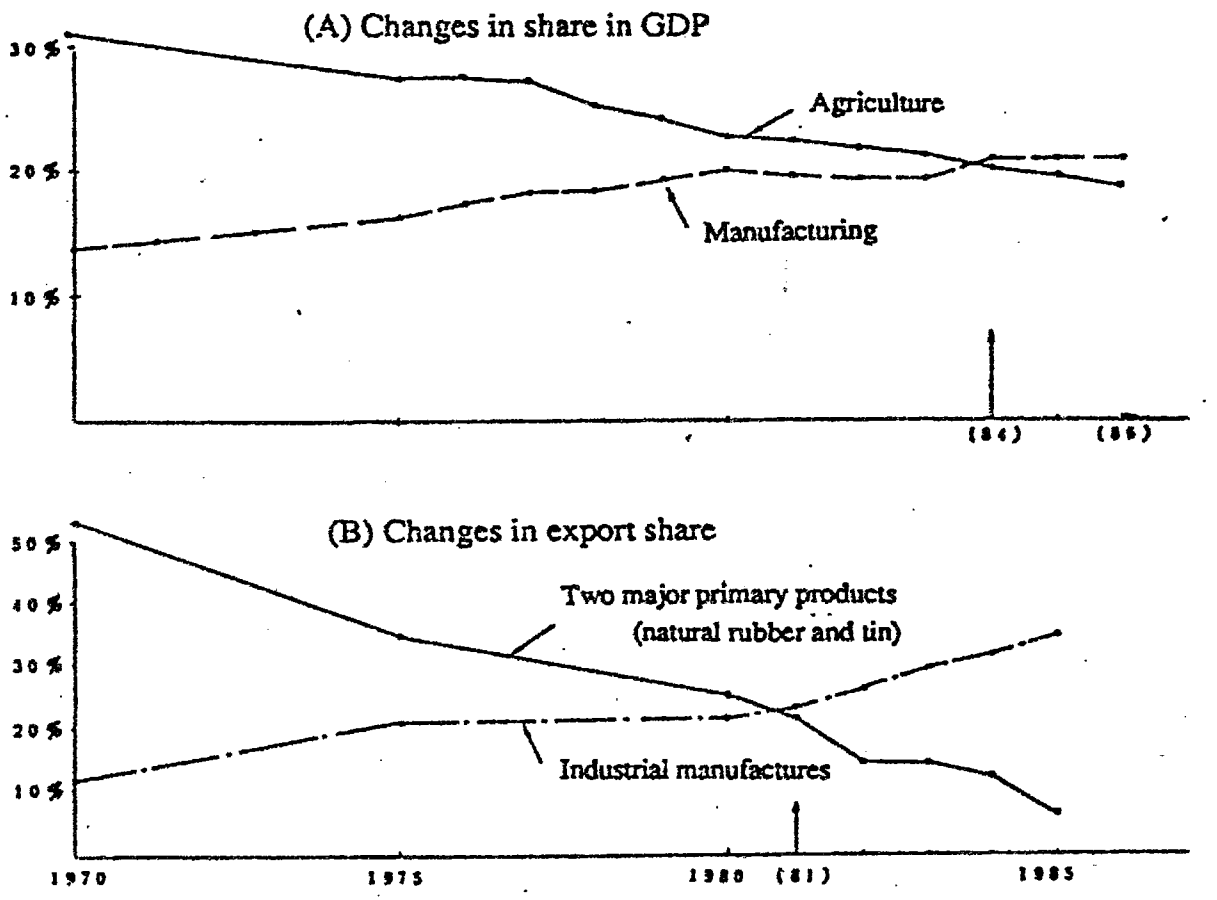

Source: Ministry of Finance, "Economic Report", each year

THE EFFECT OF ULTRAVIOLET RADIATION ON THE BONDING BETWEEN ORGANIC POLYMER AND METAL SUBSTRATE

NER CRUZ RODRIGUEZ
Industrial Technology Development Institute
Gen. Santos Ave., Bicutan, Taguig
Metro Manila, Philippines

and

KATSUTOSHI KUROSAWA
National Research Institute for Metals
2-3-12 Nakameguro, Meguro-Ku, Tokyo, Japan

ABSTRACT

The bonding between metal substrate and five (5) different coatings, namely, alkyd clear paint, melamine alkyd paint, zinc chromate primer, red lead primer and epoxy primer, as affected by ultraviolet radiation was studied. Three (3) methods of surface preparation of metal substrates were used: phosphating, polishing and derusting by wire brush. Painted specimens were subjected to accelerated corrosion using salt spray and humidity tests. Half of the total number of the specimens were subjected to weathermeter using xenon lamp as source of UV radiation. The bonding strength of the coatings in steel was measured by the pull-off adhesion test method. Visual evaluation for the appearance of rust and blister was noted after every cycle. The investigation of chemical and morphological change occuring after subjecting to corrosion tests was performed using FTIR and SEM.

Three types of failure occurred in the coating and metal system after the pull-off test: adhesion failure, cohesion failure and substrate failure. UV radiation and surface treatment affect the bonding strength and locus of failure of coating system. It was also found out that UV radiation accelerates the rusting of coated specimens but not the formation of blister.

INTRODUCTION

A basic cause of degradation of an organic coating is the chemical breakdown of the organic matrix of the coating. This is often due to photo-oxidation of the coating polymer by the mixed action of UV radiation from sunlight (*1,2-4*), oxydation from the atmosphere and water (*5-11*). Ultraviolet light (wavelength: 40 - 400 nm) decomposes some polymer structure by absorbing its energy. This type of degradation is dependent on the spectral absorption of coating polymer (*12,13*), the pigmentation of the coating, the use of UV

absorbers (*14*), temperature, radiation intensity and energy distribution and humidity (*15*).

The service life of an organic coating is determined by the durability of the coating itself and its adhesive ability on base material. The former is the stability of a coating layer as exposed to various environmental factors, and the latter is determined by the condition of the interface between the organic film and the substrate. To improve the surface condition of substrate, phosphate or chromate treatment are usually applied.

Since bond strength is composed of adhesion force and the dynamic properties of paint film and substrate, the bond strength measured by a mechanical test method is not the actual adhesion force of paint film. Accordingly, the value of bond strength obtained by a mechanical test method are quite different from those of adhesion force estimated on the basis of surface chemistry.

In this study, bonding strength of five types of organic coatings in steel were measured by mechanical test using the pull-off method after subjecting to corrosion tests. Visual evaluation and instrumental analysis were also performed.

It is then expected to determine the effect of corrosion testing with and without UV radiation and to observe the phenomena taking place on the bonding and failure occuring on the interface of organic polymer and metals with different treatments.

EXPERIMENTAL PROCEDURE

TEST SPECIMEN PREPARATION

Specimens measuring 150 X 50 X 1 mm cut from commercially produced cold rolled steel sheet were used in this experiment. These specimens were drilled (0.5 cm diameter) on the upper center portion for easy handling during preparation and testing. Specimens' surface were then polished using emery paper number 400. To remove dirt and organic impurities such as grease, oil, etc., specimens were immersed several times and vaporized with Trichloroethylene (TCE). After degreasing, specimens were kept in dessicator.

PRETREATMENT

In this study, three types of preparation for test specimens were done prior to painting: polished, zinc phosphated and derusted. Thus, all the test specimens polished and degreased previously were divided into three parts for the following pretreatment:

A. Polished (Treatment A). These specimens would serve as the untreated samples.

B. Phosphated (Treatment B). Phosphate coatings are produced by immersion, spraying, or other technique with a phosphate solution, and are secondary barriers consisting of crystalline or amorphous phosphates of the metal to be coated.

The procedure and reagents recommended by Nihon Packerizing Co. Ltd. was used in zinc phosphating of the specimens.

C. Derusted (Treatment C). Degreased/polished specimens were exposed in the atmosphere for about 42 days. Rust were then removed partially by wire brushing. Collected rust were kept in dessicator for analysis.

PAINTING

Five types of organic coatings were used:

1. Alkyd Clear Paint (Coating 1)
2. Melamine Alkyd Paint (Coating 2)
3. Zinc Chromate Primer (Coating 3)
4. Red Lead Primer (Coating 4)
5. Epoxy Primer (Coating 5)

All untreated and treated specimens were painted with five types of paints using bar coater. Test specimens painted with Melamine Alkyd Paint were cured for 15 min at 130^{o}C, while all others were dried at room temperature. Back sides were all sealed by painting with Red Lead Paint and Alkyd Paint for first and second coating, respectively. Alkyd Paint was also used for sealing the edges by dipping the specimen's sides in it. Painted specimens were hang vertically to dry.

CODING

This study is divided into two parts. The first part consist of corrosion testing by salt spray method while the second part made use of the humidity cabinet. Both parts made use of the weathermeter for UV radiation source.

The specimens were coded using four-digit numbers as shown in Figure 1. The first digit represents the type of treatment of metal, 2nd digit for the paint used, 3rd digit for corrosion test and 4th digit for the replication number.

PAINT FILM THICKNESS MEASUREMENT

When painted specimens were totally dried and cured, film thickness was measured using the Electromagnetic thickness meter, model ES8e3KB4 (Fisher (WG)).

CORROSION TESTING

Organic coatings on exterior exposure are subjected to attact by degrading elements of the weather, particularly ultraviolet light, oxygen and water. Corrosion testing was used to evaluate the behavior of films exposed in apparatus

that produces ultraviolet radiation, high temperature, and water condensation on the films.

To compare the effect of UV radiation on the bonding of organic polymers and metal, accelerated corrosion equipments were used. Weathermeter's xenon lamp was used as light source, having similar spectral distribution through UV to IR energy to that of the sunlight. Humidity cabinet (CT-3 Suga Test Instrument) controlled at constant temperature and humidity (49^{o}C, 98% RH) was also used, as well as salt spray cabinet.

Salt spray test was performed using the Standard Practice on ASTM B117, weathering test based on ASTM G26 and ASTM D3459-87 for humidity test.

Experiment I. Corrosion Testing using Salt Spray Cabinet and Weathermeter. Painted specimens were exposed on accelerated tester for several cycles. Each cycle consists of a total of 48 hour - salt spray testing for all samples, and 18 hour - UV exposure for half the number of the samples. Other half was not exposed to UV.

Experiment II. Corrosion Testing using Humidity Cabinet and Weathermeter. Specimens for this test consist of 96 hour - humidity test and (with and without) 18 hour - UV exposure per cycle. Testing was continued for several cycles.

ADHESION TEST

After every cycle, all specimens were measured for adhesion bond strength using Elcometer 106 Adhesion Tester. This instrument employs the pull-off method to measure the lift-off force required to pull a test dolly off a small area of coating away from the base material. See Figure 2.

A dolly is attached to the coating of the specimens. After curing the adhesive, the coating is cut through. The instrument claw is engaged and the lift force is applied. The force applied is recorded by means of a dragging indicator on an engraved scale.

After the adhesion test, the dollies and the test area of the specimens were examined. Specimens' photographs were also taken. Delaminated area of the specimens caused by adhesion testing were then painted to avoid galvanic contamination during the proceeding test cycles.

RUST AND BLISTER EVALUATION

Test Specimens were observed and rated after every cycles according to the degree of rust and blister based on the Standard Method of ASTM D 610-85 and ASTM D 714-87, respectively.

FTIR SPECTROSCOPY

Infrared spectroscopy has been applied for the investigation of both the chemical bonding between polymer and metal surface and the molecular orientation in the polymer film resulting from its interaction with the substrate metal.

After all the cycles were completed, representative samples, including stock specimens, of each painting systems and treatments, were subjected to FTIR analysis. Deflectance Infrared Spectroscopy Method was used using JEOL JIR-100 FTIR Spectrophotometer.

This method was used to determine and compare the changes and effect on the chemical bonding of each paints before and after accelerated testing.

SEM OBSERVATION

Surface morphology of painted specimens were observed using the JEOL-T20 Scanning Microscope with 20 KV accelerating voltage.

RESULTS AND DISCUSSION

PAINT FILM THICKNESS

Table I below shows the summary of coating measurements of the specimens, using polished-degreased sample as the base metal standard:

Table I. Coating Thickness (um) of Specimens

Treatment	Experiment I	Experiment II
A : Polished	4.5 to 15.1	18.3 to 41.8
B : Phosphated	7.1 to 18.4	19.6 to 44.4
C : Derusted		42.5 to 70.0

The coating thickness of painted specimens for Experiment II were thicker than that of Experiment I's samples, because a bigger bar coater was used. Increasing the thickness of the coating was done to insure that samples would not corrode easily. It was observed from the previous experiment (Expt. I) that after third cycle, samples were severely corroded, as will be discussed later.

It can be noticed that derusted specimens (Treatment C) had thicker coatings, which actually were oxides and rust, that were not completely removed by wire brushing, adhering to the metal surface beneath the paint.

CORROSION TEST CYCLE

It was observed from the salt sprayed specimens (Experiment I) that samples got easily rusted. Thus, testing was stopped until third cycle. It was then the basis for designing Experiment II, using Humidity cabinet for corrosion testing and the same weathermeter for UV radiation. This experiment was continued until seventh cycle.

BLISTER RATING

Figure 3 showed the graphs of Blister Rating of specimens on Experiments I and II. From the following graph, it showed that the appearance of blister on the specimens, phosphated or not, is independent of the presence or absence of UV radiation. However, it was observed that Epoxy Primer (Coating 5) increased the number and size of blister formation as the corrosion test continue.

RUST RATING

Figure 4 showed the graphs of Rust Rating of the specimens. Test specimens exposed in salt spray with and without UV (Experiment I) easily got rusted as compared to specimens exposed in humidity cabinet with and without UV (Experiment II), except Red Lead Primer (Coating 4) which remained unrusted. It can be accounted for the thicker coating of specimens used in Experiment II than in Experiment I as shown on Table 1.

Phosphated specimens (Treatment B) were generally less rusted than polished specimens (Tretment A) after every cycle. This proves that phosphate coatings provide a good base for paints. The chemical effects of phosphating on the surface converted the surface to a non-alkaline condition to protect against the spread of corrosion (*16*).

Derusted specimens (Treatment C), generally, were the most corroded. The old rust that adhere to the specimens beneath the paints served as the seed to produce more new rust.

However, notice the graph of Experiment II for Alkyd Clear Paint, this showed polished specimens (Treatment A) more rusted than the derusted (Treatment C) specimens. This could be attributed to some difficulty encountered on the evaluation of derusted specimens (Treatment C). The rust color of the specimens were still visible after painting with Alkyd Clear Paint, that even after several cycles, the growth of new rust were not clearly distinguished. See Figure 4b.

The significant effect of UV exposure on the early rusting of specimens were clearly seen in Coatings 2, 3 and 5 of Experiment I. The same result was observed in Coating systems 1 and 5 of Experiment II.

However, the opposite result was obtained on Coating systems 1, 2, 3 and 5 for derusted specimens (Treatment C); and for coating system 2 (Melamine Alkyd Paint) - polished and phosphated. It showed less rusting on the UV radiated specimens. For the meantime, the reason for this phenomena couldn't be explained.

ADHESION TEST RESULT

In adhesion test, if the coating fully adhered to the dolly, the test was claimed 100% valid. However, most of the time, only a portion of the coating was removed and partial adhesion failure between the adhesive and the dolly occured. After taking the strength value, observation and examination was also done to the dolly and specimens so as allowances were made in cases of partial adhesion failure occurence.

Types of Failure

There are three types of failure observed on the specimens after the test: adhesion failure, cohesive coating failure and substrate failure (*17*). Adhesion failure means that the failure occured on the metal and coating interface, Cohesion failure occured at the bulk of the coating itself and Substrate failure means that failure occured on the metal substrate itself.

As shown in Figure 5a, Alkyd Clear Paint (Coating 1), Melamine Alkyd Paint (Coating 2) and Epoxy Primer (Coating 5) decreased bonding strength significantly after 3 cycles. However, Zinc Chromate (Coating 3) and Red Lead Primer (Coating 4) showed a small change in the bonding strength. Based on the observation done on the dollies and test specimens, Coating systems 1, 2 and 5 had Adhesion failure, and Coating systems 3 and 4 had Cohesion failure. Thus, measurement taken in Coatings 1, 2 and 5 were actually Adhesion Strength, and Cohesion Strength for Coatings 3 and 4. The same pattern was observed in the failure of the specimens in Experiment II as shown in Figure 5b.

The third kind of failure, Substrate failure, was observed in all painting systems with Treatment C (rusted, wire brushed) in Experiment II.

Thus, adhesion strength of organic coating to metal decreases after every cycle while cohesion strength remains constant.

Effect of UV Radiation on Bonding Strength and Locus of Failure

It was observed from the Red Lead Primer (Coating 4) and Epoxy Primer (Coating 5) specimens that UV radiated specimens had lower cohesion and adhesion strength,

respectively, than with no UV radiation, as seen in Figure 5b.

In the UV radiated specimens, it was observed that depth of failure on the paints' bulk is deeper, near the base metal. Paints failed in bigger area than that without UV.

Diagram 1. Cross Section of Specimen After Adhesion Test

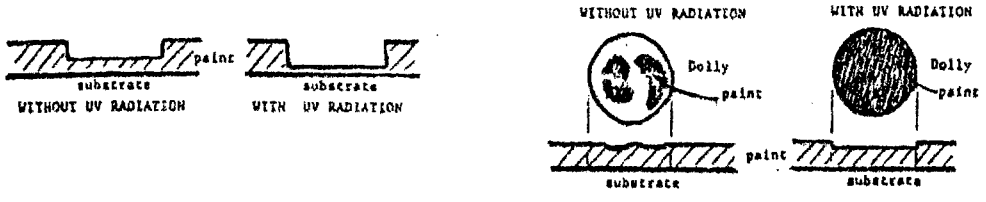

Epoxy Primer (Coating 5), when observed after every test cycle showed that failure occured from the center bulk of the paint to the paint's surface. It showed that this paint still hardened after corrosion testing.

Diagram 2. Stages of Failure of Epoxy Primer Painted in Metal

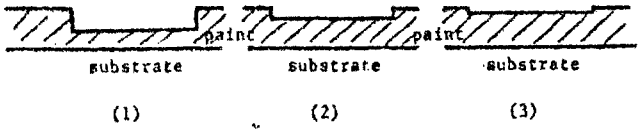

This proves that UV radiation affected the locus of failure of coatings.

Other graphs did not show a good correlation on the effect of UV on the bonding strength of paints. It was because most of the tests were not 100% valid, meaning that only a portion of the coating was removed during the Adhesion Test. However, the testing of polished Alkyd Clear Paint (Coating 1 Treatment A) showed a 100% valid test from cycle 1 to 7. In Figure 5b, non-UV radiated specimens showed slightly higher adhesive strength than UV radiated specimens.

Effect of Phosphating on Bonding Strength and Locus of Failure

For comparing the effect of varying treatments to the bonding strength of coating and metal, Coatings 3 and 4 are good basis of comparison since both had recorded a 100% cohesion strength from cycle 1 to 7. However, the graphs in Figure 5b showed only a slight difference of bonding strength on polished and phosphated specimens. The effect of treatment was more on the depth of failure, or locus of failure. The paints' failures on the polished specimens were near the base metal, however, phosphated specimens' paint failure occured near the paint's surface.

Diagram 3. Cross Section of Specimens With Different Treatment After Adhesion Test

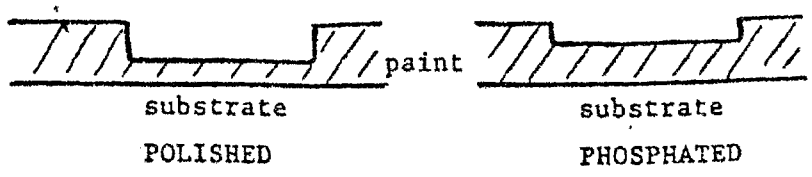

On the other hand, Alkyd clear paint showed a significant bonding strength difference between phosphated and polished specimens. This proves that phosphating increases the bonding of the coating and the substrate.

Generally, bonding between coating and substrate becomes weaker when rust or other corrosion product started to appear on the paint and substrate interface. However, when the paint-substrate interface remains intact, the bonding strength remains constant. In this case, failure may occur on the paint's bulk itself.

FTIR RESULTS

Alkyd Clear Paint and Melamine Alkyd Paint subjected to salt spray test, with and without UV radiation, were both rusted after 3rd cycle. As shown in Figure 6, FTIR spectra of these test specimens are similar to that of rust sample. However, spectra of Zinc Chromate Primer, Red Lead Primer and Epoxy Primer coated specimens after 3rd cycle showed no new band formation.

On the other hand, spectra of Melamine Alkyd Paint, Zinc Chromate Primer and Epoxy Primer coated specimens subjected to humidity test showed no new band formation. Corroded Alkyd Clear Paint coated sample was not analyzed anymore.

On Figure 7, Red Lead Primer coated specimen showed a band intensity increase at around 1300 cm^{-1} after humidity test and a decrease after UV radiation. At 1170 cm^{-1}, band intensity decreased more after UV radiation. The absorption bands in this region are due to the C-O-C stretching vibrations of the phthalate ester. New band was also formed on wavenumbers around 940, 840, 775 and 680 cm^{-1}. Exposure at UV radiation either shifts the band, and increases or decrease the band intensity.

Increase or decrease of the band intensity in a particular position means that molecular vibration, either bending or stretching, of the organic paint was affected by UV radiation. Visible effect of UV on the deterioration of Red Lead Primer was seen in SEM photographs showing the appearance of cracks on the surface. See Figure 8.

STRUCTURAL SURFACE MORPHOLOGY

SEM photographs on Figure 8a showed that UV radiation increases the pores on the specimens' surface. However, varying metals substrate preparation, in Figure 8b, shows no significant difference on the surface morphology of paint. The formation of pores from the surface contributed to the decrease on the bonding between paint and metal interface or to the bonding of the paint bulk itself.

CONCLUSION

From this study, the following were derived:

1. Ultraviolet radiation accelerated the degradation of coatings as seen in the early appearance of rust. However, appearance of blister was independent of the presence of UV radiation.

2. Phosphate coatings provide a good base for paints by enhancing paint adhesion to metal substrate.

3. Three types of failure occured on the coating and metal system during the adhesion test: Adhesion failure, Cohesion failure and Substrate failure. After corrosion testing, adhesion bond between coating and metal substrate decreases, while cohesive bond on the coating itself remains constant.

4. Ultraviolet radiation decreases the bonding strength between coating and substrate system. Radiated painted specimens failed near the substrate, while that without UV radiation failed near the paint surface. Paint failure existence on bigger area was also observed on radiated specimens. UV radiation to Epoxy Primer painted specimen, however, cause a hardening effect on the paint itself.

5. FTIR analysis showed that exposure at UV radiation either shift, increase or decrease the band intensity of the spectra, as obviously observed on the Red Lead Primer coated specimen, which also showed presence of cracks. SEM photographs showed the increase of pores on radiated specimens, a factor that may contribute to the decrease of bonding on paint and metal interface or to paint itself.

ACKNOWLEDGEMENTS

The authors wish to thank Japan International Cooperation Agency for sponsoring this study through the National Research Institute for Metals in Tokyo, Japan. The invaluable assistance of Dr. Hirata and Dr. Fukuda is gratefully acknowledged.

REFERENCES

1 D.R. Bauer, J. Appl. Polym. Sci., 27(1982)3651.
2 M. Tsuda and S. Oikawa, Polymer, 17(1979)3759.
3 S.W. Shalaby, Polymer, 17(1979)419.
4 P. Cassidy and T. Aminabhavi, J. Macromol. Sci., Rev. Macromol. Chem., C21 (1), (1981)89.
5 A.D. English and H.J. Spinelli, J. Coat. Technology, 56(1984)43.
6 D.R. Bauer, Prog. Org. Coat., 14 (1986) 193.
7 A.C. Somersall and J.E. Guillet, in A.C. Somersall and J.E. Guillet (eds.), Polymer Stabilization and Degradation, ACS Symp. Ser. No. 280, Am. Chem. Soc., Washington, DC, 1985, p.211.
8 J.L. Gerlock, H. Van Oene and D.R. Bauer, Eur. Polym. J., 19(1983)11.
9 J.L. Gerlock and D.R. Bauer and L.M. Briggs, in S.S. Labana and R.A. Dickie (eds.), Characterization of Highly Cross-Linked Polymers, ACS Symp. Ser. No. 243, Am. Chem. Soc., Washington, DC, 1984, p.285.
10 J.L Gerlock and D.R. Bauer, J. Polym. Sci., Polym. Lett. Ed., 22(1984)447.
11 J.L. Gerlock, D.R. Bauer, L.M. Briggs and R.A. Dickie, J. Coat. Technol., 57(1985)37.
12 G. Kaempf, H.G. Voelz, A. Klaeren and W. Papenroth, in G.D. Parfitt and A.V. Patsis (eds.), Proc. 6th Int. Conf. Org. Coat. Sci. Technol., Vol.4, p.239, Technomic (Lancaster, PA), 1980.
13 G. Kaempf J. Coat. Technol., 51(1979)51.
14 A. Jurgetz, H. Rothbacher and C. Bliefert, Farbe + Lack, 91(1985)921.
15 G.P. Bierwagen, The Science of Durability of Organic Coatings: A foreword., Progress in Organic Coatings, 15(1987) pp.183-184.
16 M.F. Maker and A.M. Pradel. In Metal Finishing Guidebook and Directory., (N.Hall,ed.), Metals and Plastic Pub, Inc., 1987, p.644.
17 C.G. Munger, Mat. Perf., 22, 7(1983)33.

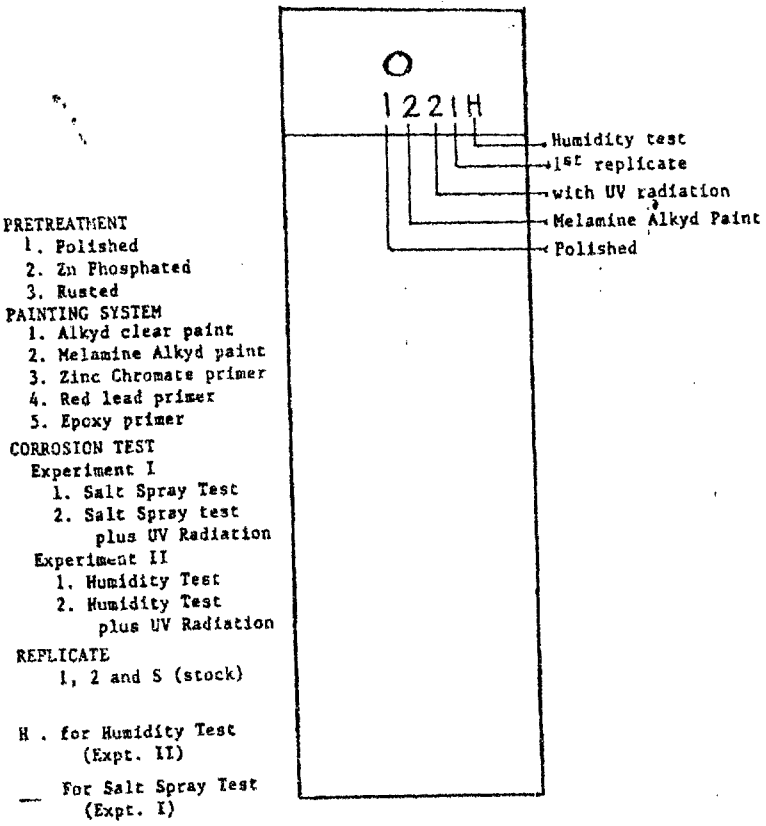

Figure 1. Coding System of Specimens

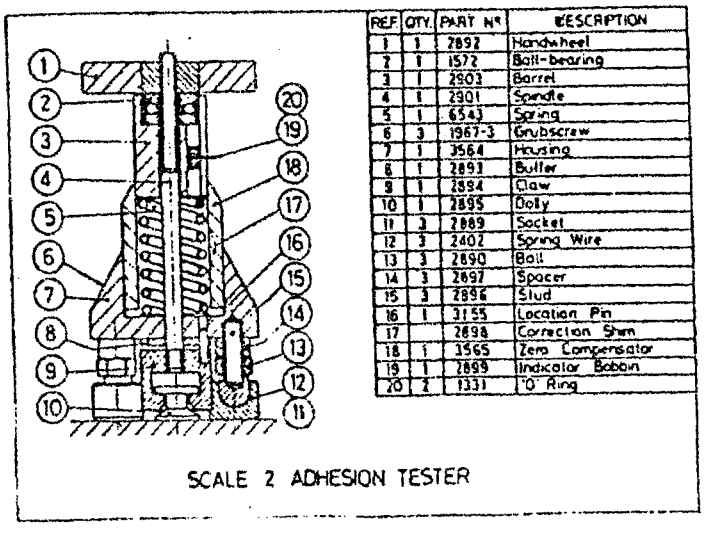

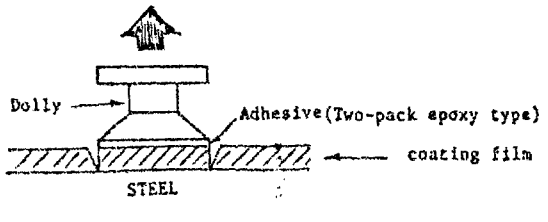

Figure 2. Adhesion Tester

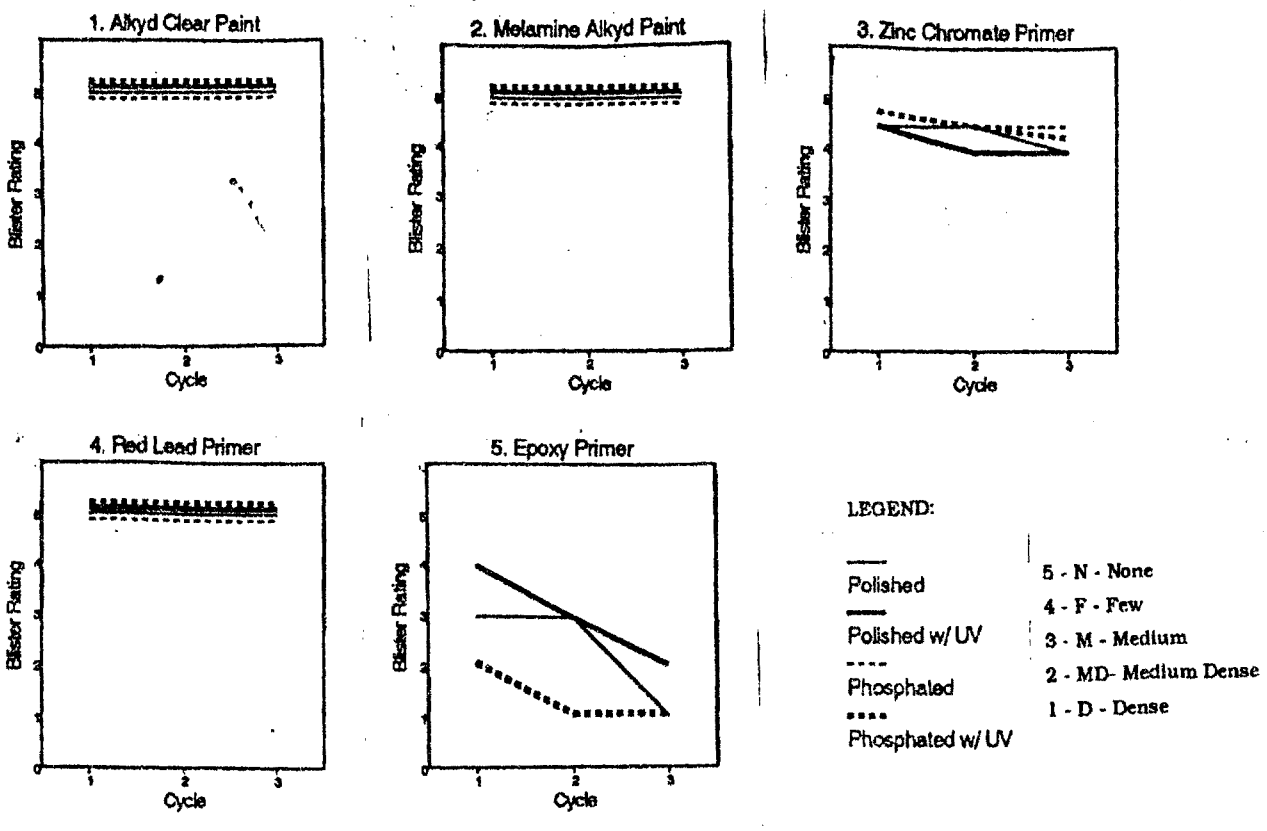

Figure 3a. Blister Rating of Specimens Subjected to Salt Spray Test (Experiment I)

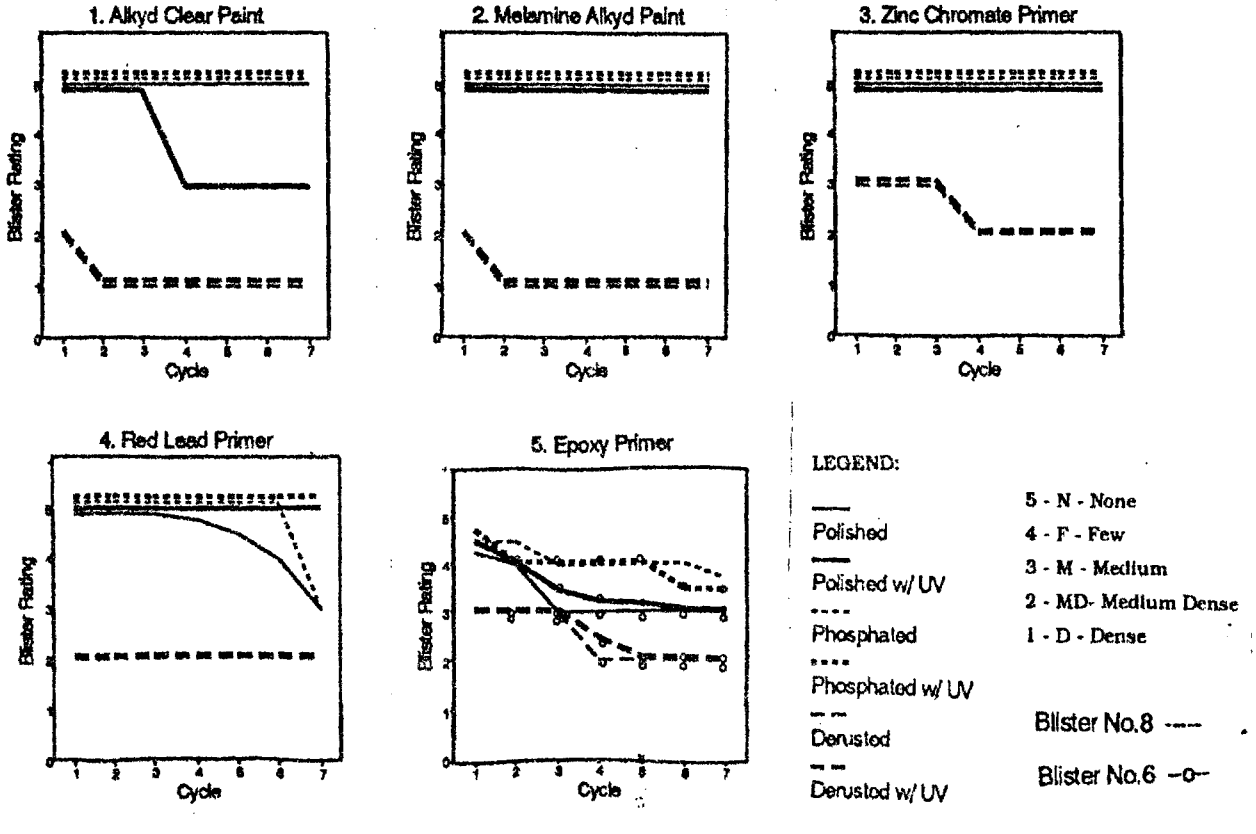

Figure 3b. Blister Rating of Specimens Subjected to Humidity Test (Experiment II)

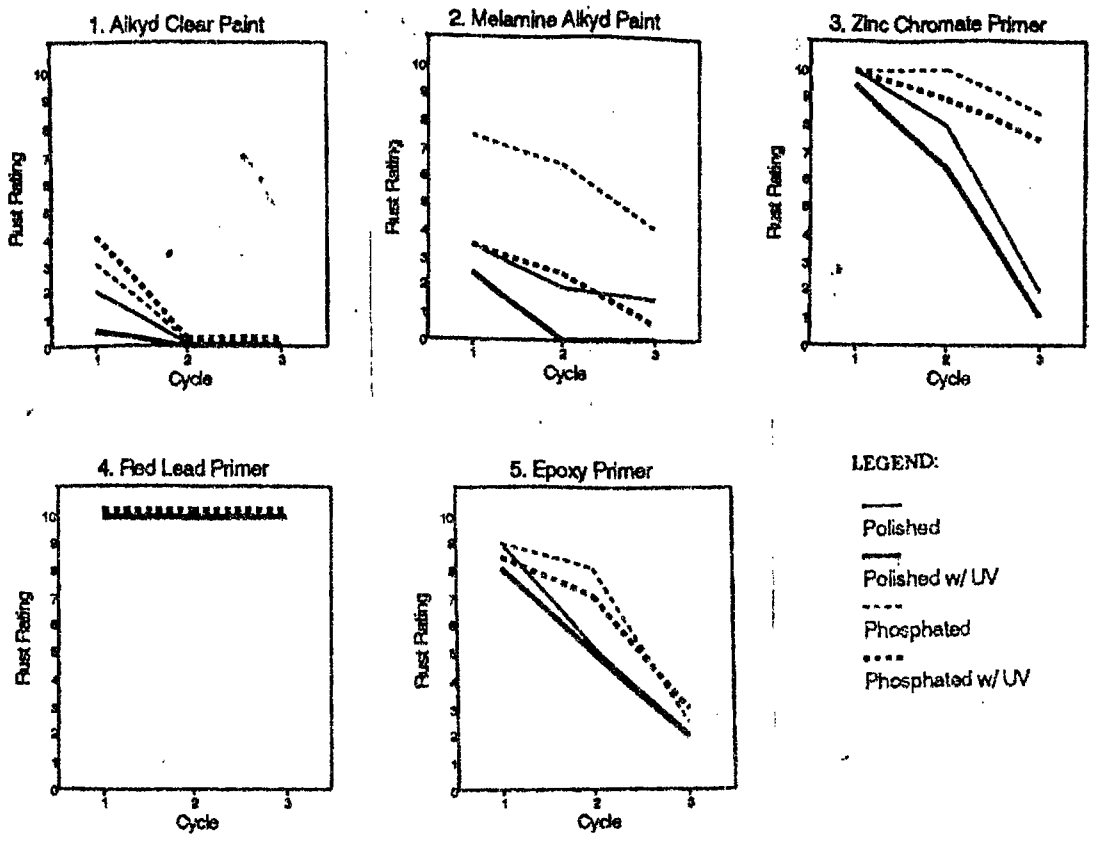

Figure 4a. Rust Rating of Specimens Subjected to Salt Spray Test (Experiment I)

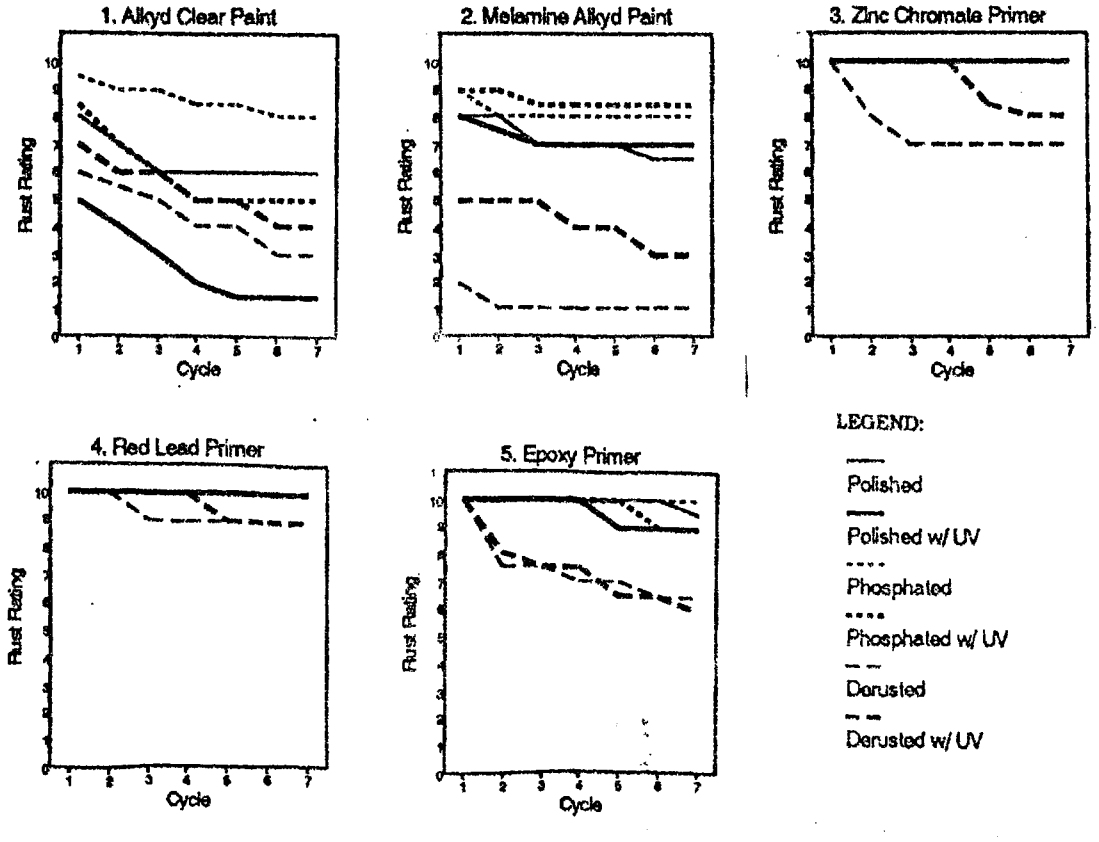

Figure 4b. Rust Rating of Specimens Subjected to Humidity Test (Experiment II)

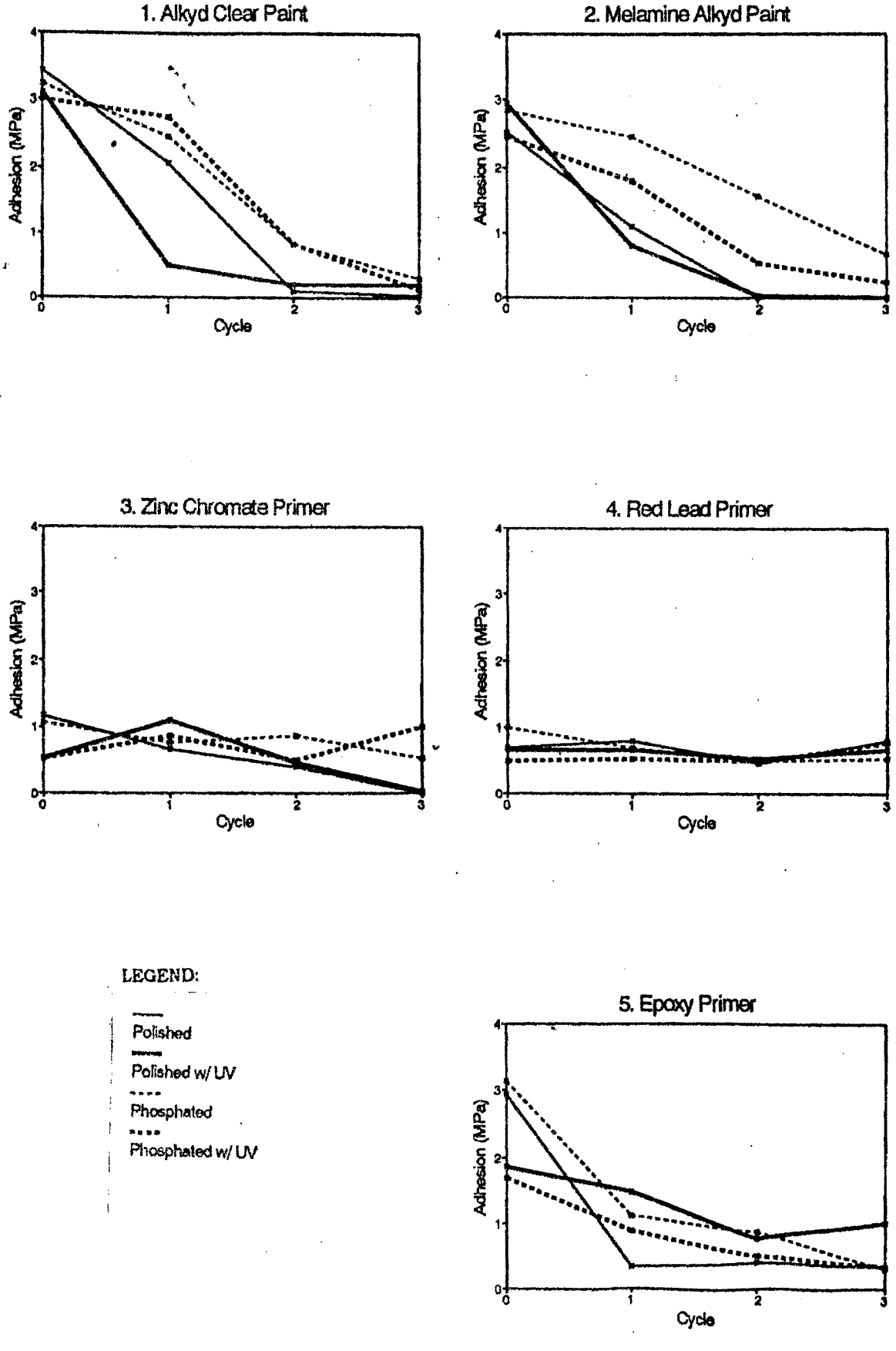

Figure 5a. Adhesion Test Results of Specimens Subjected to Salt Spray Test (Experiment I)

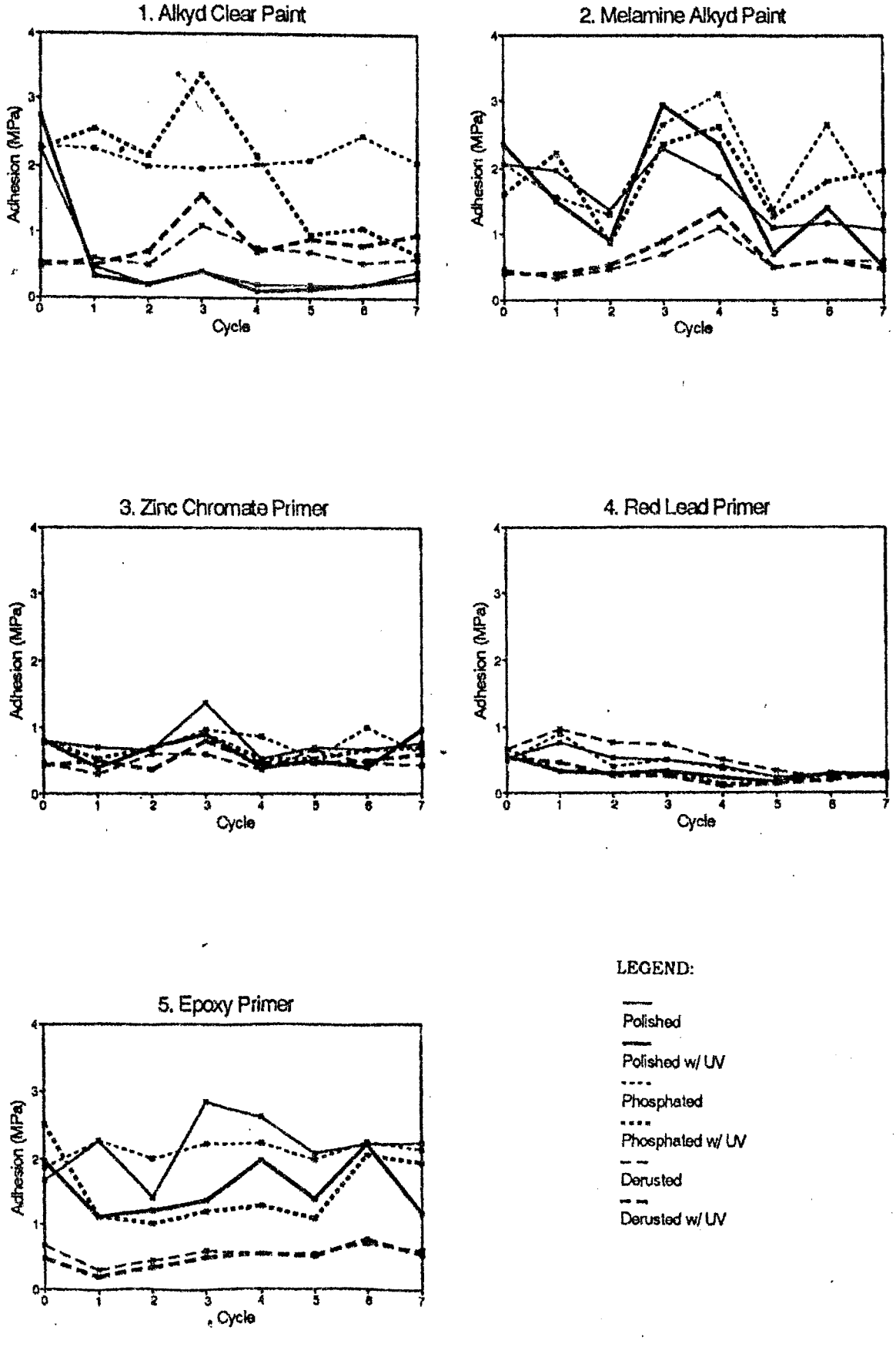

Figure 5b. Adhesion Test Results of Specimens Subjected to Humidity Test (Experiment II)

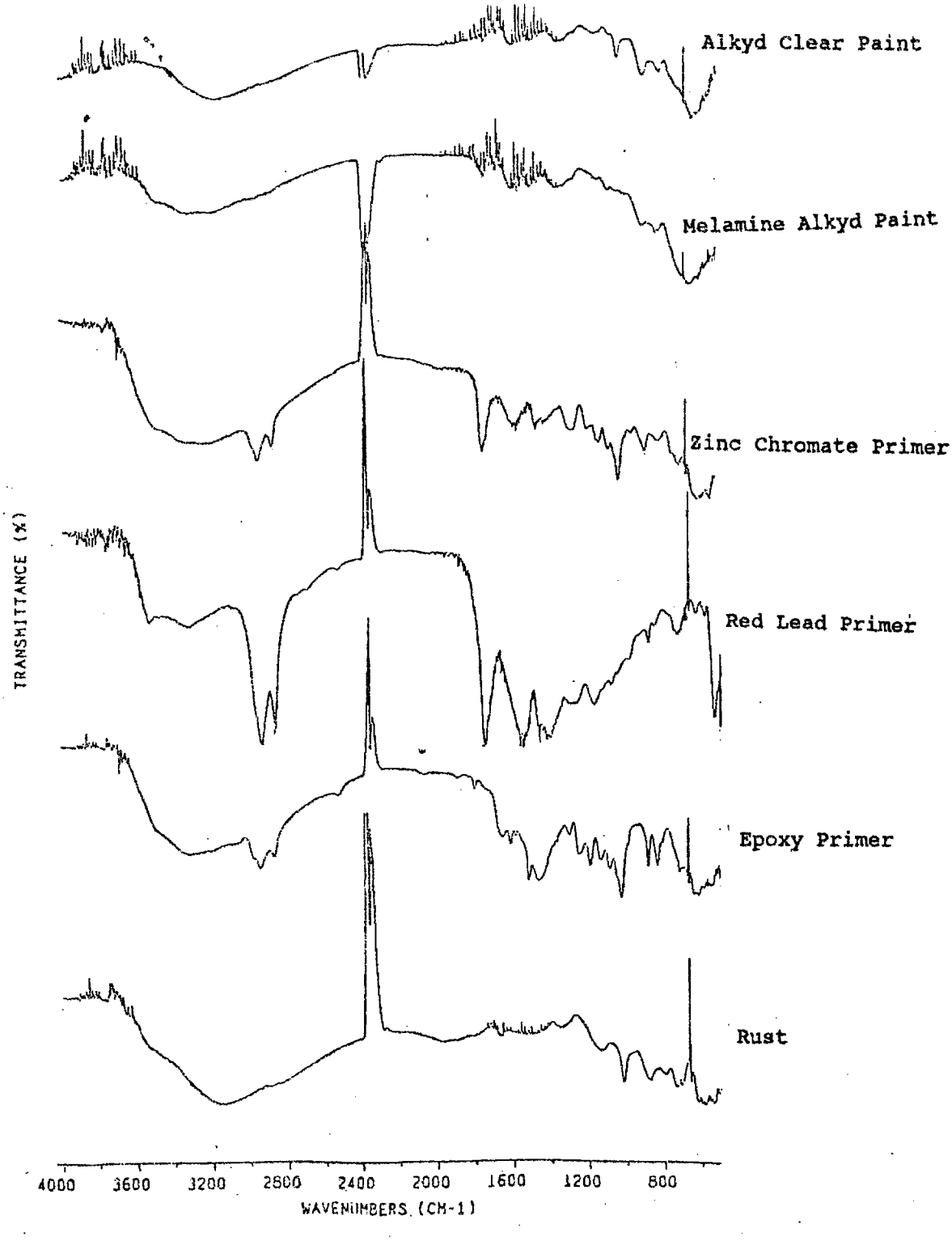

Figure 6. FTIR Spectra of 5 Types of Coatings After 3rd Cycle of Salt Spray and Weathering Test (Preparation: Polished)

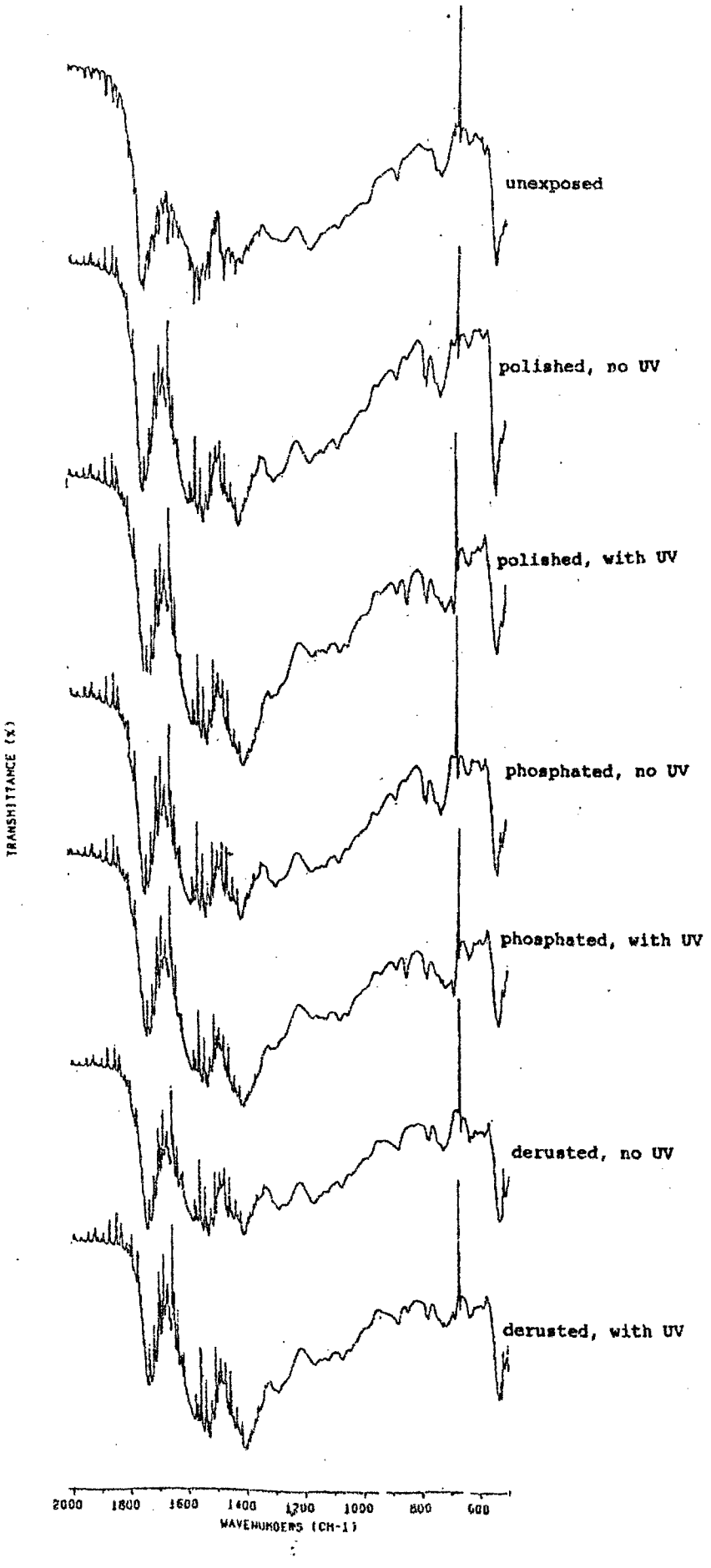

Figure 7. FTIR Spectra of Red Lead Primer Coated Specimens After 7th cycle Humidity Test

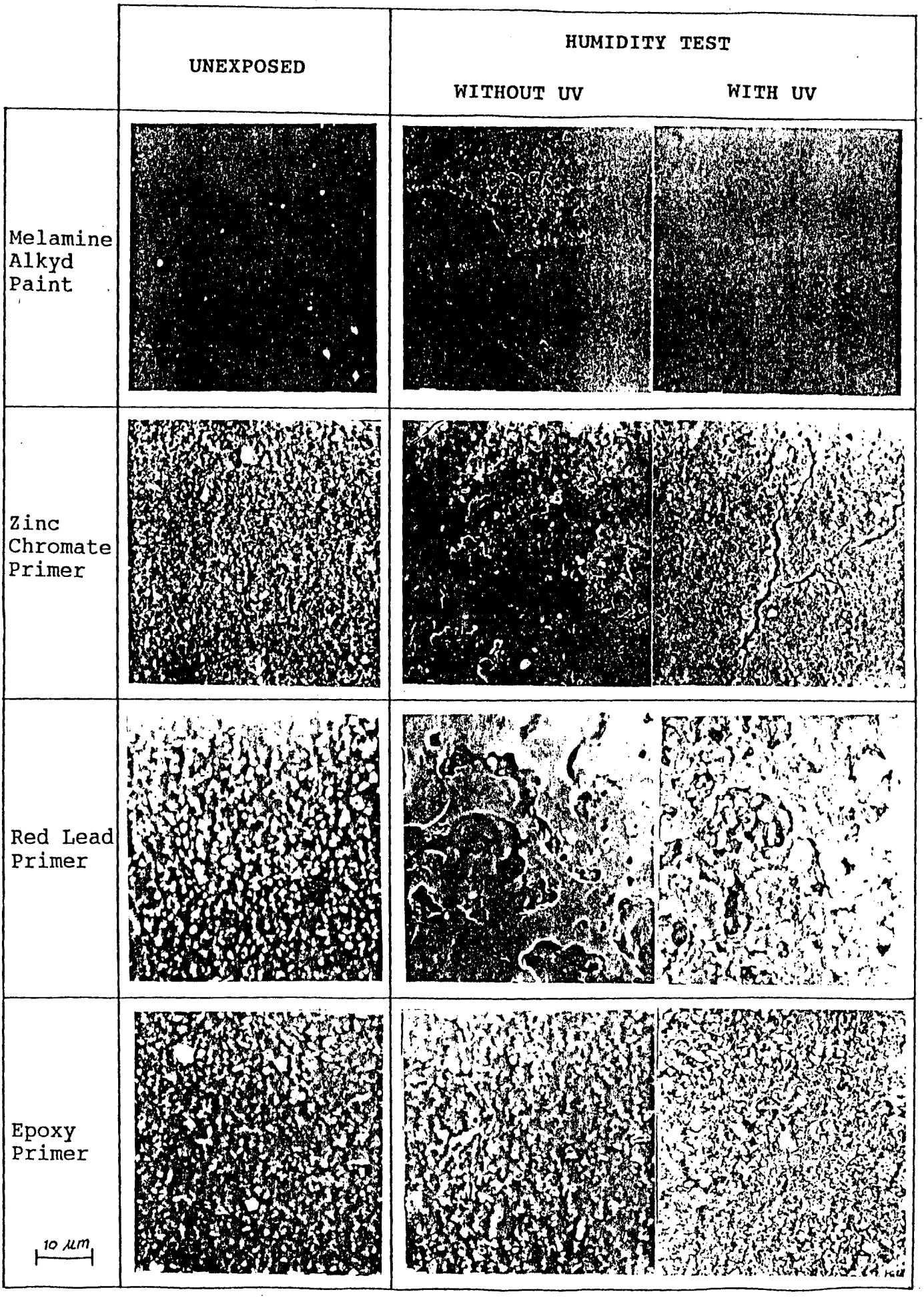

Figure 8a. SEM Morphology of Several Types of Coatings Before and After 7th cycle Humidity Test

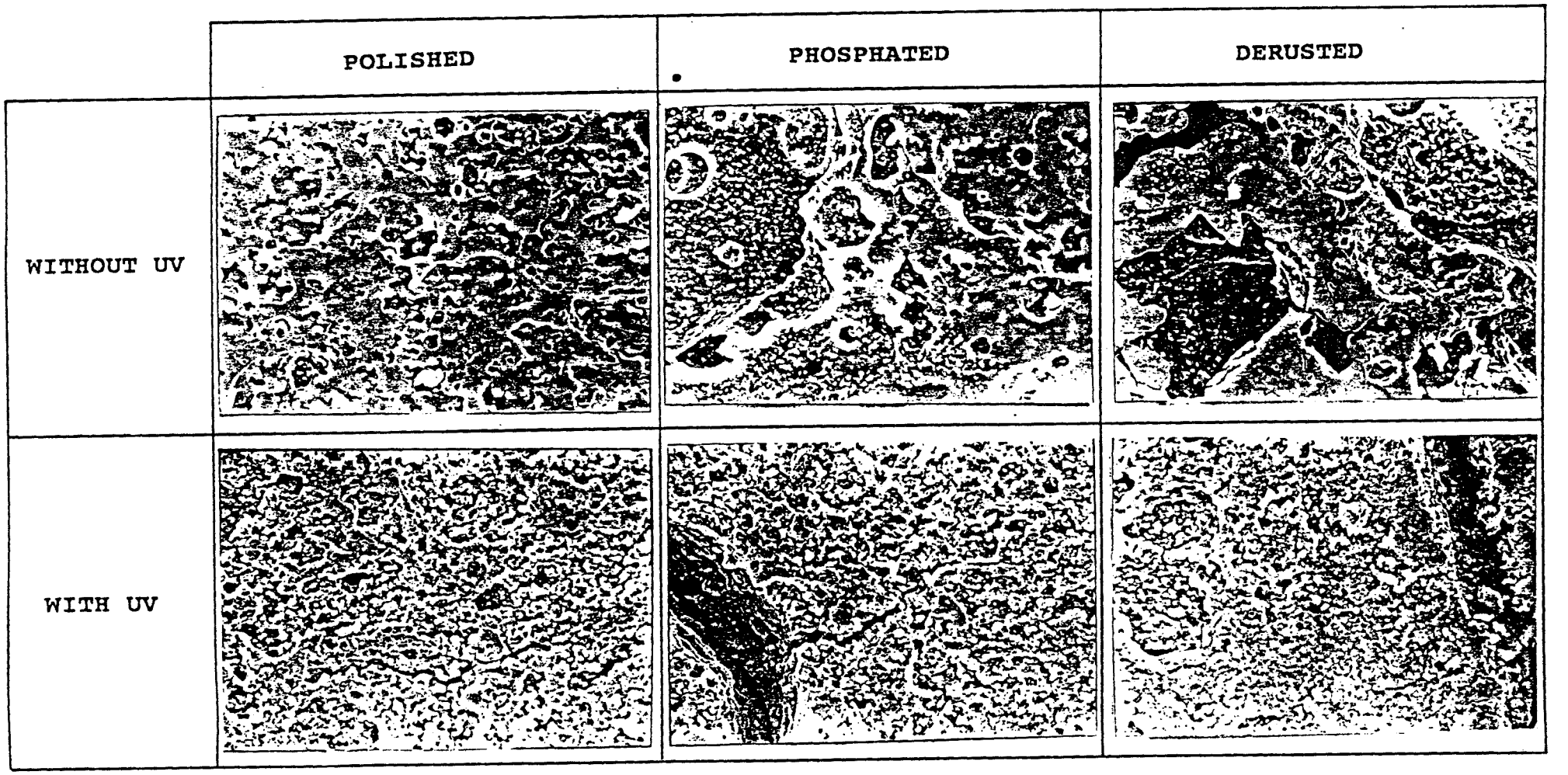

Figure 8b. SEM Morphology of Red Lead Primer With Different Types of Preparations After 7th Cycle Humidity Test

BANGKOK METROPOLIS AND ITS AIR POLLUTION PROBLEMS

Dr. Supat Wangwongwatana

Air Quality and Noise Management Division
Department of Pollution Control
60/1 Soi Phibun Watthana 7
Rama 6 Road, Bangkok 10400
Thailand

ABSTRACT

Bangkok Metropolis which includes Bangkok City and five surrounding provinces, namely Samut Prakarn, Prathum Thani, Nakorn Prathom, Nonthaburi, and Samut Sakorn, is suffering from deteriorating air quality as a result of transportation exhaust emissions and to some extend from industrialization. Ambient air quality standard for total suspended particulate matter are violated. Carbon monoxide concentrations monitored at several tempory curbside stations were found to be in excess of Thai standards which are set less stringent than standards of other international jurisdiction. Curbside concentrations of ambient lead exceed US EPA standards although they are below current Thai standards. Concentrations of other pollutants such as nitrogen dioxide, ozone and sulfur dioxide are currently below respective Thai standards, however, annual levels are increasing.

Particulate matter in the ambient air are mainly from diesel vehicle emissions and two stroke motorcycles, as well as other sources such as construction dust. Carbon monoxide, lead, hydrocarbon and benzene emissions are almost entirely from gasoline driven vehicles. Chronic traffic congestion in Bangkok Metropolis contributes to exceptionally high levels of pollutants. Poorly maintained vehicles coupled with maltuning and overfuelling for high power performance which result in very rich air-to-fuel ratios also lead to excessive emissions of carbon monoxide, unburned hydrocarbon, and smoke.

The Royal Thai Government has placed a high priority on improving air quality of the nation, particularly within Bangkok Metropolitan area. Several measures have been taken to alleviate air pollution problems. They include (i) phasing-out of lead in gasoline; (ii) introduction of unleaded gasoline; (iii) other improvement on gasoline quality; (iv) introduction of catalytic converters; (v) improvement of diesel fuel quality; (vi) introduction of compressed natural gas (CNG) buses; (vii) introduction of low-smoke lubricating oil for two-stroke gasoline engines; (viii) vehicles inspection program; (ix) establishment of emission standards for new vehicles; (x) improvement of traffic condition; (xi) establishment of industrial emission standards; (xii) development of green area.

Air Pollution Problems in Bangkok Metropolis

Thailand is gradually transforming from an agrarian to an industrialized economy and has recorded one of the highest rates of economic growth in the world in recent years. The average rate of economic growth during the 1980s was an impressive 7.8 percent per annum. This has raised the standard of living of the Thai people. However, while the country's economy is flourishing, it environmental quality, on the other hand, is receding.

Bangkok City, the capital and chief port of Thailand, bears another name of "Krung-thep" which has a meaning in Thai of "City of Angels". The city by itself covering an area of about 1,568 square kilometers and having population of 5.9 million people is in the stage of rapidly growing urbanization. It is expanding to cover other five surrounding suburban provinces, namely Samut Prakarn, Prathum Thani, Nakorn Prathom, Nonthaburi, and Samut Sakorn, to form the Bangkok Metropolitan Region (BMR) which cover a total area of 6,886 square kilometers and having population of 8.9 million people. BMR alone contains almost 75 percent of Thailand's total energy consumption. BMR is thus being considered as one of the world's largest urban areas or "Mega Cities" or "Super Cities", cities with population of more than 4 million.

Increasing urban populations and growing levels of industrialization have led to a series of environmentally-related problems in many of the world's cities, not least of which is worsening of air quality. Bangkok is not exceptional and so far is the city having the most polluted air in Thailand, typical for many other cities of the developing world. The city has been being plagued with air pollution problems for some time as a result of high concentration of energy-intensive activities, such as power generation, transportation and manufacturing. The problem is escalated and worsening every year due to increasing numbers of population, industries, and automobiles. Consequently, the health and the quality of life of the people residing in the city are being jeopardized. People will likely suffer pulmonary impairments leading to some restricitions on activity. Susceptible individuals will have increased rates of respiratory illness.

It is not an unusual scene in Bangkok nowadays to see Bangkokians on the streets, for example policemen, pedestrains, busdrivers and passengers, and motorcyclists, covering their noses an mouths with simple surgical masks to protect themselves from inspiring suspended particulate into their lungs, while some of them even wear much more sophisticated respirators to also remove gaseous air pollutants from inspired air.

Air Pollution from Road Tansport

The number of vehicles in Bangkok has soared, from 600,000 in 1980 to 2.3 million in 1991, of which about 1 million are motorcycles, more specifically, 2 stroke-engine motorcycles. All of them are practically uncontrolled vehicles and poorly maintained. Catalytic converter has not yet been legally required for gasoline-engine vehicles. Leaded gasoline is still being used, although lead content has currently been reduced, thus high levels of suspended particulate lead are expected. Not until the first of May of 1991 that unleaded gasoline was first introduced in Bangkok and subsequently in other provinces. Since the beginning of 1992, lead content in the gasoline has been reduced nationwide to 0.15 gram

per litre from previously 0.4 gram per litre. This is equivalent to a reduction of 62.5 percent.

Levels of traffic in Bangkok City exceed the capacity of its road system which has only 112 main roads with a total length of 524 kilometers and 4,280 smaller roads. It is estimated that the roads occupy just only 9 percent of the city area which is very low compared to 22 percent in London and 24 percent in New York City. As a consequence, major traffic arteries are normally congested. Cars travel at an average speed of less than 7 kilometers per hour in the business areas in Bangkok and at an average speed of less than 20 kilometers per hour in other areas. Slow speeds, frequent stops, deceleration and acceleration result in greater incidence of incomplete combustion which causes higher emissions of carbon monoxide, hydrocarbons and particulate matter.

Diesel vehicles are very popular because diesel fuel is 25 percent cheaper than gasoline. They are used primarily for commercial purposes to deliver goods and materials rather than being used as passenger cars. Most diesel trucks are operated in an overloaded condition. Engine is intentionally adjusted to produce higher power by increasing the amount of fuel injected into the cylinders. High level of black smoke emission is the consequence of such tampering which contributes to high level of particulate matter in the air.

The number of motorcycles increases sharply in the last two years as a result of traffic congestion. Bangkokains switch to use motorcycles in order to go around Bangkok faster. Motorcycles are currently being used as public taxis for carrying passengers in addition to delivering messages. Due to excessive use of poor quality lubricating oil and poor engine maintenance, they emit large quantities of white smoke which contributes greatly to the already high suspended particulate level in the air.

Air Pollution from Industry

The Bangkok Metropolis, the most densely populated area in the country, accounts for over 50 percent of the 52,000 factories and 23 industrial estates in the country and will continue to be so in the foreseeable future. In 1990, there are 19,892 factories registered in Bangkok City, out of a total of 26,226 factories in the Bangkok Metropolis. Many of them are small scale factories. At present, industries contribute to air pollution problems in Bangkok in a lesser degree compared to transport sector. The problems are localized rather than widespread. However, emissions from industry are expected to grow rapidly in the next 10 years, at an average rate of 5 to 7 percent per year.

Air pollution generated by industries is largely a result of industrial energy consumption. Air pollutants of major concerns are soot, sulfur dioxide, nitrogen oxides, and odor. The growth in lignite and coal consumption in the industrial sector will have a significant impact on air quality.

Ambient Air Quality Standards

The Office of the National Environment Board (ONEB) established the National Primary Ambient Air Quality Standards (NPAAQ) for six principle criteria air

pollutants since 1981. They are summarized in details in Table 1. Some of these standards are quite high in values when they are compared to the respective standards of the World Health Organization (WHO). The revision of these NPAAQ standards taking into account the latest information on their effects on human health are thus being in consideration. It is expected that the new NPAAQ standards will be much stricter than the current ones.

Currently, there is no longer the Office of the National Environment Board. Three new departments, including Office of Environmental Policy and Planning, Department of Pollution Control and Department of Environmental Quality Promotion, are established under the new Improvement and Conservation of National Environmental Quality of 1992 to replace the former ONEB.

Table 1 Thailand's National Primary Ambient Air Quality Standard

Air Pollutants	1 hr average value (mg/m^3)	8 hr average value (mg/m^3)	24 hr average value (mg/m^3)	1 year average value (mg/m^3)	Methods of Measurement
Carbon Monoxide CO	50	20	--	--	Non-Dispersive Infrared Detection
Nitrogen Dioxide (NO_2)	0.32	--	--	--	Gas Phase Chemiluminescence
Sulfur Dioxide (SO_2)	--	--	0.30	0.10*	Pararosaniline
Total Suspended Particulate Matter (TSP)	--	--	0.33	0.10*	Gravimetric, High Volume Air Sampling
Photochemical Oxidant (O_3)	0.20	--	--	--	Gas Phase Chemiluminescence
Lead (Pb)	--	--	0.01	--	Wet Ashing and Atomic Absorption Spectrophotometer

Note: * = Geometric Mean

Ambient Air Quality Monitoring in Bangkok Metropolis

The ONEB has begun its ambient air monitoring program in Bangkok since 1983. At present, the Department of Pollution Control taking over the monitoring activity maintains 7 permanent continuous ambient air quality monitoring stations in Bangkok City. These stations are located in areas representing different types of land use, such as residential, industrial, commercial and mix areas. Characteristics of these stations are summarized in Table 2 and their locations are shown in Figure 1. Relocation and upgrading of these stations are being carried out by the department to better monitor the quality of air in Bangkok.

Recently, the monitoring network in Bangkok City has been expanded. Four additional permanent continuous on-line curbside air quality monitoring stations are installed, location of which are also shown in Figure 1. Each of them is also equipped carbon monoxide and suspended particulate matter monitors and noise meter with an on-site display board to continuously and instantaneously display real-time in-situ air quality to the public.

In addition, the department also performs short-term temporary (2 weeks period) curbside air quality monitoring on a regular basis at 22 most congested streets in Bangkok City. Locations are shown in Figure 2. Two air pollutants, namely carbon monoxide and suspended particulate matter, and noise are monitored.

In 1988, five movable permanent air quality monitoring stations were installed in Samut Prakarn province with the assistance from Japanese government. Locations of these stations are illustrated in Figure 3. Samut Prakarn province is one of the five satellite provinces surrounding Bangkok City and is characterised by a large numbe of industries. Sulfur dioxide, nitrogen oxides, and suspended particulate matter are continuously monitored at these stations.

The Department of Pollution Control is planning to upgrade and expand its ambient air quality monitoring network to cover the whole area of the Bangkok Metropolis. Air pollution emission inventory database together with the computerized simulation system for forcasting air quality in the Bangkok Metropolis are being developed with the technical assistance from the Royal Swedish government.

Current Air Quality in the Bangkok Metropolis

The results from the long-term air quality monitoring indicate that the Bangkok Metropolis is having air pollution problems in an increasing magnitude with regard to suspended particulate matter, carbon monoxide and lead, respectively. Results are still not conclusive in respect of other air pollutants, namely sulfur dioxide, nitrogen oxides and ozone.

Total Suspended Particulate Matter (TSP)

Monitoring results show that annual geometric mean concentrations of total suspended particulate matter (TSP) exceed Thailand's NPAAQ standards of 0.1 mg/m^3 at all ambient air quality monitoring stations in Bangkok City. Near the main streets where traffic is heavy, short-term 24-hour average TSP concentrations range from 0.2 to 0.7 mg/m^3 which far exceed the daily NPAAQ standard of 0.3 mg/m^3. The natural background level of SPM in Thailand as measured in rural

Table 2 Characteristics of Permanent Ambient Air Quality Monitoring Stations Located in Bangkok City

Station Number	Land Use Classification	Pollutant Monitored
1. Office of the National Environment Board (ONEB)	Urban Residential	TSP, CO, NO_2, O_3, Pb, SO_2, Wind Speed and Direction
2. Chankasem Teachers' College	Suburban Residential	TSP, Pb, CO
3. Ban Somdet Teachers'	Mixed	TSP, Pb, CO, Wind Speed and Direction
4. Rat Burana Post Office	Industrial	TSP, Pb, CO, SO_2, Wind Speed and Direction
5. Queen Saovabha Memorial Institute	Commercial	TSP, Pb, NO_2, O_3
6. The Meteorological Department, Sukhumwit	Urban Residential	TSP, Pb, CO
7. Bangna Meteorological Office	Industrial	TSP, PB, CO, NO_2, SO_2, Wind Speed and Direction

areas is about 0.05 to 0.07 mg/m^3. The TSP concentraions show an increasing trend over the past years. More than 60 percent by weight of TSP was found to be smaller than 10 micrometer in diameter. The particle size distribution shows two modes at about 0.4 and 4 micrometer. This obviously indicates potential adverse health effects to the people, particularly those who live or work near heavily traffic congested areas.

One study analyzed the composition of TSP and concluded that particulate matter or black smoke from diesel vehicles contributes to suspended particulate matter in the air about 40 percent. Another 40 percent is from construction and fugitive sources, such as soil dust from road surface and uncovered land. The remaining 20 percent is from other sources which include industries, sea, and other natural sources.

Carbon Monoxide

Ambient 1-hour and 8-hours average carbon monoxide concentrations at all permanent ambient air quality monitoring stations satisfy the NPAAQ standards. Carbon monoxide concentrations in residential areas of Bangkok City are generally low -around 1 ppm.

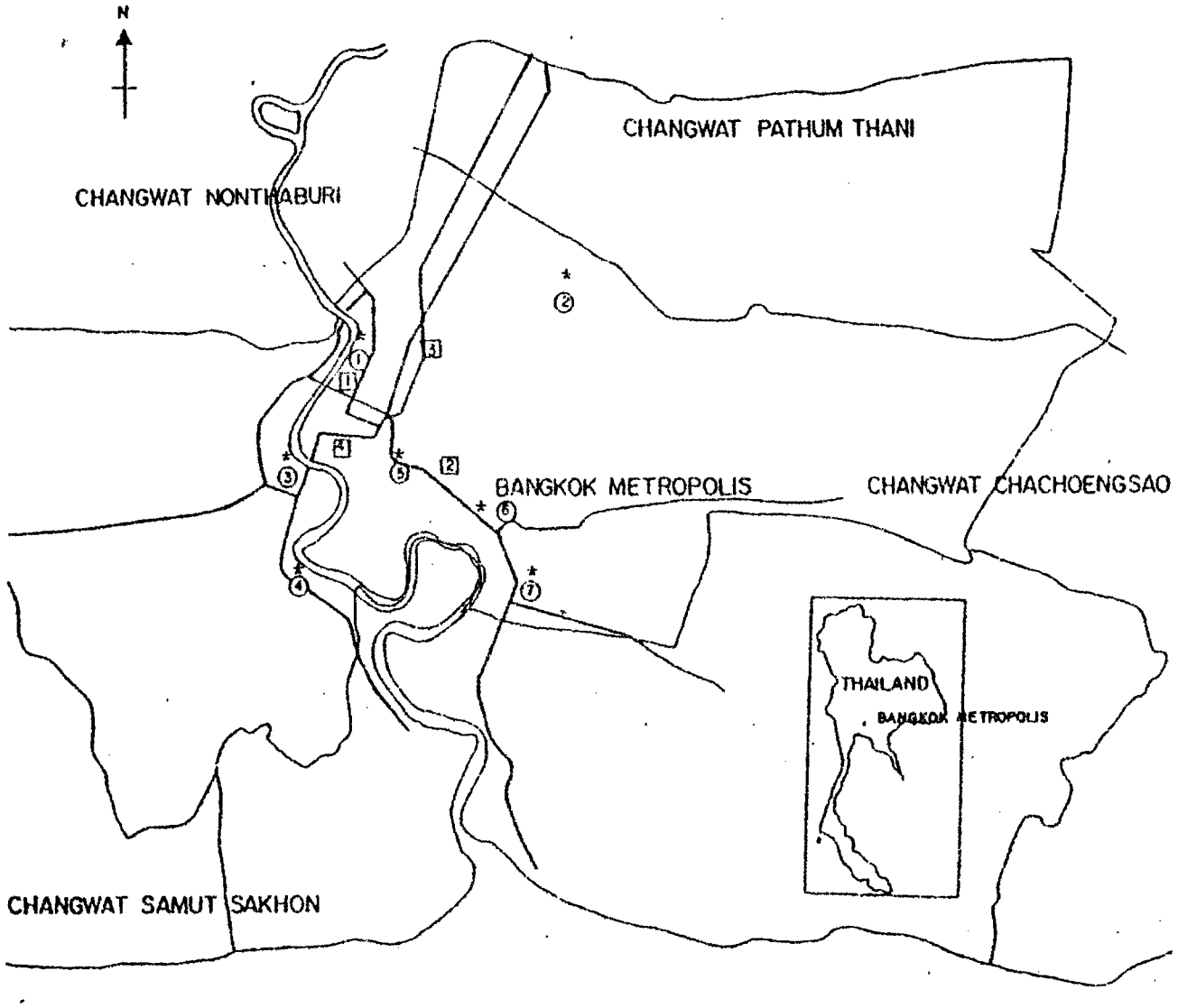

* ○ Ambient air monitoring stations.

□ Ambient air monitoring stations with sign-board on curbside

Figure 1 - Locations of Permanent Ambient Air Quality Monitoring Stations in Bangkok City

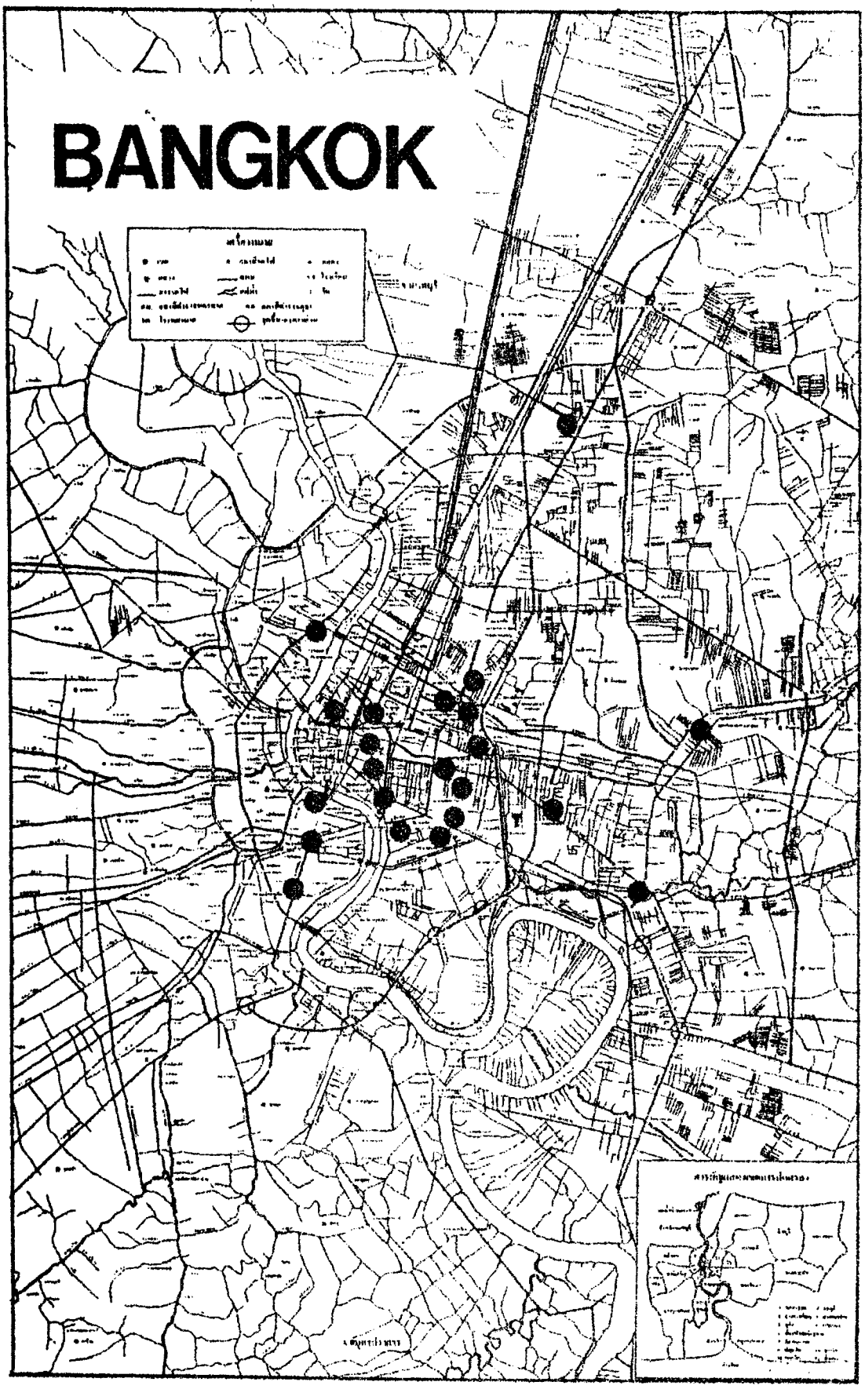

Figure 2 - Locations of 22 Short-Term Temporary Curbside Air Quality Monitoring Stations in Bangkok City

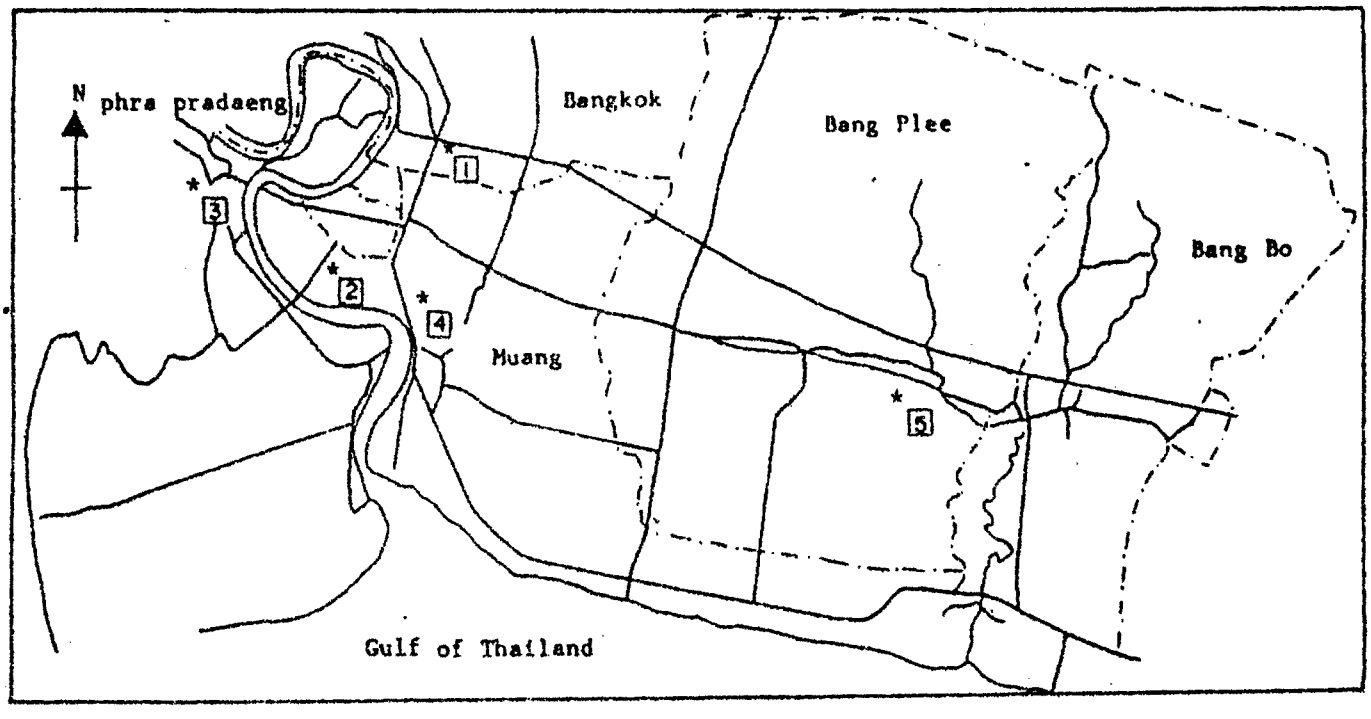

Monitoring Station

*MS1 Bangna

*MS2 Power Plant, EGAT

*MS3 Mineral Department Office

*MS4 Samutprakarn Provincial Office

*MS5 Housing and Industrial Estate

Figure 3 - Five Movable Permanent Air Quality Monitoring Stations in Samut Prakarn Province

However, carbon monoxide concentrations are much higher when get closer to the streets, particularly ones which are heavily congested. Carbon monoxide accumulation is found in certain locations, typically characterized by heavy traffic, narrow streets and tall building on both sides of the street. The eight-hours average concentrations of carbon monoxide are generally close to, sometimes exceed, the standard of 20 mg/m^3. A concentration of 30 mg/m^3 was recorded in one of the streets in Bangkok. Although, one-hour average concentrations of carbon monoxide still meet the standard of 50 mg/m^3, a maximum concentration of 49 mg/m^3 was recorded.

Surprisingly, carbon monoxide levels in Bangkok City have not increased substantially for the past five years although the number of gasoline-driven vehicles have increased annually at a rate of more than 10 percent in the past two years. This may be as a result of the pronounced "heat island's effect" in the city center which produces rapid vertical mixing and thus helps dispersing carbon monoxide from the street level in seconds.

Lead (Pb)

Ambient daily average concentrations of lead in Bangkok do not normally exceed the NPAAQ standard for lead of 0.01 mg/m^3. In 1990, ambient lead concentrations ranged from 0.0003 - 0.00086 mg/m^3. Concentrations of lead monitored in 1985 to 1987 at five out of eight roadside stations were found to be greater than 0.001 mg/m^3. A concentration of 0.004 mg/m^3 was reported in 1988 at one roadside location and as high as 0.006 mg/m^3 of roadside daily lead concentration was detected in 1989. The results indicate that there is an increasing trend of lead concentration in Bangkok.

Other Air Pollutants

Measurements of SO_2, NO_x, and O_3 taken at the roadside in central Bangkok showed that their ambient concentrations are relatively low on average, and do not normally exceed the relevant NPAAQ standards. These measurements do not show the effect of SO_2 emissions from industrial plants and power stations, most of which are located in the outskirts of Bangkok.

Ambient concentrations of NO_x and O_3 were not as high as might be expected given the large number of vehicles in the city. The atmospheric photochemical reactions involving NO_x (NO and NO_2), HC and O_3 are very complex and depend on many factors, one of which is the degree of wind dispersion. Wind may carry polluted air away from the city before NO is fully converted to NO_2 and thus the subsequent formation of O_3.

Government Measures Towards Improving Air Quality

The public and the government are voicing serious concern about the increasing trend of air pollution problems, particularly in the Bangkok Metropolis. A concerted effort is being made by the government to restore the quality of the air together with industries, the public and non-governmental organizations (NGOs). A number of measures adopted by the government to mitigate air pollution

problems, particularly those caused by the transport sector, are aimed not only at exhaust gas emission controls but also at the improvement of fuel and engine specifications and the improvement of the road network to maintain better traffic flow. These measures are summarized below.

Phasing-Out of Lead in Gasoline

At the end of 1989, the government made a decision to reduce lead content in gasoline from 0.45 to 0.4 grams per litre and targeted to allow no more than 0.15 gram per litre by September 1993. The government decided later to phase out leaded gasoline at an earlier schedule. The maximum allowable lead in gasoline was reduced from 0.4 to 0.15 grams per litre in January 1992 and the premium leaded gasoline will be totally phased out by 1996.

Introduction of Unleaded Gasoline

On the 1st of May 1991, the government introduced the first time ever in Thailand premium unleaded gasoline (ULG) after it was found that more than 80 percent of existing gasoline-driven motor vehicles in Thailand can run on ULG. In order to encourage the use of ULG, ULG is currently sold at prices below that of leaded gasoline by about 0.30 baht per litre through restructuring gasoline tax and further subsidizing the incremental cost over leaded gasoline.

The decision to introduce ULG was made for two reasons. The first reason is to reduce lead in the ambient air as early as possible and the second one is to prepare the gasoline market so that ULG will be available at the gas stations nation-wide by the time new motor vehicles equipped with catalytic converters are introduced in 1993. Within five months of its introduction, premium ULG gained 25 percent of the total premium gasoline consumption in Bangkok and are widely distributed all over the country.

On 4th of February 1992, the Cabinet decided that all government owned gasoline-driven motor vehicles in Bangkok which have hard valve seats must use unleaded gasoline.

Other Improvement on Gasoline Quality

It is being proposed by the government to set the maximum aromatic and benzene contents in both leaded and unleaded gasoline to 50 amd 3 percent by volume, respectively. These limits if imposed would reduce emissions of carcinogenic compounds. Currently, there is no maximum limit for aromatic content while the current maximum allowable benzene content is set at 5 percent by volume.

In addition, it is also being proposed to require both leaded and unleaded gasoline to contain oxygen between 1 to 2 percent by volume. The minimum oxygen content (1 percent by volume) can be achieved through the use of any one of the following oxygenated compounds: 5.5 percent by volume of methyl tertiary butyl ether (MTBE) or 2.75 percent by volume of fuel grade ethanol (E 100). The addition of oxygenated compounds would curtail carbon monoxide emissions.

Introduction of Catalytic Converters

To reduce emissions of air pollutants other than lead, namely carbon monoxide, nitrogen oxides and hydrocarbons, all new gasoline-driven motor vehicles whose engines are larger than 1,600 cc will be required to have catalytic converters by January 1, 1993. Catalytic converters will be required for all new gasoline-driven motor vehicles whose engines are smaller than 1,600 cc by September 1, 1993. The government has decided to reduce tax on catalytic converters to as low as 5 percent in order to reduce the burden on the car byers.

Improvement of Diesel Fuel Quality

The current sulfur content of diesel fuel of not more than 1 percent by weight will be reduced to not more than 0.5 percent by weight by September 1, 1993. In the mean time, all oil refineries and distributors are encouraged to voluntarily sell low-sulfur (0.5%) diesel fuel. In addition, all buses owned by state enterprises in Bangkok have been required to use low-sulfur diesel fuel since March of 1991.

To reduce emissions of black smoke from diesel-driven buses and trucks, it is scheduled to lower the 90 percent distillation temperture of diesel fuel from 370 °C to 357 °C on September 1, 1992. However, low-distillation temperature (357 °C) diesel fuel is currently available in most gas stations.

To encourage the use of better quality diesel fuels, gas stations are required to sell low-sulfur and low-distillation temperature diesel fuel at the same price as high-sulfur and high-distillation temperature diesel fuel. This is made possible by adopting two measures: first to reduce excise tax for diesel fuel by 0.11 baht per litre and second to subsidize diesel importers and refineries by reducing the oil fund deduction by 0.3 baht per litre of diesel imported or produced. The cost to the country resulting from the improvement of diesel fuel quality is more than 1,000 million baht per year.

Introduction of Compressed Natural Gas (CNG) Buses

The Bangkok Mass Transit Authority (BMTA) is purchasing 82 CNG buses at a total cost of 400 million bahts to replace old diesel buses. This is a measure designed to reduce black smoke on Bangkok's streets. CNG buses will first be used mainly on streets in Bangkok which have most polluted air. It is anticipated that the use of CNG buses would reduce black smoke emissions by a factor of 7.5 compared to conventional diesel fuel.

Introduction of Low-Smoke Lubricating Oil for Two-Stroke Gasoline Engines

The government is promulgating a new, mandatory standard for low-smoke lubricating oil to reduce white smoke emitted by some 900,000 two-stroke motorcycles in Bangkok. White smoke is the product of combustion of gasoline blended with lubricating oil used in two-stroke engines. Tax on the additives being used in the production of low-smoke lubricating oil will be reduced in order to lower the price of such oil.

Vehicle Inspection Program

The government has earmarked an initial budget of 28 million baht for the implementation of an annual inspection program for vehicle emissions. Initially, the program will begin with the inspection of 100,000 government-owned vehicles in Bangkok. This is to ensure that all government-owned vehicles are in compliance with the standards. If inspected vehicles are found to emit air pollutants exceeding the relevant allowable limits of emission standards, services are required for those vehicles to bring emission levels down to meet the standards. In the near future, the program will be extended to personal private vehicles. The establishment of private inspection centers will be encouraged to sufficiently provide services to a large number of vehicles in Bangkok.

On-the-road inspection of emissions from in-used vehicles in Bangkok is being carried out citywide by the Police Department and the Department of Land Transport. Five hundred baht fine is imposed on vehicles violating the emission standards. The violating vehicles must meet the standards before they can be driven on the streets again.

Establishment of Emission Standards for New Vehicles

Type-approval and conformity of production emission standards for new vehicles are being drafted by the government and will be put into force by 1992. This is to ensure that people will be furnished with good quality and low polluting vehicles from the beginning.

Improvement of Traffic Condition in Bangkok

Traffic congestion is one of the most important factors, in addition to such factors as large number of vehicles and poor vehicle maintenance, which contributes to the deteriorating air quality in Bangkok. Carbon monoxide and hydrocarbons are emitted from vehicles in larger quantities when they are under idling condition. The government is implementing several measures to alleviate the traffic condition in Bangkok and more actions are being planned for the future.

- Several fly-over bridges across major congested intersections and elevated roadways are being constructed.
- Express-ways and ring-road networks are being expanded so that unnecessary trips passing through the city center can be avoided or reduced.
- Several major mass transit systems are being implemented and some are pending for the approval from the government. They include the sky-train system, elevated municipal railways, and the electric train system in the central business districts.
- Parking is prohibited on major streets.
- City truck terminals at the outskirts of Bangkok are being planned in order to reduce the number of large trucks entering the city center.
- Flexible working hours has recently been introduced in government offices to solve traffic congestion during rush-hours.
- An underground oil pipeline system to transport oil products directly

from the oil refinery and oil depots in Bangkok to the Don Maung Airport and to major industrial areas is under construction. This would help reducing the number of oil trucks on the roadways.

Establishment of Industrial Emission Standards

The Department of Industrial Works (DIW) is responsible for issuing industrial emission standards which are designed to ensure that the ambient air quality standards are achieved. The DIW has proposed a set of industrial emission standards which are expected to receive formal Ministerial notification in the near future. The new establishment of air-polluting industries and the burning of lignite or coal in the inner Bangkok are also prohibited. In addition, reformulation of fuel oil which are frequently used by industries, particularly with respect to its sulfur content, is under investigation its cost-benefit.

Development of Green Areas

One of the government's major policies to remedy air pollution in Bangkok is to conserve and to increase green areas in the city as much as possible in order to provide sinks for air pollutants and at the same time to produce more oxygen to the air for the people. More public parks will be built in the future and tree planting are being encouraged.

Impact on Ambient Air Lead Concentrations from the Elimination Lead in Gasoline

Efforts that the government has put in to eliminate lead from the gasoline are being paid off. Unleaded gasoline (ULG) was introduced into the market in May 1, 1991 while lead content in the leaded gasoline has been reduced to 0.15 gram per litre from 0.4 gram per litre since January 1, 1992. Figure 4 shows the impact on ambient air lead concentrations in Bangkok since the introduction of ULG and low leaded gasoline. The consumption of ULG is quite stable, about 25 percent of total premium gasoline consumption. Although the ambient air concentrations (monthly mean of daily average concentration) of lead from May to December of 1991 still show an increasing trend after the introduction of ULG in May of 1991, but the concentrations are lowest when compared to those of previous years (from 1986 to 1990) during the same period of time (May - December), as shown in Figure 5. High level of pollution is typical at the end of the year, during winter season.

Monitoring results show a large drop in ambient air concentrations of lead after the introduction of low leaded gasoline in January 1992, from more than 0.3 microgram per cubic metre in December 1991 to 0.15 microgram per cubic metre in February 1992. There is a slight increase in ambient air lead concentration in March 1992 but that is probably a result of a corresponding increase in the gasoline consumption.

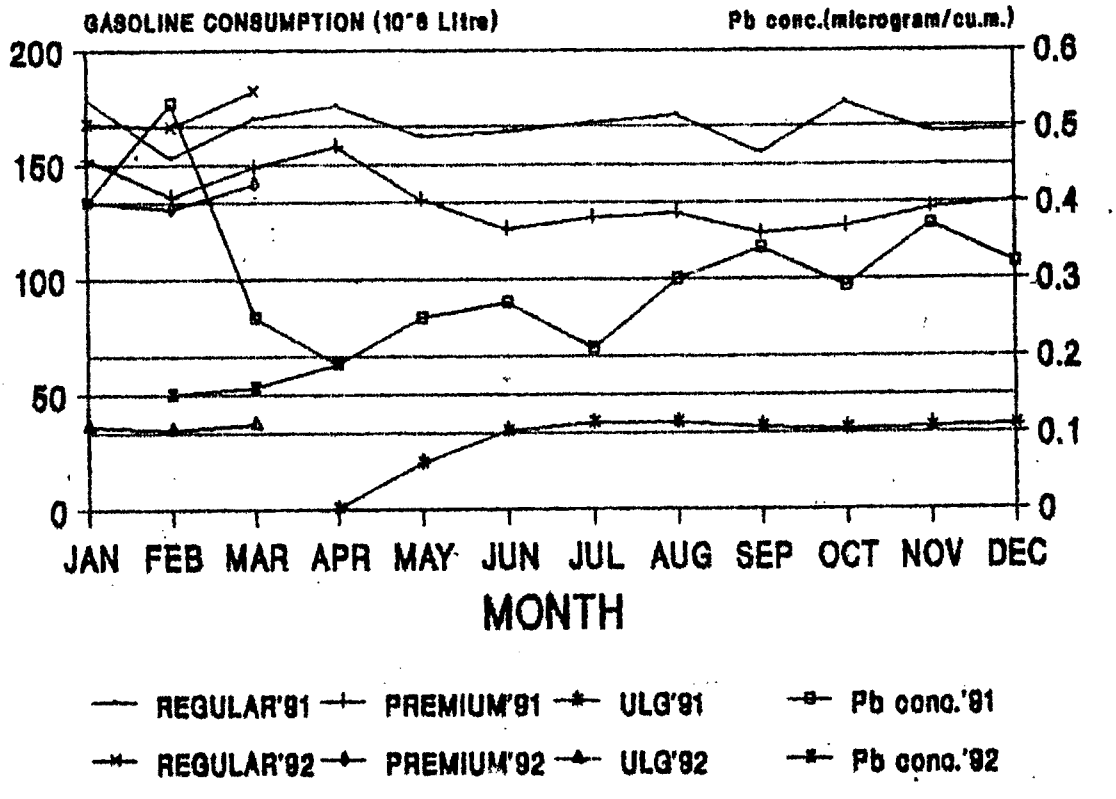

Figure 4 Ambient Air Lead Concentrations (monthly means of daily average concentrations) in Bangkok versus Gasoline Consumption.

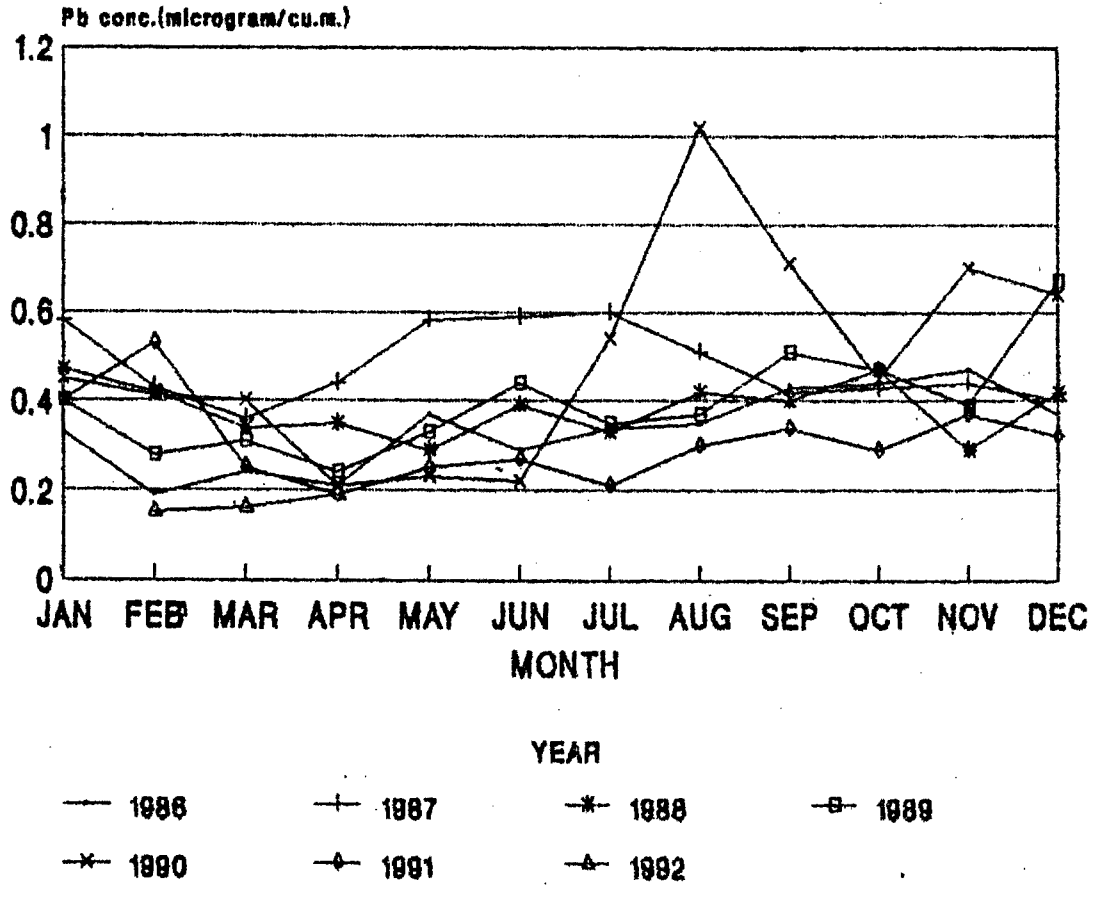

Figure 5 Ambient Air Lead Concentrations (monthly means of daily average concentrations) in Bangkok from 1986 to 1992

COATINGS FOR PIPELINES AND OTHER UNDERGROUND STRUCTURES

Mr.Vinit La-ongsuwan

TOA Paint (Thailand) Co.,Ltd.

I. Purpose of Coating

Pipe Coating on Underground Structures isolate metal from Contact with Sucounding environments. Since a perfect Coating Cannot be assured, Cathodic Protection is used in Conjunction the Coating system to provide the first line of defense against corrosion

II. Desirable Characteristic of a pipe coating

A) Effective Electrical Insulator

Since soil Corrosion is an electrochemical process, a pipe coating has to stop the current by isolating the structure from the environment.

B) Ease of Application

The Coating material must be suitable and properly applied to be effective. Coating application specifications and good construction practices combined with proper inspection contribute to the quality of the finished coating system.

C) Applicable to piping with a minimum of defects.

This characteristic correlates with ease of application. No Coating is perfect, and this is why cathodic protection is required. Do not buy a pipe coating that has too many holidays (voids in coating) even before it leaves the mill.

D) Adhesion to pipe surface

Coating adhesion is important to eliminate water migration between the metal substrate and the pipe coating. The coating adhesion assures permanence and ability to withstand handling during installation without losing effectiveness

E) Resist development of holidays

Once the coating is buried, two areas that may destroy or degrade coatings are soil stress and environmental contaminants. Soil stress, brought about in certain soil that are alternately wet and dry, creates tremendous forces that may split or cause thin areas. Adhesion, cohesion and tensile strength are important properties to evaluate in order to minimize this problem. The coating's resistance to chemicals, hydrocarbons and acidic or alkaline conditions has been known in order to evaluate performance in known contaminated soils.

F) Handling, Storage and Installation

The ability of a coating to withstand damage is a function of its impact, abrasion and ductile properties. Pipe coatings are subjected to a great deal of handling from propper handling, shipping and stockpiling are recommended, coatings vary in their ability to resist damage. Outside storage requires resistance to ultraviolet rays and temperature changes. These properties must be evaluated to assure proper performance.

G) Constant Electrical resistivity

Since corrosion is an electrochemical reaction, a coating with a high electrical resistance over the life of the system is important. The percentage of initial resistance drop is not an indicative of the pipe coating quality as the overall level of electrical resistivity.

H) Resistant to Disbonding

Since most pipelines are eventually cathodically protected, it is necessary for the coating to withstand cathodic disbondment. The amount of cathodic protection is directly proportional to the quality and integrity of the coating. Cathodic protection does two things. First it drives water through a coatng that would ordinarily resist penetration. It also may produce hydrogen at the metal surface where current reaches it, and the hydrogen break the bond between the coating and metal surface. No coating is completely resistant to damage by cathodic protection, but it is very important to choose a coating that minimizes these effects.

I Ease of repair

Recognizing that some damage may be occure and that the weld area must be field coated, compatible field materials are required to make repairs and complete the coating after welding. Manufacturers' recommendations should be followed. Variable in conditions influence selection of materials.

All nine of these characteristics (A-I) are important when evaluating the selection of a pipe coating

The following factors should also be considered when selecting a pipe coating:

1 Type of Soil or Backfill

Soil Conditions and backfill influence the coating system selected and thickness specified . Soils are rated by thier shrink-swell factor (soil stress). High shrink-swell soils can damage conventional coatings. Ideally, trenches should be free of projections and rocks, permitting the coating to bear on smooth surface. When backfilling, rock and debris should not strike the pipe coating.

2 Accessibility of Pipeline

When a pipelene is inaccessible or in a marine evironment , the best system should be selected with less emphasis on initial cost. Experience under similar conditions for at least five years or will designed laboratory tests on new products are the best criteria for coating selection.

3 Operating Temperature of Piping

Surface temperature and environmental conditions must be considered, because, once buried, a coating experiences a wet heat condition, which is more detrimental than dry heat and have coating effectiveness. A modified disbondment test, " Cathodic Diabonding fo Pipeline Coatings " determines resistance to elevated temperature.

4 Ambient Temperatures During Construction and Installation.

Temperatures during construction and installation are often more critical than operating temperature. For instance, some thermoplastic systems such as mastics, tapes, or enamels may become brittle in freezing temperature. Above recommended operating temperatures, thermoplastic systems may be cold flow. Extra care in handling, transport and storage is needed under extreme conditions.

5 Geographical and Physical Location

Pipe source and coating plant location often determines the coating or area cost factor in selection. Severe environments, such as river crossing, pipe inside casings, exceptionally corrosive soils, high soil stress area and rocky conditions require special consideration. On large projects in remote areas the economics may favor a railhead or field coating site.

6 Handling and Storage

Handling shipping and stock piling are important in the selection process. Some coatings require special handling and padding. All require careful handling.

Most underground coatings are not designed for above ground use and are affected by excessive above ground storage. Coal tar asphalt enamel and mastic coatings are protected from ultraviolet deterioration by whitewash or kraft paper. In polyethylene, the addition of 2.5 percent carbon black is the most satisfactory

deterrent. Stock should be rotated, first - in, first - out, to minimize the potential problem. Long term storage requirement could determine coating selection.

7 Costs

Evaluating of pipe coating properties with the above considerations assist in selection. The most misunderstood factor is " Costs " In pipe coating economics the end has to justify the means. The added cost of coatings and cathodic protection has to pay for itself through reduced operations costs and longer life. "True" protection costs include not only initial costs of coating and cathodic protection but also installation, joint coatings and repairs. Field engineering and facilities to correct possible damage to other underground facilities may add costs.

II Description of Coating Systems.

A) Enamels

Bituminous enamels are formulated from coal tar pitches or petroleum asphalts and have been used as protective coating for over sixty five years. These bituminous enamels are coal tar Enamel and asphalt enamel. These enamels are the corrosion coating, combined with glass and/or felt to obtains mechanical strength for handling. These material should meet the requirements of the National Association of Corrosion Engineers. National Association of Pipe Coating Applicators or The American Water Works Association. Enamel coatings have been the Workhorse coating of the industry and provide efficient long-life corrosion protection.

Bituminous enamel systems may be used within a temperature range of 30°F to 180°F (-1.1°c to 82°c) when temperature fall below 40°F (4.4°c), Precautions should be taken to prevent cracking and disbonding during field installation. Enamels are affected by ultraviolet rays and should be protected by kraft paper or whitewash. Enamels also affected by hydrocarbons. A barrier coat is recommended when contamination exist. This coating is available on all size of pipe. Recently enamel use has declined for the following reasons :-

- Reduced suppliers
- ; Environmental and Health Standard
- Increased acceptance of plastic coating
- Utilization of raw materials as fuel

Pipe should be bare and free of mill coatings for the best surface preparation. Prior to blast cleaning, the pipe is heated to drier off surface moisture and loosen mill scale. Blast cleaning uses sand, steel shot or grit or combination for the desired profile and cleaned surface. Blasting operations remove all rust, scale and other impurities from the surface.

The blast cleaned surface is primed and when dry, coating and wrapping is performed by hot application of bituminous coating.

B) Asphalt Mastic

Asphalt-Mastic pipe coating is a dense mixture of sand, crushed limestone and fiber bound with a selected air-blown asphalt. These

materials are proportioned to secure maximum density of approximately 132 pounds per cubic foot (2.718 Kgs per ltr.) this mastic material is available with various type of asphblts. Selection is based on operation temperature and climatic conditions to obtained maximum flexibility and operating characteristics. This coating is a thick 1/2 " to 5/8 " (1.27 cm to 1.6 cm), extruded mastic resulting in a seamless corrosion coating

Asphalt mastic systems may be designed for installation and use within are operating temperature range of 40^{o}F to 190^{o}F (4.4^{o}c to 88^{o}c). Precautions should be taken when handling in freezing temperatures. Whitewash protects it from ultraviolet rays, and this should be maintained when in storage. This system is not for aboveground or in hydrocarbon-contaminated soils. This coating is available on $4\frac{1}{2}$ " to 48 " (11.4 cm to 122 cm) pipe

The application procedure is as follows. Prior to blast cleaning, the pipe is heated to drive off surface moisture and loosen mill scale. A combination of shot and grit removes all rust, scale and other impurities to the standard clean of SSPC-SP 6 to SSPC-SP 10 . Pipe is then spray coated with asphalt primer prior to extrusions of the hot mastic mixed to the circumference of the pipe. The extrusion forms a seamless coating bounded to the pipe. The whitewash is applied to reflect the sun's rays and to facilities stockpiling .

C) Extruded Plastics - Polyethylene and Polypropylene

There are two systems available . One is an extruded polyethylene sleeve, shrunk over a 10-mil asphalt mastic. The other is a dual extrusion where a butyl adhesive is extruded onto the blast-Cleaned pipe following by multiple fused layer of polyethylene. The latter utilizes multiple extruders in proprietary method, which obtain maximum bond with minimum stress. The sleeve type is available on 1/2 " through 24 " (1.3 cm through 61 cm) pipes, while the dual extrusion is presently available on 2 $\frac{1}{2}$ " through 103 " (6.35 cm through 262 cm) pipe. The operating temperature range for polyethylene system is from - 40°F to 180°F (-40°c to 82°c) and for polypropylene it is -5°F to 190°F (-21°c to 88°c). Polyethylene systems have been successfully field bent (1.9° per pipe diameter length), at-40°F (-40°c). Swelling may be occur in hydrocarbon environments. Polyethylene has excellent dielectric strength. With proper selection of polyethylene resins and addition of 2 $\frac{1}{2}$ % carbon black, a dual extrusion system has withstood long-term above ground storage and above ground use.

Application methods follow : Both method preheat bare pipe prior to grit blast cleaning to a commercial (SSPC-SP6) blast clean with sleeve type coating, the adhesive under coating is applied by flood- coating the hot material over the pipe before it pass through an adjustable wiper ring that control thickness. After mastic is applied, the pipe pass through the centre of the crosshead die where plastic is extruded in a cone shape around

the pipe. Immediately the plastic is water, quenched to shrink around the undercoating and pipe. Following electrical inspection, pipe ends are trimmed for cut back, and the coated pipe is stockpiled.

In the dual extusion system, the cleaned pipe is rotated at a calibrated rate. The first of two extruders applied a film of butyl adhesive of predetermine width and thickness, fusing the film to the rotating pipe in two layers. While the butyl is still molten, high molecular weight polyethylene is applied form the second extruder in multiple layers of a predetermined thickness. producing a bonded coating 50 to 100 mill thick. Water quenching, electrical inspection, and cut back in complete prior to stockpeling.

Polyethylene systems have been in used in Europe for approximately fifteen years with both crosshead and side extrusion methods. In addition to the butyl adhesive or asphalt mastic adhesive, some system use polypropylene copolymer adhesive. This System require high temperature (200°c or 392°F) heating for application of the adhesive.

D. Fusion-Bonded Thermosetting Powder Resins

These coatings are applied to preheated pipe surfaces 400°F to 500°F (204°c to 260°c) with or without primers. On some resins pose-curing is required. This coating is applied in 12 to 25 mil thickness. The fusion-bonded powder coatings have good mechanical and physical properties and may be used above or below ground. On above ground installations, to eliminate chalking and to maximize service life, topcoat with a urethane paint. of all the

pipe coating systems, the fusion-bonded thermosetting resin systems are the most resistant to hydrocarbons, acids and alkaline

These coatings are available in 3/4 " - 43 " (1.9 cm - 122 cm) diameter pipe.

Thermal-bonded powder resins require great care to apply them properly. Prior to cleaning, pipe is heated to remove moisture and loosen mil scale. It is necessary to clean the surface to a near-white metal finish as define in SSPC-SP 10

The pipe is heated uniformly to the recommended application temperature ($400^{o}F$ - $500^{o}F$/$204^{o}c$ - $260^{o}c$.) If primer is required there are minimum overcoat times. Powder resin is applied by electrostatic deposition to a 12 - 25 mil thickness.

Certain resins required post-heat treatment for proper cure inspection by a minimum of 100 volts per mill of thickness is recommended.

E.) Liquid Epoxy and Phenolics.

There are many liquid systems available that cure by heat and/or chemical reaction, some are solvent types and other are 100 % solids. Their use is mostly in larger diameter pipes where conventional systems may not be available or where the may offer better resistance to operating temperatures in $200^{o}F$ ($93^{o}c$) range.

Generally epoxies have an amine or polyamide curing agent and require a near-white blast cleaned surface SSPC-SP 10. coal tar epoxies have coal tar pitch added to the epoxy resin. A coal

tar epoxy cured with a low molecular weight amine is specially resistant to an alkaline environment such as occure on a cathodically protected structure some coal tar epoxies become brittle when expose to sunlight.

For a mill-applied system the pipe is place on coating rollers mounted on a tracked dolly that automatically feeds the pipe in to agrit blasting machine. It is cleaned inside and out. Then it is transfered into a spray booth when the interior and exterior can be simultaneously coated with two separate spray coat to provide a dry film thickness of 12 mils, after which the coated pipe is subjected to hot air blowers for proper curing prior to inspection at 100 volts permill.

F.) Mill Applied Tape Coating Systems

For normal construction conditions, prefabricated applied tapes are applied as a three layer system consisting of primer, corrosion preventive tape (inner layer) and a mechanical protective tape (outer layer) This system is available on 2 " Through 120 " pipe and is recommended for temperature up to 140°F (60°c.) but there are tape systems presently available for temperature up to 200°F (93°c). The primer's function is to Provide a bonding medium between the pipe surface and the adhesive or sealant on the inner layer. The inner layer tape consist of a plastic backing and adhesive. This layer protects aginst corrosion, so it has to provide a high electrical resistivity and low moisture absorption and permeability along with are effective bond to the primed steel. It is always a minimum thickness of 15 mils, with the total

system a minimum of 40 mils. The outer layer tape consist of a plastic film and adhesive of the same types of materials used in the inner layer tape. The purpose of the outer layer tape is to provide mechanical protection to the inner layer tape and also to be resistant to the elements during outdoor storage. The outer layer tape is always a minimum of 25 mils.

Bare pipe is heated prior to blast cleaning to remove moisture and loosen mill scale. Abrasive blast cleaning is used to obtain SSPC-SP 6. A quick-drying primer is applied to the blast cleaned pipe surface at a coverage of approximately one gallon per eight squares of tape applied. The inner-wrap tape is applied over dry primer with proper mechanical equipment that applied the inner layer to the pipe under tension (10 lbs per inch of width minimum), resulting in a tight, wrinkle-free coating. The spiral overlap should be approximately on inch. The outer-wrap tape is simultaneously applied under tension (12-14 lbs, per inch of width minimum) to obtain a tight wrinkle-free coating. The laps of the inner and outer wraps should not be on top of each other, but should be staggered.

Polyvinyl, polyethylene and coal tar tape are widely used for joint coating protection of for odd shapes or bends or milled applied applications.

G.) Wax Coatings

Wax coatings are used on limited basis. Microcrystalline wax coatings are usually used with a plastic over wrap. Wax

waterproofs the pipe and the wrapper protects the wax coating from contact with the soil and afford some mechanical protection. The most popular use of wax coating is the over-the-ditch application with a combination machine that cleans, coats wraps and lowers into the ditch in one operation.

B.) Polyurethane Foam Insulation

This is a system controlling heat transfer in above ground, below ground, and marine pipelines. While generally used with a corrosion coating, if the proper moisture vapor barrier is used over the urethane foam, effective corrosion protection is obtained. This is a plant applied process where the carrier pipe is centered within the outer jacket, which contains and molds the foam as well as provides effective moisture vapor barrier. Metered quantities of foam components are rapidly introduced between the carrier pipe and the outer jacket. The foam is restrained by end caps and rises on a first basis forming a uniform composite unit. When properly jacketed, usually with polyethylene or coated steel, the system is moistured and corrosion-resistance, sufficiently strong to resist crushing, and flexible enough to permit allowable fieldbending.

1.) Concrete

Mortar lining and coating has the longest history of protecting steel or wrought iron from corrosion when steel is encased in concrete, a protective iron oxide film forms. As long as the alkalinity is maintained and the concrete is impermeable to chlorides and oxygen, corrosion protection is obtained.

Today, Concrete as corrosion coating is limited to internal lining. The external application is applied over a corrosion coating for armor protection and negative bouyancy in marine environments. A Continuous reinforced concreate coating has proved to be the most effectively controlled method.

IV Application Specification .

A.) Selection of Application

A major cause fo pipeline coating failure is improper application. A quality material poorly applied is of little value and the quality of a pipe coating is only as good as the quality of application. To assist in evaluation of an applicator, the following points should be considered

1. Experience

2. Reputation .

This is an asset earned by consistent performance Not only good quality work but also solving problems and correcting mistakes help to develop a reputation.

3. Realiability .

There are many Variables in application of coatings. A realiable work force, well maintained equipment and consistent quality performance are prerequisites for an applicator

4. Conformance to Coating Manufacturer's Specification

The manufacturer's established minimum specifications for application of materials should be met.

5. Modern, Automated Equipment.

Capital expenditure on automated application equipment is an important part of the success of pipe coatings. Elimination of human errors through automation and controls continues to be an important factor in improved pipe coatings.

6. Quality Control

Knowledge of applicator's quality control procedures on materials, application, and finish product is essential in the selection of an applicator.

B.) Inspection Procedures

The good inspection is on important part of the quality installation. Inspection should begin with stockpile of bare pipe through coating operations, load out, coated pipe stockpile, field inspection, joint coating procedure and back fill of coated pipe. Knowledge of the coating syetem, plant facilitiex, quality control methods, shipping requirements, handling, joint coating, field conditions, field holiday detection and repair are requirement for proper installation. Experience and common sense in inter pretation of specification and analysis of test result will contribute to obtaining the best possible coating results.

C.) Coating Evaluation

The American Society of Testing and Materials (ASTM), National Association of corrosion Engineers (NACE), and the American Water Works Association (AWWA) have developed standard test

for pipe coating. Eleven standard test methods are now available from ASTM, which were developed in conjuction with the American Gas Association. A summary of these test procedures are as the following:

1. Physical and Mechanical Test.

   a. Abrasion Resistance of Pipeline Coatings.

   b. Bendability of pipeline coating

   c. Impact Resistance of Pipeline coatings (Limestone Drop Test)

   d. Impact Resistance of Pipeline coatings (Falling weight Test)

   e. Penetration Resistance of Pipeline Coatings.

2. Electrical and Electrochemical Tests.

   a. Cathodic Disbonding of Pipeline Coatings

   It is an accellerated test for measuring the rate of coating damage and adhesion-loss caused by the application of cathodic protection to holidays in coated pipe.

   b. Water Penetration into pipeline Coatings.

   It is a method for measuring the rate and approximate depth of water absorption by a coating.

   c. Test for Joints, Fitting and Patches in Coated Pipelines.

   It is an adaptation of the water Penetration Test to evaluate patch and joint performance.

   d. Disbonding Characteristics of Pipeline Coating by Direct Soil Burial.

It is a method for measuring the cathodic disbonding of pipeline by using soil as the electrolyte.

3. Chemical and Atmospheric Tests.

a. Effect of Outdoor Weathering Pipeline Coatings.

It is a standard procedure for exposing coated pipe samples to local atmospheric conditions. The Controlled exposure period permits subsequent evaluation for ultraviolit deterioration disbondment, loss of impact resistance, or other pertinent characteristics.

b. Chemical Resistance of Pipeline Coatings

It is a standard method for evaluating the deterioration of coating properties after exposure to chemical liquids and their vapors.

D.) Summary

It is not easy to select the best systems to meet any given environment or soil condition. Knowledge of operation and installation conditions is the begining of the process. Steel source and job. location may limit the coatings available to each project. Selection of a quality applicator is the most important consideration and frequently is the most neglected. Following coating and applicator selection, inspection at the coating mill and especially on the job site during construction will go far in assuring that a high quality pipe coating system has been installed.

PRESERVATION OF SHIP'S HULL

BY

COMMANDER MANA NAKNAEWDEE

RTN DOCKYARD PON PRACHUL

THAILAND

ABSTRACT

The operational readiness of a modern, technologically sophisticated fleet is of paramount importance to the defense of our nation. Preservation of ship's hull comprise a key element in the maintenance program required to achieve and retain this readiness

The Royal Thai Navy is committed to providing this protection in the most reliable and cost effective manner available. This is being achieved through an active program (1) pursue paper about corrosion and protection (2) develope procedure about prevention,protection and control ship's hull corosion (3) find the principle to assign process that use to repair the ship's hull (Painting System Selection).

This paper mainly describes RTN Dockyard PomPrachul' experiences with regard to select painting system for fleet of Royal Thai Navy.

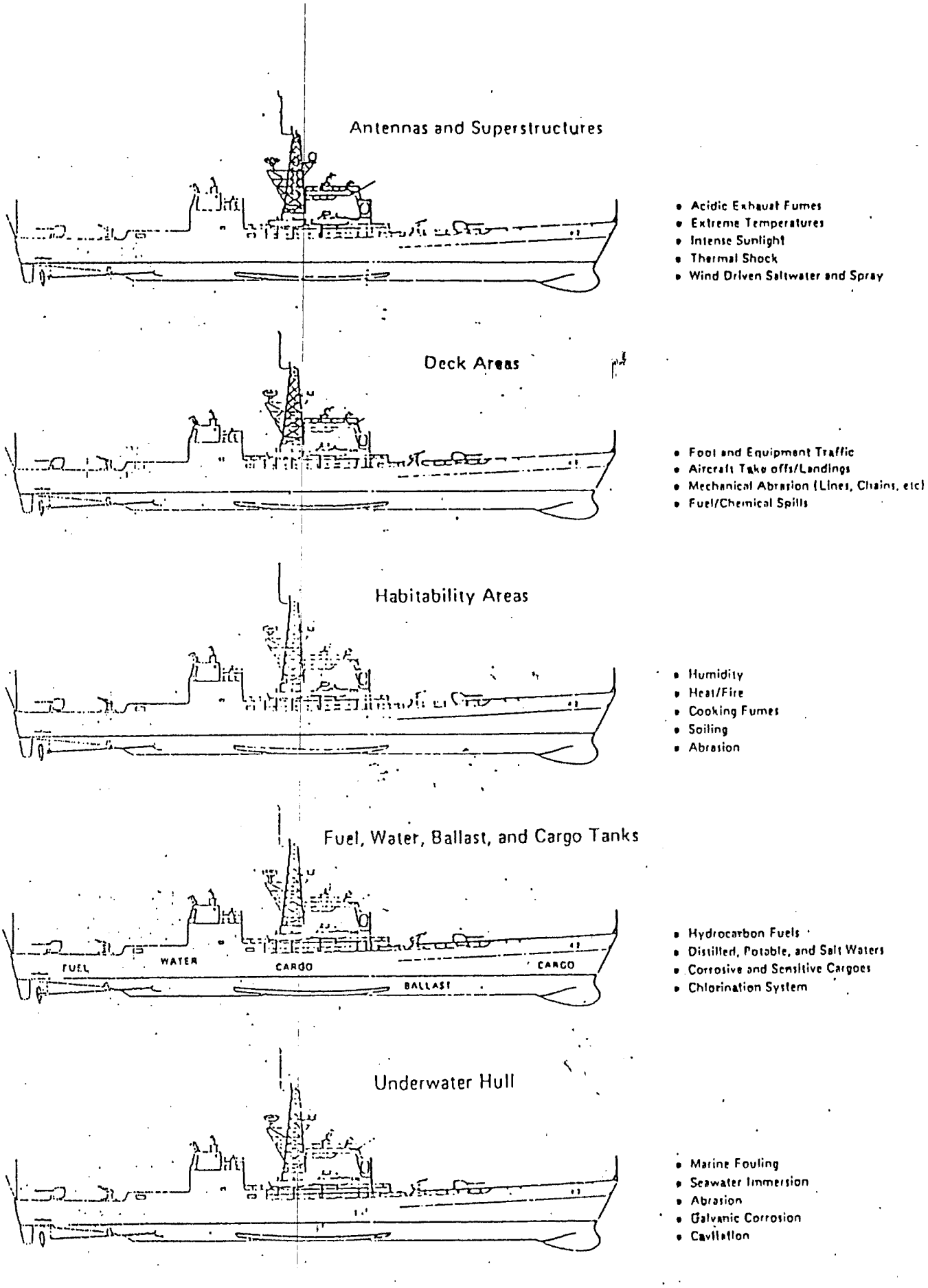

FIGURE 1
Environments that are destructive to shipboard coatings.

1. INTRODUCTION

Coated surfaces on Navy ships are subjected, as shown in figure 1, to a variety of destructive conditions (e.g., a salt laden, high humidity atmosphere; total seawater immersion; and acidic exhaust gases) with temperatures ranging from those of the tropics to those of the Arctic. They must be resistant to physical damage from such forces as cavitation, drag (friction), impact with waves and mooring structures, and abrasion by chains. Each coating system must adhere tightly to the particular substrate (ferrous and nonferrous metals, wood, plastics, and elastometers) to which it is applied, and it must resist deterioration from a varitety of chemicals (e.g., distilled, potable, and salt water, hydrocarbon fuels and lubricants; and sanitary wastes) In addition, antifouling coatings must prevent the attachment and growth of marine organisms on immersed surfaces. These organisms increase frictioal drag, which results in loss of speed and maneuverability and increased fuel consumption. Fouling may also promote localized corrosion, damage to coatings, reduced buyoyancy, and inoperable equipment. Thus, ships of the Navy require a combination of versatile and speciallzed coatings to meet many differint requirements to keep them operational. Many of these coatings may also prove to be as cost effective on commercial ships as on those of the Navy.

Environment that are destructive to shipboard coatings

1. Antennas and Superstructure
   - 1.1 Acidic Exhaust Fumes
   - 1.2 Extreme Temperature
   - 1.3 Intense Sunlight
   - 1.4 Wind Driven Saltwater and Spray
2. Deck areas
   - 2.1 Foot and Equipment Traffic
   - 2.2 Aircaft ake offs / Landing
   - 2.3 Mechanical Abrasion (Line, Chains, etc)

2.4 Fuel, Chemical Spills

3. Habitability areas

3.1 Humidety

3.2 Heat/Fire/Cooking Fumes

3.3 Soiling

3.4 Abrasion

4. Fuel,Water,Ballast and Cargo Tanks

4.1 Hydrocarbon fuel

4.2 Distilled, Patable and Salt waters

4.3 Corrosive and Sensitive Cargoes

4.4 Chlorination System

5. Underwater hull

5.1 Marine Fouling

5.2 Seawater Immersion

5.3 Abrasion

5.4 Galvanic Corrosion

5.5 Gavitation

2. BACKGROUND

Coating materials and techniques utilized by the Navy have generally changed in much the same manner as those of the commercial sector. Prior to World War 2, most of the maintenance painting was done by sailors using chipping hammers and other hand tools to clean steed surfaces and drushes to aply drying oil (e.g., alkyd) paints. Since that time both cleaning and application techniques and coating materials have improved greatly. All shipyard and maintenance depot painting is done by civilian (civil service or contractor) personnel who clean steel surfaces to a near white blast (SSPC.SP 10) with automated equlpment wherever possible to reduce emission of particulates, and apply coatings with modern spray equipment. The everyday maintenance painting is still accomplished by less experienced ship personnel.

In the last forty years, paints used on Navy ships have changed from the drying oil (alkyd) formulations, such as Navy Formula 1(1944), of the early forties to vinyls, such as Navy Formula 119, of the early fifties to epoxies, such as MIL-P-23236 (1982) currently in use today. The drying oil paints were relatively easy to aply since they did not require a high not require a high level of surface preparation, but they had limited resistance to marine service. The vinyl paints were much more durable, but they required a higher level of surface preparation and more coats to achieve a desired thickness. The epoxies have proved to be more cost effective in that, even though they still require a relatively high level of surface preparation and should be applied at temperatures above 60 ° F,they provide a very durable barrier in fewer coats.

Maintenance painting of ships in service is covered in great detail in Navy Ships Technical Manual, Chapter 9190.* This document provides information on when to paint, surface preparation, frequency of repainting and thickness of paint films, coatings to be used, and application procedures. Touching-up by currently recommended practices is emphasized. Strict safety precautions meeting all governmental reguiations are specified for painting operations. Chapter 9190 also provides information on cathodic protection of ships.

3. ENVIRONMENTAL ZONE

General Considerations. Because of the wide diversity of available systems, the adverse conditions under which they must. sometimes be applied, environmental testrictions, and the need for minimizing maintenance, the choice of a suitable painting system is not always an easy one. There is, of course, no one "best" painting system, but rather a dynamic competition among alternative materials and methods whose choice often depends both upon technological factors and pollcy considerations.

Since environmental factors are often to dominant ones, they will be considered here first, followed by other important considerations such as cost, appearance, and design.

Effects of Environment on Corrosion Rates. Among the technological factors in the choice of a painting system, environment is usually the controlling one. For example, one rule of thumb advocates that steel need not be painted at all when the corrosion rate is uniform and below a certain level; when the environment is too severe, on the other hand, alternative materials of construction should be considered instead of painting.

Environmental Zone Chart. illustrates the "environmental zone" concept of SSPC. it suggests painting systems for consideration in rural, urban, commercial, and marine environments and in several special exposures. Usse of the term "environmental zone" in this context is not meant to parallel the common meaning of the term, which implies geographical location but, rather, defines the type of environment (atmosphere) to which the coated steel will be exposed. As an example of this more specialized meaning of environmental zone, consider a steel framed building, part of which is devoted to office space, and another part of which is devoted to chemical laboratory and pilot plant space where acidic fumes are frequently generated. Each of these areas is exposed to a significantly different environment. Another example is the roadway and superstructure of a bridge located in a geographical area where freezing and road salt use are common. The upper portions of such a bridge to be protected simply against weather exposure, whereas the roadway steel and adjacent structural components must be protected against de-icing salt in solution.

For purposes of classifying environmental exposures according to their severity., they have been divided into environmental zones from essentially non-corrosive dry interiors - Zone 0 - to severe chemical exposurers - Zone 3. Special conditions are listed in Table 1. Exposure conditions may be such as to require little or no protection by painting; conversely, they may indicated the need for elaborate surface preparation, pretreatment, and properly selected primer, intermediate, and finish coats, and finish coats.

Table 1. includes a concise description of each environmental zone together with typical painting system(s) recommended for minimum performance. More durable systems may be used, of course, to achieve better performance or longer coating life within any one environmental zone.

This classification of environment is probably the most useful type of designation, since most available data on paint exposures is defined in these broad terms. The SSPC is also investigating a more precise environmental classification in terms of time-of-wetness, chioride level, sulfur dioxided content, pH, conductivity, surface contamination, etc.

In Table 1, Painting System numbers have been rounded off to show the generic class of systems that are satisfactory. For example, SSPC-PS 4 includes Painting System Guide 4.00 and Painting System Specifications SSPC-PS 4.01 through 4.05.

Such guides as Table 3 arte intended to aid the specifier in selecting a painting system (including surface preparation, coatings, and application) but are, of course, no substitute for the knowledge and judgment entailed in an intelligent choice.

Influence of Geographical Locations on Environmental Zones:

Inland, rural locations, far from coastal salt water, are free from the corrosive influence of airborne salt. The presumption that the atmosphere in these areas, located far from centers of heavy industry, are therefore "virtually unpolluted," has been drastically reversed. It is now seen that even rural locations, hundreds of miles distant from industrial plants and electrical power generating stations, can sometimes be subjected to acid rain generated by sulfur dioxied emissions. Rain water with a pH as low as 3-4 has been observed not only in rural, but also in wilderness locations. Thierefore, preparers of painting system specifications must now cultivate a realistic awareness of present atmospheric conditions prevailing in rural locations that were traditionally considered bening with respect to corrosion of steel.

Heavy industrial environments, such as those involving coke plants, are severe enough to be classified in the chemical category. These environments are marked by reduced paint life and high corroaion rates.

Marine atmosphere is typiffied by frequent and relatively high concentrations of salt mist, but it does not imply direct contact with salt spray or splashing waves; it contains a high concentration of chlorides in contrast to the high concentration of sulphur dioxide in the industrial atmosphere.

Fresh and salt water immersion have important differences because of osmotic and electrolytic effects.

Alternative immersion refers to frequent, perhaps fairly long immersion in water alternated with exposure to the atmosphere above the water - for example, the boottopping area of a ship's hull, or steel in the tidal range.

Condensation and high humidity exposure refers to almost continuous condensation; exposure to high humidity alone (with little or infrequent condensation) is not considered to be in this class of exposure.

Chemical environments are those in which strong concentrations of highly corrosive gases, fumes, or chemicals - either in solution, or as concentrated liquids or solids - contact the surface. The severity of exposure may vary tremendously from mild concentration in a yard area to direct immersion in the chemical substance.

Underground refers to buried surfaces in direct contact with the soil, which may be high in salinity or acidity.

It should be understood that surfaces presumed to be exposed to the weather are indeed open to the elements. Structures open to pollution, but sheltered from rain, are particulaary vulnerable.

Special Service Requirements. Some painting systems for special services, including resistance to abrasion, fouling, graffiti, mildew, and skidding are listed in Table 2

Table 1

TYPICAL SSPC PAINTING SYSTEMS FOR ENVIRONMENTAL ZONES

Environmental Zone	Zone Conditions
0	Dry interiors where structural steel is imbedded in concrete, encased in masonry, or protected by membrane or non-corrosive contact type fireproofing
1A	Interior,normally dry (or temporary protection) Very mild (oil base paints now last ten years or more).
1B	Exteriors, normally dry (includes most areas where oil base paints now last six years or more).
2A	Frequently wet by fresh water. involves condensation, splash, spray or frequent immersion.(oil base paints now last 5 years or less.)
2B	Frequently wet by fresh water. involves condensation, splash, spray or frequent immersion.(oil base paints now last 3 years or less.)
2C	Fresh water immersion
2D	Salt water immersion
3A	Chemical exprosure, acidic (pH 2.0 to 5.0)
3B	Chemical exprosure, acidic (pH 5.0 to 10.0)
3C	Chemical exprosure, neutral (pH 10.0 to 12.0)
3D	Chemical exprosure, presence of mild solvents. Intermittent contact with aliphatic hydrocarbons (mineral spirits, lower alcohols, glycols,etc.)
3E	Chemical exprosure, severe. Includes oxidizing chemicals, strong solvents,extreme pHs, or combinations of these with high temperatures

Table 2

TYPICAL RECOMMENDATIONS FOR SPECIAL SERVICE CONDITIONS

Type of Service*	Discussion and Recommendations
Abrasion Resistant	Urethane coatings probably have more abrasion resistance per mil than any other generic class. These are available as proprietary materials. Expoxies such as madified SSPC-PS 13 can be specially formulated so that removal, even by blast cleaning, is difficult, especially when they are sand reinforced. Zinc-rich coatings, such as SSPC-PS 12, especially the ignorganic types, tend to"polish"and not abrade off steel surfaces Coal tar epoxy paints, such as SSPC-PS 11, or selected proprietary products, especially when reinforced with garnet or other hard 30 to 70 mesh materials. Sand reinforcement in SSPC-PS 2,3,4,10,11,or13 Gravel, sand, slate granules in SSPC-PS 9 or 10
Anti-Sweat	Preformed plastic and foam spray have superseded paints for most anti-sweat functions.
Anti-fouling	These paints are covered in SSPC-PS 19 and in Volume 1 of the Steel Structures Painting Council Manual.
Graffiti Resistant	SEE SSPC-PS 17 and polyester urethane guides with recommended ratios of polyol, isocyanate, and NCO.
Skid Resistant	Any type of paint that is suitable for application on floors can be converted to a specifically skid resistant pain by incorporation of a finely divided material such as silica, aluminum oxide, or ground shells.
Mildew Resistant	1. Wash with phosphate-free detergent. 2. Rinse with sodium hypochlorite solution (Hilex, Clorox, Purex, etc.) and allow to dry without rinsing. 3. use a paint suitable for specific and exposure.
Piping	Color codes for identifying piping are given in ANSI A13.1 1975, "Piping and Piping Systems."
Safety Colors	Standards for safety colors are given in ANSI Z53.1-1979, "Color Coding."

4. ASSIGN THE SHIP'S AREA BY ENVIRONMENT ZONE

SHIP 'S AREA	ENVIRONMENT ZONES	SPECIAL CONDITIONS
1. BOTTOM	2D	FOULING
2. BOOTTOPING	2B	FOULING, ABRASION
3. TOP SIDE	2B	LIGHT,RAIN,ABRASION
4. DECK	1B	LIGHT,ABRASION,SKID
5. EXTERNAL SUPERSTRUCTURE	1B	LIGHT,RAIN,COLOR
6. INTERNAL SUPERSTRUCTURE	1A	CLEAN,COLOR

5. PAINTING SYSTEM

A term intended to include, with equal emphasis, not only the well accepted components of a system such as surface preparation and paint materials, but also the application, inspection, and safety functions.

Painting System compose of

1. Surface Preparation
2. Standard of Surface Preparation
3. Primer
4. Anticorrosion
5. Intermediate Coat
6. Topcoat

6. PANIT SPECICATION

A form of standard that is a precise statement of a set of requirements to be satisfied by a material.

Example:

1. Zine Rich
2. Vinyl
3. Chlorinated Rubber
4. Bituminus
5. Phenolic
6. Alkyd
7. Epoxy
8. Cool Tar Epoxy
9. Urethane
10. Polyester
11. Miscellaneous

7.PAINTING SYSTEM SELECTION

Although environment is usually the primary factor in the choice of a coating system, other factors such as costs, application, surface preparation, appearance, design, available facillties, and availability of specifications must also be considered.

EXAMPLE

Guide for Selecting Painting Systems for Ship Bottoms

Surface Preparation	Primer	Anticorrosive	Intermediate	Top Coat
Abrasive Blast Cleaned		Bituminus Aluminum Pigmented	Bituminus	Conventional Antifouling
Abrasive Blast Cleaned	Wash Primer	Vinyl 2 or 3 Coated	Vinyl	Vinyl Antifouling
Abrasive Blast Cleaned		Chlorinated Rubber 2 Coated	Chlorinated Rubber	Chlorinated Rubber Antifouling
Abrasive Blasted Cleaned		Coal Tar Epoxy 2 Coated	Vinyl Tar	Vinyl Antifouling or Self Polishing Copolymer
Abrasive Blasted Cleaned		Catalyzed Epoxy 2 Coated	Epoxy Tar	Self Polishing Copolymer

Conclusion

Today to select paint for maintenance our ship will considers painting system more than each paint. We will consider from, Environment, Surface Preparation and first coated (Primer) is dominant

REFERENCES

1. Systems And Specification (Steel Structures Painting Manual) Volume 1 and Volume 2
2. Coatings And Inspection Manual (What, When and How) : Jotun Marine Coating
3. Worldwide Marine Maintenance Manual : International Paint
4. Whatever The Marine Coating Problem, We have got it covered : Sigma Coating
5. Chugoku Product of Quality
6. Service Life Performance of Marine Coatings and Paint System : Journal of Coatings Technology, June 1980, pp. 55-63
7. Performance of Selected Marine Coatings : Journal of Coatings Technology, February 1980, pp. 35-45
8. Coating Systems Guide for Hull, Deck, and Superstructure, : Technical and Research Bulletin 4-10 Society of Naval Architects and Marine Engineers, 1973

CORROSION & PROTECTION

MISS TAVEEPORN KHUMTHONG

Thai Kansai Paint Co.,Ltd.
180 Moo 3, Theparak rd., Amphur Muang, Samutprakarn 10270

Abstract

A number of cars move here and there around every district in the world, which make much difference of weathering, traffic and driving conditions.

Under the circumstances, automotive paint film is requested to protect car body sufficiently from corrosion or to be more upgraded on corrosion resistance.

Herein, we oversee the current market situation of CED paint, which is well-known for automotive anti-corrosive primer, and foresee what direction it will go toward.

In consequence, the applicability of the CED paint to anti-corrosive steels is enhanced and the integrated corrosion resistance of car body can be made dramatically better by not only the paint resin modification but also chemical treatment improvement and steel substrate adjustment.

Presentation of Corrosion Mechanism and Protection Method will be covered following these subjects :

1. Classification and its origin of Automotive Rust
2. Mechanism of Corrosion
3. Regulation of Automotive Rust
4. Protection Method
   - 4.1 Development of material & film performance
   - 4.2 Painting process of automobile
   - 4.3 CED Mechanism
   - 4.4 CED in future

CORROSION AND PROTECTION

AN ARTICLE

BY

MISS TAVEEPORN KHUMTHONG

CORROSION AND PROTECTION

<CONTENTS>

INTRODUCTION

It is greatly required that automotive paints should be provided with not only superb but also widely applicable qualities in the motorization age of today.

Fig.1 shows the briefing on the object of automotive coating. A number of cars. move here and there around every district in the world,which makes much differenceof weathering, traffic and driving conditions.

Under the circumstances,automotive paint film is requested to protect car body sufficiently from corrosion or to be more upgradeed on corrosion resistance.

What is more, we encounter at present the period called the epoch of sense,led by the requirements of personality.Such an epoch calls for further better film appearance, making mantenance of coated film free and R & D of advanced color styling.

That s why the requests for automotive paints qualities are so diversified.

Herein,we oversee the current market situation of CED paint which is well-knownfor automotive anticorrosive primer,and foresee what direction it will go toward

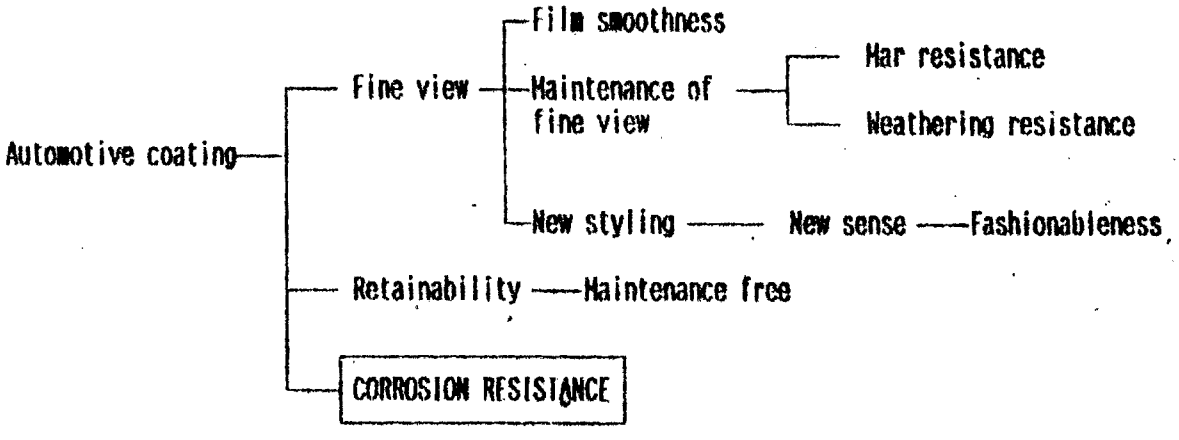

Fig.1 Object of application

The automotive paint market asked for superior corrosion resistance of coating film for autobody and a CED paint could satisfy this demand thoroughly

This market has called upon to improve further a variety of the CED paint qualities since then,however. It is necessary that the first generation CED paint has high anti corrosive property,and as a result,it build up tough film. The tough film leads to bigger-internal stress of film and consequently ,it brings out poor film adhesion, i.e.secondary adhesion after warm water submergence,to zinc-galvanized steel.The adhesion of the CED paint to the Zn-galvanized steel has attracted more considerable concern with the increase of the use of the Zn-galvanized steel for car.

In term of paint quality,it is important to make relaxation of the film internal stress.

The more advantageous manner to do it,is to introduce straight chain molecule into the main-structure of resin incorporated in CED paint.The film defect can be eliminated through this approach of the paint resin modification.

And future trend of CED PAINT ARE DESCRIBED ALSO

CED paint is the most popular for corrosive protection of automotive application.

RUST OF AUTOMOBILE

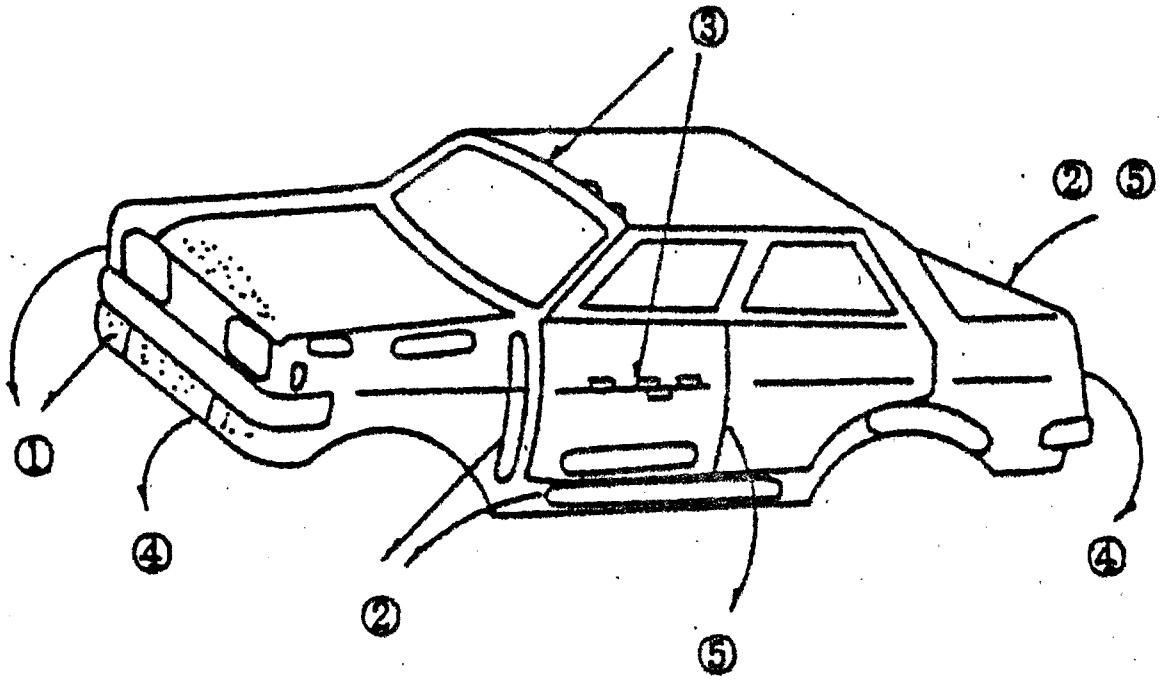

Dry or half dry circumstance	①	Chipping damage and rust
	③	Rust from reinforce fixing place
	⑤	Rust from edge
Wet circumstance	②	Rust from hollow section
	③	Rust from reinforce fixing place
	④	Rust from clearance
	⑤	Rust from edge

CLASIFY OF AUTOMOBILE RUST AND ITS ORIGIN

BODY PART	KIND OF RUST		ORIGIN	
Inner Panel	Gravity Corrosion	Rust from hollow section	Corrosive Reactant	Internal accumulation of water, salt, mud
				Insufficient of pretreatment and film thickness
Outer Panel	Surface Corrosion	Damage by chipping	Damage and corrosion reactant	Damage by clipping stone
				Creepage of rust
			Soft dipping and corrosion reactant	Rust from slightly damage
Overall Body		Rust from clearance	Insufficient corrosion resistant	No treatment and no coating in clearance
		Rust from edge	Interface cutting of substrate	Insufficient of edge-covering Creepage from edge

MECHANISM OF CORROSION

SCAB CORROS. MODEL

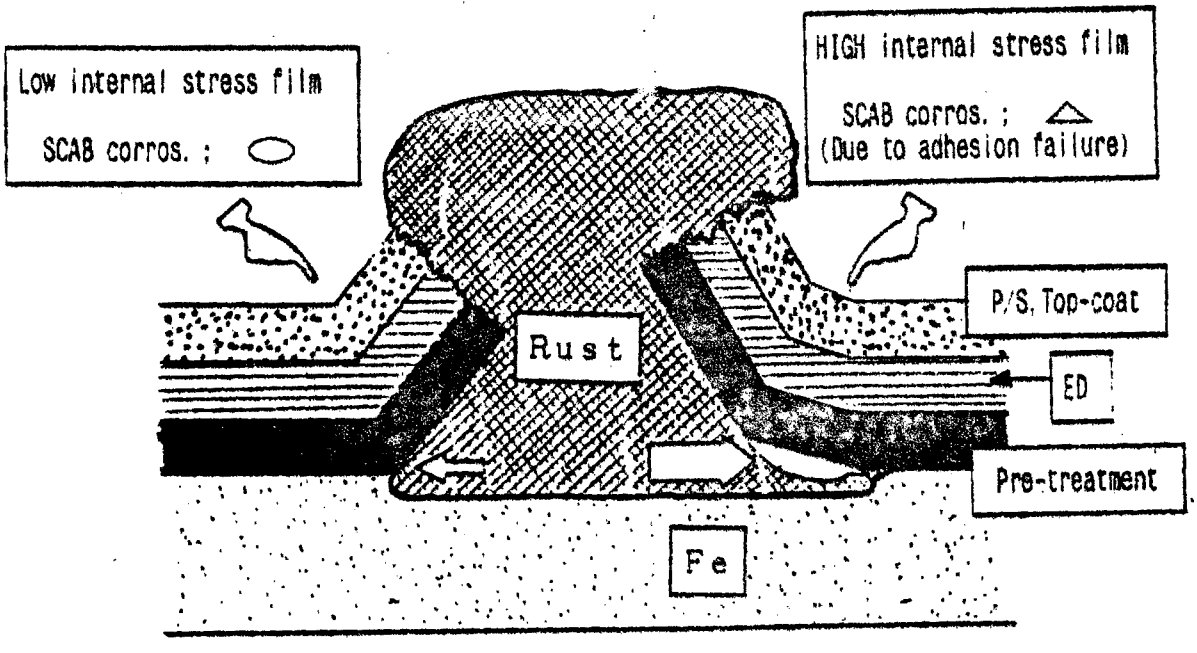

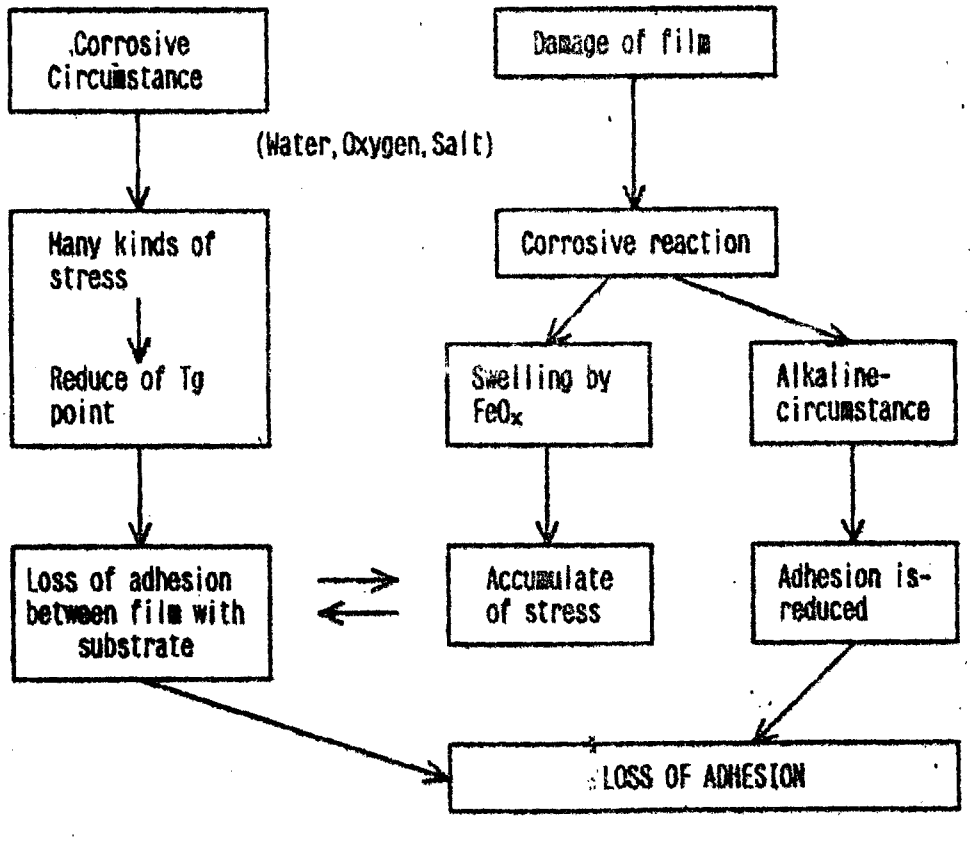

REGULATION OF AUTOMOBILE RUST

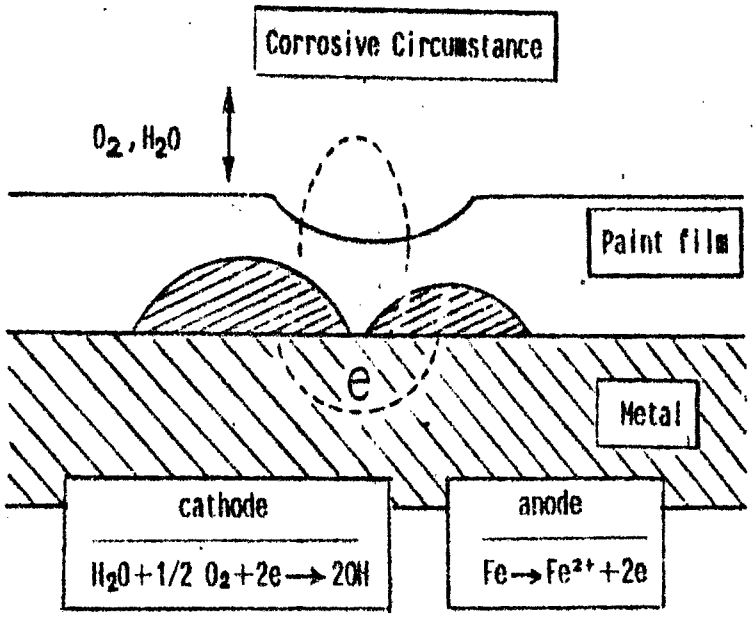

STEP 1 — Circumstance of corrosive reaction

Water accumulation between film with substrate

Corelation film and substrate → Wet Adhesion

STEP 2 — Supply corrosion reactant

Constant supplying of corrosion reactant → Permeability of paint film

STEP 3 — Inhibition of corrosive reaction → Anticorrosive pigment (Inhibitive action)

Film properties

AUTOMOBILE RUST & PROTECTION METHOD

CORROSION TYPE	BODY PART	ORIGIN	PROTECTION
Surface corrosion	Floor Hood, Fender Door, Roof	Damage of film	-Anticorrosive substrate -Dipping pretreatment type -CED PAINT APPLICATION
	Edge	Insufficient covering	-Anti dipping sealer -Stone guard coating -Sufficient film thickness -Edge treatment
Gravity corrosion	-Clearance -Hemming -Hollow section -Body under	Insufficient of-pretreatment	-Anti corrosive substrate -Dipping pretreatment type -CED paint application -Rust proof oil, wax apply -Body shape development
Galvanic corrosion	Interval attached portion	Ion inductive between 2 kind of difference metal	-Dipping pretreatment type -CED PAINT APPLICATION -Spacer application

MATERIAL AND PROCESS MODIFY

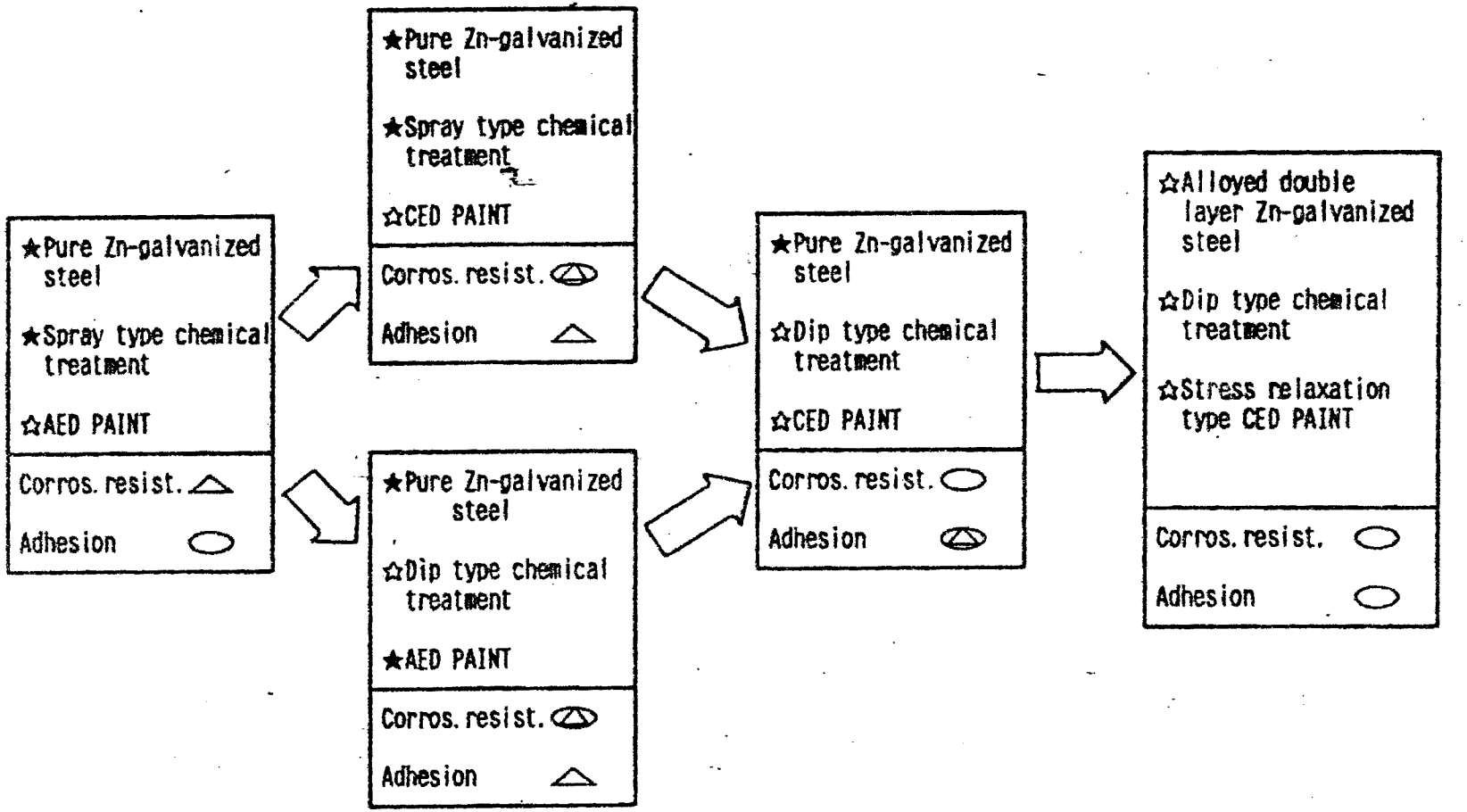

IMPROVEMENT OF CAR BODY PROTECTION

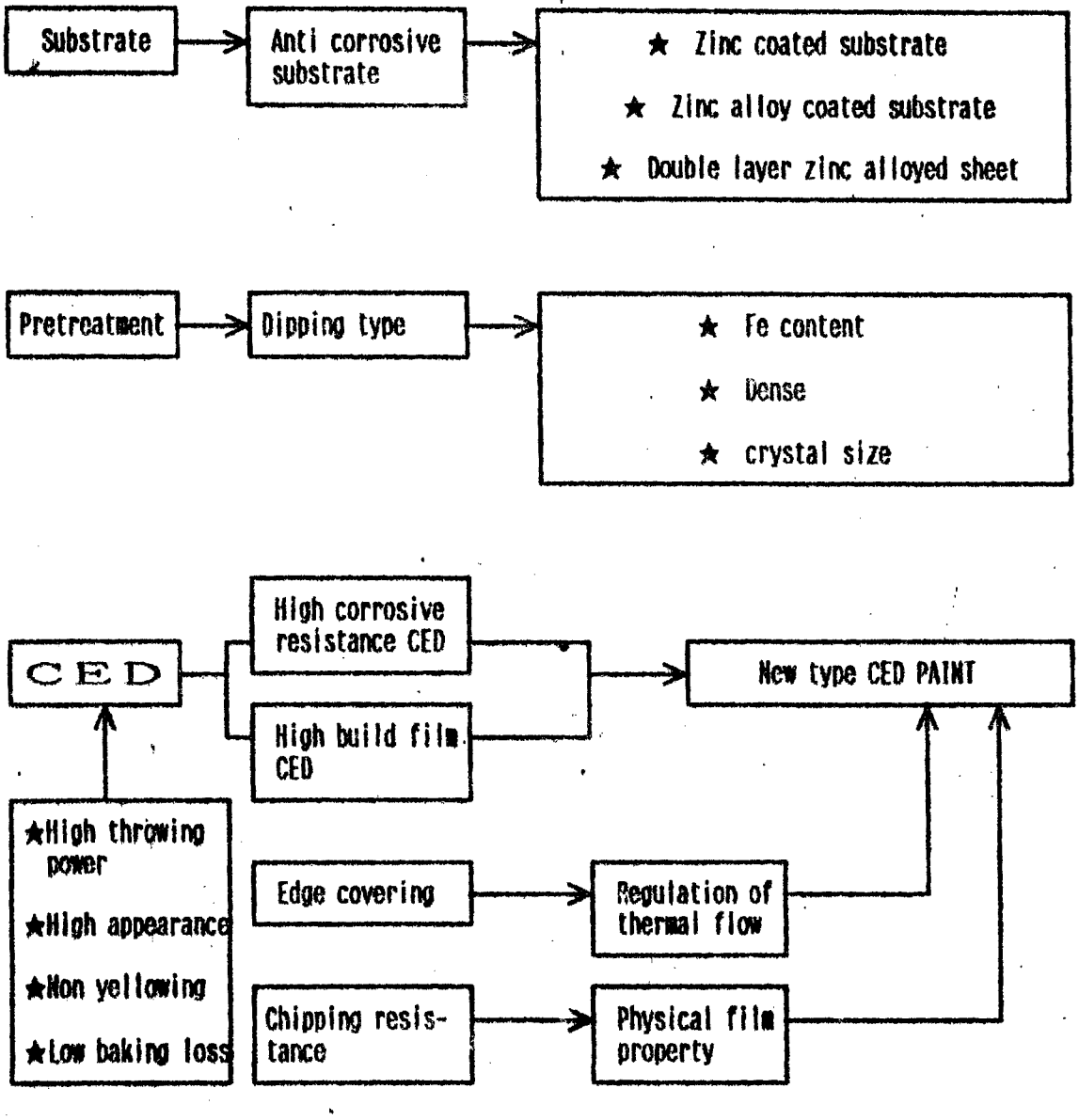

THE MECHANISM OF CATHODIC ED

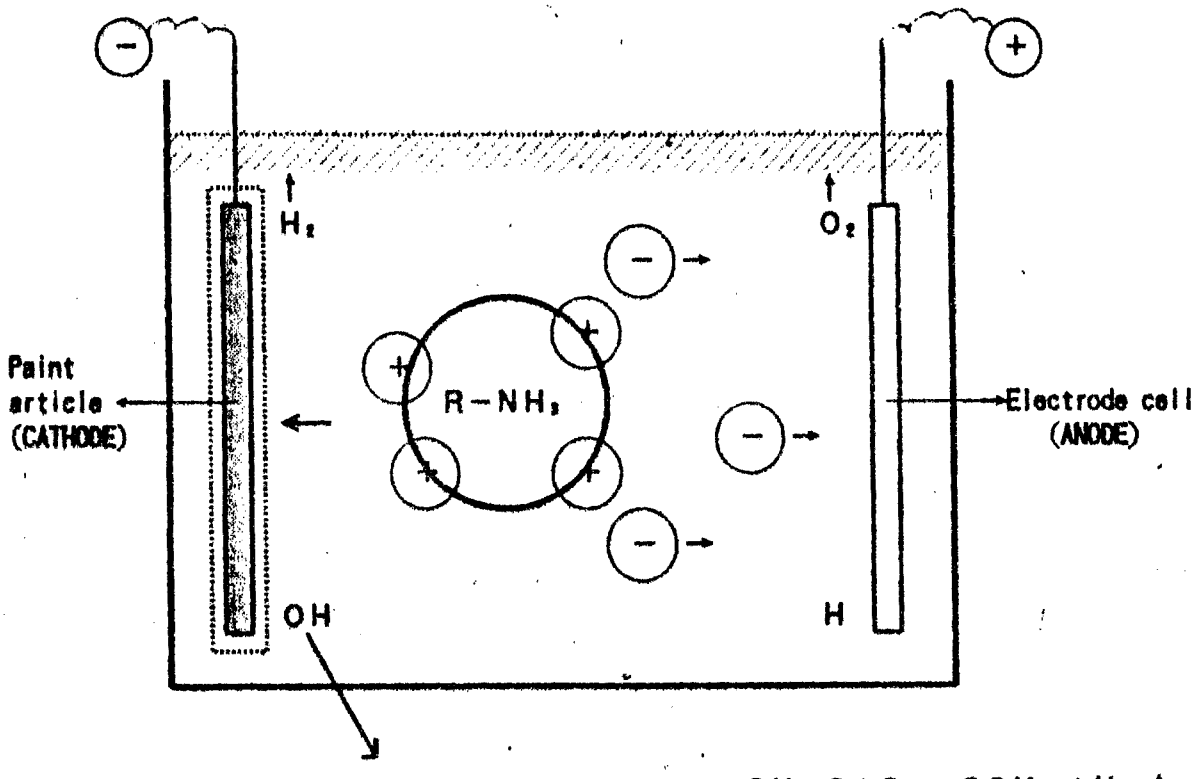

pH UP → Surface of electrode
↓
Loss of electrolicity → Insoluble
↓
Coagulation → Deposit
↓
Making of film

$$2H_2O + 2e \rightarrow 2OH + H_2\uparrow$$

$$R-\overset{|}{\underset{|}{N}}H + OH \rightarrow R-\overset{|}{\underset{|}{N}} + H_2O$$

Insoluble resin

CATHODIC ED IN FUTURE

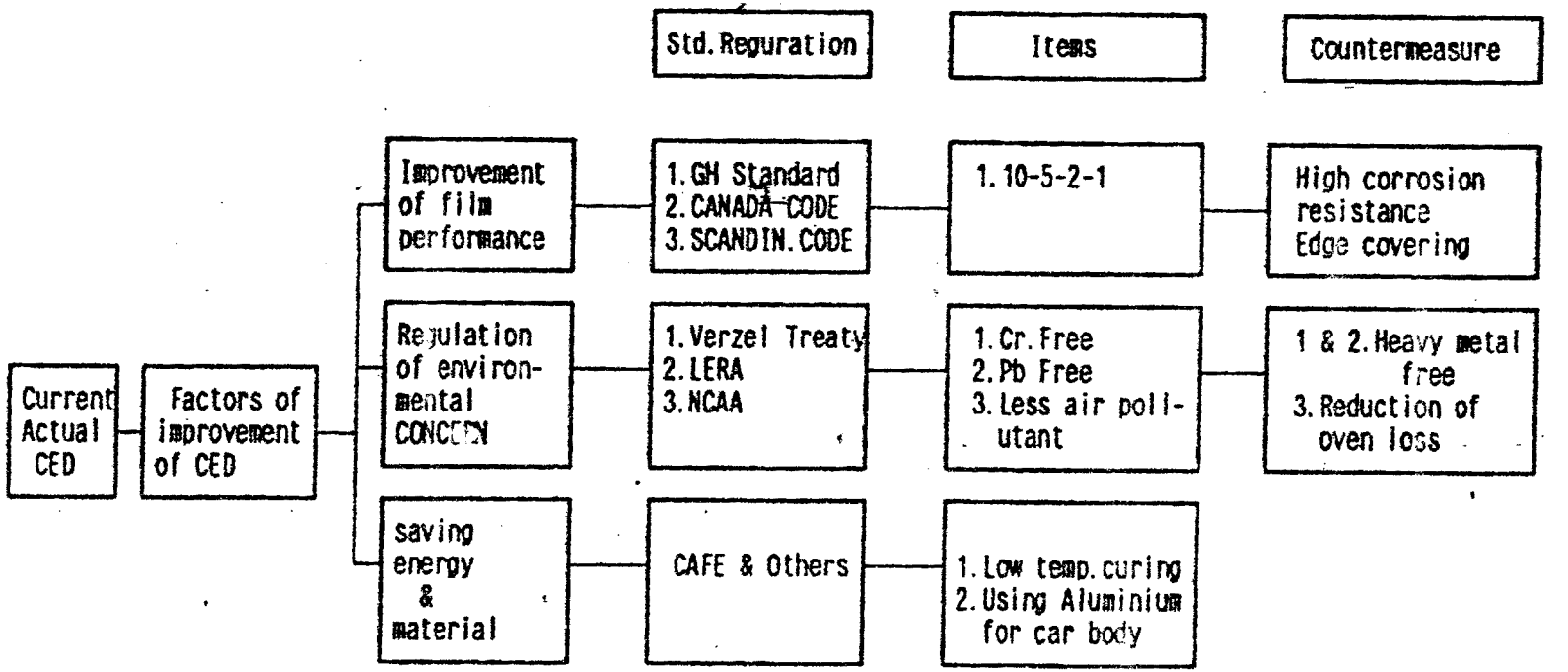

NOTICE

- VERZEL Treaty —Reguration of waste
- CAFE — Corporate Average Fuel Economy
- LERA — Lead Exposure Reduction Act
- NCAA — New Clean Air Act

Study on the properties of organic paints for steel structure subjected to natural exposure

Soravuth Judabong
Metal and Material Technology department
Thailand Institute of Scientific and Technological Research

ABSTRACT

Painted steel with five types of paints namely, Long oil alkyd, Tar epoxy, Chlorinated rubber, Polyurethane and Fluoride were exposed in different natural environments in Thailand and were evaluated for their durability. After 2 years of exposure,the properties of chalking, gloss and colour difference (ΔE) noticeably changed but no severe deterioration. Fluoride paint exhibited very good chalking resistance and gloss retension while the poor one was Tar epoxy. Colour difference varied from 2-10 and was relatively higher on the non-white colour samples. Polyurethane and Long oil alkyd showed better adhesion. The electrical properties of paint films were acceptable.

1. Introduction

Atmospheric corrosion can lead to the deterioration of steel structure, many construction materials deteriorate much more rapidly in tropical environment than in other parts of the world, this includes organic coatings that are used to protect metal. In this study, different paintings used for heavy steel construction were evaluated for their durability after 2 years exposure in natural environments.

2. Objective

- To evaluate the durability of organic coated metal by outdoor exposure tests.

3. Methodology

3.1 Test specimen

There are six painting systems, B1-B6 for this study as concluded in Table 3.1. The size of specimen was 200x100x3.2 mm, the steel substrate is shot blast to obtain roughness Rz 60 before coat. The coating is done by air spray method.

3.2 Exposure condition

3.2.1 Exposure sites

The exposure locations are selected from typical urban (Bangkok), rural (Chiangmai), Industrial (Prapadang) and marine (Huahin) as shown in map (fig 3.1). The exposure environmental factor are given in Table 3.2

The samples were fixed at the angle of 5 less than the lattitude of the place.

3.2.2 The effect of inclined angle

The inclined angle of 0°, L-5°, 30°, 45° and 90° are tested at marine site (50 meters from the coast) only.

3.2.3 The effect of distance from the coast

The Specimens are exposed at the distance of 60, 150 and 1,000 meters from the coast with the inclined angle of 45°

3.3 Test method

The tested samples were collected annually and evaluated as items listed in Table 3.3

4. Results and discussion

4.1 Surface appearance

The sample increased in chalking up to 20-30% of the surface area after 2 years, B2 (Tar epoxy) showed the highest chalking which was around 30% in all environments while B5 (Fluoride) chalked lower than the others. (Fig. 3.2)

Slight blistering of size less than 1 mm in diameter was found on some samples. No serious checking was observed. However, pitting was observed by using magnifying lens, on B1 (Long oil alkyd) from all site. Industrial and marine environment tended to promote more pitting.

The specimen inclined angle had similar effect on chalking, blistering and checking. Pitting revealed on every samples and tended to increase with the increasing of inclined angle.

4.2 Evaluation of weatherability

Colour difference (ΔE) of the samples increased in a wide range from 2-10 as shown in Fig 3.3. The non-white colour samples tended to show higher colcur change more than the white ones. B6 (Polyurethane-green) increased up to 6-9, B2 (Tar epoxy) 4-7, B1 (Long oil alkyd) 3-6, B5 (Fluoride), B3 (Chlorinated rubber) and B4 (Polyurethane) less than 3. Yet, it was difficult to differentiat the influence of environment on colour change due to the variety of test results (Fig. 3.4).

The specimen inclined angle had similar effect on ΔE after 2 year exposure, this was also for distance from the coast.

The gloss property was measured in term of gloss retension, B5 (Fluoride) showed higher gloss retension than the others while the lower one was B2 (Tar epoxy). The gloss retension of B5 ranged from 60-95%, the lower ones came from urban and industrial atmosphere. The gloss retension of B2 was less than 10% at all exposure site. Test results of the other samples are as follow B6 and B4 (Polyurethane) 26-60% , B1 (Long oil alkyd) 10-20% except in rural 40-50%, B3 (Chlorinated rubber) 10-30% (Fig 3.5). The industrial and urban environment tended to have more effect on gloss retension, followed by marine and rural environment (Fig 3.6).

The specimen inclined angle had similar effect on gloss retension and also for distance from the coast.

4.3 Anticorrosion property

The electrical properties (impedance) of paint films after 2 years exposure were satisfactory. The value of Rx, Cx and tan δ slightly differed from that before exposure and were not exceed the judgement standard as mentioned before.

B2 (Tar epoxy) tended to loss the insulating property more than the other samples. The samples collected from urban, rural and industrial area had higher values of tan δ which are 0.4-0.6 while those of the others were less than 0.3 (Table 3.6).

The specimen inclined angle and distance from the coast was found no significant difference on the electrical properties of the paint samples.

4.4 Adhesive property

The adhesion of B4 (Polyurethane) B6 and B1 (Long oil alkyd) was better than those of the others, the flaking area was around 15% while for the others was 15-35% (Fig. 3.7). The position

that failure occured on the samples are as follow : B1 (Long oil alkyd), B2 (Tar epoxy), B3 (Chlorinated rubber) between first coat and substrate, B4 (Polyurethane) B5 (Fluoride) between second coat and first coat, B6 (Polyurethane) between the first coat and substrate for sample from marine and in the first coat (cohesive breakdown) for

samples from other sites. B2 (Tar epoxy) showed somewhat more flaking despite the good adhesion by nature, it was expected due to the exceeding of a) retained, shear stress between substrate and paint film caused by different thermal expansion during exposure and/or b) the shear stress initiated during preparation of cross-cut.

5. Conclusion

The painted samples were found no severe damage on the surface. Most chalking was found on B2 (Tar epoxy) with 30% chalked area, while none chalk on B5 (Fluoride). The beginning of pitting was observed on B1 (Long oil alkyd) at all environments. Industrial and marine environment tended to promote more pitting.

The sample colour change (ΔE) varied from 2-10. The non-white paint noticeably changed more in ΔE. For gloss property, the gloss retension of specimen varied from 10-95%, B5 (Fluoride) was considered better than others while the poor one was B2 (Tar epoxy). B1 (Long oil alkyd), B3 (Chlorinated rubber) were considerably low gloss retension, which probably influenced by the environment of industrial and urban.

The adhesion of B4, B6 (Polyurethane) and B1 (Long oil alkyd) were considered better than those of the others. Besides, the electrical properties of the paint film were acceptable.

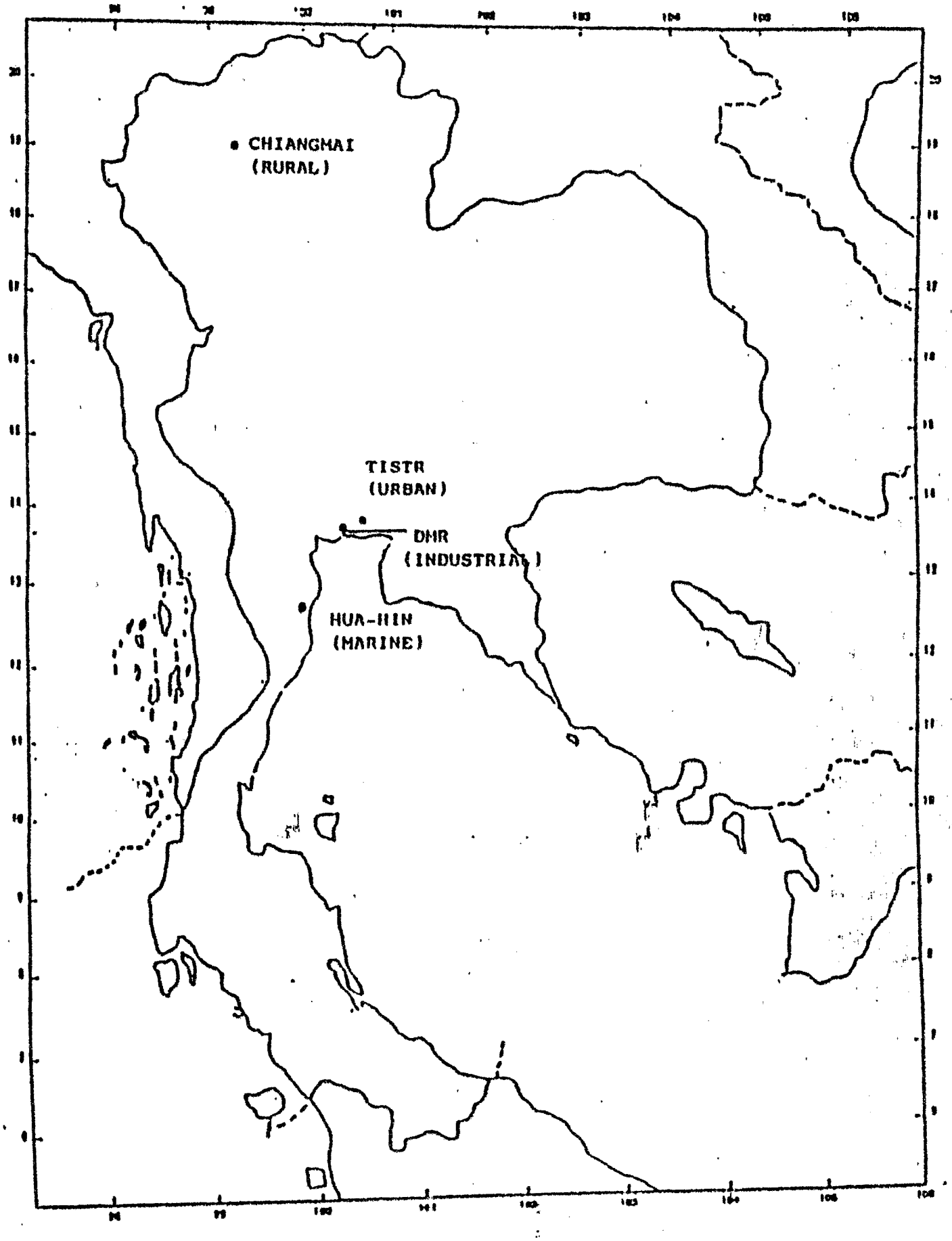

Fig.3.1 Exposure Location in Thailand

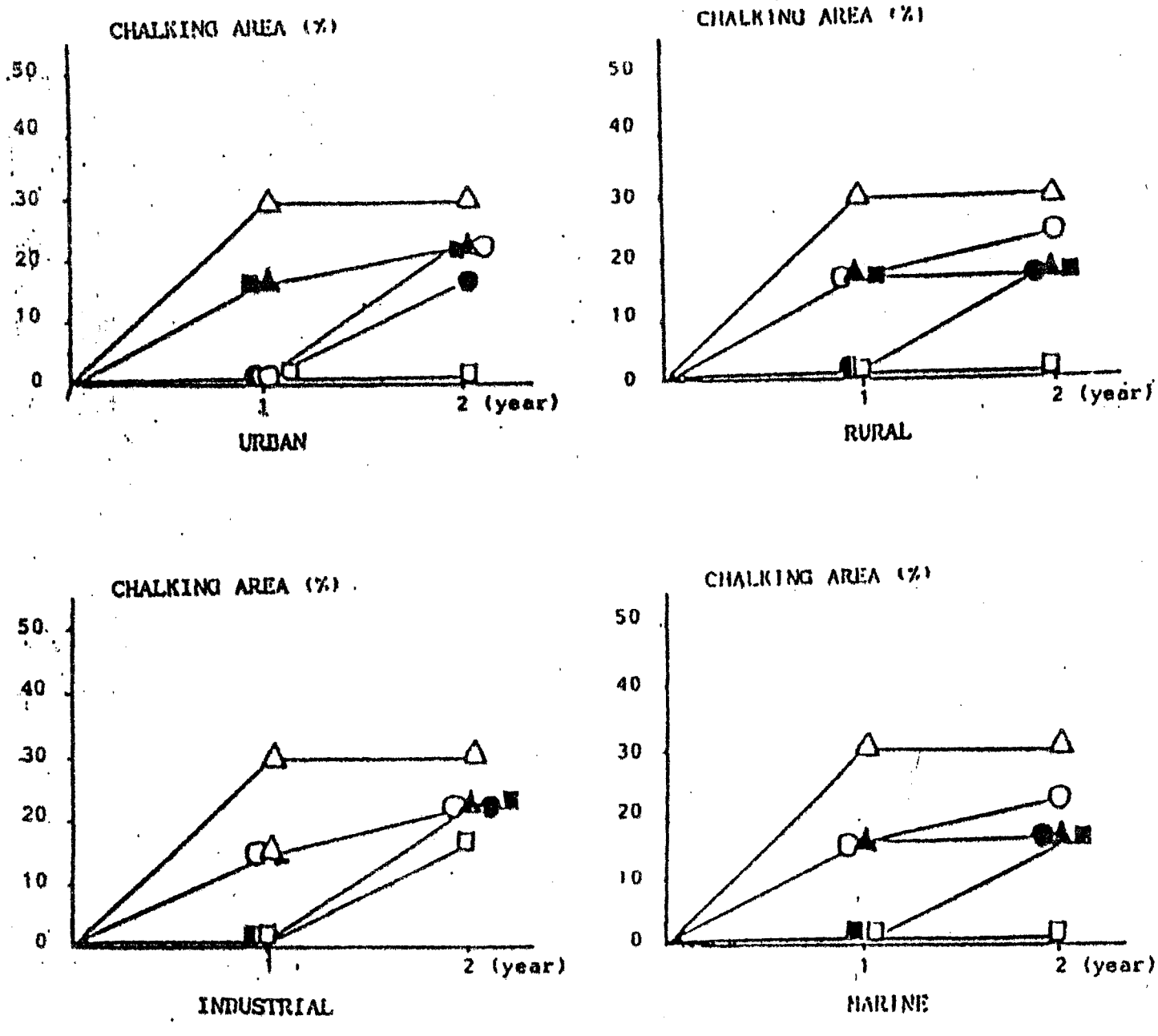

Fig 3.2 Chalking of specimens at different environments

▲ B-1 : Long oil alkyd (white)

△ B-2 : Tar epoxy (black)

○ B-3 : Chlorinated rubber (white)

● B-4 : Polyurethane (white)

□ B-5 : Fluoride (white)

■ B-6 : Polyurethane (green)

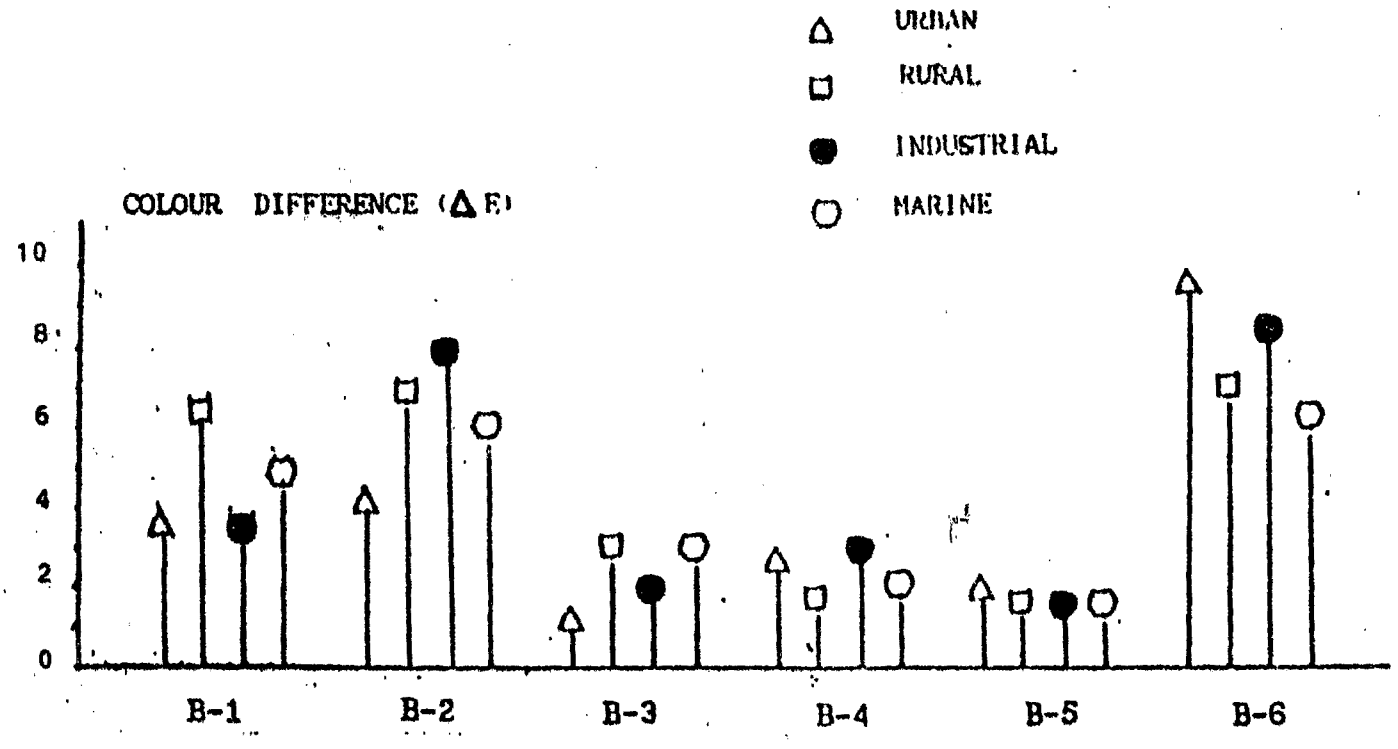

Fig 3.3 Colour difference (ΔE) of specimens after 2 years exposure

B-1 : Long oil alkyd (white)

B-2 : Tar epoxy (black)

B-3 : Chlorinated rubber (white)

B-4 : Polyurethane (white)

B-5 : Fluoride (white)

B-6 : Polyurethane (green)

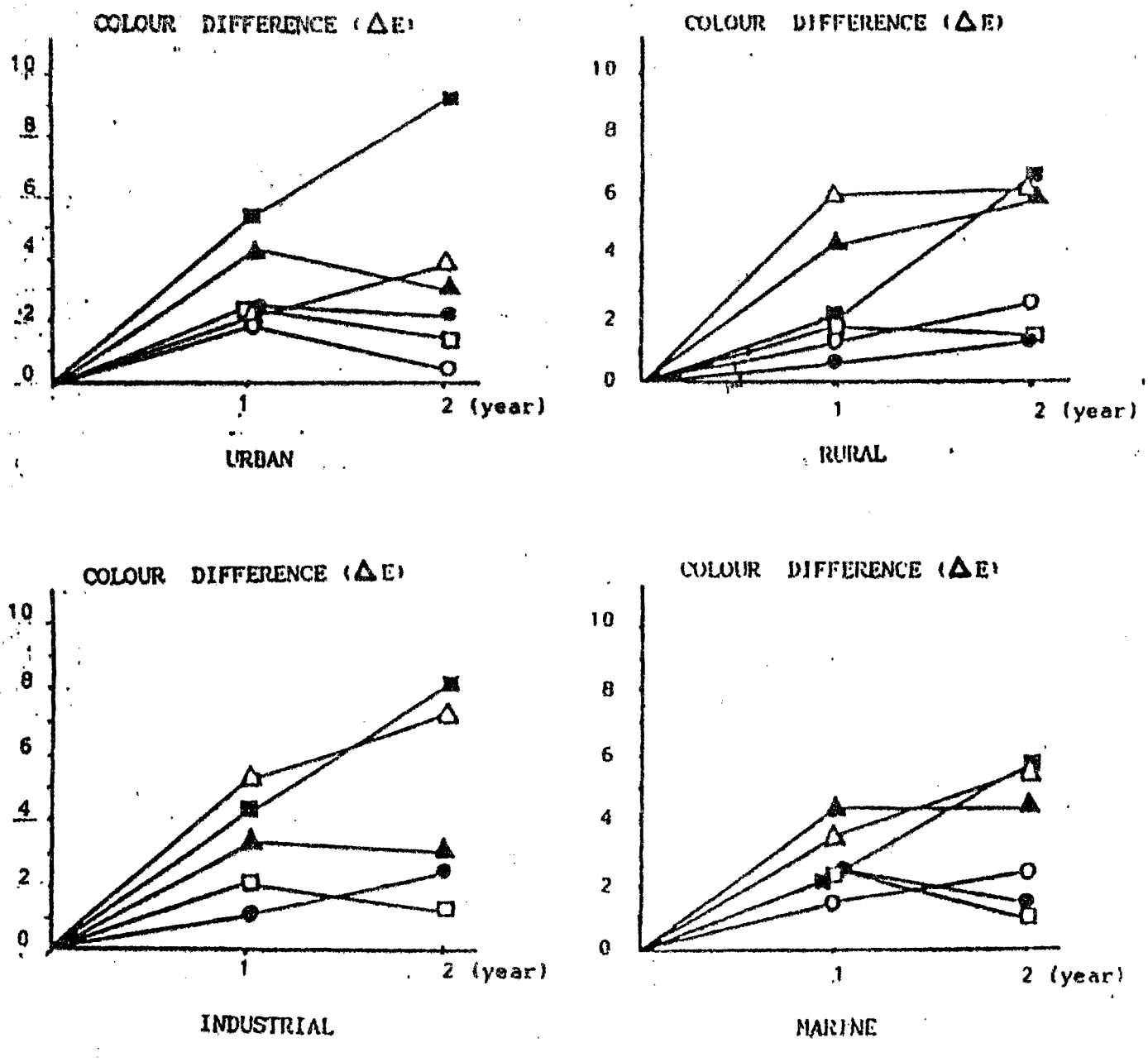

Fig 3.4 Colour difference (ΔE) of specimens at different environments

▲ B-1 : Long oil alkyd (white)

△ B-2 : Tar epoxy (black)

○ B-3 : Chlorinated rubber (white)

● B-4 : Polyurethane (white)

□ B-5 : Fluoride (white)

■ B-6 : Polyurethane (green)

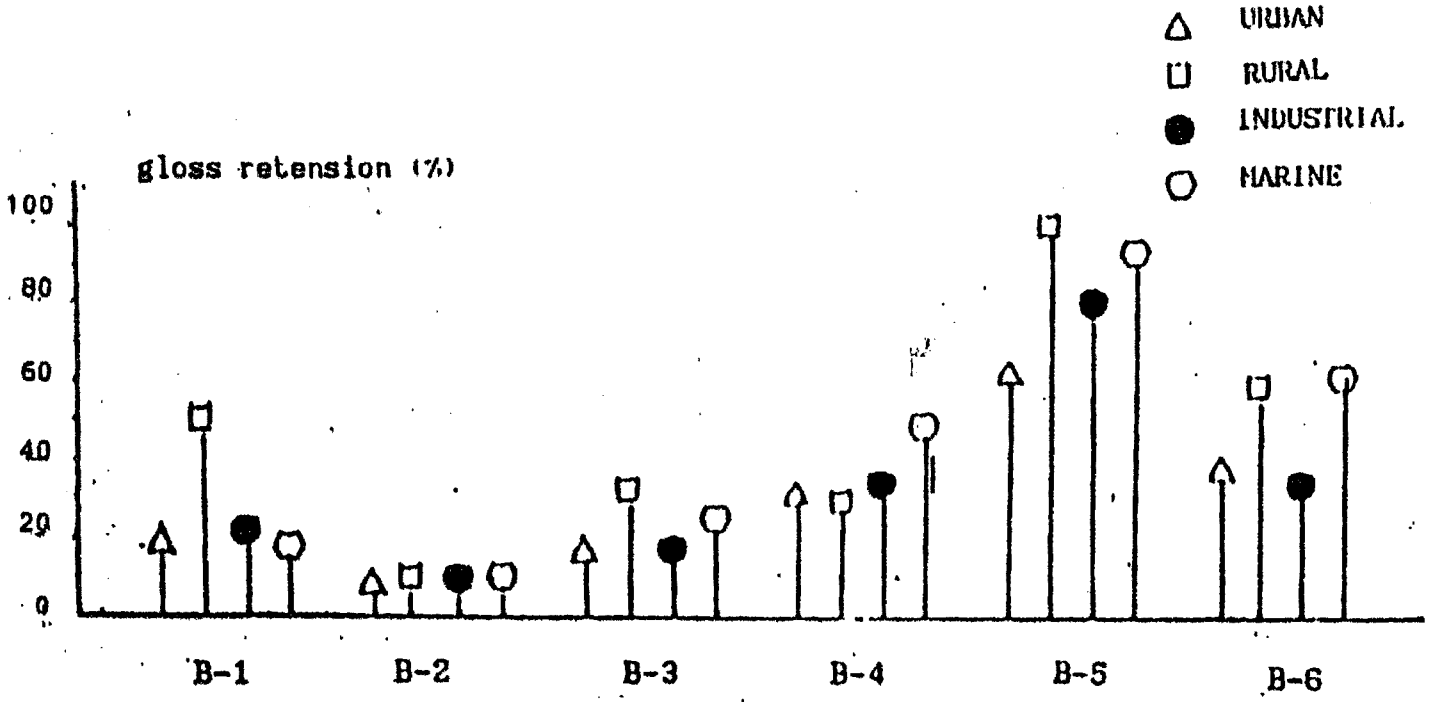

Fig 3.6 gloss retension of various paint samples, 2 years exposure

B-1 : Long oil alkyd (white)

B-2 : Tar epoxy (black)

B-3 : Chlorinated rubber (white)

B-4 : Polyurethane (white)

B-5 : Fluoride (white)

B-6 : Polyurethane (green)

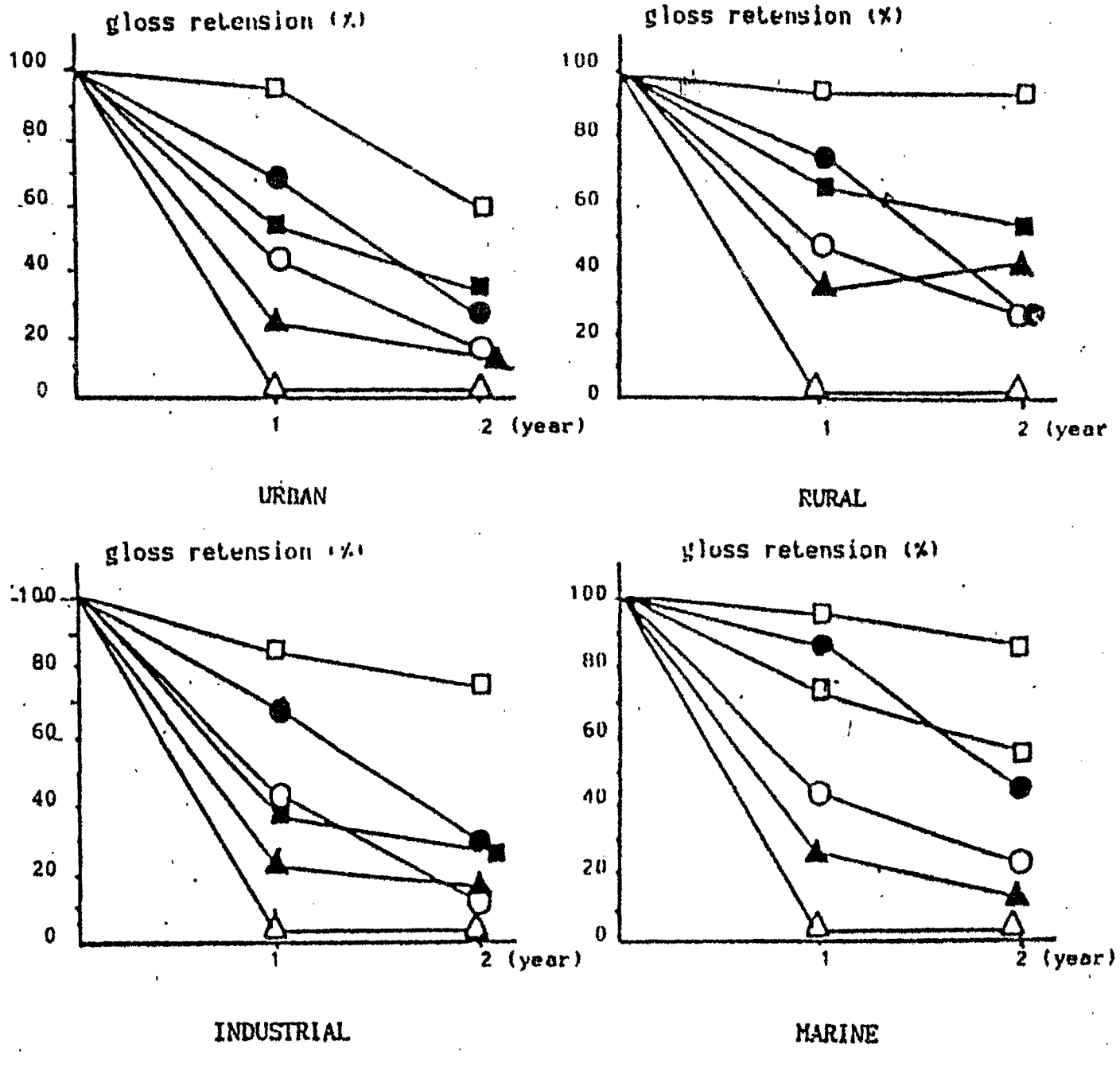

Fig 3.6 gloss retension of specimens at different environments

▲ B-1 : Long oil alkyd (white)

△ B-2 : Tar epoxy (black)

○ B-3 : Chlorinated rubber (white)

● B-4 : Polyurethane (white)

□ B-5 : Fluoride (white)

■ B-6 : Polyurethane (green)

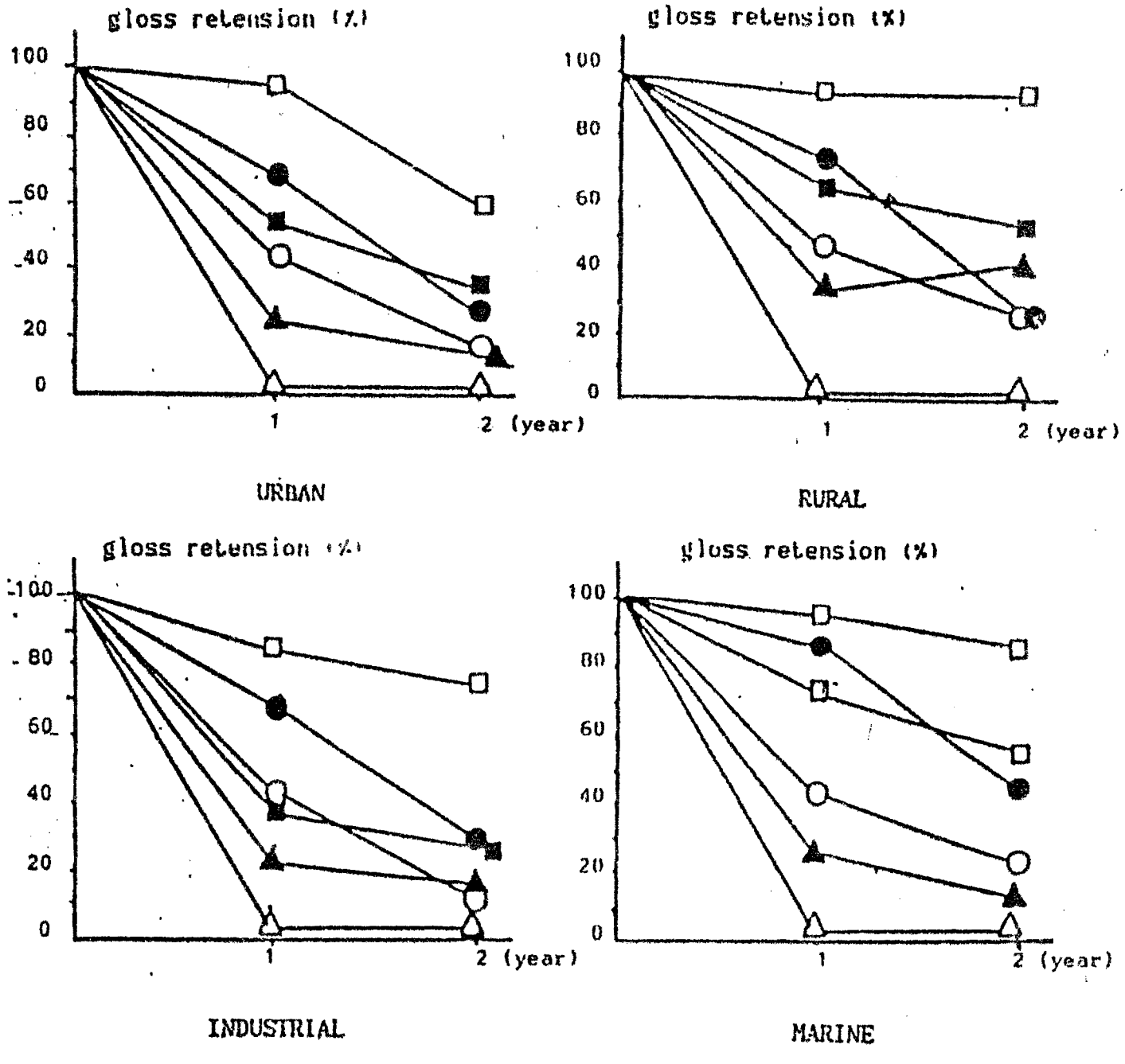

Fig 3.6 gloss retension of specimens at different environments

▲ B-1 : Long oil alkyd (white)

△ B-2 : Tar epoxy (black)

○ B-3 : Chlorinated rubber (white)

● B-4 : Polyurethane (white)

□ B-5 : Fluoride (white)

■ B-6 : Polyurethane (green)

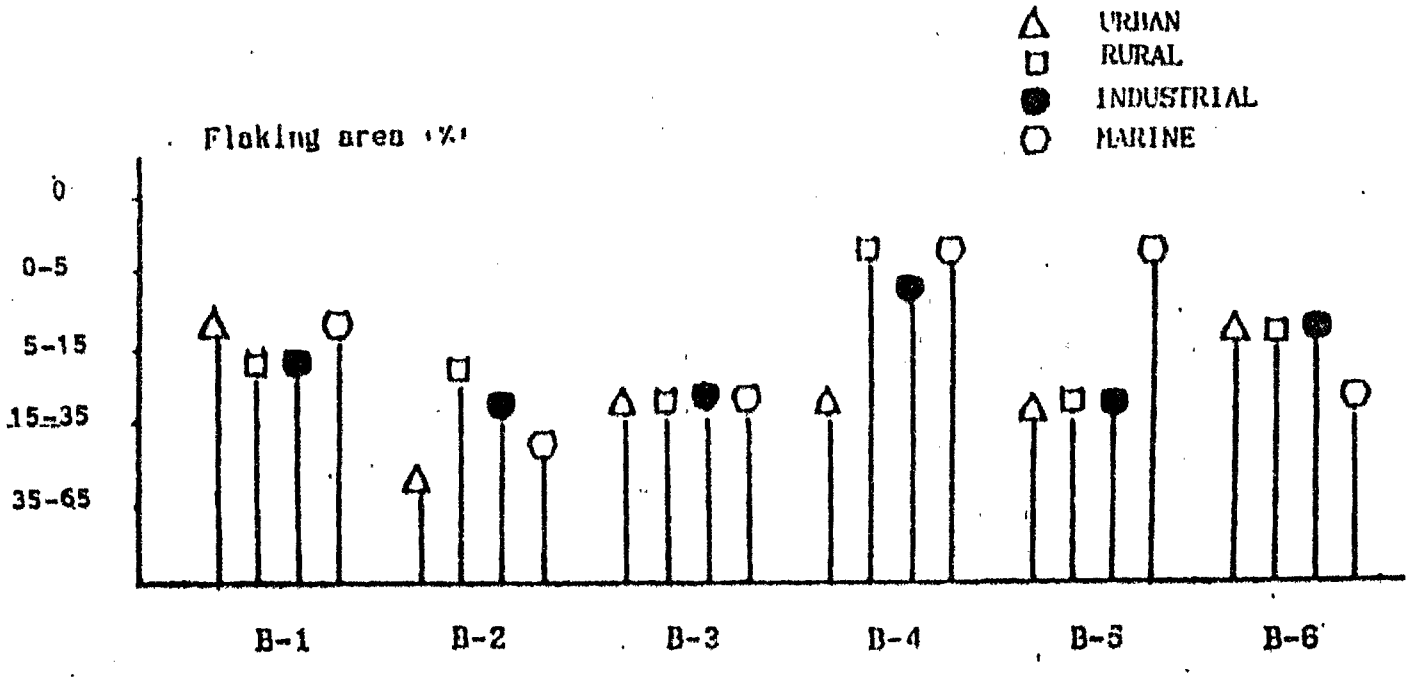

Fig 3.7 Adhension of specimens after 2 years exposure

B-1 : Long oil alkyd (white)

B-2 : Tar epoxy (black)

B-3 : Chlorinated rubber (white)

B-4 : Polyurethane (white)

B-5 : Fluoride (white)

B-6 : Polyurethane (green)

Table 3.1 Painting System and Process for Outdoor Exposure Test

Panel No.[a]		Test panel	1st Coat		2nd Coat		3rd Coat		4th Coat		5th Coat		Remark
			Common name	DFT (um)	Common name	DFT (um)	Common name	DFT (um)	Common name	DFT (um)	Common name	DFT (um)	
B-1	M-1	Steel (Shotblast Rz = 60) 200 x 100 x 3.2	Long exposure wash primer	20	Lead cyanamide rust preventive primer	35	Lead cyanamide rust preventive primer	35	Long oil alkyd undercoat	35	Long oil alkyd top coat	35	
B-2	M-2		Inorganic zinc shop primer	20	Tar expoxy paint	20	TAR expoxy paint	90	TAR expoxy paint	90	-------	90	
B-3	M-3		Epoxy zinc shop primer	20	Chlorinated rubber primer	35	Chlorinated rubber primer	35	Chlorinated rubber undercoat	35	Chlorinated rubber top coat	35	
B-4	M-4		High-build inorganic zinc primer	75	Epoxy primer	60	Epoxy primer	60	Epoxy undercoat	35	Polyurethane top coat	35	over-thinned coat prior to 2nd Coat

Panel No.[2]		Test panel	1st Coat		2nd Coat		3rd Coat		4th Coat		5th Coat		Remark
			Common name	DFT (um)	Common name	DFT (um)	Common name	DFT (um)	Common name	DFT (um)	Common name	DFT (um)	
B-5	M-5		High-build inorganic zinc primer	75	Epoxy primer	60	Epoxy primer	60	Fluoride undercoat	35	Fluoride top coat	35	Over-thinned coat prior to
B-6	M-6	Hot dip galvanized steel 200 x 100 X 3.2	Epoxy primer	60	Epoxy primer	60	Epoxy undercoat	35	Polyurethane top coat	35			

Table 3.2 Environmental factors of the exposure sites

Environmental factors	Exposure sites			
	Urban	Rural	Industrial	Marine
Temperature (°C)				
Max.	31.4	31.4	30.0	31.4
Min.	25.7	19.6	24.0	22.2
Avg.	28.6	26.3	28.3	27.05
Relative humidity (%)				
Max.	84.2	82.7	88.7	94.6
Min.	68.5	51.2	67.7	72.0
Avg.	76.4	71.7	81.3	82.7
Pollutants				
SO_2 (mg/day/dm^2)				
Max.	1.01	0.12	1.23	0.02
Min.	0.00	0.00	0.28	0.00
Avg.	0.28	0.005	0.52	<0.001
NaCl (μgCl/day/dm^2)				
Max.	228.37	58.78	164.68	376.12
Min.	0.00	0.00	0.00	0.00
Avg.	45.48	15.34	34.82	119.81
NO_2 (mg/day/dm^2)				
Max.	0.32	0.04	0.15	0.15
Min.	0.06	0.00	0.03	0.00
Avg.	0.104	0.006	0.078	0.015
^-Cl (mg/day/dm^2)				
Max.	16.38	0.00	15.70	13.88
Min.	0.00	0.00	0.00	0.00
Avg.	1.76	0.00	2.48	4.33

Table 3.3 Evaluation items for the tested samples.

Property	Evaluation Method
1. Specimen appearance	Chalking (ASTM D 659) Blistering (ASTM D 714) Checking (ASTM D 660)
2. Weatherability	Colour difference (ASTM 2244) Gloss (ASTM D 523)
3. Anticorrosion properties	Impedance : The impedance of paint film were measured in term of resistance, statistic capacity and dielectric loss factor which related to the film properties. The test results were evaluated using judgment standard for paint film degrastation and judment standard in a quideline on repair painting for flood gate steel pipe as shown in Table 3.4 and 3.5
4. Adhesive properties	Cross - cut tape test (ASTM 3359)

Table 3.4 Judgment Standard in a Guideline on Repair Painting for Floodgate Steel Pipe (1969)

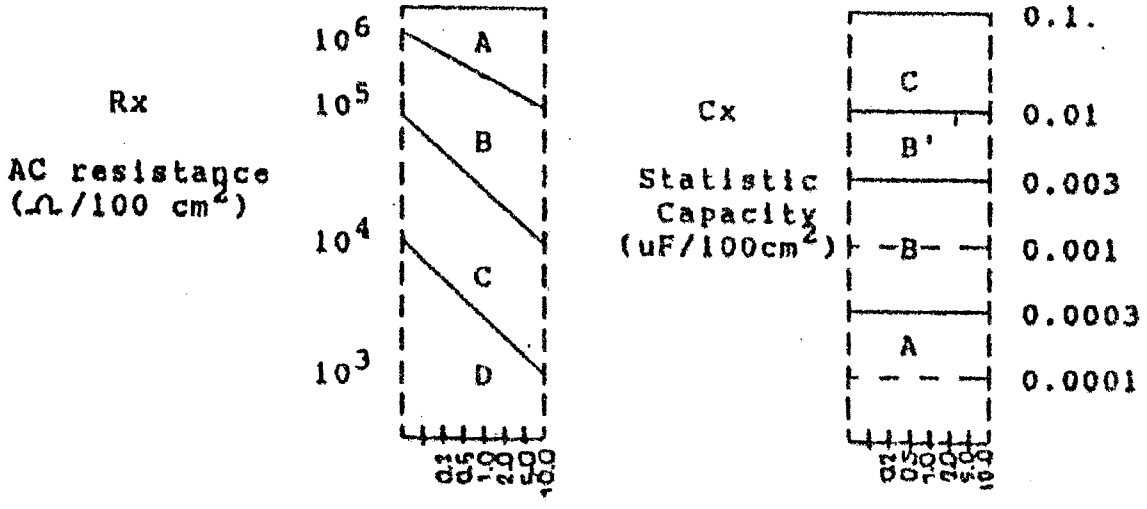

Degree of Degradation	Impedance Value		Condition of Paint film
	Resistance	Capacity	
I	A . B	A	No degradation
II	C	B	Degradation of top coat only
III	C	B	Corrosion and blistering
IV	D	C	Remarkable degradation

Table 3.5 Judgment Standard for Paint Film Degradation.

Resistance (KΩ)	Tan δ	Film Condition
10 or less	1.0 or more	Bad
10 - 100	0.5 - 1.0	Poor
100 - 500	0.3 - 0.5	Fair
500 - 1000	0.2 - 0.3	Good
1000 - more	0.2 or less	Very Good

Frequency : 1 KHz

Table 3.6 Impedance of paint films

T.P. No.		Date		Exposure time		1.0 Khz					
						Start Impedance			End Impedance		
		Start (d.m.y.)	End (d.m.y.)	t'(d)	t (y)	Rx	Cx	tanδ	Rx	Cx	tanδ
B1	U	23 Jun 89	22 Jun 90	364	1	3.2×10^{6}	0.1×10^{-8}	0.07	2.2×10^{6}	9.5×10^{-10}	0.08
	R	15 Jun 89	12 Jun 90	362	1	3.0×10^{6}	0.1×10^{-8}	0.07	2.3×10^{6}	10.0×10^{-10}	0.07
	I	27 Jun 89	27 Jun 90	365	1	3.0×10^{6}	0.1×10^{-8}	0.07	1.6×10^{6}	10.2×10^{-10}	0.12
	M	19 Jun 89	4 Jun 90	350	1	2.8×10^{5}	0.1×10^{-8}	0.07	1.4×10^{6}	9.2×10^{-10}	0.12
	U		21 Jun 91	728	2				6.0×10^{5}	1.4×10^{-9}	0.19
	R		12 Jun 91	727	2				5.0×10^{5}	2.1×10^{-9}	0.15
	I		27 Jun 91	730	2				5.6×10^{5}	1.3×10^{-9}	0.21
	M		4 Jun 91	715	2				6.5×10^{5}	1.4×10^{-9}	0.17
B2	U	23 Jun 89	22 Jun 90	364	1	12×10^{6}	0.3×10^{-8}	0.06	10.8×10^{6}	2.5×10^{-10}	0.06
	R	15 Jun 89	12 Jun 90	362	1	11×10^{6}	0.3×10^{-8}	0.06	10.4×10^{6}	2.5×10^{-10}	0.07
	I	27 Jun 89	27 Jun 90	365	1	11×10^{6}	0.3×10^{-8}	0.06	9.3×10^{6}	3.0×10^{-10}	0.06
	M	19 Jun 89	4 Jun 90	350	1	11×10^{5}	0.3×10^{-8}	0.06	3.4×10^{6}	2.0×10^{-10}	0.23
	U		21 Jun 91	728	2				8.0×10^{5}	4.0×10^{-10}	0.49
	R		12 Jun 91	727	2				9.1×10^{6}	4.0×10^{-10}	0.44
	I		27 Jun 91	730	2				9.0×10^{5}	3.0×10^{-10}	0.55
	M		4 Jun 91	715	2				1.8×10^{6}	6×10^{-10}	0.15

Table 3.6 Impedance of paint films

T.P. No.	Date		Exposure time		1.0 Khz					
					Start Impedance			End Impedance		
	Start (d.m.y.)	End (d.m.y.)	t'(d)	t (y)	Rx	Cx	tanδ	Rx	Cx	tanδ
B3 U	23 Jun 89	22 Jun 90	364	1	1.7×10^{6}	0.04×10^{-8}	0.07	1.3×10^{6}	15.0×10^{-10}	0.08
R	15 Jun 89	12 Jun 90	362	1	2.1×10^{6}	0.1×10^{-2}	0.07	1.7×10^{6}	11.3×10^{-10}	0.08
I	27 Jun 89	27 Jun 90	365	1	2.0×10^{6}	0.1×10^{-8}	0.07	1.6×10^{6}	13.0×10^{-10}	0.08
M	19 Jun 89	4 Jun 90	350	1	2.1×10^{6}	0.1×10^{-8}	0.07	1.7×10^{6}	12.0×10^{-10}	0.08
U		21 Jun 91	728	2				4.7×10^{5}	1.7×10^{-9}	0.18
R		12 Jun 91	727	2				5.1×10^{5}	1.5×10^{-9}	0.21
I		27 Jun 91	730	2				5.2×10^{5}	1.5×10^{-9}	0.2
M		4 Jun 91	715	2				5.8×10^{5}	1.4×10^{-9}	0.19
B4 U	23 Jun 89	22 Jun 90	364	1	3.4×10^{6}	0.7×10^{-2}	0.01	8.0×10^{6}	1.0×10^{-10}	0.20
R	15 Jun 89	12 Jun 90	362	1	3.2×10^{6}	0.7×10^{9}	0.07	4.1×10^{6}	7.0×10^{-10}	0.05
I	27 Jun 89	27 Jun 90	365	1	3.6×10^{6}	0.7×10^{-9}	0.06	3.0×10^{6}	1.0×10^{-10}	1.10
M	19 Jun 89	4 Jun 90	350	1	4.1×10^{6}	0.6×10^{-9}	0.06	8.5×10^{6}	6.0×10^{-10}	0.10
U		21 Jun 91	728	2				7.5×10^{5}	7×10^{-10}	0.30
R		12 Jun 91	727	2				6.2×10^{5}	1.2×10^{-9}	0.21
I		27 Jun 91	738	2				9.0×10^{5}	7.0×10^{-10}	0.25
M		4 Jun 91	715	2				7.0×10^{5}	7.0×10^{-10}	0.32

Table 3.6 Impedance of paint films

T.P. No.	Date		Exposure time		1.0 Khz					
					Start Impedance			End Impedance		
	Start (d.m.y.)	End (d.m.y.)	t'(d)	t (y)	Rx	Cx	tanδ	Rx	Cx	tanδ
B 5 U	23 Jun 89	22 Jun 90	364	1	3.5×10^{6}	0.7×10^{-9}	0.05	2.1×10^{6}	1.0×10^{-10}	0.78
R	15 Jun 89	12 Jun 90	362	1	3.9×10^{6}	0.6×10^{-9}	0.05	7.0×10^{6}	0.5×10^{-10}	0.9
I	27 Jun 89	27 Jun 90	365	1	3.5×10^{6}	0.6×10^{9}	0.05	3.3×10^{6}	6.0×10^{-10}	0.08
M	19 Jun 89	4 Jun 90	350	1	3.2×10^{6}	0.7×10^{-9}	0.06	3.9×10^{6}	1.0×10^{-10}	0.42
U		21 Jun 91	728	2				7.4×10^{5}	9×10^{-10}	0.24
R		12 Jun 91	727	2				6.5×10^{5}	1.0×10^{-9}	0.24
I		27 Jun 91	730	2				6.1×10^{5}	1.0×10^{-9}	0.26
M		4 Jun 91	715	2				7.1×10^{5}	1.0×10^{-9}	0.22
B 6 U	23 Jun 89	22 Jun 90	364	1	5.0×10^{6}	0.6×10^{-9}	0.05	3.3×10^{6}	5.0×10^{-10}	0.12
R	15 Jun 89	12 Jun 90	362	1	5.2×10^{6}	0.5×10^{-9}	0.06	3.4×10^{6}	5.8×10^{-10}	0.08
I	27 Jun 89	27 Jun 90	365	1	4.7×10^{6}	0.5×10^{-9}	0.05	5.8×10^{6}	5.2×10^{-10}	0.05
M	19 Jun 89	4 Jun 90	350	1	4.3×10^{6}	0.7×10^{-9}	0.05	3.4×10^{6}	5.8×10^{-10}	0.08
U		21 Jun 91	728	2				7.3×10^{5}	9×10^{-10}	0.24
R		12 Jun 91	727	2				2.7×10^{5}	2.6×10^{-9}	0.22
I		27 Jun 91	730	2				8.75×10^{5}	8×10^{-10}	0.23
M		4 Jun 91	715	2				6.3×10^{5}	1.2×10^{-9}	0.21

Table 3.6 Impedance of paint films

T.P. No.	Date		Exposure time		1.0 Khz					
					Start Impedance			End Impedance		
	Start (d.m.y.)	End (d.m.y.)	t'(d)	t (y)	Rx	Cx	tanδ	Rx	Cx	tanδ
Specimen Inclined angle										
0°	19 Jun 89	4 Jun 91						9.3×10^{5}	1.4×10^{-9}	0.12
5 - 5°	19 Jun 89	4 Jun 91						7.8×10^{5}	1.4×10^{-9}	0.14
30°	19 Jun 89	4 Jun 91						9.2×10^{5}	1.3×10^{-9}	0.13
45°	19 Jun 89	4 Jun 91						9.1×10^{5}	1.5×10^{-9}	0.11
90°	19 Jun 89	4 Jun 91						7.6×10^{5}	1.7×10^{-9}	0.12
Distance from Coast (meters)										
50°	19 Jun 89	4 Jun 91						9.3×10^{5}	1.5×10^{-9}	0.11
150°	19 Jun 89	4 Jun 91						7.0×10^{5}	1.6×10^{-9}	0.14
1000°	19 Jun 89	4 Jun 91						6.5×10^{5}	2.0×10^{-9}	0.12